

1. Report No. FHWA/TX-88+381-1		2. Government Accession No.		3. Recipient's Catalog No.	
4. Title and Subtitle TIME DEPENDENT DEFLECTIONS OF PRETENSIONED BEAMS				5. Report Date August 1987	
				6. Performing Organization Code	
7. Author(s) D. J. Kelly, T. E. Bradberry, and J. E. Breen				8. Performing Organization Report No. Research Report 381-1	
9. Performing Organization Name and Address Center for Transportation Research The University of Texas at Austin Austin, Texas 78712-1075				10. Work Unit No.	
				11. Contract or Grant No. Research Study 3-5-84-381	
12. Sponsoring Agency Name and Address Texas State Department of Highways and Public Transportation; Transportation Planning Division P. O. Box 5051 Austin, Texas 78763-5051				13. Type of Report and Period Covered Interim	
				14. Sponsoring Agency Code	
15. Supplementary Notes Study conducted in cooperation with the U. S. Department of Transportation, Federal Highway Administration. Research Study Title: "Optimum Design of Bridge Girders Made Using High Strength Concrete and Deflection of Long-Span Prestressed Concrete"					
16. Abstract <p>Eight long-span (127-ft) pretensioned AASHTO Type IV bridge beams made with high strength concrete and low-relaxation strand were instrumented in the field. Longtime deformations and internal beam temperatures were measured. Measurements were taken periodically from the time the beams were cast, through construction, and continued for one year after they were placed in service. Deformation measurements included concrete surface strains, prestressing strand strain, and quarter point and midspan camber or deflection. Internal concrete temperatures were measured with thermocouples which were located in critical locations of the beam. The measured time dependent camber or deflection was compared to the results of several previously reported analytical techniques. These analytical results did not accurately predict the measured response.</p> <p>A modification of the PCI multiplier technique for calculating longtime camber and deflection was developed and programmed for use on a microcomputer. These new multipliers were used to accurately predict the time dependent response of the instrumented beams. This technique was then used to calculate the sensitivity of time dependent camber or deflection to some of the more important variables such as concrete strength, creep, and construction time schedule. Based on the results of the sensitivity study, one could expect camber or deflection of long span beams, similar to those studied, to vary from 2 to 6 in. at erection and from -0.75 to 2 in. at the end of the service life.</p>					
17. Key Words field measurement, deformations, girders, prestressed, pretensioned, long-span, low relaxation strand, casting, storage, erection, traffic			18. Distribution Statement No restrictions. This document is available to the public through the National Technical Information Service, Springfield, Virginia 22161.		
19. Security Classif. (of this report) Unclassified		20. Security Classif. (of this page) Unclassified		21. No. of Pages 232	22. Price

Lack of
Technical Support
with Page Layout
Standard Form

Plans

TIME DEPENDENT DEFLECTIONS OF PRETENSIONED BEAMS

by

D. J. Kelly, T. E. Bradberry, and J. E. Breen

Research Report 381-1

Research Project 3-5-84-381

"Optimum Design of Bridge Girders Made Using High Strength Concrete
and Deflection of Long-Span Prestressed Concrete Beams"

Conducted for

Texas

State Department of Highways and Public Transportation

In Cooperation with the

U. S. Department of Transportation
Federal Highway Administration

by

CENTER FOR TRANSPORTATION RESEARCH
BUREAU OF ENGINEERING RESEARCH
THE UNIVERSITY OF TEXAS AT AUSTIN

August 1987

The contents of this report reflect the views of the authors who are responsible for the facts and accuracy of the data presented herein. The contents do not necessarily reflect the official views or policies of the Federal Highway Administration. This report does not constitute a standard, specification, or regulation.

P R E F A C E

This report is the first report in a series which summarizes an investigation of the feasibility of utilizing high strength concretes and improved low relaxation steels in pretensioned bridge girders. This report summarizes a field measurement program in which deformations of long span pretensioned girders with low relaxation strand were monitored from initial casting, through storage, erection and bridge completion, and through the first year of traffic.

This work is part of Research Project 3-5-84-381, entitled "Optimum Design of Bridge Girders Made Using High-Strength Concrete and Deflections of Long-Span Prestressed Concrete Beams." This report specifically summarizes the work referred to in the second part of the project title. The research was conducted by the Phil M. Ferguson Structural Engineering Laboratory as part of the overall research programs of the Center for Transportation Research of The University of Texas at Austin. The work was sponsored jointly by the Texas State Department of Highways and Public Transportation and the Federal Highway Administration under an agreement with The University of Texas at Austin and the State Department of Highways and Public Transportation.

Liaison with the State Department of Highways and Public Transportation was maintained through the contact representative, Mr. David P. Hohmann and the former Area IV Committee Chairman, Mr. Robert L. Reed. Mr. R. E. Stanford was the contact representative for the Federal Highway Administration.

This research involved a great deal of coordination with field operations. The authors are particularly indebted to Jesse Lawrance and Heldenfels Bros., Inc., for their cooperation during girder fabrication. Messrs. Ronald Bailey, Buddy Johnson, Orville Miller, and E. V. Weese of the State Department of Highways and Public Transportation all provided invaluable assistance in field operations. Numerous students from the Ferguson Laboratory assisted in readings over the long life of the project. The authors are particularly indebted to Tommy Bush, Reid Castrodale, David Hartmann, David Olvera, Tim Overman, Alan Phipps, Guillermo Ramirez, Akbar Vasseghi, Charles Walker, and David Yates in this regard.

This portion of the overall study was directed by John E. Breen, who holds the Nasser I. Al-Rashid Chair in Civil Engineering. Co-directors supervising other portions of Project 381 were Ned H. Burns

and Michael E. Kreger. The installation of instrumentation and early readings of the girders was under the direction of Timothy E. Bradberry, Research Engineer. The longer term monitoring of the girders and development of the time dependent computer analysis were under the direction of Dominic J. Kelly, Research Engineer.

S U M M A R Y

Eight long-span (127 ft) pretensioned AASHTO Type IV bridge beams made with high strength concrete and low-relaxation strand were instrumented in the field. Longtime deformations and internal beam temperatures were measured. Measurements were taken periodically from the time the beams were cast, through construction, and continued for one year after they were placed in service.

Deformation measurements included concrete surface strains, prestressing strand strain, and quarter point and midspan camber or deflection. The strain measuring systems did not work properly, and so most of the strain data were invalid. Camber and deflection were measured using a reference piano wire with a constant force retensioning system based on use of a standard weight. This measuring system worked extremely well. The average beam camber at erection was 3.3 in. After the composite slab had been cast the average camber was 1.4 in. Long-term camber after approximately 1000 days averaged 1.1 in. and varied from 0.2 in. to 1.8 in.

Internal concrete temperatures were measured with thermocouples which were located in critical locations of the beam. Average beam temperatures of as much as 15° F less than the ambient temperature were measured. In general, the thermal gradients were near linear before the beam became composite and highly nonlinear afterwards.

The measured time dependent camber or deflection was compared to the results of several previously reported analytical techniques. These analytical results did not accurately predict the measured response.

A modification of the PCI multiplier technique for calculating longtime camber and deflection was developed. These new multipliers were used to accurately predict the time dependent response of the instrumented beams. The procedure was programmed for convenient use on a personal computer. A program listing and user guide is included. This technique was then used to calculate the sensitivity of time dependent camber or deflection to some of the more important variables such as concrete strength, creep, and construction time schedule. Based on the results of the sensitivity study, one could expect camber or deflection of long span beams, similar to those studied, to vary from 2 to 6 in. at erection and from -0.75 to 2 in. at the end of the service life.

I M P L E M E N T A T I O N

This report summarizes a field monitoring program of the deformation of long span prestressed concrete girders using high strength concrete and low relaxation strand. The computation of deflections is shown to be highly dependent on a knowledge of actual field conditions including both actual material properties and actual construction schedules.

A typical long span girder example (Type IV beam on a 127 ft span) is presented to indicate that final, long term camber can vary from as low as -0.75 in. to +2.0 in. depending on material properties, environment, and construction schedules. A relatively user-friendly program for use on a microcomputer is provided so that design or field personnel can easily update deflection predictions as actual material properties and construction time schedules become known. The program results indicate that minor factors like the location of temporary supports during storage can affect final deformations appreciably.

This report shows that girder deformation can be calculated fairly accurately when material properties and construction schedules are known. A number of suggestions are made for use by those updating the SDHPT programs used for pretensioned girder design. Implementation of the microcomputer program CAMBER in field offices would give a practical method for establishing expected girder sags or cambers. This should assist field personnel in deciding on final camber allowances when setting deck forms.

C O N T E N T S

Chapter		Page
1	INTRODUCTION	1
	1.1 General	1
	1.2 Previous Experimental Studies	5
	1.3 Methods of Analysis	8
	1.4 Field Program	8
	1.5 Objective and Scope	9
2	BRIDGE DETAILS, INSTRUMENTATION, AND COMPANION TESTS	11
	2.1 General	11
	2.2 Beam and Composite Bridge Details	11
	2.3 Materials	17
	2.3.1 Beams	17
	2.3.2 Deck Panels	20
	2.3.3 Cast-in-Place Slabs	20
	2.4 Laboratory Tests	20
	2.4.1 General	20
	2.4.2 Compressive Strength	20
	2.4.3 Elastic Modulus	20
	2.4.4 Creep and Shrinkage	20
	2.5 Field Instrumentation	22
	2.5.1 Instrumentation Location	22
	2.5.2 Concrete Surface Strain	22
	2.5.3 Prestressing Strand Strain	26
	2.5.4 Concrete Temperature	26
	2.5.5 Camber and Deflection Measuring System ..	26
	2.6 Data Reduction	30
3	FIELD OPERATIONS	33
	3.1 Bridge Construction	33
	3.2 Measurements	42
	3.3 Problems Encountered	43
	3.3.1 Missed Zero Readings	43
	3.3.2 Varying Support Conditions	43
	3.3.3 Site Access Difficulties	43
	3.3.4 Difficulties Caused by the Construction Technique	43
	3.3.5 Problems with Instrumentation	46

Chapter		Page
4	OBSERVED BEHAVIOR	49
	4.1 General	49
	4.2 Field Measurements	49
	4.2.1 Camber and Deflection	49
	4.2.2 Concrete Surface Strains	56
	4.2.3 Strain of the Prestressing Strand	56
	4.2.4 Concrete Temperature Variations	63
	4.3 Companion Tests	72
	4.3.1 Concrete Compressive Strength	72
	4.3.2 Elastic Modulus of Concrete	77
	4.3.3 Concrete Creep and Shrinkage	82
	4.4 Thermal Movements	88
	4.5 Comparison of Observed Behavior	92
	4.5.1 Creep Curves	92
	4.5.2 L-Series Camber and Deflection Response .	94
	4.5.3 H-Series Camber and Deflection Response .	96
	4.5.4 L-Series vs H-Series Camber and Deflection Response	98
5	ANALYTICAL TECHNIQUES AND RESULTS	103
	5.1 General	103
	5.2 SDHPT's PSTRS10-Prestress Loss, Maximum Camber, and Slab Dead Load Deflection	104
	5.3 AASHTO - Prestress Losses	105
	5.4 PCI Design Handbook - Prestress Loss, Elastic Camber and Deflections, and Longtime Camber or Deflection	114
	5.4.1 Prestress Loss	114
	5.4.2 Elastic Camber and Deflection	116
	5.4.3 Longtime Camber and Deflection	125
	5.5 Suttikan's PBEAM - Prestress Loss, Elastic Camber and Deflections, and Time Dependent Response	132
	5.5.1 PBEAM	132
	5.5.2 Prestress Loss	138
	5.5.3 Elastic Camber and Deflection	140
	5.5.4 Time Dependent Camber and Deflection	143
	5.6 Proposed Multipliers - Time Dependent Camber and Deflection	149
	5.7 General	156

Chapter		Page
6	ASSESSMENT OF ANALYTICAL TECHNIQUES	161
	6.1 Prestress Loss	161
	6.2 Elastic Camber and Deflection	166
	6.3 Time Dependent Camber and Deflection	167
	6.4 Sensitivity of Camber Predictions to Material Properties and Construction Schedule	170
	6.4.1 General	170
	6.4.2 Concrete Strength	172
	6.4.3 Age at Release	174
	6.4.4 Creep	174
	6.4.5 Humidity	174
	6.4.6 Low-Relaxation Strand Substituted for Stress-Relieved Strand	176
	6.4.7 Replaced Beam	178
	6.4.8 Construction Schedule	178
	6.4.9 Combinations of Variables	180
7	SUMMARY, CONCLUSIONS, AND RECOMMENDATIONS	185
	7.1 Summary	185
	7.2 Conclusions	185
	7.2 Recommendations	187
	REFERENCES	189
	APPENDIX A	195

T A B L E S

Table		Page
2.1	Properties of Beam Concrete	19
2.2	Instrumentation on Each Beam	24
3.1	History of L-Series Beams	34
3.2	History of H-Series Beams	35
3.3	Layers of Panels Placed on Beams	41
3.4	Average Measured Deck Thickness	41
3.5	Support Conditions	44
5.1	Design Values Used to Calculate Prestress Loss	110
5.2	Parameters Used to Calculate Prestress Losses for Instrumented Beams	110
5.3	Transformed Cross Section Properties Used to Calculate Prestress Loss	111
5.4	Concrete Elastic Moduli (ksi) Used to Calculate Elastic Response	120
5.5	Elastic Response Calculated Using the PCI Design Handbook Moment Area Equations	122
5.6	Comparison of Measured and PCI Design Handbook Calculated Elastic Camber and Deflections	124
5.7	Multipliers Suggested by PCI to Be Used as a Guide in Estimating Longtime Cambers and Deflections for Typical Members [23]	126
5.8	Elastic Cambers and Deflections Predicted Using PBEAM	141
5.9	Comparison of Elastic Response Predicted with PBEAM and the Measured Elastic Response	142
5.10	Calculated Elastic Camber and Deflection That Occurs When a Beam Is Placed Into and Taken Out of Storage	154

Table		Page
6.1	Comparison of Calculated and Measured Elastic Responses (in.) for Beam L-01	168
6.2	Comparison of Calculated and Measured Elastic Responses (in.) for Beam H-i2	168

F I G U R E S

Figure		Page
1.1	Components of beam camber or deflection	2
1.2	Components of time dependent camber and deflection ...	4
2.1	Location and designation of instrumented beams in the right main lane bridge	12
2.2	Location and designation of instrumented beams in the left main lane bridge	13
2.3	Span and support dimensions	14
2.4	AASHTO Type IV prestressed concrete I-beam	15
2.5	Deck panel details	15
2.6	Composite deck design dimensions	16
2.7	Strand pattern for the L-series beams in the right main lane bridge	16
2.8	Strand pattern for the H-series beams in the left main lane bridge	18
2.9	Mild reinforcing steel	18
2.10	Creep test setup	21
2.11	Location of instrumentation stations	23
2.12	Demec mechanical strain gage	25
2.13	Details of surface strain and camber or deflection instrumentation	27
2.14	Location of strain gages and thermocouples at midspan and quarter point stations of the L-series beams	28
2.15	Location of strain gages and thermocouples at midspan and quarter point stations of the H-series beams	28
2.16	Deflection instrumentation	29

Figure		Page
2.17	Ruler and anchor bolt at beam end	29
2.18	Standard weight deflection procedure for establishing and maintaining a fixed tension in the piano wire	31
3.1	Instrumentation station before concrete is cast	36
3.2	Instrumentation station after release while still in the prestressing bed	36
3.3	Typical beam support while in storage	38
3.4	Steel girders for the gantry system	38
3.5	Cranes used to launch beams	39
3.6	Beam placed in the bridge	39
3.7	Beams next to steel girder in their temporary location	40
3.8	Fiberboard glued to the top of beams before placing deck panels	40
3.9	Cart used to access instrumentation	45
3.10	Temporary bracing in the way of Demec points	45
4.1	Time dependent camber and deflection response of beam L-01	50
4.2	Response of beam L-01	51
4.3	Time dependent camber and deflection response of beam L-02	53
4.4	Time dependent camber and deflection response of beam L-i1	54
4.5	Time dependent camber and deflection response of beam L-i2	55
4.6	Time dependent camber and deflection response of beam H-01	57

Figure		Page
4.7	Time dependent camber and deflection response of beam H-o2	58
4.8	Time dependent camber and deflection response of beam H-i1	59
4.9	Time dependent camber and deflection reponse of beam H-i2	60
4.10	Measured strain at the midspan of L-o2	61
4.11	Measured strain distribution at the midspan of L-o2	61
4.12	Surface strain readings affected by the epoxy	62
4.13	Typical measured strand strain	64
4.14	Temperature distribution in a beam during the morning of a sunny summer day	66
4.15	Temperature distribution in a beam on a cold overcast winter day	66
4.16	Temperature distribution in a beam on a hot summer day	67
4.17	Temperature distribution on an overcast spring day while in storage	68
4.18	Midspan temperature distributions in composite beam L-i1 on a sunny winter day	68
4.19	Quarter point temperature distribution in composite beam L-i1 on a sunny winter day	69
4.20	South end temperature distribution in composite beam L-i1 on a sunny winter day	69
4.21	Midspan temperature distributions in composite beam L-i1 on an unusually hot winter day	70
4.22	Quarter point temperature distributions in composite beam L-i1 on an unusually hot winter day ...	70
4.23	South end temperature distributions in composite beam L-i1 on an unusually hot winter day	71

Figure		Page
4.24	Midspan temperature distributions in composite beam L-i1 on an overcast spring day	71
4.25	Quarter point temperature distributions in composite beam L-i1 on an overcast spring day	73
4.26	South end temperature distributions in composite beam L-i1 on an overcast spring day	73
4.27	Cylinder compressive strengths corresponding to beams L-i1 and L-i2	74
4.28	Cylinder compressive strengths corresponding to beams L-i1 and L-i2 that were broken the first 100 days after casting	74
4.29	Cylinder compressive strengths corresponding to beams L-o1 and L-o2	75
4.30	Cylinder compressive strengths corresponding to beams H-o1 and H-o2	75
4.31	Cylinder compressive strengths corresponding to beams H-o1 and H-i2	76
4.32	Variation of 14-day strength of beam cylinders	76
4.33	Variation of 28-day strength of beam cylinders	78
4.34	Elastic modulus vs the compressive strength for the beam concrete	79
4.35	Data Pauw used to develop the formula that AASHTO recommends to be used for calculating concrete elastic modulus [37]	80
4.36	Elastic modulus predicted using AASHTO, ACI 363, and a proposed formula vs measured values	81
4.37	Creep coefficient for cylinders corresponding to beams L-i1 and L-i2	83
4.38	Shrinkage and thermal strain of unloaded cylinders corresponding to beams L-i1 and L-i2	84

Figure		Page
4.39	Strain of unloaded cylinders corrected for thermal effects using changes of ambient temperatures	84
4.40	Creep coefficient for cylinders corresponding to beams H-o1 and H-o2	86
4.41	Shrinkage and thermal strain of unloaded cylinders corresponding to beams H-o1 and H-o2	87
4.42	Strain of unloaded cylinders corrected using changes of ambient temperatures	87
4.43	Temperature induced camber in a composite beam on an unseasonably warm winter day	89
4.44	Temperature induced camber in a composite beam on a sunny winter day	90
4.45	Temperature induced camber in a composite beam on an overcast day	91
4.46	Comparison of creep curves	93
4.47	Camber and deflection responses of the L-series beams	95
4.48	Camber and deflection responses of the H-series beams	97
4.49	Camber and deflection responses of typical L- and H-series beams	99
5.1	Comparison of prestress losses for the L-series beams calculated using AASHTO specifications	107
5.2	Comparison of prestress losses for the H-series beams calculated using AASHTO specifications	108
5.3	Comparison of prestress losses for the L- and H-series design beams calculated using AASHTO specifications ..	113
5.4	Comparison of prestress losses for the L-series beams calculated using the PCI Design Handbook (1985)	115
5.5	Comparison of prestress losses for the H-series beams calculated using the PCI Design Handbook (1985)	117
5.6	Comparison of prestress losses for the L- and H-series design beams calculated using the PCI Design Handbook (1985)	118

Figure		Page
5.7	Initial response at midspan of a beam with a two-point depressed strand pattern	119
5.8	Longtime response for the L-series design beam predicted using the PCI multipliers and designer assumed timing of events	127
5.9	Longtime response for the H-series design beam predicted using the PCI multipliers and designer assumed timing of events	127
5.10	Longtime response for the beams L-i1 and L-i2 predicted using PCI multipliers and actual timing of events	129
5.11	Longtime response for the beams L-o1 and L-o2 predicted using PCI multipliers and actual timing of events	129
5.12	Longtime response for the beams H-o1 and H-o2 predicted using PCI multipliers and actual timing of events	130
5.13	Longtime response for the beams H-i1 and H-i2 predicted using PCI multipliers and actual timing of events	130
5.14	Comparison of time dependent camber predicted using PCI multipliers and the measured response for beam L-o1	131
5.15	Comparison of time dependent camber predicted using the PCI multipliers and the measured response for beam H-i2	131
5.16	Model cross section of beam used to run PBEAM	134
5.17	Concrete stress-strain curve used for PBEAM [25]	135
5.18	Creep curve for the L-series beams used as input for PBEAM	137
5.19	Creep curve for the H-series beams used as input for PBEAM	137
5.20	Time dependent prestress loss for beam L-o1 predicted using PBEAM	139

Figure		Page
5.21	Time dependent prestress loss for beam H-i2 predicted using PBEAM	139
5.22	Time dependent camber for beam L-i1 predicted using PBEAM	144
5.23	Time dependent camber for beam L-i2 predicted using PBEAM	144
5.24	Time dependent camber for beam L-o1 predicted using PBEAM	145
5.25	Time dependent camber for beam L-o2 predicted using PBEAM	145
5.26	Time dependent camber for beam H-o1 predicted using PBEAM	146
5.27	Time dependent camber for beam H-o2 predicted using PBEAM	146
5.28	Time dependent camber for beam H-i1 predicted using PBEAM	147
5.29	Time dependent camber for beam H-i2 predicted using PBEAM	147
5.30	Comparison of time dependent camber predicted using PBEAM and measured camber for beam L-o1	148
5.31	Comparison of time dependent camber predicted using PBEAM and measured camber for beam H-i2	148
5.32	Time dependent camber for beam L-i1 predicted using the proposed multipliers	155
5.33	Time dependent camber for beam L-i2 predicted using the proposed multipliers	155
5.34	Time dependent camber for beam L-o1 predicted using the proposed multipliers	157
5.35	Time dependent camber for beam L-o2 predicted using the proposed multipliers	157
5.36	Time dependent camber for beam H-o1 predicted using the proposed multipliers	158

Figure		Page
5.37	Time dependent camber for beam H-o2 predicted using the proposed multipliers	158
5.38	Time dependent camber for beams H-i1 and H-i2 predicted using the proposed multipliers	159
5.39	Comparison of time dependent camber predicted using the proposed multipliers and measured camber for beam L-o1	160
5.40	Comparison of time dependent camber predicted using the proposed multipliers and measured camber for beam H-i2	160
6.1	Comparison of calculated prestress losses for the L-series design beams	162
6.2	Comparison of calculated prestress losses for beams L-o1 and H-i2	163
6.3	Comparison of calculated time dependent camber for beam L-o1	169
6.4	Comparison of calculated time dependent camber for beam H-i2	171
6.5	Sensitivity of time dependent camber to concrete strength	173
6.6	Sensitivity of time dependent camber to beam age at release	173
6.7	Sensitivity of time dependent camber to the creep coefficient	175
6.8	Sensitivity of time dependent camber to the relative humidity	175
6.9	Effect that substituting low-relaxation strand for stress-relieved strand without changing the design of the beam has on time dependent response	177
6.10	Comparison of the cambers for a typical beam and a new beam which is used in place of a rejected beam	179

Figure		Page
6.11	Comparison of the cambers for a beam in a fast track construction schedule to one in a slow track schedule	181
6.12	Range of time dependent response predicted using combinations of variable concrete strengths, creep, and construction time schedule	182

C H A P T E R 1

INTRODUCTION

1.1 General

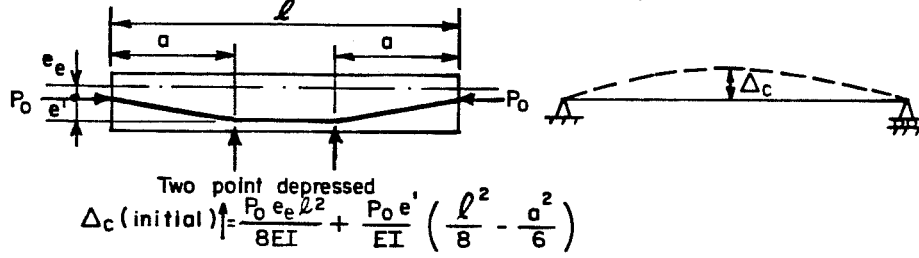
When designing and constructing bridges utilizing pretensioned, prestressed concrete beams, both the designer and the constructor must consider camber or deflection of the beams. Because the beam and slab concretes shrink and creep, while the prestressing steel relaxes, the camber or deflection changes with time. Being able to accurately predict the camber or deflection with time is important. Excessive camber or deflection can result in a rough driving surface. Differences in the camber of adjacent beams during bridge erection may require using a thicker cast-in-place slab to correctly level the slab, while satisfying the minimum slab thickness requirement above every beam. Accurate knowledge of the expected cambers during the construction process can facilitate erection.

Prediction of net beam camber or deflection is difficult, because it is the small difference of several large camber and deflection components. These components, shown in Fig. 1.1, are the camber caused by the prestressing force, and the deflections caused by the beam weight and by the weight of the composite deck. Formulas to calculate these midspan elastic camber and deflections for simply supported beams are also included in Fig. 1.1. The actual magnitude of camber or deflection for each component changes with time, because the components are affected by time dependent material properties.

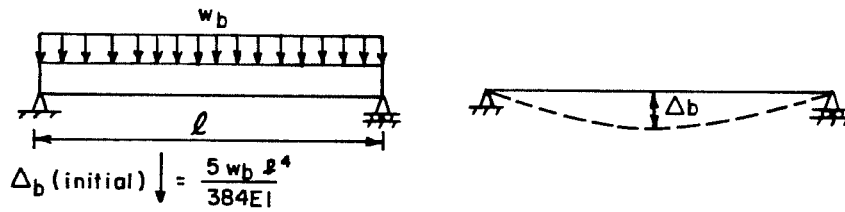
The time dependent material properties which affect the deflection components include concrete creep and shrinkage, and prestressing steel relaxation. Creep is the time dependent strain that is caused by a sustained stress applied to the member. Shrinkage is the time dependent strain that occurs as moisture leaves the concrete. Relaxation is the loss in stress that occurs when the prestressing steel is held at a constant strain. Because the concrete does not remain at a constant stress nor the prestressing steel at a constant strain, creep and relaxation interact and affect the magnitude of each other.

The camber caused by the prestressing force is affected by creep and the magnitude of the prestressing force. As shown in Fig. 1.2a, creep causes the camber to grow with time. When the composite deck is cast, the moment of inertia of the beam is increased. This causes the camber to grow at a slower rate. The magnitude of the prestressing force is reduced by creep, shrinkage, and relaxation. Because the prestressing force is being reduced, camber is lost as shown in Fig. 1.2a. This elastic deflection (lost camber) is affected by the

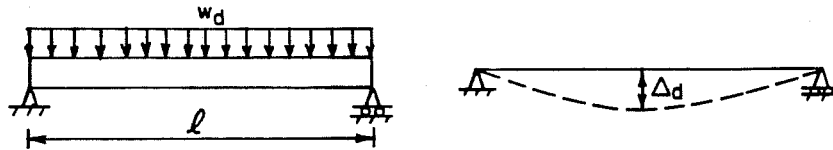
a. Camber caused by the prestressing force :



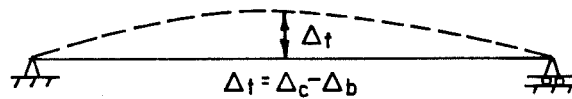
b. Deflection caused by the beam weight :



c. Deflection caused by the composite deck weight :



d. Net camber or deflection before the deck is added :



e. Net camber or deflection after the deck is added :

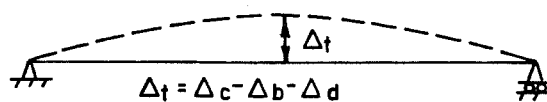


Fig. 1.1 Components of beam camber or deflection

strength or elastic modulus of the concrete while the loss is occurring. The growth of camber due to creep is also reduced as prestressing force losses occur, because smaller stresses are imposed by the force.

When the composite deck is added, the beam deflects downward. This causes the prestressing strand below the beam center of gravity to stretch and regain some of the lost prestressing force. As a result, the deflection caused by the loss of prestressing force is slightly reduced as shown in Fig. 1.2a.

The deflection component caused by the beam weight increases due to creep, as shown in Fig. 1.2b. When the composite deck is cast, the time dependent deflection grows at a slower rate due to the increased moment of inertia. The deflection component caused by the deck also increases due to creep as shown in Fig. 1.2c.

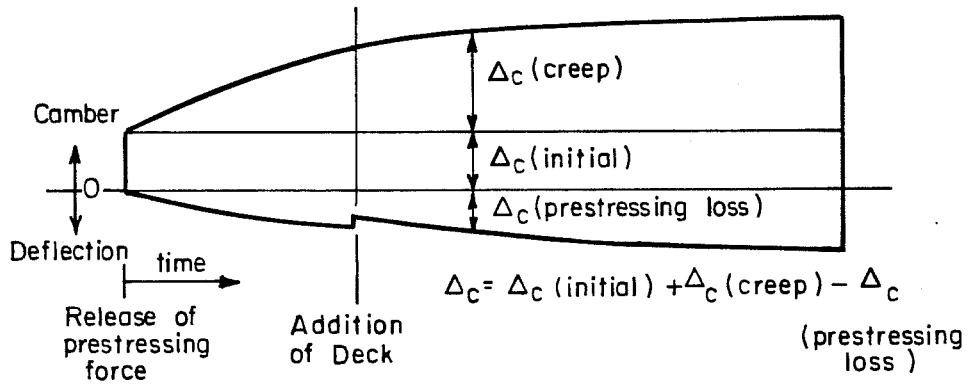
As a beam ages, the camber and deflection components continue to grow. With time, components of time dependent camber and deflection caused by creep can become as great as two times the initial elastic components. Because each component increases with age, the net camber or deflection is the small difference of increasingly larger components. Because these components are large in comparison to the net camber or deflection, it is difficult to accurately predict the net response.

With the development of higher strength concrete, (concrete with strengths greater than 6000 psi), and low-relaxation prestressing strand, bridges with longer spans are being built. Longer spans are desirable in situations where the bridge must span over existing roads or to minimize environmental impact. Longer spans are also being used to minimize the construction cost by reducing the required number of bents.

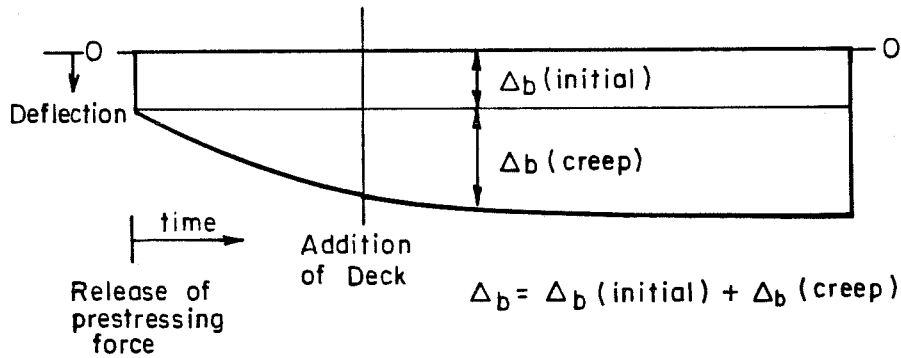
Unfortunately, the net camber or deflection becomes more difficult to accurately predict when longer spans are used. The deflection caused by the beam weight is a function of the span length to the fourth power (see Fig. 1.1). Deflection predictions become much more difficult and sensitive for longer spans.

When comparing net camber or deflection predicted by an analytical technique to the measured response, the error should not be considered as the difference between the measured and analytical net response divided by the measured net response. Theoretically, the error should be considered as the difference in the sums of the absolute values of the components, divided by the sum of the absolute values of the components for the actual beam. Unfortunately, it is impossible to separately measure the responses due to the prestressing force and the weight of the beam. Therefore, when percentage error is determined in this report, it will be the difference in the predicted and the measured

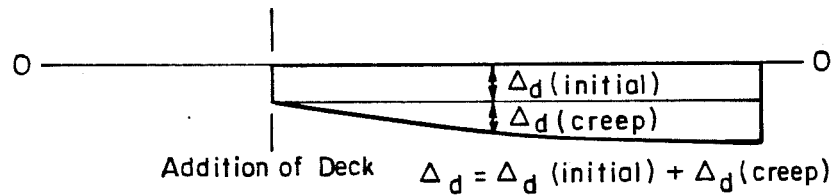
a. Time dependent camber caused by prestressing force:



b. Time dependent deflection caused by the beam weight:



c. Time dependent deflection caused by the deck weight



$$\Delta_{\text{Total}} = \Delta_c - \Delta_b - \Delta_d$$

Fig. 1.2 Components of time dependent camber and deflection

net response divided by the sum of the absolute values of the components calculated by the analytical technique.

1.2 Previous Experimental Studies

In the past, numerous experimental studies have been performed to gain an understanding of how prestressed concrete beams behave with time. These studies vary from experiments to determine time dependent material properties to field and laboratory studies in which the time dependent response was measured.

Several studies have been performed to determine the creep, shrinkage, and age strength gain characteristics of concrete. The ACI Committee 209 report [1] combines the results of several of these studies and makes specific recommendations for the prediction of these properties. That report also includes an excellent list of references. One of the most important is Hansen and Mattocks' "Influence of Size and Shape of Member on the Shrinkage and Creep of Concrete" [2]. Many shrinkage and creep tests have been performed on standard concrete cylinders. When applying the results of such tests to predict the time dependent response of a beam, one must account for the difference in the size and shape of the beam.

The ACI Committee 209 report primarily considers normal strength concrete ($f'_c \leq 6000$ psi). More recently, Ngab, Nilson, and Slate [3] found that less creep and slightly more shrinkage occurred in high strength concrete than normal strength concrete. They measured the creep coefficient to be 50 to 75% that of normal strength concrete. The measured shrinkage was not significantly greater. Carrasquillo, Nilson, and Slate [4] found that at early ages high strength concrete had a higher rate of strength gain than normal strength concrete. At later ages the differences were negligible. They also found that the AASHTO formula for predicting the elastic modulus overestimates the measured modulus for concrete with strength greater than 6000 psi.

Several research projects have investigated the relaxation characteristics of prestressing strand. Magura, Sozen, and Siess [5] studied the relaxation of stress-relieved strand. Their results were used to develop the widely used equation for predicting the amount of relaxation that will occur for strands initially tensioned to any stress. It appears in the PCI's "Recommendations for Estimating Prestress Losses" [6]. This equation was modified by steel manufacturers to predict the loss of low-relaxation strand [7].

More recently, Buckler and Scribner [8] performed tests on stress-relieved and low-relaxation strand to study the stress relaxation characteristics in prestressing strand subjected to varying stresses.

They found that the Magura, et al. equation for estimating the relaxation of stress-relieved strand worked well. However, the modified equation for low-relaxation strand underestimates the relaxation. Tests were also performed in which the stress was intentionally reduced as when the prestressing force is released. They found that for greater reductions in stress, less relaxation occurred after the stress reduction.

Only a few laboratory studies of the time dependent deflection response of pretensioned, prestressed concrete simply supported beams have been performed.

Rao and Dilger [9] studied the instantaneous and time dependent camber and deflection of six beams with and without additional nonprestressing reinforcement. The beams were 6 by 20 in. in cross section with a 2.5 by 24 in. composite slab. Super-imposed dead load was added to three of the beams. The camber and deflection response was measured for 150 days. This investigation was performed to check the accuracy of the "varying stiffness method."

Corley et al. [10] studied the behavior of four beams, 4 by 6 in. in cross section with a 6 ft clear span. Two of the beams remained unloaded while a dead load was placed on the others shortly after release. Measurements were taken for two years. The purpose for the experimental study was to determine how accurately the time dependent response could be predicted by the "rate of creep" and "superposition" methods.

Zundeleovich et al. [11] investigated the difference in camber and deflection response of noncomposite beams made with normal and lightweight concrete. The responses of nine specimens, 4 by 6 in. in cross section with a 15 ft span length, were measured. The results were compared for beams made with one of three different types of Hawaiian aggregates.

Sinno and Furr [12,13] tested four full size 50 ft long Texas Highway Department Type B bridge beams to determine the difference in elastic and time dependent camber for beams designed with straight and draped strands. The straight strands were blanketed at the ends of the beams to prevent overstressing at release. Two beams were made using lightweight concrete and two with normal weight concrete. One lightweight and one normal weight concrete beam was made using straight strands. The other two beams were made using draped strands. They found that the straight blanketed strand beams could be designed to have less elastic and time dependent camber than the draped strand beams.

Branson, Meyers, and Kripanarayanan [14] studied the differences in time dependent behavior of beams made with different

weight concretes. The beams were 6 by 8 in. in cross section. The beams were simply supported with a 15 ft span length. Twelve sand-lightweight and three all-lightweight beams were tested. A composite slab was added to six of the beams. Field measurements of five sand-lightweight beams, 45 in. deep, in a composite bridge were also taken.

They found that the greatest camber and prestress losses occurred in the all-lightweight beams, while the least camber and prestress loss occurred in the normal weight beams. A prestress loss of approximately 30% for the sand-lightweight beams was measured in the field. Losses for similar normal weight and all-lightweight beams would be approximately 25 and 35%, respectively. Specific comparisons of camber were not given. The measured creep and shrinkage was not significantly different for the lightweight concrete. Therefore, they determined that the greater losses and cambers for the sand- and all-lightweight concrete beams were the result of the smaller elastic moduli.

Only a few other field investigations have been performed in which the time dependent response of simply supported, pretensioned prestressed beams have been measured.

Sinno and Furr [12,13] compared the time dependent responses of lightweight and normal weight concrete composite beams. Time dependent strain and camber of highway bridge beams were measured. The measured strains were used to calculate the prestress loss. They found that the lightweight concrete beams had greater initial and time dependent camber, and greater prestress loss than comparable normal weight beams.

The measured beam camber and prestress loss were compared to those predicted by a computer program written by Sinno [19]. They found good agreement between the measured and predicted responses when experimental creep and shrinkage data of the beam concrete were used as input to the program.

Sokal and Tyrer [15] measured the camber and internal concrete temperature of a 57 in. deep highway I-beam for a 60-day period. Low-relaxation prestressing strand was used. The beam was steam cured. Internal beam concrete temperature was measured and the measured camber adjusted for thermal movements. The camber grew from 1.1 in. immediately after release to 2.2 in. at 60 days. The measured camber was compared to the camber predicted using CEB recommendations [20]. They found that for the environmental conditions in which the beams were stored, the use of CEB data resulted in overprediction of the camber.

Gamble et al. [16,17,18] measured the time dependent strain and deflection response of prestressed pretensioned I-beams in three bridges located in Illinois. These beams were designed using standard

Illinois Department of Transportation design procedures. They were designed using typical span lengths and construction materials. Other information about these studies and the results are given in Bradberry's report [21].

1.3 Methods of Analysis

In the past, several analytical techniques have been proposed for predicting the time dependent behavior of prestressed concrete members. The techniques are used to calculate prestress loss, camber, or both. They vary in complexity from simple approximate formulas that can easily be solved by hand to complex computer programs. Only techniques which can be used to predict the response of composite, pretensioned, prestressed concrete beams are mentioned in this section.

Techniques proposed for calculating the prestress loss or time dependent camber which can be easily performed by hand include the procedure in the AASHTO Specifications [22,48], the PCI Design Handbook procedure [23], PCI's "Recommendations for Estimating Prestress Losses" [6], and Tadros, Ghali, and Dilgers' recommendations [24]. The AASHTO and PCI Design Handbook procedures are used to calculate the loss for the beams in this study. The PCI Design Handbook multipliers are used to predict the camber. These procedures will be discussed in Chapter 5.

Computer programs and techniques best suited for use on a computer have been developed by Suttikan [25], Sinno and Furr [26,27], Branson and Kripanarayanan [28], Hernandez and Gamble [29], Rao and Dilger [9], and Huang [49]. The earlier work of Gamble has been reflected in the current AASHTO procedures [22,48]. The extensive work at Lehigh University is generally too complex for non-computerized application [49]. The technique proposed by Suttikan and modifications to the techniques proposed by Sinno and Furr, and Branson and Kripanarayanan were used to predict the response for the beams in this study. These techniques will be discussed in Chapter 5.

1.4 Field Program

As part of this investigation, time dependent deformations of long span pretensioned beams made with high strength concrete and low-relaxation prestressing strand were measured. Previous laboratory and field investigations have been limited to prestressed beams of normal strength concrete and typical span lengths. Only one investigation has been performed in which the deformations of a beam made with low-relaxation strand were measured [15]. This project was initiated in order to gain a better understanding of how long span beams made with high strength concrete and low-relaxation strand deform with time.

This report summarizes this project. It is based on the thesis of Kelly [46] who relied heavily on the initial work of Bradberry [21]. Bradberry developed the instrumentation and instrumented eight beams in the prestressing yard. He reported on the deformations that were measured until the beams were first placed in the bridge. Kelly was then responsible for deformations measured during construction of the bridges, measurements in service, and comparison of measured and calculated deformations. Measurements were continued until April 1987 by Ramirez and Yates after Kelly completed his thesis.

1.5 Objective and Scope

The objectives of this portion of Project 381 were:

1. Measure the elastic and time dependent deformation response of prototype beams during field construction operations and early service life.
2. Test material samples from the instrumented beams to determine the short and long term material properties
3. Evaluate the accuracy of currently available analytical techniques for predicting time dependent behavior
4. Revise and improve such analytical techniques, as might be required
5. Determine the sensitivity of time dependent behavior to variations in material properties and the construction time schedule.

Descriptions of the bridge details, instrumentation used, and the companion tests performed to determine material properties are given in Chapter 2. Chapter 3 includes a description of the construction process, information about when measurements were taken, and problems encountered with the construction process and instrumentation. The measured bridge response and the results of companion material tests are presented in Chapter 4. The results of several analytical techniques are presented and compared to the measured results in Chapter 5 along with a description of a substantially revised analytical technique which was adapted for use on a microcomputer. In Chapter 6, the results of the analytical techniques are compared to each other in order to determine which techniques most accurately predict the measured behavior. The results of the sensitivity study based on the microcomputer analysis are also presented in Chapter 6. Chapter 7

includes a summary, conclusions, and recommendations. Appendix A is a User's Guide for the microcomputer program CAMBER used to predict girder deflections. A full listing of program CAMBER in FORTRAN 77 is presented in Ref. 46. Full details on all aspects of this study are presented in Ref. 46.

CHAPTER 2

BRIDGE DETAILS, INSTRUMENTATION, AND COMPANION TESTS

2.1 General

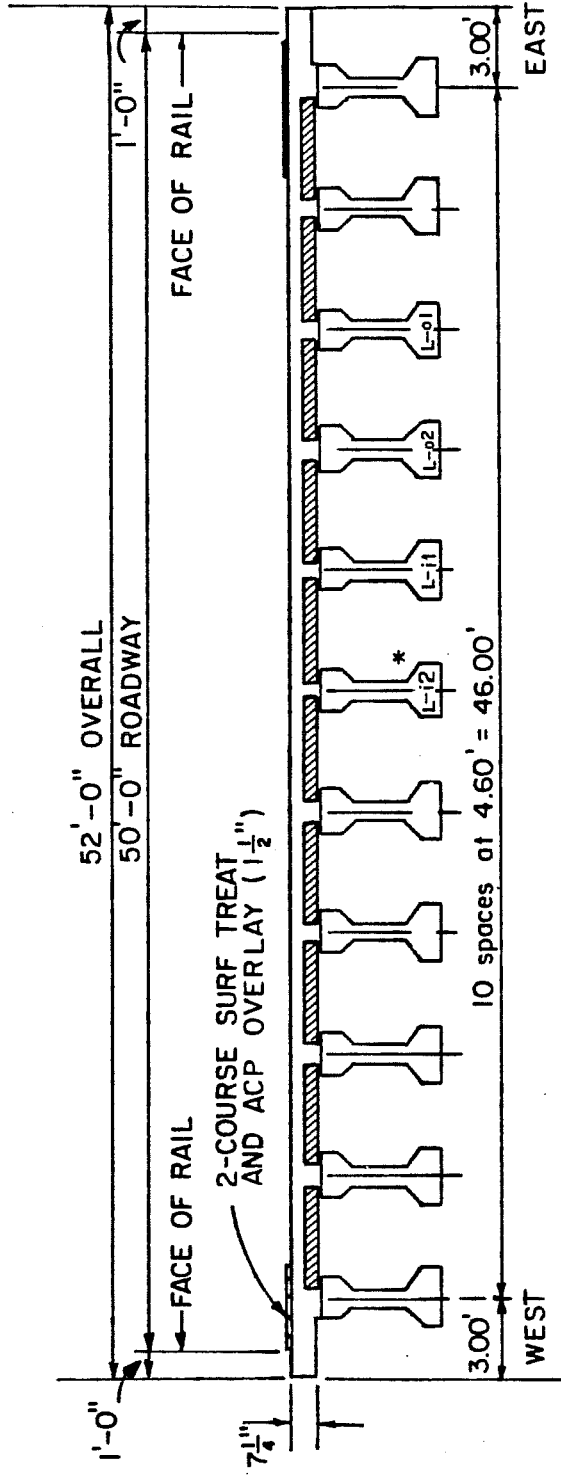
This chapter includes information about the beam and bridge design, materials used, companion tests, field instrumentation, and data reduction. Other detailed information on the selection and design of instrumentation, and companion test procedures can be found in Bradberry's report [21].

2.2 Beam and Composite Bridge Details

The two composite prestressed concrete beam and reinforced concrete slab bridges studied were part of the right and left main lanes of Loop 1 in Austin, TX. These particular bridges extend over the environmentally sensitive Barton Creek wooded area. Long spans and special construction techniques which minimize environmental impact were used. Each bridge carries two lanes of traffic. Only the first span on the north end of each bridge was instrumented.

Eight beams were instrumented at the time they were cast. Figures 2.1 and 2.2 show the location and designation of the instrumented beams. Those in the right main lane bridge will be referred to as the L-series beams. The "L" stands for lower initial stress, 0.70 times the guaranteed ultimate tensile strength (f'_s), in the prestressing strand. Those in the left main lane bridge will be called the H-series beams. The "H" stands for higher initial stress, $0.75f'_s$. The second symbol of the beam designation is either an "o" or an "i". The "o" stands for beams placed towards the outside of the span, while the "i" stands for beams placed towards the middle or inside of the span. The third and final symbol is a "1" or a "2", referring to the casting position in the prestressing bed.

The spans were designed to use eleven, simply supported 128.74-ft long, AASHTO Type IV beams spaced 4.60 ft on centers. The distance between supports and support details are shown in Fig. 2.3. Dimensions and properties of a Type IV beam appear in Fig. 2.4. Rather than using a 7-in. thick cast-in-place slab, the contractor exercised the option to use 4-in. thick precast, prestressed concrete deck panels with a 3.25-in. cast-in-place slab. Panel dimensions and reinforcement details are given in Fig. 2.5. Composite deck design dimensions are shown in Fig. 2.6. The 3.25 in. cast-in-place slab thickness has a tolerance of -0.5 to +2.0 in.



* Explanation of Beam Designations

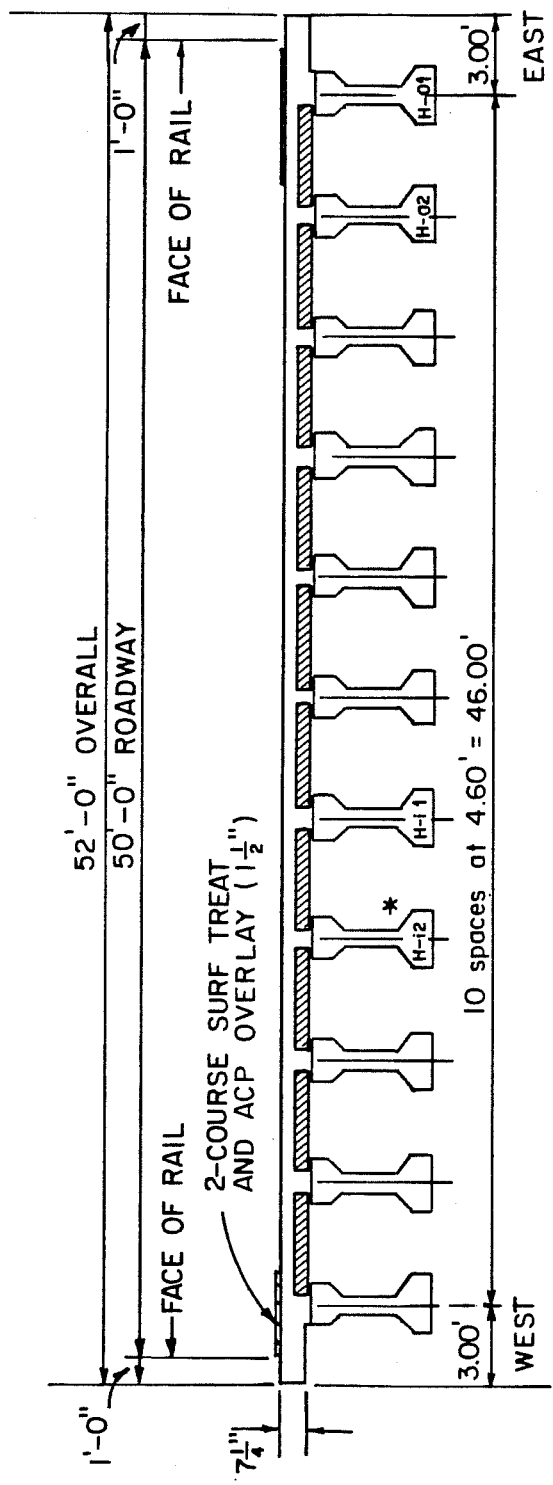
L - initial strand stress of 0.70 times the guaranteed ultimate tensile strength

i - placed towards the inside of the span

o - placed towards the outside of the span

1 or 2 - refers to the casting position in the prestressing bed

Fig. 2.1 Location and designation of instrumented beams in the right main lane bridge



* Explanation of Beam Designations

H- initial strand stress of 0.75 times the guaranteed ultimate tensile strength

i- placed towards the inside of the span

o- placed towards the outside of the span

1 or 2- refers to the casting position in the prestressing bed

Fig. 2.2 Location and designation of instrumented beams in the left main lane bridge

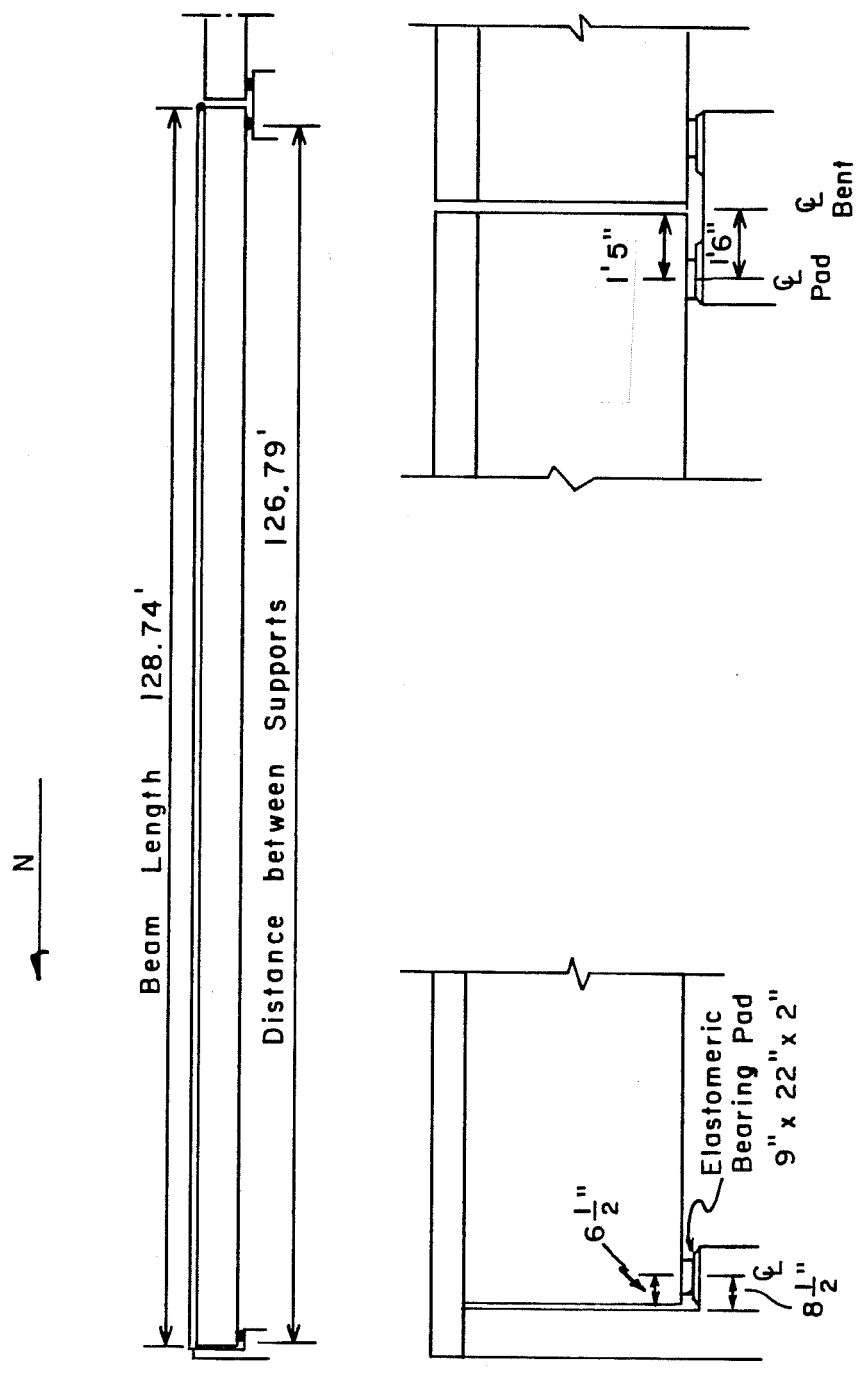


Fig. 2.3 Span and support dimensions

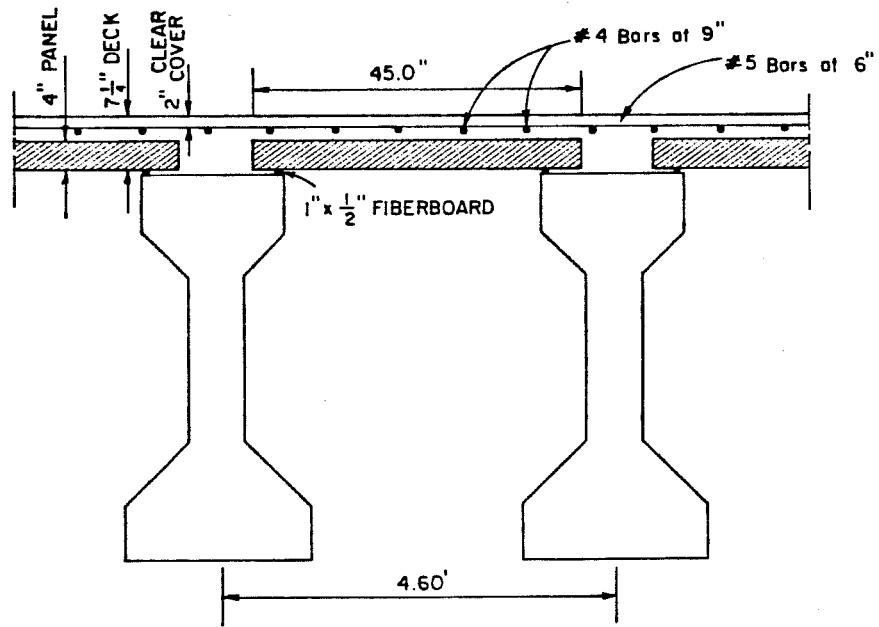


Fig. 2.6 Composite deck design dimensions

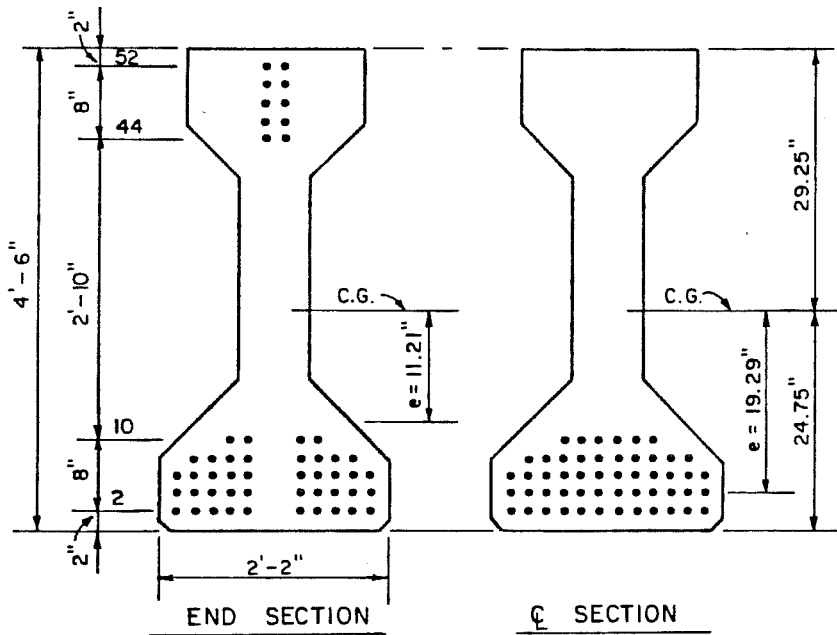


Fig. 2.7 Strand pattern for the L-series beams in the right main lane bridge

The L-series beams were designed assuming the use of normal stress-relieved strand placed on a 2 in. by 2 in. grid pattern. The strand pattern consisting of 52 individual 1/2-in. diameter grade 270 strands, 10 of which were draped, is shown in Fig. 2.7. The drape points were specified to be between 6 ft-5 in. and 8 ft-5 in. on each side of the beam centerline. The initial strand tension was designed to be $0.70f_s'$ for a total initial force of 1504 kips.

The H-series beams were designed assuming the use of low-relaxation strand. The use of a higher effective prestress level is permitted with low-relaxation strand. This results in fewer strands for otherwise similar beams. These beams had 46 individual 1/2-in. diameter grade 270 strands, 10 of which were draped, as shown in Fig. 2.8. They were initially tensioned to $0.75f_s'$ for a total initial force of 1425 kips. Drape point locations were the same as for the L-series beams. Note that the "L" and "H" designations refer to the initial strand stress level and not the total force.

Details of mild steel reinforcement used for all instrumented beams are given in Fig. 2.9. The four #11 bars in the top flange were added to control flexural cracking during release. Only the outer two bars extend the entire beam length. The inner two bars extended for 30 ft in each direction from the beam centerline. Additional vertical web reinforcement, #3 bars at 4-in. spacing, was added to the end 2 ft of each beam to prevent splitting.

Texas State Department of Highways and Public Transportation (SDHPT) Type T5 traffic rails were used on both bridges. The design weight of the rail is 325 lb/ft. A two-course surface treatment and an asphaltic concrete pavement overlay with a total thickness of 2 in. was used. The design weight of this material is 135 pcf.

2.3 Materials

2.3.1 Beams. All beams were cast using Texas (SDHPT) class H concrete [30]. The concrete mix included Type III cement, crushed limestone aggregate, entrained air, and superplasticizer admixture. The cement factor, water-to-cement ratio, and design strengths for each beam are given in Table 2.1.

The prestressing steel used was 1/2-in. diameter, grade 270, seven-wire strand. Low-relaxation strand was used for all the beams, even though L-series beams in the right main lane were designed assuming normal relaxation stress-relieved strand would be used. However, the actual number of strands and the initial stress levels in the strand were maintained as specified in the design. The strand in beams L-i1, L-i2, H-o1, and H-o2 was manufactured by Florida Wire and Cable Co.,

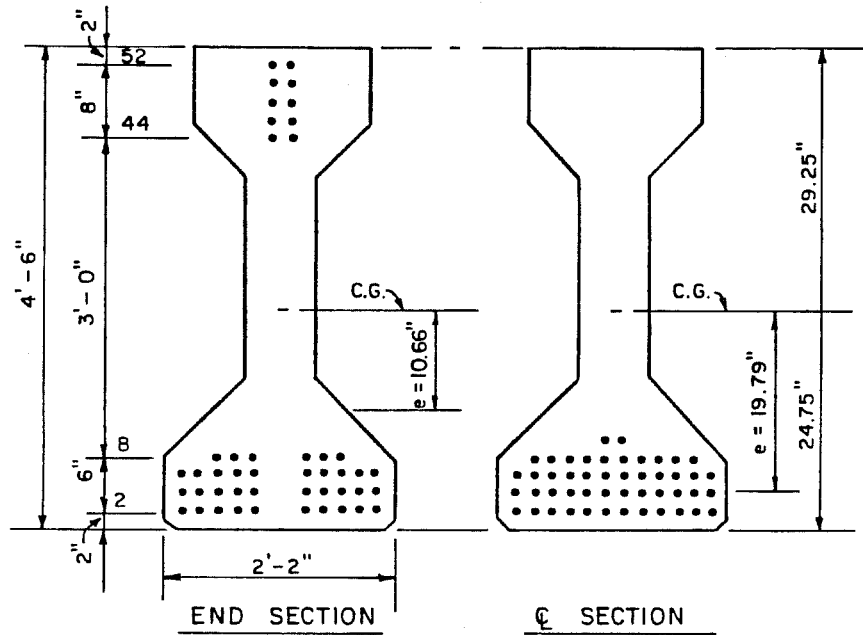


Fig. 2.8 Strand pattern for the H-series beams in the left main lane bridge

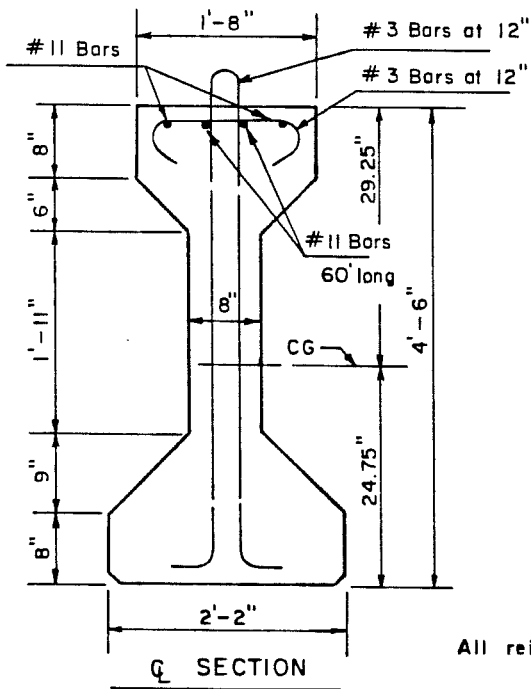


Fig. 2.9 Mild reinforcing steel

All reinforcement is GR60.

TABLE 2.1 Properties of Beam Concrete

Beams	Date Cast	Cement Factor (sacks/cu.yd.)	Water/Cement (by wt)	Design Release Strength (psi)	Design 28-day Strength (psi)
L-i1					
L-i2	6/25/84	6.5	.40	5270	6660
L-o1					
L-o2	7/9/84	6.5	.40	5270	6660
H-o1					
H-o2	10/2/84	7.0	.40	5025	6500
H-i1					
H-i2	11/12/84	7.0	.38	5025	6500

Note: All beams have Type III cement, crushed limestone aggregate, and air entraining and superplasticizer admixtures.

while the strand in beams L-o1, L-o2, H-i1, and H-i2 was manufactured by Shinko Wire America, Inc. The elastic modulus of the strand was assumed equal to 28,000 ksi for calculations. The nonprestressing reinforcement was grade 60 deformed bars with an assumed elastic modulus of 29,000 ksi.

2.3.2 Deck Panels. The deck panels were cast using Texas SDHPT class H concrete [30]. The specified release and 28-day compressive strengths were 4000 and 5000 psi, respectively.

2.3.3 Cast-in-Place Slabs. Texas SDHPT class S concrete [30] was used for the slabs. The mix included six sacks of Type I cement per cu. yd. of concrete, crushed limestone aggregate, and 6% entrained air. The specified water-to-cement ratio was 0.39 by weight. The 28-day design strength was 5000 psi. Grade 60 deformed bars were used for the slab reinforcement.

2.4 Laboratory Tests

2.4.1 General. In order to obtain information that could be used as input for analytical techniques, tests were performed on 6-in. diameter standard concrete cylinders, made with the concrete used to cast the instrumented beams and the cast-in-place slabs. These cylinders were stored in an outdoor, uncontrolled environment similar to that of the beams. Other than not storing the cylinders in a controlled environment, test procedures generally followed ASTM specifications.

2.4.2 Compressive Strength. Compressive strength tests were performed at various ages in order to obtain the shape of the age-strength gain curve of the concrete used in the beams as well as the 28-day strengths of the cast-in-place slab concretes. Compression tests followed ASTM C39-83b [31].

2.4.3 Elastic Modulus. Concrete stress-strain tests were performed following ASTM C469-81 [32]. A compressometer which met ASTM C-469-81 requirements was used to measure the strain. Concrete elastic moduli were determined from the test results.

2.4.4 Creep and Shrinkage. Creep tests were performed following ASTM C512-76 [33]. The tests were performed outdoors in an uncontrolled environment similar to the environment to which the beams were exposed.

Figure 2.10 is a picture of a creep test frame that was used. The cylinders were initially loaded using a hydraulic ram and load cell. Sustained load was maintained by springs monitored by dial gages. Periodically, the sustained loads were readjusted to the initial value.

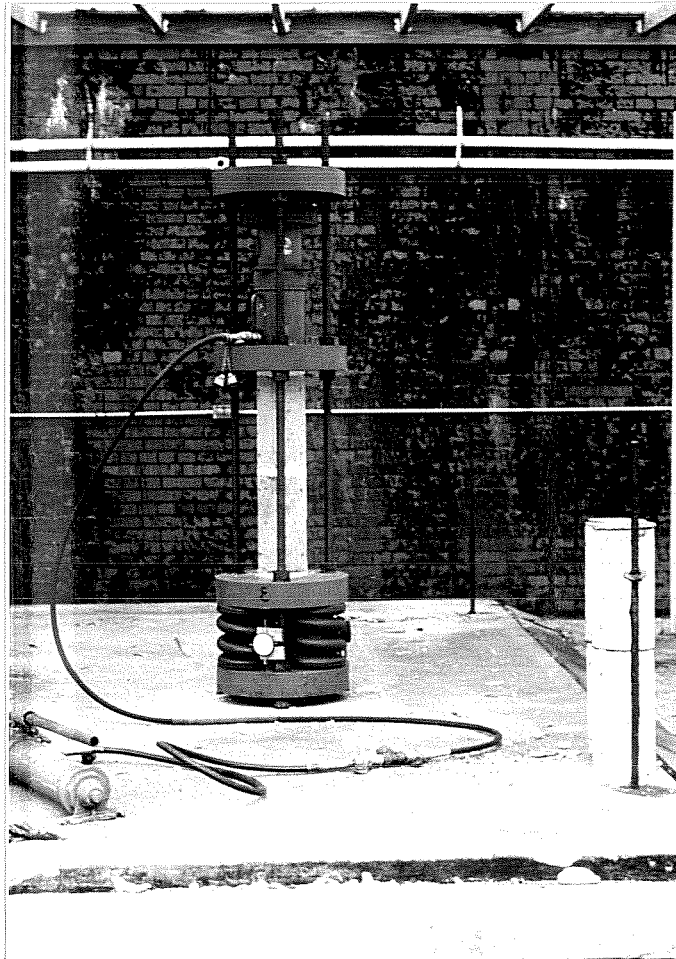


Fig. 2.10 Creep test setup

A general tolerance of plus or minus 5% was maintained. The strain of the concrete cylinders was measured using a Demec mechanical strain gage. Whenever measurements of the creep (loaded) specimens were taken, strain of companion unloaded specimens was also measured. In order to determine the creep strain, the thermal and shrinkage strain of the unloaded specimens was subtracted from the measured strain of the loaded specimens. Therefore, the net strain was due only to creep.

2.5 Field Instrumentation

2.5.1 Instrumentation Location. As mentioned in Sec. 2.2, eight beams were instrumented at the time they were cast and monitored for approximately three years thereafter. Instrumentation was used to measure concrete surface strains, prestressing strand strain, internal concrete temperature, and camber or deflection. Four beams in each bridge were instrumented.

Instrumentation was attached near the midspan, southern quarter point, and south end of each beam. Distances from the south end of a beam to instrumentation locations are given in Fig. 2.11. Table 2.2 lists the instrumentation attached to each beam. Only two beams in each bridge were fully instrumented. The other beams only had instrumentation for measuring surface strains and camber.

2.5.2 Concrete Surface Strain. Concrete surface strains were measured using a Demec mechanical strain gage. Figure 2.12 is a schematic of the gage. Each division of the dial corresponds to 8.1 microstrains. Two Demec points, small circular pieces of steel with a conical hole in the center, were attached to the surface of interest approximately 200 millimeters apart. The Demec points were glued to the top of stainless steel bolts which screwed into inserts which had been attached to the forms. Five-minute epoxy was used to minimize interference and time loss for the fabricator. Experience indicated that the conical holes should have been machined in the stainless steel bolt top surface to eliminate reliance on the epoxy which did not have long term durability.

Strain was calculated by taking the difference between the current readings and the initial readings made before the prestressing force was released. Effects of temperature on the gage readings were eliminated by reading a standard invar bar. It is important to understand that the use of the standard bar only eliminates the effect that temperature has on the Demec gage. The measured strain between Demec points was the total strain, including thermal strain in the beam.

The concrete surface strain was measured at the midspan, quarter point, and south end stations. At each station, five pairs of

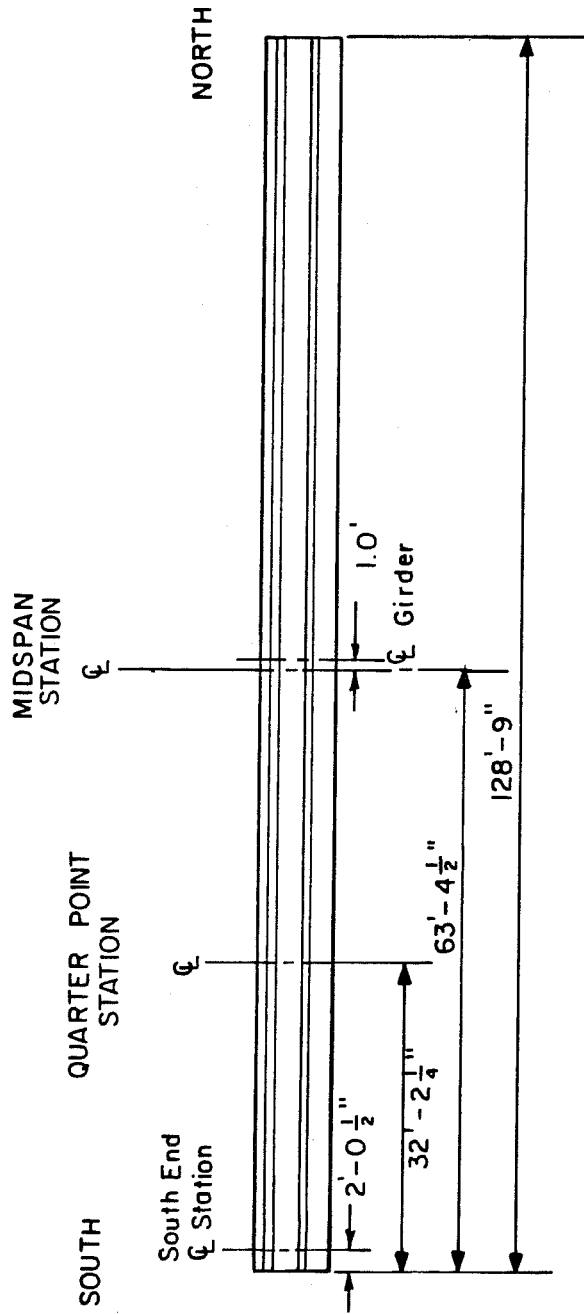


Fig. 2.11 Location of instrumentation stations

TABLE 2.2 Instrumentation on Each Beam

Beam	Date Cast	Concrete Surface Strain	Strand Strain	Concrete Temperature	Deflection/Camber
L-i1	6/25/84	yes	yes	yes	yes
L-i2	6/25/84	yes	no	no	yes
L-o1	7/9/84	yes	yes	yes	yes
L-o2	7/9/84	yes	no	no	yes
H-o1	10/2/84	yes	yes	yes	yes
H-o2	10/2/84	yes	no	no	yes
H-i1	11/12/84	yes	yes	yes	yes
H-i2	11/12/84	yes	no	no	yes

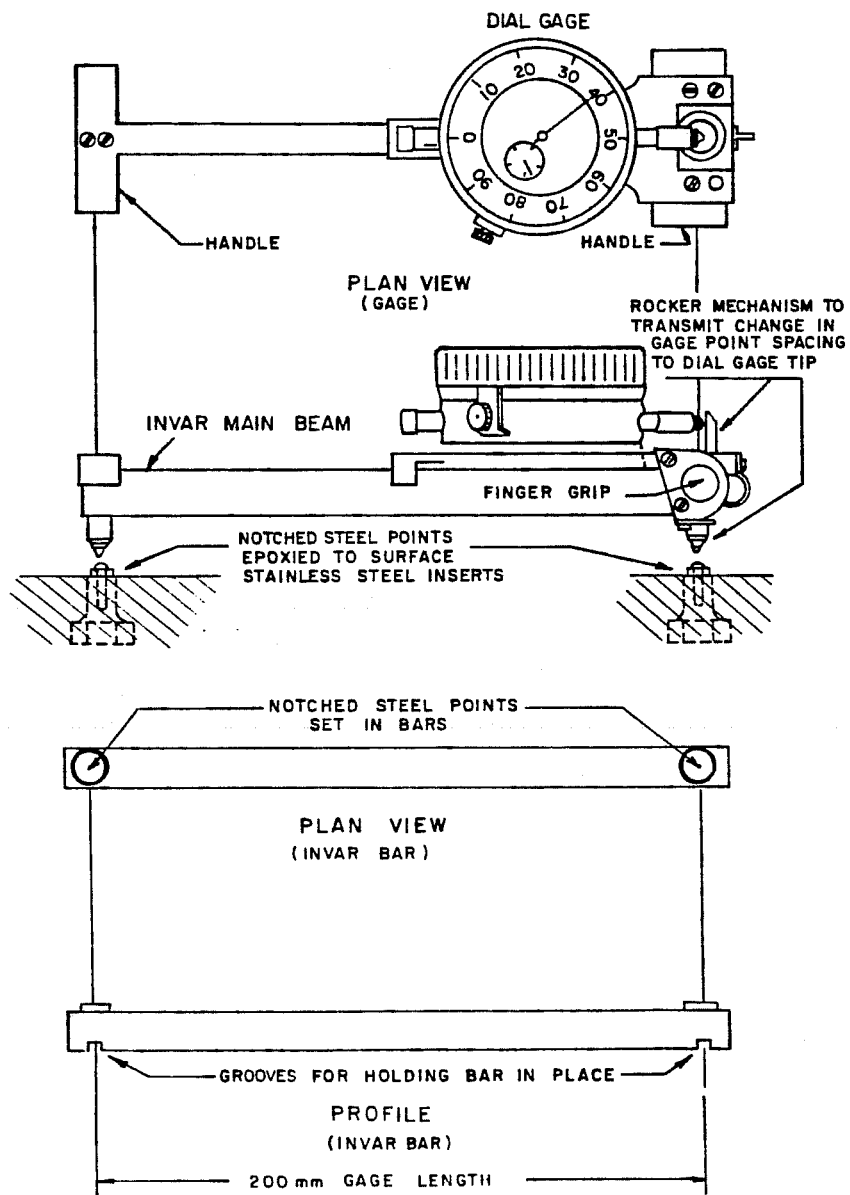


Fig. 2.12 Demec mechanical strain gage

demec points were attached to the beams at the levels shown in Fig. 2.13. The points attached at 24.8 in. from the bottom of the beam were used to measure the strain at the level of the beam neutral axis before the composite deck was added. This strain corresponds to the axial strain in the beam. The other points were used for determining the beam curvature.

2.5.3 Prestressing Strand Strain. Prestressing strand strains were measured using a strain indicator and electrical strain gages attached to the strand. Lead wires from the strain gages were permanently attached to a switch box at each instrumentation station. Each switch box was equipped with a precision resistor to give a base reading. Thus, it was theoretically not necessary to leave the indicator continuously connected or to use the same strain indicator each time readings were taken.

Strain gages were attached to the strand at the midspan and quarter point stations of two beams from the L-series and two beams from the H-series. At these stations, ten gages were attached to five strands as shown in Figs. 2.14 and 2.15. All gages were attached to the strand after it was stressed but before the concrete was cast. Therefore, the measured strain corresponds to the change in strain caused by elastic shortening, creep, shrinkage, temperature, and load effects.

2.5.4 Concrete Temperature. Internal concrete temperature and thermal gradients were measured using thermocouples which were placed in critical locations of the beams and decks. Thermocouples were installed in four beams at the midspan, quarter point, and south end stations. As shown in Figs. 2.14, 4.14 and 4.15, four thermocouples were installed at each station: one 4 in. above the beam bottom, one 4 in. below the beam top, one at the neutral axis, and one in the center of the deck. The thermocouple wires were connected to a temperature indicator. The wire (model NN-J-20) and the indicator were manufactured by Omega Engineering, Inc.

2.5.5 Camber and Deflection Measuring System. Elastic and time dependent beam camber and deflections were measured using stainless steel rulers, piano wire, and a mirror. Rulers were permanently attached to one side of the bottom flange at the midspan and quarter point stations of all beams as shown in Fig. 2.16. Rulers were also attached to both ends of the beams above the bearing pads. Size six piano wire was strung along the bottom flange of the beams and attached to anchor bolts at the beam ends as shown in Fig. 2.17. Measurements were taken by holding a mirror next to the ruler and lining up the wire with its mirror image to ensure constant viewer eye height. The observer then recorded the ruler reading where the wire crossed it. The time dependent camber or deflection was calculated by taking the difference between the current reading and the zero reading taken before prestress force transfer.

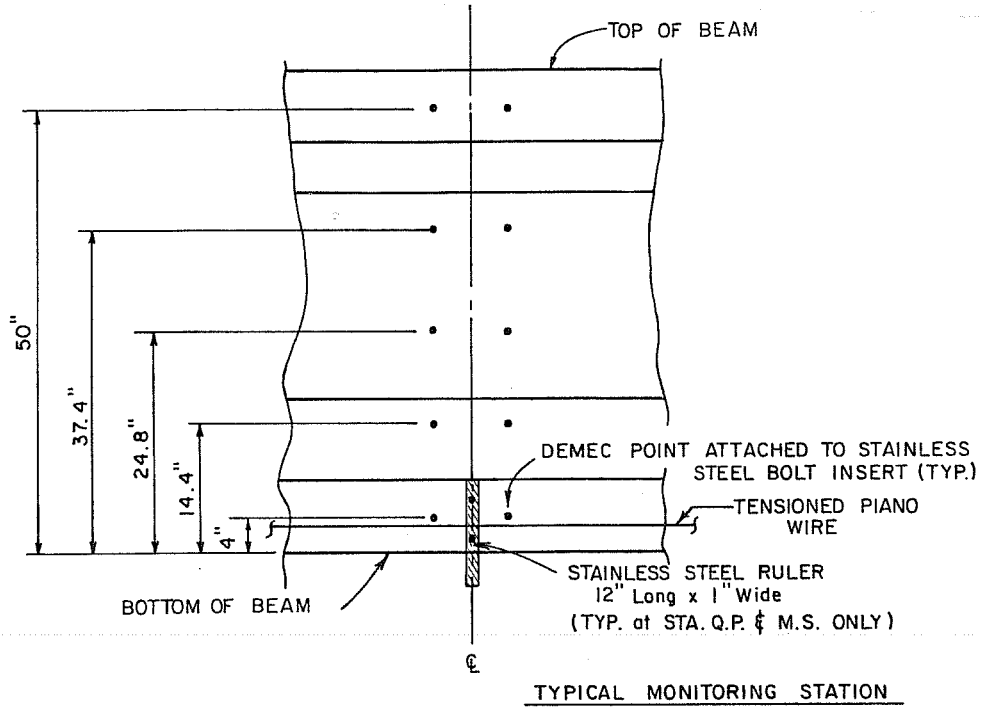


Fig. 2.13 Details of surface strain and camber or deflection instrumentation

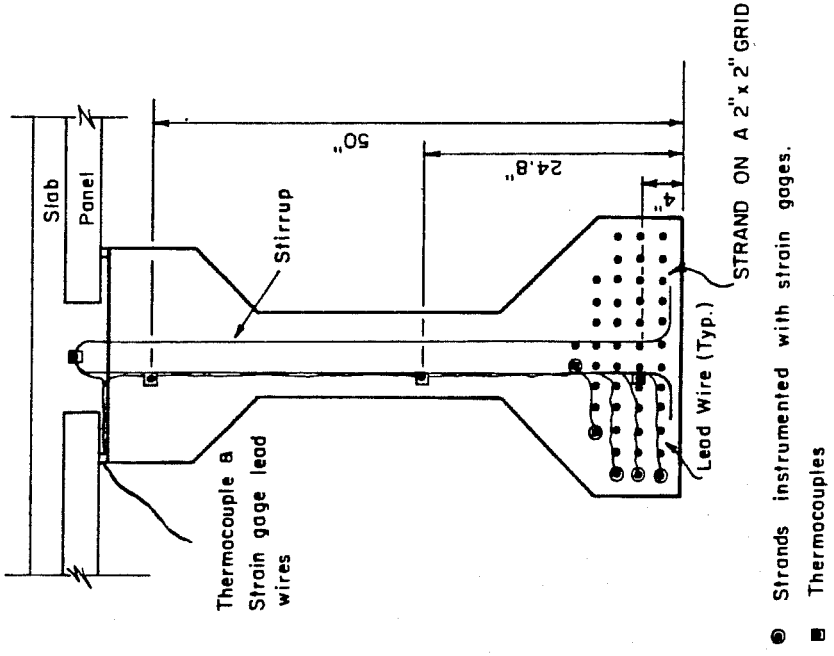


Fig. 2.15 Location of strain gages and thermocouples at midspan and quarter point stations of the H-series beams

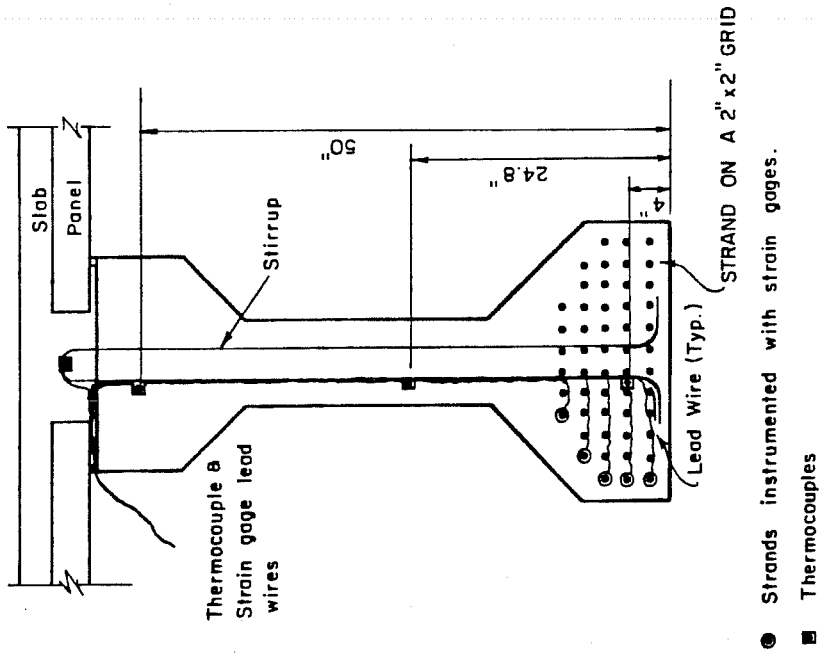


Fig. 2.14 Location of strain gages and thermocouples at midspan and quarter point stations of the L-series beams

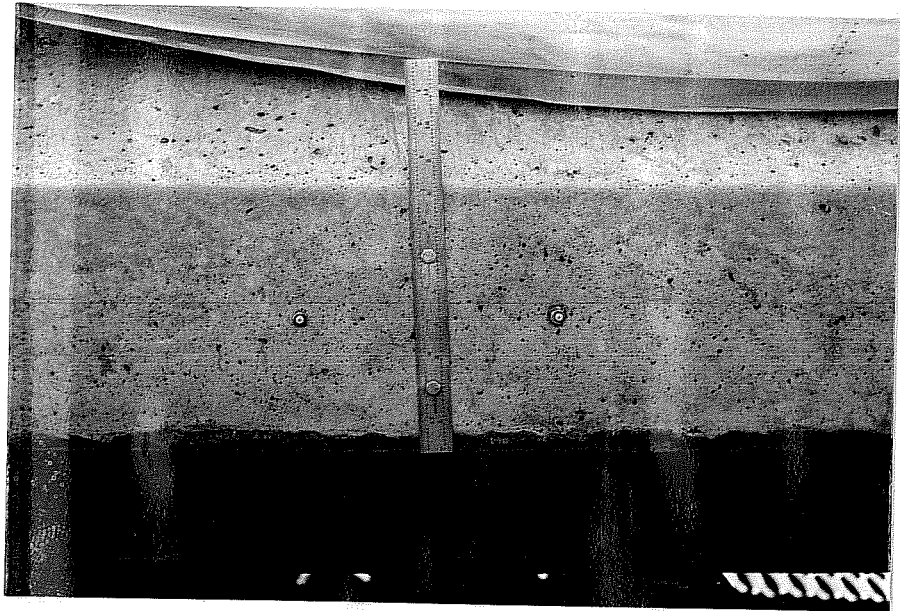


Fig. 2.16 Deflection instrumentation

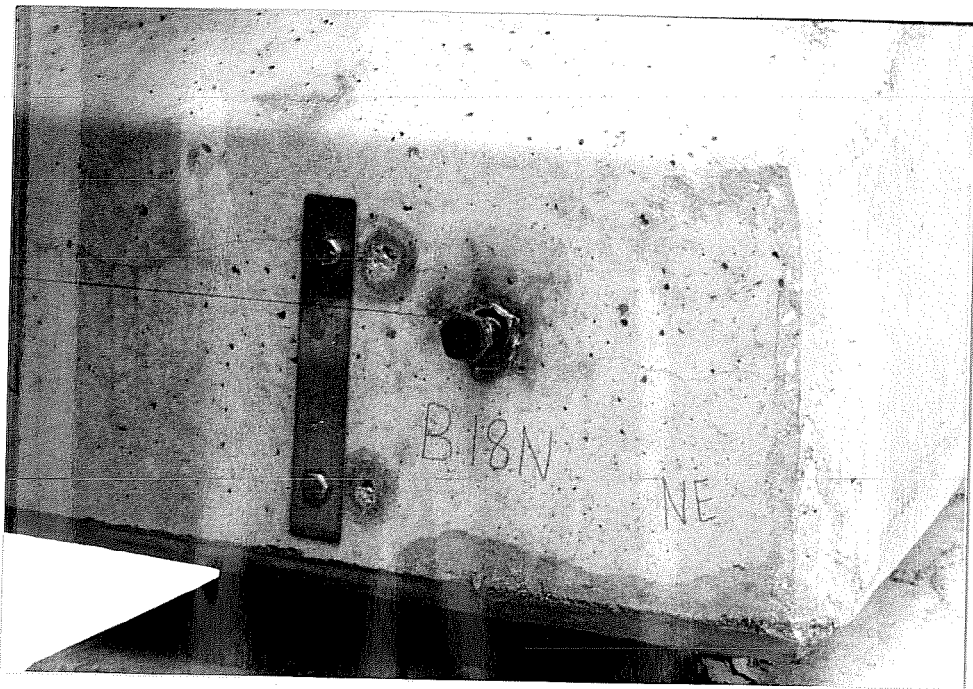


Fig. 2.17 Ruler and anchor bolt at beam end

The support region rulers were fixed to the beams as a reference for when a piano wire had to be replaced. If the new wire did not cross the end rulers at the same level as the original wire, appropriate corrections were made to the midspan and quarter point readings.

In order to obtain accurate results, the piano wires were adjusted to the same tension every time readings were taken. The tension was adjusted by turning the anchor bolt at either end of the beam. The procedure for determining the proper tension is shown in Fig. 2.18. A 32.2 gram weight was hung from the piano wire at midspan, and the resulting reading, R_a , was recorded. The difference between this reading and the reading without the weight, R_b , was determined. The tension in the wire was then adjusted until the difference became equal to the preset difference. This system was determined to be accurate to 1/64 of an inch.

2.6 Data Reduction

The measurements obtained with the beam and companion test instrumentation were reduced to strains and cambers using Super Calc 3, a spreadsheet software program used on microcomputers.

When comparing the measured response to the response predicted by an analytical technique, factors such as thermal movements and changing support conditions must be considered. Concrete expands or contracts with a change in temperature. Therefore, thermal strains are introduced due to seasonal and daily temperature fluctuations. Thermal gradients are created by temperature variations within the depth of the beam. Thermal gradients cause differential strains which create a thermal beam curvature. Depending on the direction of the curvature, the beam will either camber up or deflect down. The effect that temperature has on deformation will be discussed in Sec. 4.4.

While in storage, beams are often supported at locations different than where they will be supported in the bridge. The beams being studied were stored on 7-in. by 7-in. wooden planks located several feet from the beam ends. Since several beams had to be moved within the prestress yard, the support conditions did not remain constant throughout the storage period. Because the beams were supported several feet from their ends, the beam cambers were greater than if the beams had been supported closer to the ends as in the bridge. The increase in camber was caused by the reduced span length and negative beam dead load moments created by the portions of the beam cantilevering beyond the supports. Except for beams H-o1 and H-o2, the support conditions were carefully monitored. The difference in support

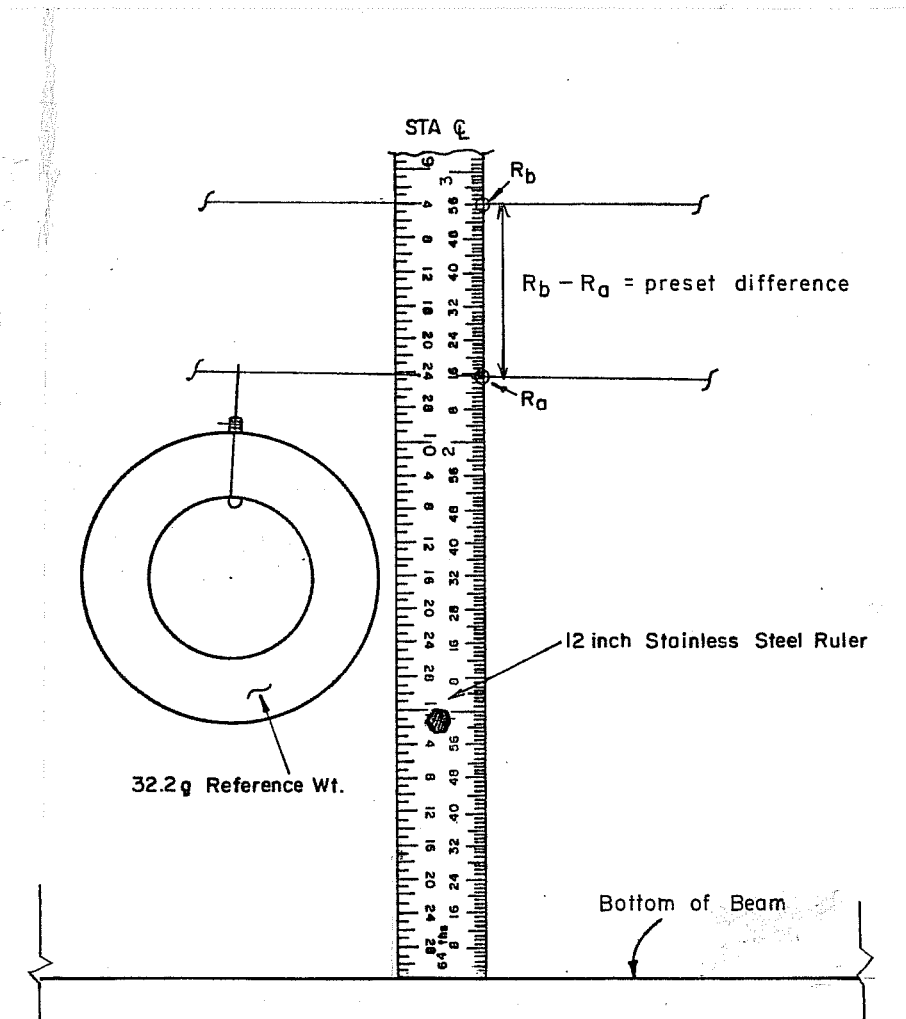


Fig. 2.18 Standard weight deflection procedure for establishing and maintaining a fixed tension in the piano wire

conditions during storage were considered when performing analytical calculations and comparing their results to the measured responses.

CHAPTER 3

FIELD OPERATIONS

3.1 Bridge Construction

Construction of the bridge included seven phases that affected the experimental program:

1. Casting the beams and releasing the prestressing force
2. Placing the beams in storage
3. Placing the beams in the bridge
4. Placing precast deck panels on the beams
5. Placing the concrete for the cast-in-place slab
6. Casting the guard rails
7. Placing an asphaltic concrete pavement overlay on the deck

These seven construction phases are discussed in this section.

The beams were cast at Heldenfels Brothers, Inc. prestress plant just south of San Marcos, TX. The instrumented beams were cast two at a time between June and November of 1984. The histories of each set of beams are given in Tables 3.1 and 3.2.

Each strand was initially stressed to approximately 2000 pounds (13 ksi). All strands were then fully stressed prior to depressing the draped strands. Location of the drape points were approximately 57 ft from each end. The strands were tensioned to the initial design stress (189 or 202.5 ksi).

The stressing operation for the instrumented beams was always performed on a Friday so that the researchers had the weekend to prepare for the casting. Strain gages were attached to strand, thermocouples were tied to stirrups, and inserts for the concrete surface strains and deflection measuring systems were attached to the forms. Figure 3.1 shows a typical instrumentation station after strain gages and thermocouples had been attached.

Usually, on the third day after the strands were stressed, mild steel reinforcement would be tied into place, the forms would be set in

TABLE 3.1 History of L-Series Beams

Time from Casting (days)				Significant Event or Finding
L-i1	L-i2	L-o1	L-o2	
-3.33		-2.50		Finished stressing strands
	-2		-2	Attached strain gages, installed thermocouples, and determined low-lax strand was being used
0.00		0.00		Beams were cast
0.88		0.69		Transfer of prestress force
0.98		0.80		Beams were placed in storage
450		436		Beams shipped to and placed in bridge
457		443		Panels were placed on beams. 1-1/2 layers of panels placed on L-i1, 1 layer on L-i2 and L-o1, and two layers on L-o2
515		501		Panels were readjusted. One layer on each beam
567		553		Slab was cast
674		660		East rail of RML bridge was cast
687		673		West rail of RML bridge was cast

TABLE 3.2 History of H-Series Beams

Time from Casting (days)				Significant Event or Finding
H-o1	H-o2	H-i1	H-i2	
-3.85		-3.00		Finished stressing strands
-3		-2		Attached strain gages and installed thermocouples
0.00		0.00		Beams were cast
1.09		0.82		Transfer of prestress force
1.13		0.84		Beams were placed in storage
149		108		Beams were shipped to bridge site
150		-		Beams were placed in the bridge but not on bearing pads
234		108		Beams were moved over and/or placed on bearing pads
241		128		Panels were placed on beams. 1/2 layer of panels on H-o1 and 1 layer on H-o2, H-i1, and H-i2
245		204		Forms were added to the side of H-o1
261		220		Slab was cast
371		330		East rail of LML bridge was cast
526		485		West rail of LML bridge was cast

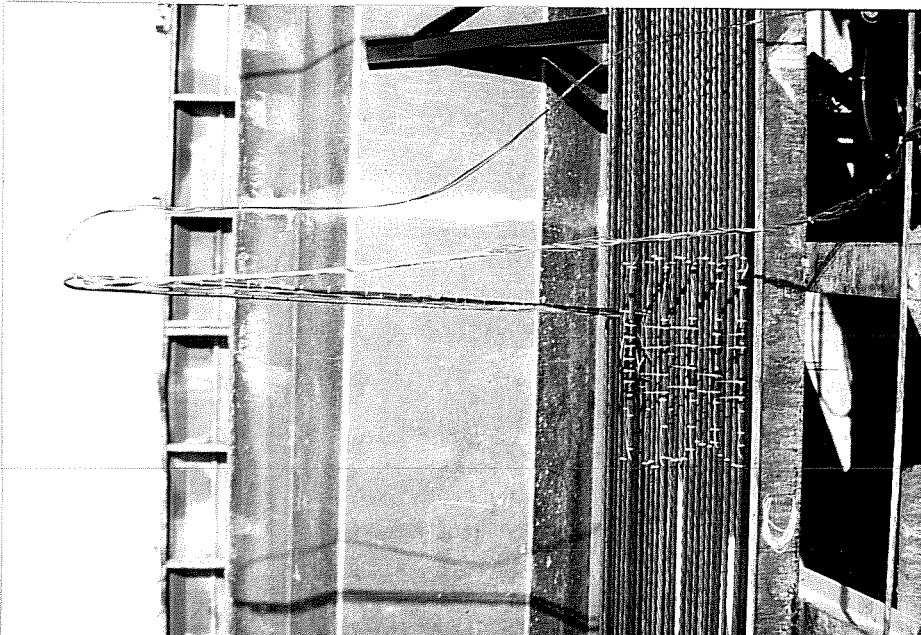


Fig. 3.1 Instrumentation station before concrete is cast



Fig. 3.2 Instrumentation station after release while still in the prestressing bed

place, and then the concrete would be cast in the afternoon or the next morning. The beams were moist cured overnight. On the day after casting, the forms were stripped and the prestressing force was released. Between these two operations, the deflection and surface strain measuring systems were attached and zero readings were taken. Figure 3.2 shows a typical instrumentation station at this stage. For all but the first casting, beams L-i1 and L-i2, initial readings were taken while the beams were still in the prestressing bed. The beams were then placed in storage at the prestressing plant on wooden planks as shown in Fig. 3.3.

Because the bridge site was located in an environmentally sensitive area, a gantry system was used to place the beams in the bridge. This system consisted of two cranes that rode on top of the rectangular steel box girders supported on the outside parts of the bent caps as shown in Fig. 3.4. After all the beams had been placed in a span, the steel girders were cantilevered to the next bent. Figure 3.5 shows a beam being taken from a truck and Fig. 3.6 shows the beam in place. Instrumented beams were placed in the left main lane bridge on February 28 and 29, 1985 and in the right main lane bridge on September 18, 1985.

Because the steel girders rested on the bent caps, four beams in each span could not be immediately placed in their final locations. The two beams closest to a steel girder were first placed a few feet towards the inside of the bridge as shown in Fig. 3.7. When the steel girders were removed from the span, these beams were moved to their final locations using a hydraulic ram and jack. Beams H-o1 and H-o2 were the only instrumented beams that were not initially placed in their proper locations.

The next step in the construction process was to place precast prestressed concrete deck panels on the beams. The 1-in. by 1/2-in. fiberboard strips were glued to the top of the beams along each edge as shown in Fig. 3.8. Instrumentation wires from the girders were protected from panel loads by placing them between fiberboard protectors and leading them to the space between girders. The panels were then placed on top of the fiberboard. The deck panels were at least six months old when the slabs were cast. Therefore, the assumed average age of the panels at deck casting used for analytical techniques should not significantly affect results.

Because four beams in each span were not yet in their correct locations, the panels could not be placed on them. Instead, panels were stacked on top of other panels. Table 3.3 gives the number of panel layers that were initially placed on each instrumented beam. The desired number of layers was one (one half on each side) except for H-o1 which should have had only one half layer. Once the steel girders were

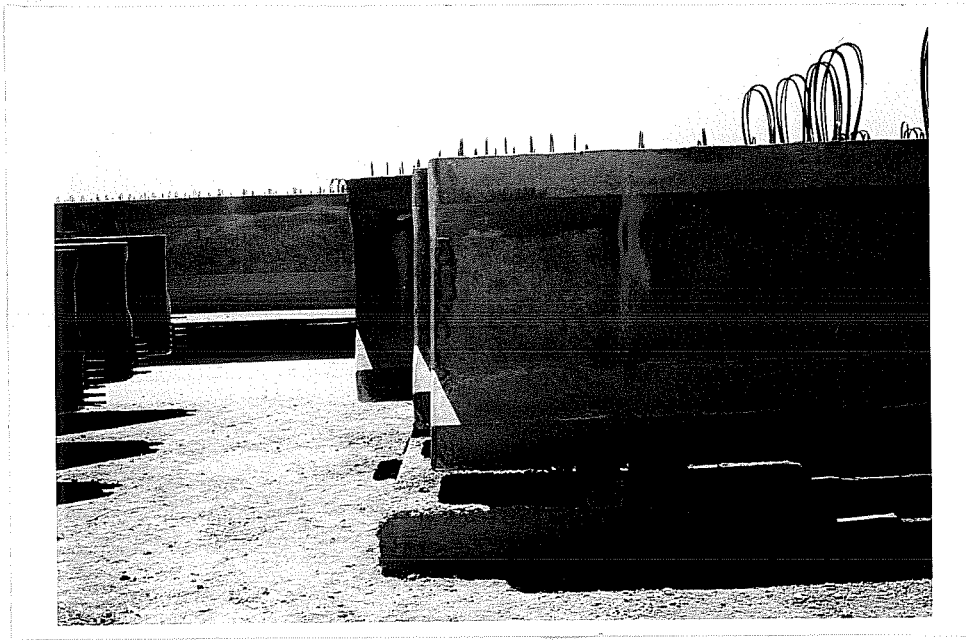


Fig. 3.3 Typical beam support while in storage

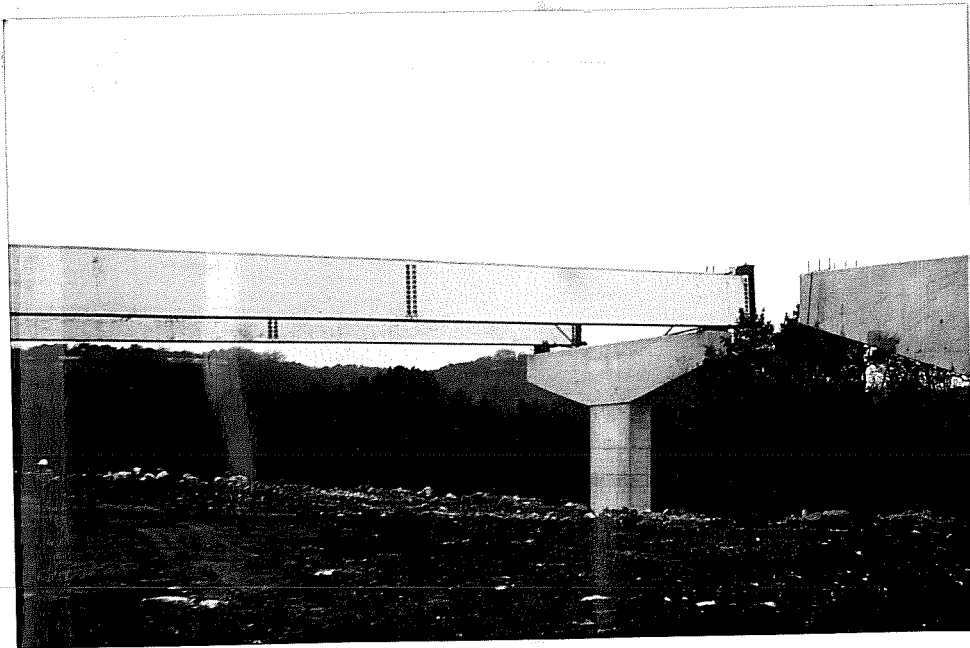


Fig. 3.4 Steel girders for the gantry system

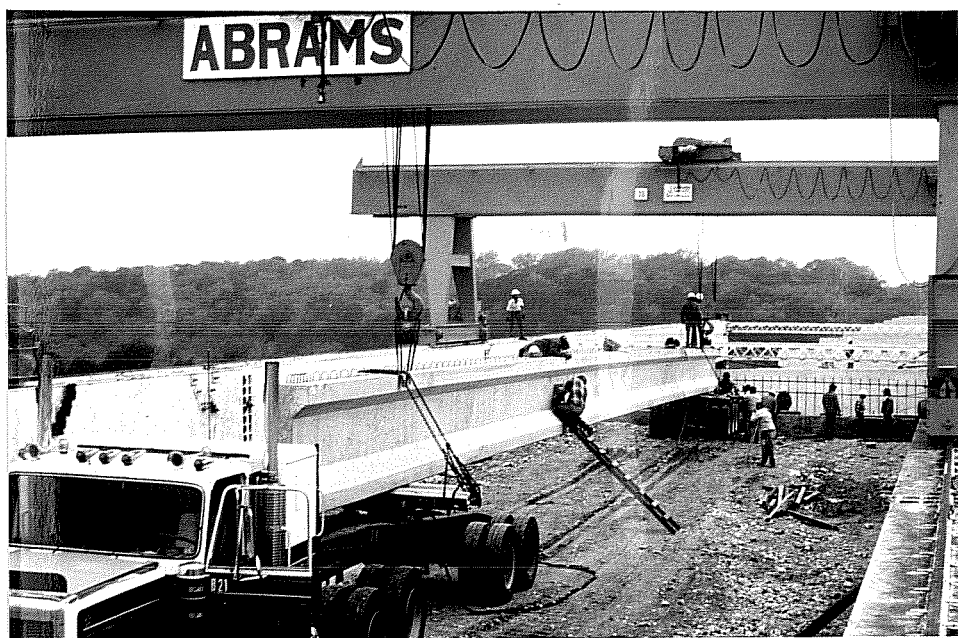


Fig. 3.5 Cranes used to launch beams

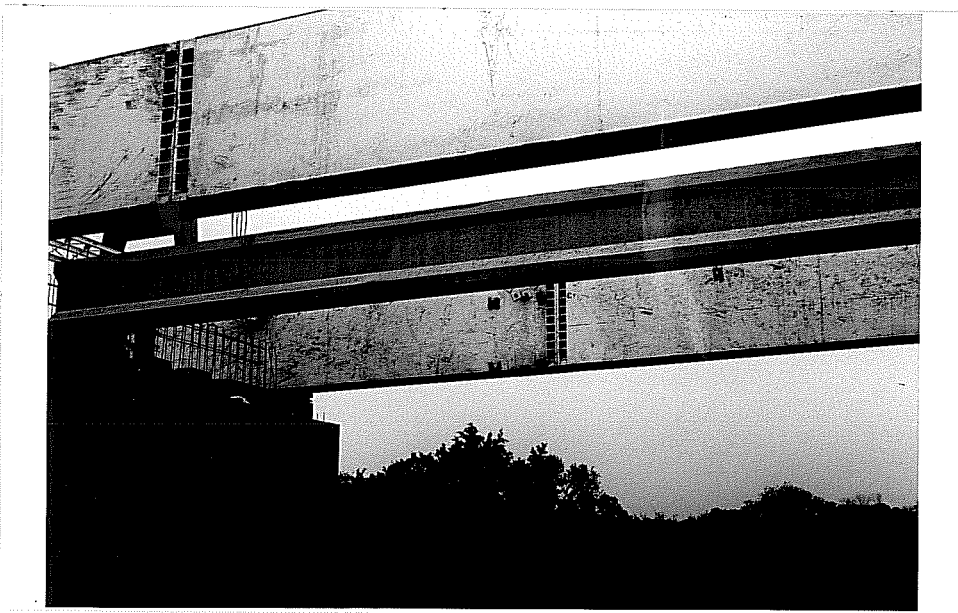


Fig. 3.6 Beam placed in the bridge

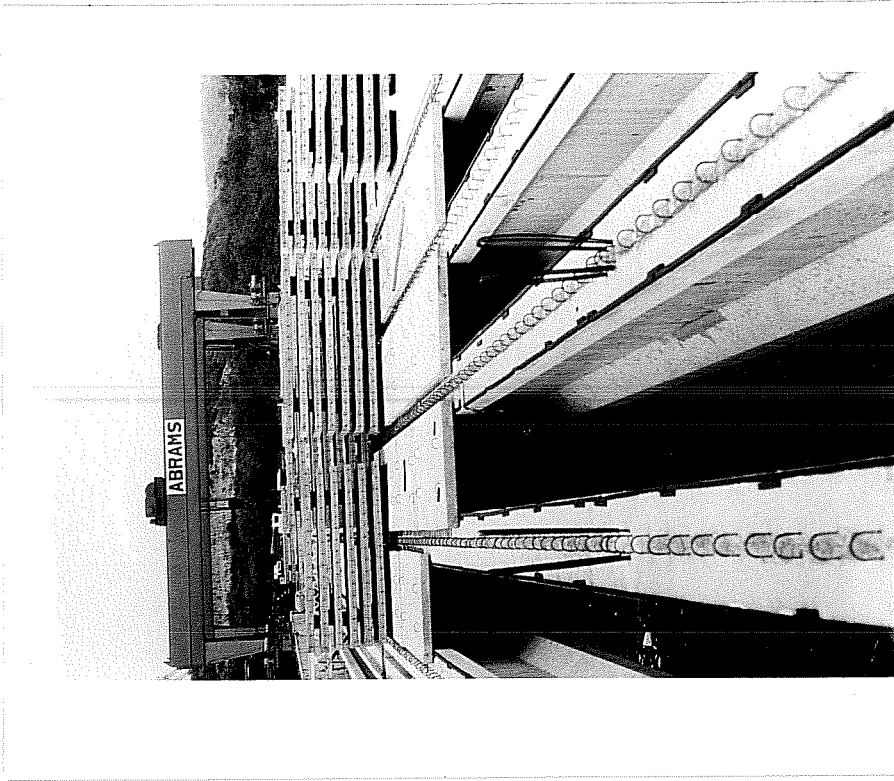


Fig. 3.8 Fiberboard glued to the top of beams before placing deck panels

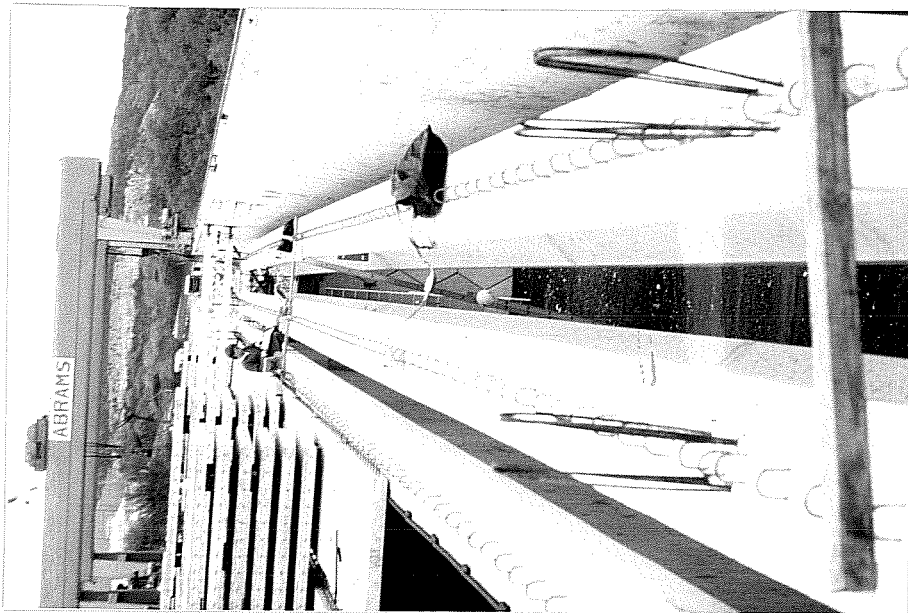


Fig. 3.7 Beams next to steel girder in their temporary location

TABLE 3.3 Layers of Panels Placed on Beams

Beam	Number of Initial Layers	Number of Final Layers
L-i1	1-1/2	1
L-i2	1	1
L-o1	1	1
L-o2	2	1
H-o1	0	1/2
H-o2	0	1
H-i1	1	1
H-i2	1	1

TABLE 3.4 Average Measured Deck Thickness

Beams	Thickness (in.)
L-i1 and L-i2	8.00
L-o1 and L-o2	7.75
H-o1	7.75
H-o2	8.25
H-i1 and H-i2	7.50

removed, the outer beams and stacked panels were moved to their correct locations.

The slab for the span with instrumented beams in the left main lane bridge was cast on June 20, 1985, and the slab for the right main lane bridge on January 13, 1986. While a slab was being cast, the field engineer measured the slab thickness above the panels at the quarter points and midspan. Table 3.4 gives the total deck thicknesses, slab plus panel, which were used for analytical calculations.

The traffic rails were cast using slip-forms, and cured using membrane curing compound. Only the rail on the east side of the left main lane bridge had a significant effect on an instrumented beam. This rail, which was cast on October 8, 1985, was placed above beam H-01, and so most of its load was carried by that beam. The rail was not completed in one cast. The last 22 ft of the rail was not cast with the rest of the rail. Several months passed before the rail was completed and the overlay was placed on the slab.

3.2 Measurements

Measurements were taken at appropriate intervals depending on the rate at which the camber was changing. If no noticeable changes were occurring, readings would be taken monthly until the bridge was completed. When a significant change in load occurred, if at all possible, readings would be taken no more than one week before and after the change.

The first measurements were taken while the beams were still in the prestressing bed but before release. These were the zero readings and all subsequent readings were compared to them when reducing the data.

Initial readings were taken immediately after release while still in the prestressing bed for all beams except L-11 and L-12. Readings were also taken as soon as the beams were placed in storage. Readings were then taken at appropriate intervals until it was time to ship them to the bridge site. When possible, readings were taken one or two days before shipping and then within a week after shipping. As will be discussed in Sec. 3.3.4, readings of beams H-01 and H-02 could not be taken within this time interval.

Once in position in the bridge, beam readings were taken at appropriate intervals. Readings were taken within one week before and after the panels and the slab were added. After the slab was cast readings did not change much, and so measurements were taken at one

month intervals. After the bridge was opened to traffic, readings were taken at about six month intervals.

3.3 Problems Encountered

3.3.1 Missed Zero Readings. During the first cast, release of the prestress force had begun before all zero surface strain readings had been taken. As soon as it was discovered that release had begun, the proper person was notified and further release was suspended until after the readings were completed. The result was that the measured concrete surface strains of beams L-i1 and L-i2 were of lower magnitude than the true strains. The difference was the amount of strain that had occurred during the premature release. Fortunately, all other zero readings were taken before release had begun.

3.3.2 Varying Support Conditions. While being stored, the beams were not supported at the same points as they were in the bridge. They were usually supported farther from the ends. Beams were also moved without notice from the fabricator. Table 3.5 gives the support conditions during storage. Unfortunately, the support conditions for beams H-o1 and H-o2 were never measured. As mentioned in Sec. 2.6, the varying support conditions must be considered when comparing measured response to analytical results.

3.3.3 Site Access Difficulties. Because there was a road passing underneath the bridge, traveling carts which were suspended from the beams were made to access the instrumentation. The road, which was also part of the construction project, was heavily traveled by the contractor making it unsafe to access the instrumentation using a ladder. Instead, carts which rolled between beams, as shown in Fig. 3.9, were built. The carts were accessed by a ladder placed against the abutment wall. This system worked extremely well.

3.3.4 Difficulties Caused by the Construction Technique. Difficulties encountered during construction include access to beams H-o1 and H-o2, temporary bracing in the way of Demec points, form work in the way of piano wires, and thermocouple wires damaged when attaching forms to beam H-o1.

As mentioned in Sec. 3.2, beams H-o1 and H-o2 were not initially placed in their correct locations in the bridge. These beams remained in their temporary locations for three months. During this time, the beams were too close to one another to place a cart between them. The only way to access the instrumentation was with a ladder. This was dangerous and difficult, and so its use was kept to a minimum. After the beams were moved to their final locations, a cart was installed.

TABLE 3.5 Support Conditions

Beam	Time from Casting (days)	Distance from Support Center to Beam End (ft)	
		North End	South End
L-i1	1.0	3.33	7.00
	207	3.42	6.83
	332	3.29	6.71
	450	0.54	1.42
L-i2	1.0	3.00	7.50
	207	3.00	7.25
	332	3.08	5.67
	450	0.54	1.42
L-o1	0.8	3.79	4.04
	85	5.67	7.18
	294	3.92	6.17
	317	4.64	4.88
	384	3.71	4.54
	436	0.54	1.42
L-o2	0.8	3.75	4.08
	85	5.42	7.47
	294	4.58	5.38
	317	5.08	5.21
	436	0.54	1.42
H-i1	0.84	16.25	8.29
	1.75	3.25	4.58
	67	4.10	5.42
	108	0.54	1.42
H-i2	0.84	4.42	3.25
	67	4.75	5.83
	108	0.54	1.42

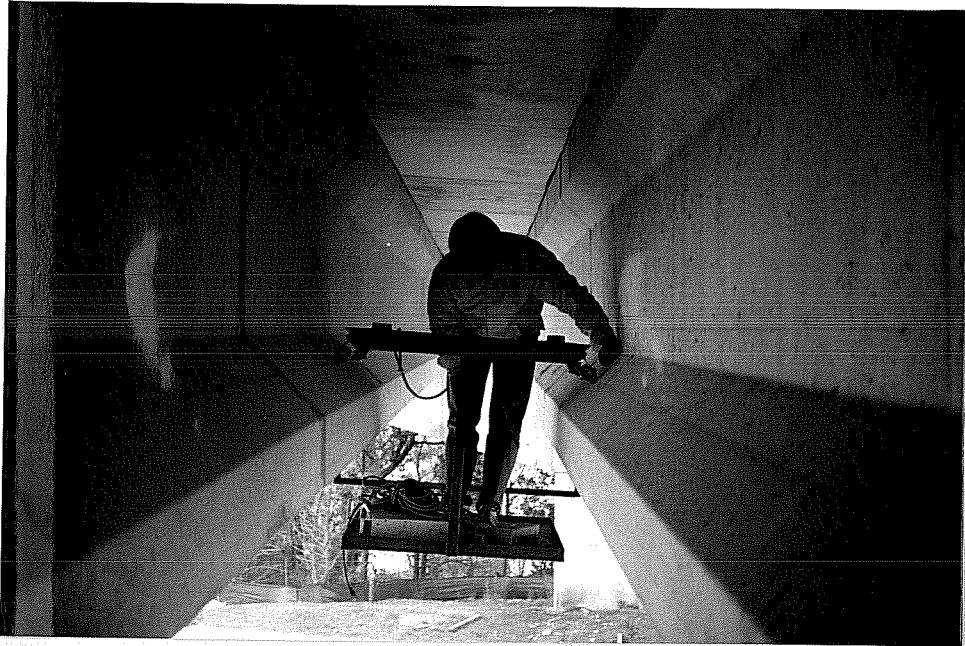


Fig. 3.9 Cart used to access instrumentation

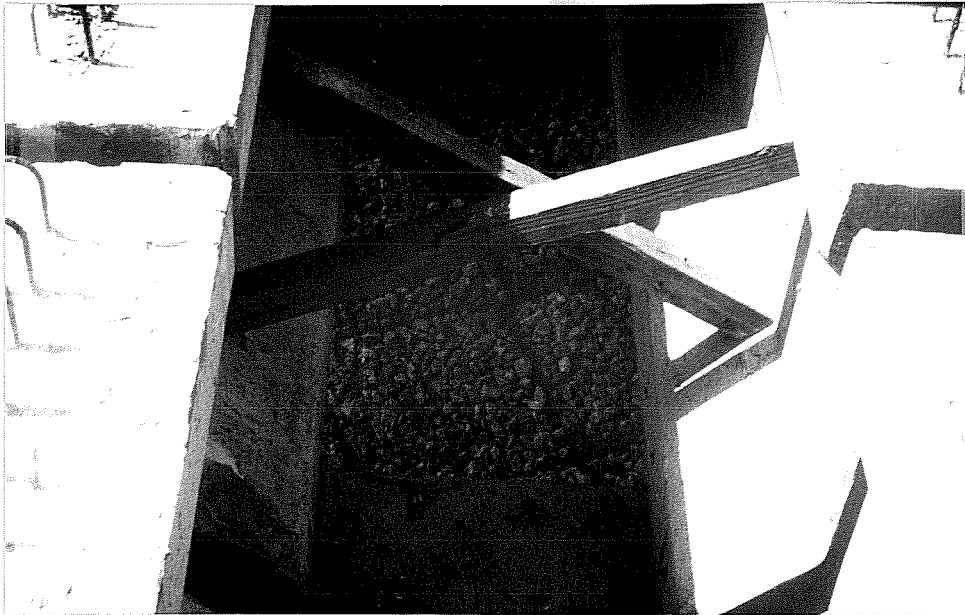


Fig. 3.10 Temporary bracing in the way of Demec points

Before the panels were placed on the beams, temporary bracing was installed between the beams. The bracing, which is shown in Fig. 3.10, was in the way of some Demec points at the south end of the beams. After the slab was cast, the bracing was removed and readings were resumed. Several other points at the south end were knocked off during construction. Since readings at the south end were not considered as important as midspan and quarter point readings, new points were not glued to the beams.

At the north end of the left main lane bridge, bracing to hold up deck forms, where panels could not be used, was placed too close to the sides of the beams. This broke the piano wires. Notches were cut into braces so that a new piano wire could be attached to the beam.

Some thermocouple wires were burned at several locations when slab form suspender rods were welded to the portion of the stirrups sticking out of the top of the beam. Fortunately, all the wires could be repaired to work properly.

3.3.5 Problems with Instrumentation. Problems encountered with the instrumentation include a missing insert for a piano wire anchor bolt, Demec points falling off, and strain gage readings becoming wildly erratic. These problems are discussed in this section.

When the forms were pulled from beam H-01, the piano wire anchor bolt insert at the south end was missing and most likely shaken loose while vibrating the concrete during the cast. In order to obtain camber and deflection data, the piano wire was tied to a Demec point bolt and a ruler was glued to the side of the beam, 15 in. from the center of the bearing pad. Thus, the magnitude of the measured readings was slightly low. The maximum error that this caused was less than 2.5%, or less than a tenth of an inch for the maximum camber.

During the winter of 1985, almost all the Demec points fell off the beams and creep test specimens. The five-minute epoxy worked well during the dry hot summer, but when the cooler temperatures and wet weather came the epoxy no longer held the points to the stainless steel bolts and concrete cylinders. In January of 1985, new points were glued to the bolts using the epoxy that the prestressing plant uses to patch beams. This epoxy worked extremely well. However, it took several hours to dry which makes it impractical to have been used initially. The magnitude of the measured strains are incorrect by the minor amount of strain that occurred between the last readings before points fell off to the first readings taken using the new points. This also includes the difference in thermal strains between these readings.

If a similar project is done in the future, it is recommended that the five-minute epoxy not be used. A system in which conical holes are drilled into the steel bolts, such as was done by Pauw and Breen [34], is recommended.

The strand strain readings appeared to work well at first, but after anywhere from a few days to approximately 120 days all the gages started to give erratic readings. The gages started indicating that the strands were gaining force rather than losing it. It was not understood why all the gages no longer worked properly. The gages may have become unattached to the strand, or chemicals in the concrete may have attacked the gages. Another possibility is that moisture penetrated the switch boxes affecting the precision resistors or connections. Further investigation and development of long-term strain instrumentation for strand in prestressed concrete is recommended for future investigations of long-term prestress losses.

Although the concrete surface strain and prestressing steel strain instrumentation performed poorly, very reliable data was obtained with the temperature and deflection measuring systems. These systems are highly recommended for use in future studies.

C H A P T E R 4

OBSERVED BEHAVIOR

4.1 General

Data obtained from the field instrumentation and the companion tests are presented in this chapter. As mentioned in Sec. 3.3, some of the instrumentation did not work properly. Therefore, throughout this chapter, emphasis is placed on the reliable data. For those cases in which instrumentation did not work properly, limited results are presented to illustrate the nature of the problem.

4.2 Field Measurements

4.2.1 Camber and Deflection. The measured time dependent camber and deflection responses of the instrumented beams are given in Fig. 4.1 and Figs. 4.3 to 4.9. Each figure shows the response of an instrumented beam at its midspan and southern quarter point. In order to clearly explain these plots, the response of beam L-01 shown in Fig. 4.1 will be discussed in detail. Figure 4.2 is a detailed description of the camber for various support and load conditions to which L-01 was subjected. This figure is helpful in understanding various steps in Fig. 4.1. After the detailed explanation for beam L-01, major variations in behavior of the other beams are also explained.

As shown in Figs. 4.1 and 4.2a, the initial camber was measured immediately after release while beam L-01 was still in the prestressing bed. The first point (1.89 in. at time 0) on the beam midspan camber curve of Fig. 4.1, corresponds to the initial camber at midspan (see Fig. 4.2a). At this stage, the span length, L_0 , was approximately 128 ft.

After initial readings were completed, the beam was placed in storage on wooden block supports which effectively shortened the span. The effective span length in storage, L_s , was 120.9 ft as shown in Fig. 4.2b. This reduction in span length created an additional midspan camber of 0.7 in. The total midspan camber at this stage was 2.59 in. and is represented by the second point on the midspan curve of Fig. 4.1 at time 0.12 days.

Beam L-01 remained in storage for 435 days. While in storage, the camber continued to grow. During this period of time, the beam was moved four times, resulting in various effective spans. The span

Time Dependent Beam Camber

Beam L-01

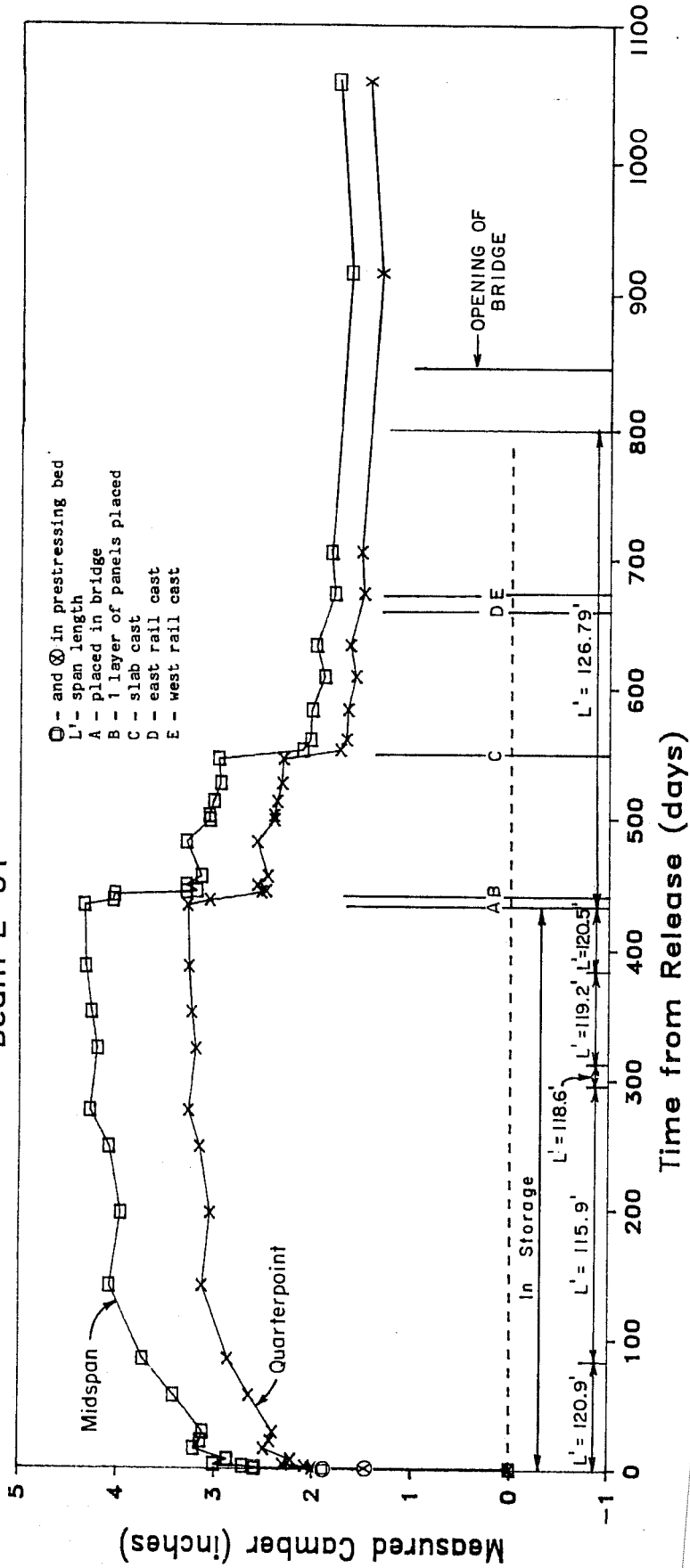
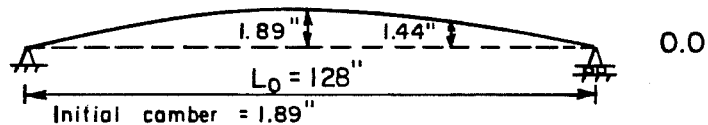


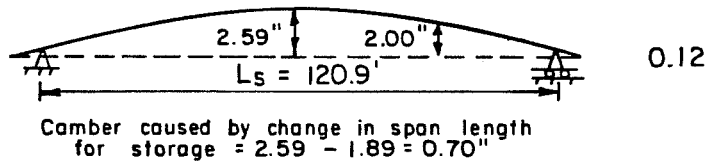
Fig. 4.1 Time dependent camber and deflection response of beam L-01

a. Prestressing bed after release :

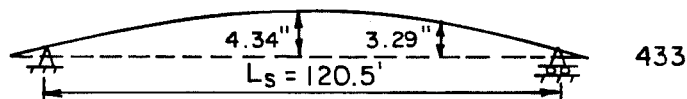
Time: (days)



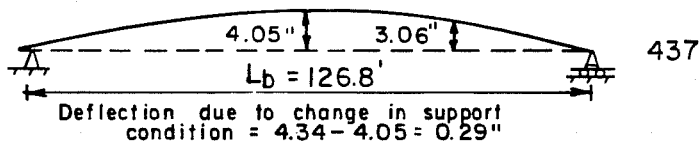
b. First placed in storage :



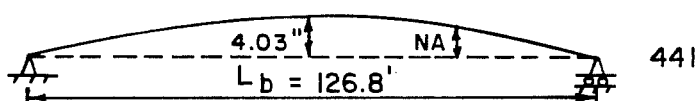
c. Last measurements in storage :



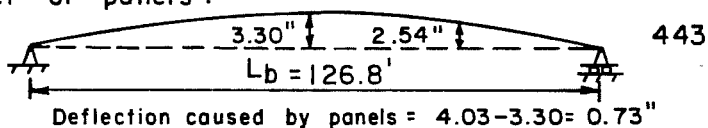
d. First measurements in bridge :



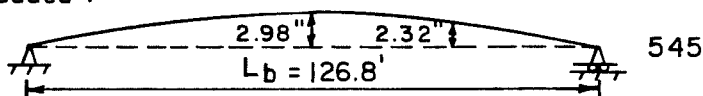
e. Before panels were added :



f. One layer of panels :



g. Last measurements before cast-in-place slab was added :



h. After slab addition :

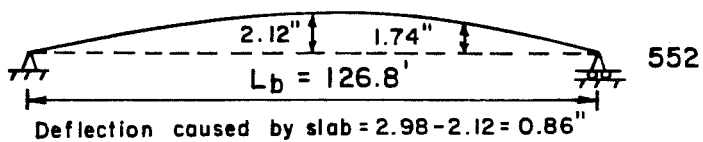


Fig. 4.2 Response of beam L-01

lengths for the different storage support conditions are given just above the time axis in Fig. 4.1. Although the change in support conditions did cause changes in elastic cambers and deflections, these were small compared to the total beam camber. As shown in Figs. 4.1 and 4.2c, the total midspan camber had grown to 4.34 in. at time 433 days.

When the beam was transported to Austin and placed in the bridge as shown by point A of Fig. 4.1 and by Fig. 4.2d, the camber decreased by about 0.3 in. This loss in camber was a direct result of increasing the span length to the final bridge span, L_b , of 126.8 ft.

Soon after the beam was placed in the bridge, one layer of deck panels was placed on it. This occurred 442 days after the prestressing force was released and is indicated by point B in Fig. 4.1 and shown in Fig. 4.2e and f. The layer of deck panels caused an elastic deflection of about 0.73 in. The beam continued to deflect downward with time until the slab was cast (see Fig. 4.1 between points B and C).

The slab was cast 552 days after release of the prestressing force. This event is indicated by point C in Fig. 4.1 and is shown in Fig. 4.2g and h. The weight of the slab caused the beam to deflect 0.86 in. This left beam L-01 with 2.12 in. of camber at midspan which is continuing to decrease slightly with time.

Although very small, additional camber was also lost when the traffic rails were cast. The addition of the east and west rails are marked by points D and E of Fig. 4.1. A small amount of camber (approximately 0.15 in.) was also lost when the asphalt overlay was finally added and the bridge opened to traffic.

Figure 4.3 shows the response of beam L-02 which was very similar to the response of beam L-01. The only significant difference was the additional deflection caused by a second temporary layer of deck panels which was initially placed on beam L-02. When the extra layer of panels was removed (point C in Fig. 4.3) the camber increased. As shown in Fig. 4.4, beam L-i1 also had additional deflection caused by an extra half layer of deck panels. This deflection was also regained when the half layer of panels was removed.

The initial readings of beams L-i1 and L-i2 shown in Figs. 4.4 and 4.5 appear to have been significantly greater than those of the other beams. These initial readings do not correspond to release in the prestressing bed and were not taken until after the beams were placed in storage. When compared to the first readings of other beams after they were moved to storage, the initial cambers are in good agreement.

Time Dependent Beam Camber

Beam L-o2

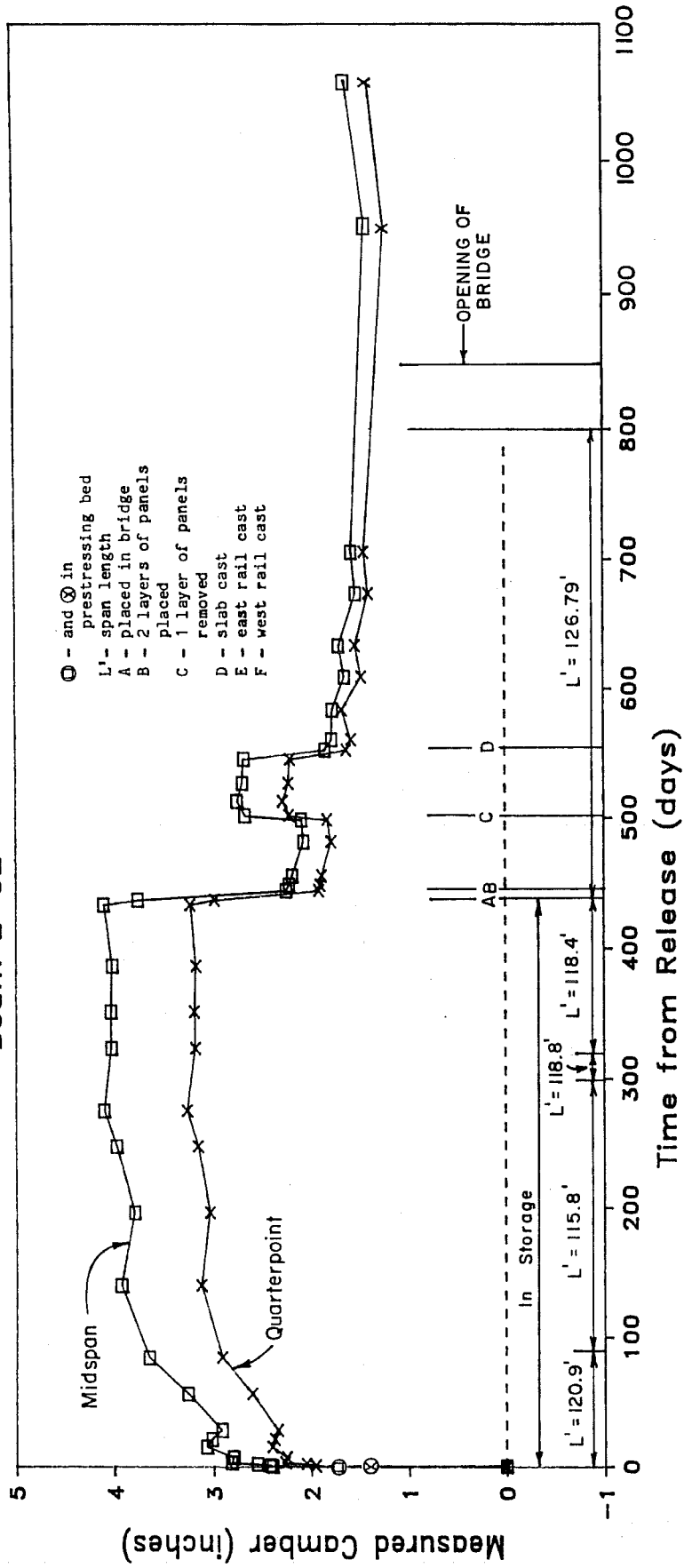


Fig. 4.3 Time dependent camber and deflection response of beam L-o2

Time Dependent Beam Camber

Beam L-11

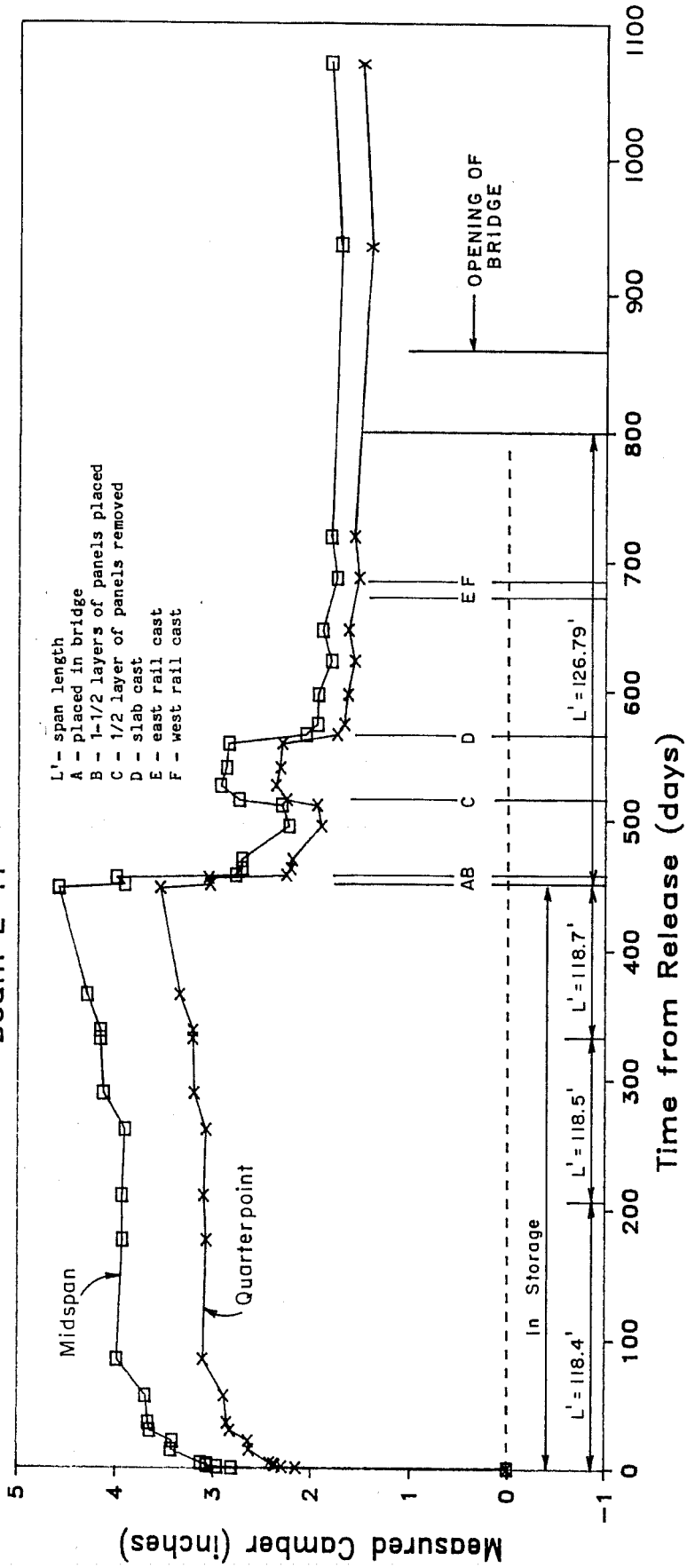


Fig. 4.4 Time dependent camber and deflection response of beam L-11

Time Dependent Beam Camber

Beam L-i2

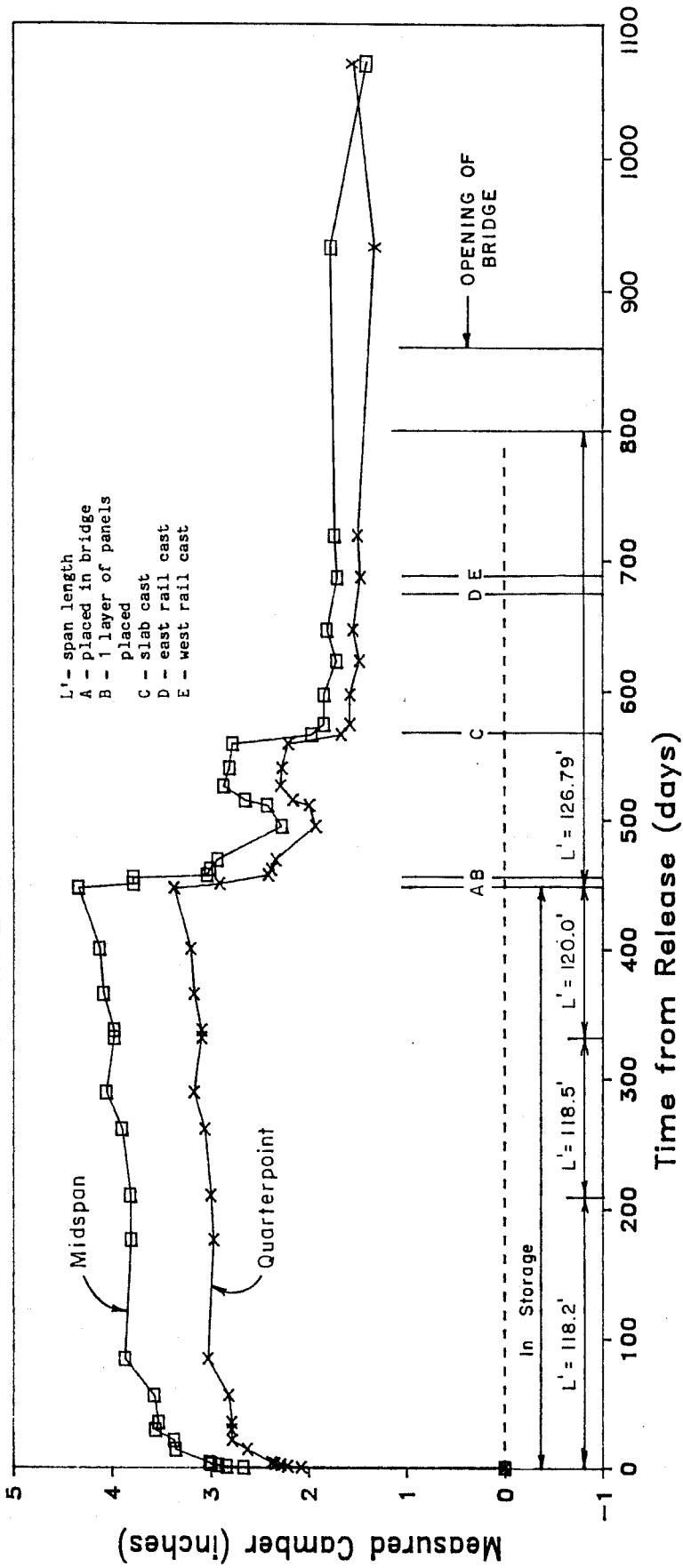


Fig. 4.5 Time dependent camber and deflection response of beam L-i2

After the panels were placed on beams L-i1 and L-i2, approximately 0.5 to 0.75 in. of additional downward movement is seen to have occurred. Some of this downward movement was gradually regained before the slab was cast. This time period occurs between points B and C in Figs. 4.4 and 4.5. This movement occurred because slab reinforcement and forms were temporarily stored on these beams. The weight of the reinforcement alone was approximately 20 kips. The magnitude of this weight is large enough to account for the observed behavior. As the forms were being attached to the outside beams and the reinforcing bars were being spread over all the beams, beams L-i1 and L-i2 regained some of the lost camber.

The camber and deflection responses of the H-series beams, Figs. 4.6 to 4.9, were also similar to the response of beam L-o1. The only significant difference was that they remained in storage for much less time.

The dashed lines in Figs. 4.6 and 4.7 represent the time periods when the instrumentation on beams H-o1 and H-o2 could not be accessed as discussed in Sec. 3.3.4. The dashed lines are shaped in such a fashion as to show how the beams most likely behaved during these periods.

Longer term readings (after the opening of the bridges to traffic) were continued only for about half of the instrumented girders because of the difficulty and danger of access as well as the fact that all girders were showing similar trends.

4.2.2 Concrete Surface Strains. As was discussed in Sec. 3.3.5, the concrete surface strain measuring system did not work properly because of failure of the epoxy used to attach the Demec points to the inserts cast into the beams. Figure 4.10 shows the measured strains at the midspan station of beam L-o2 before the epoxy lost adhesion due to moisture susceptibility. The corresponding strain distributions across the beam profile are given in Fig. 4.11. Judging from Figs. 4.10 and 4.11, one would conclude that the system worked very well. However, once the epoxy softened and points began to fall off the inserts, readings became very erratic. Figure 4.12 shows the midspan strain at different levels on beam H-i1. The epoxy used to attach the Demec points became bad within a couple of months after release of the prestressing force. Figure 4.12 illustrates how unreliable the readings became within 100 days.

4.2.3 Strain of the Prestressing Strand. As was mentioned in Sec. 3.3.5, the strand strain measuring system did not work properly. Figure 4.13 shows the measured strain in a prestressing tendon. Since strain gages were applied after strands were pretensioned, the measured strain reflects the strain that occurred after the tendon was initially

Time Dependent Beam Camber

Beam H-o1

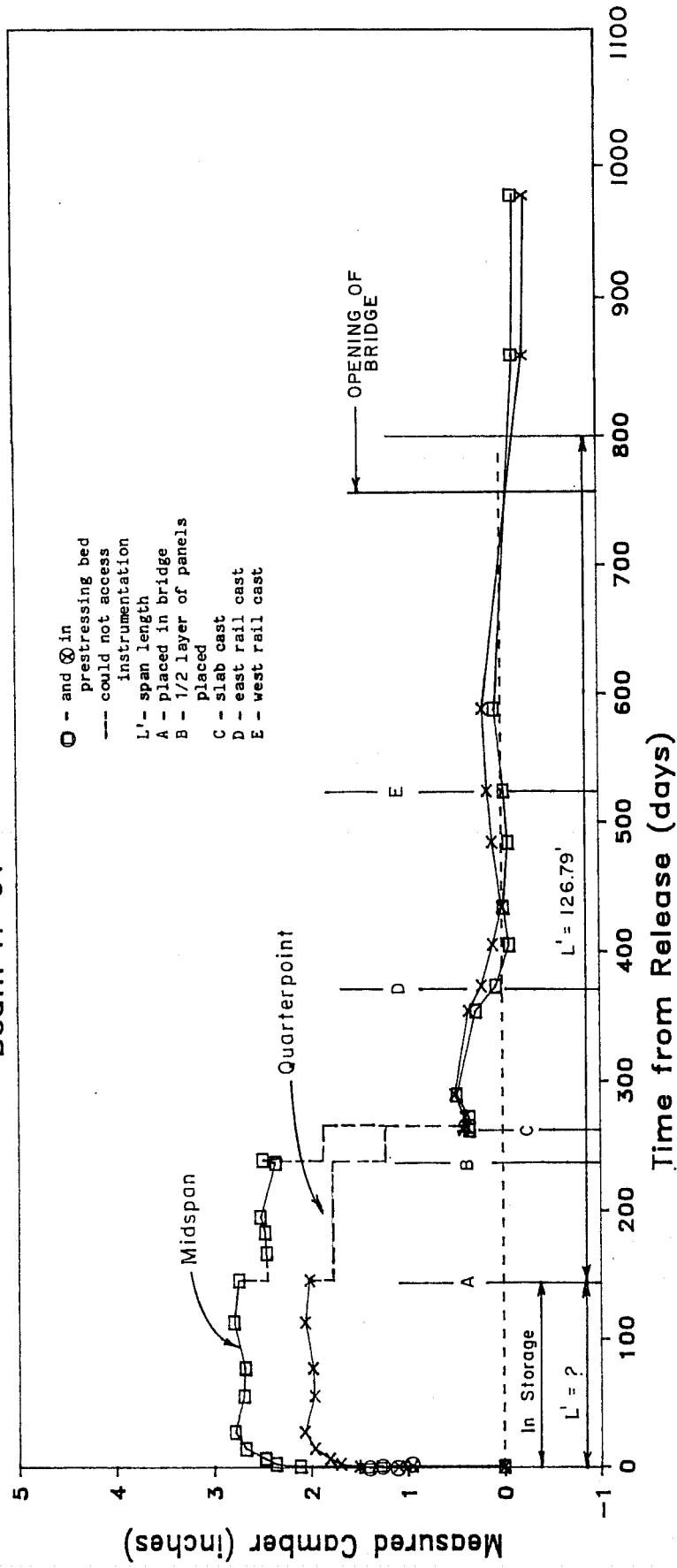


Fig. 4.6 Time dependent camber and deflection response of beam H-o1

Time Dependent Beam Camber

Beam H-o2

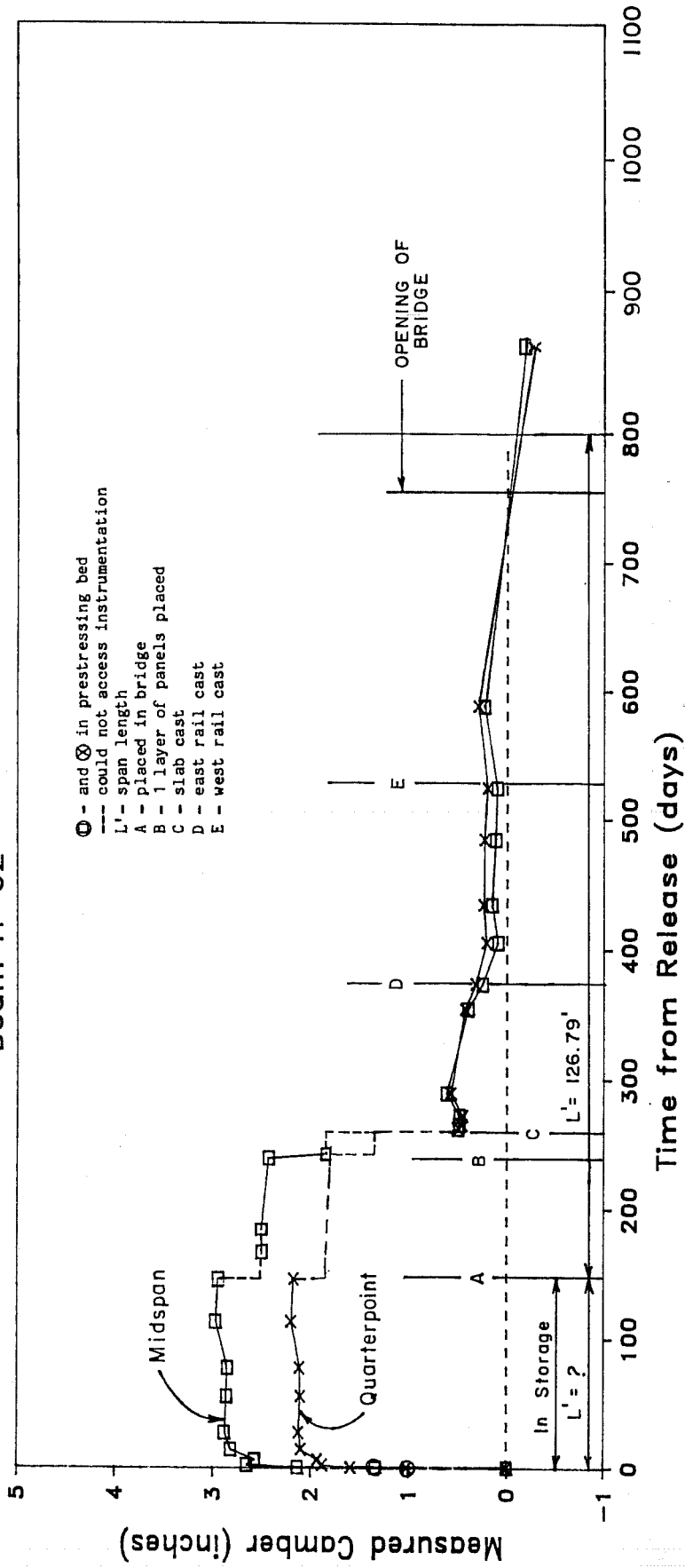


Fig. 4.7 Time dependent camber and deflection response of beam H-o2

Time Dependent Beam Camber

Beam H-i1

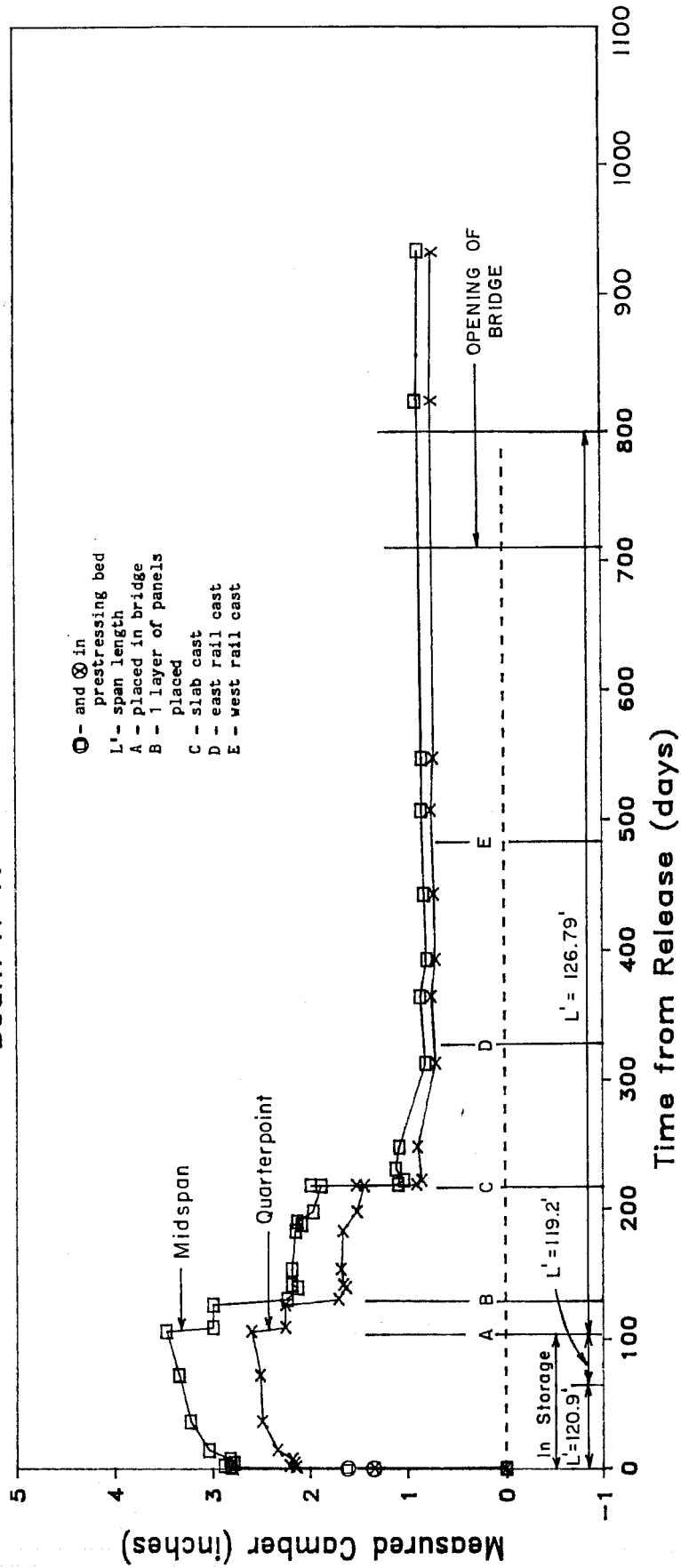


Fig. 4.8 Time dependent camber and deflection response of beam H-i1

Time Dependent Beam Camber Beam H-i2

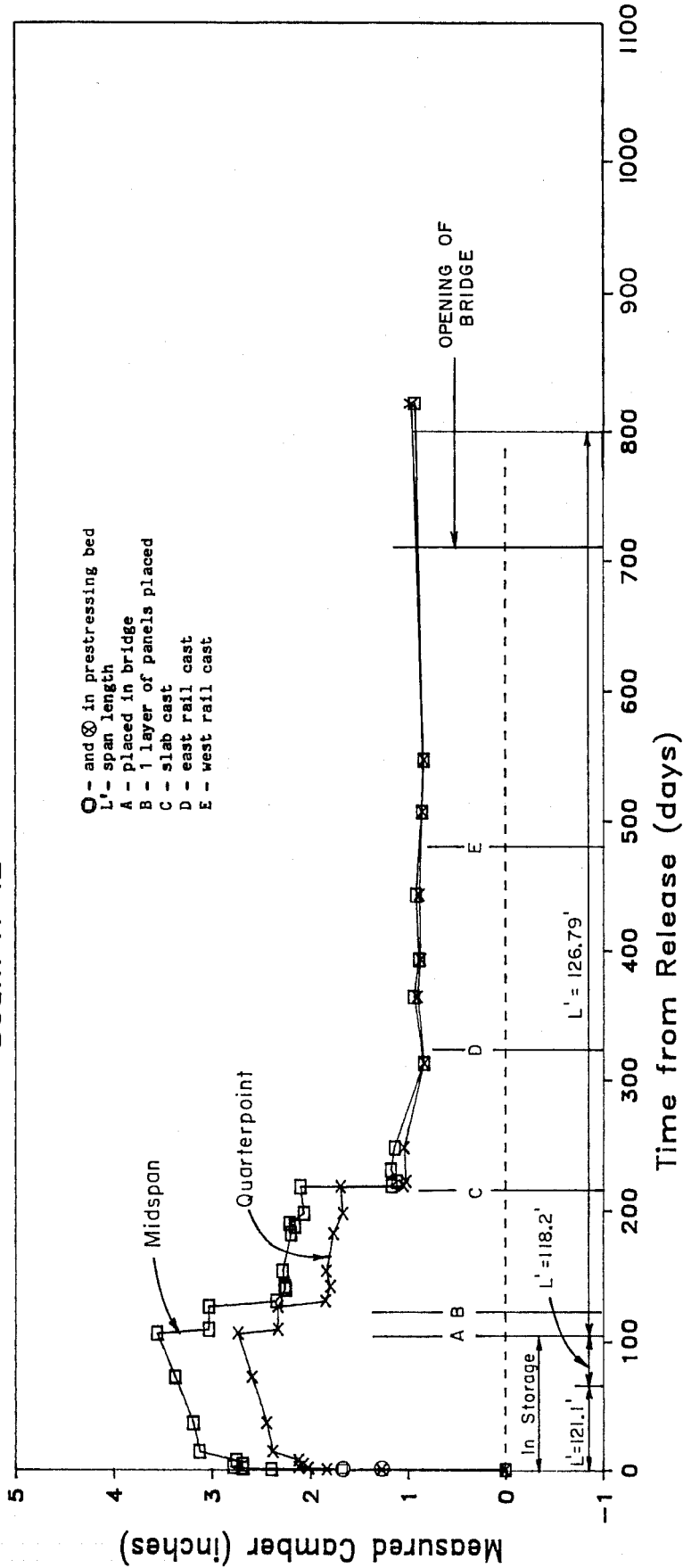


Fig. 4.9 Time dependent camber and deflection response of beam H-i2

Concrete Surface Strain Midspan of Beam L-o2

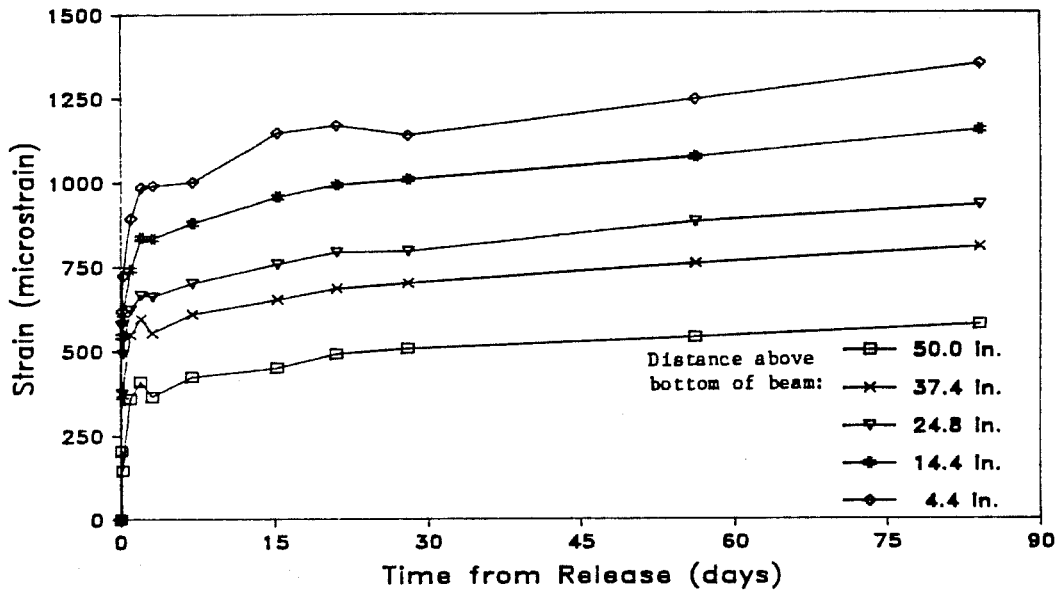


Fig. 4.10 Measured strain at the midspan of L-o2

Concrete Surface Strain Distribution — Midspan of Beam L-o2

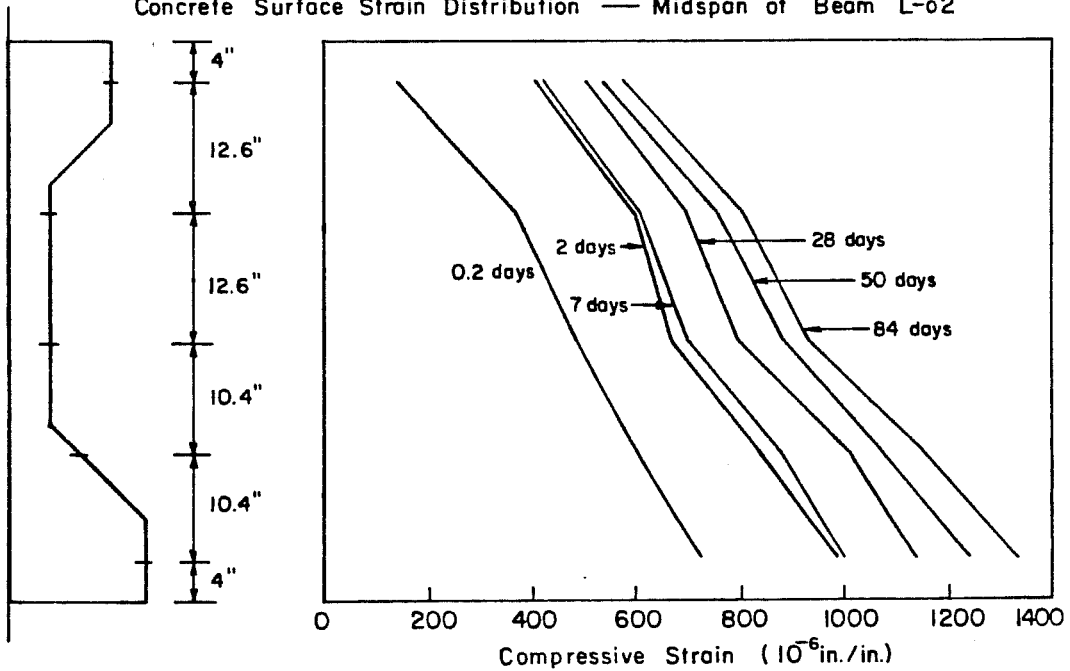


Fig. 4.11 Measured strain distribution at the midspan of L-o2

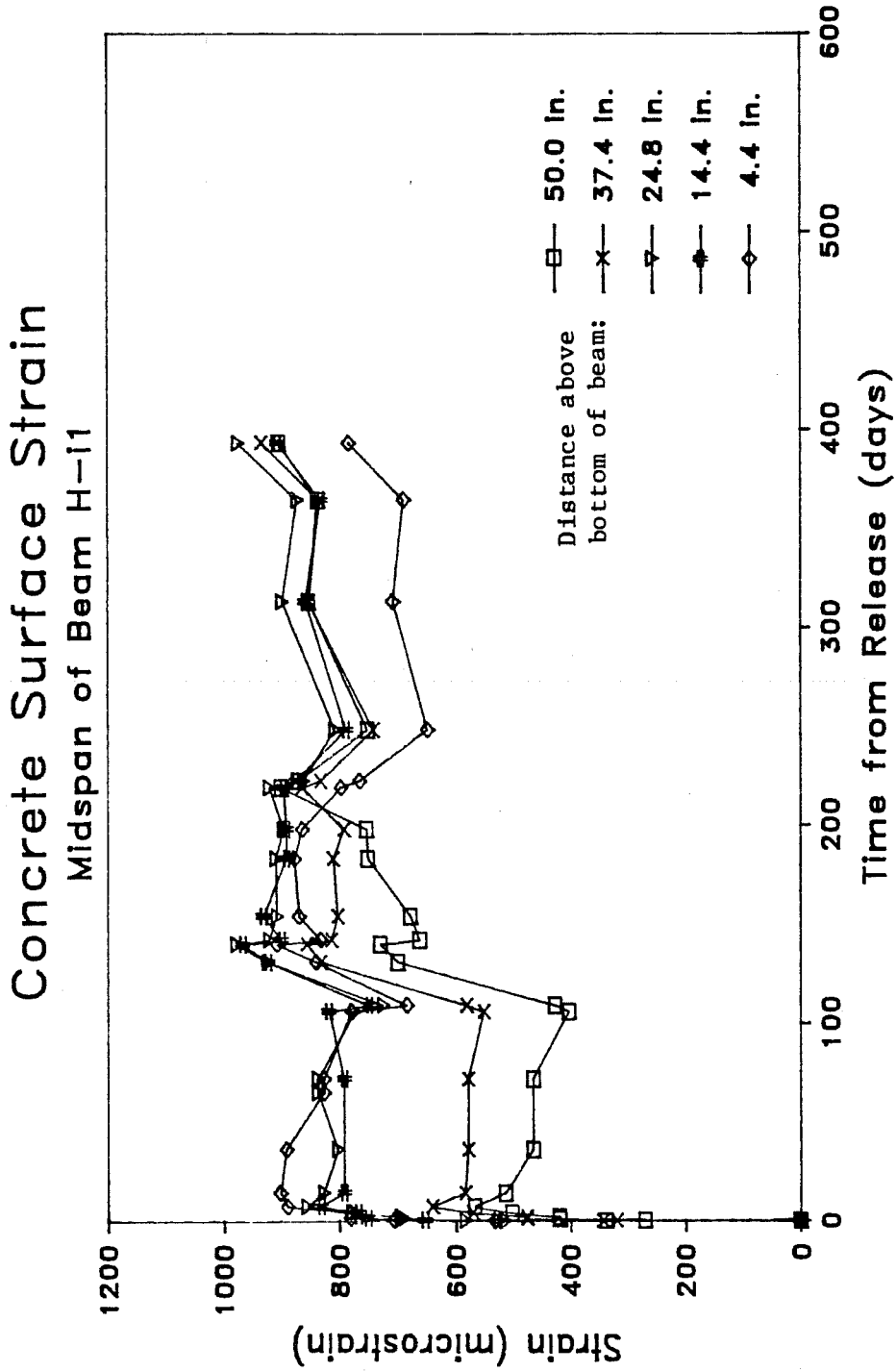


Fig. 4.12 Surface strain readings affected by the epoxy

tensioned. Thus elastic shortening upon release and similar losses would indicate compressive strains. The measured strain should reflect all losses except the loss due to relaxation. The measured strain shown in Fig. 4.13 was at the quarter point of beam L-01. The strand was located 10 in. above the bottom of the beam. The two curves in the figure are the strains measured by two different gages that were attached to the same strand and were located approximately 6 in. from one another. Thus both gages should ideally show almost identical behavior.

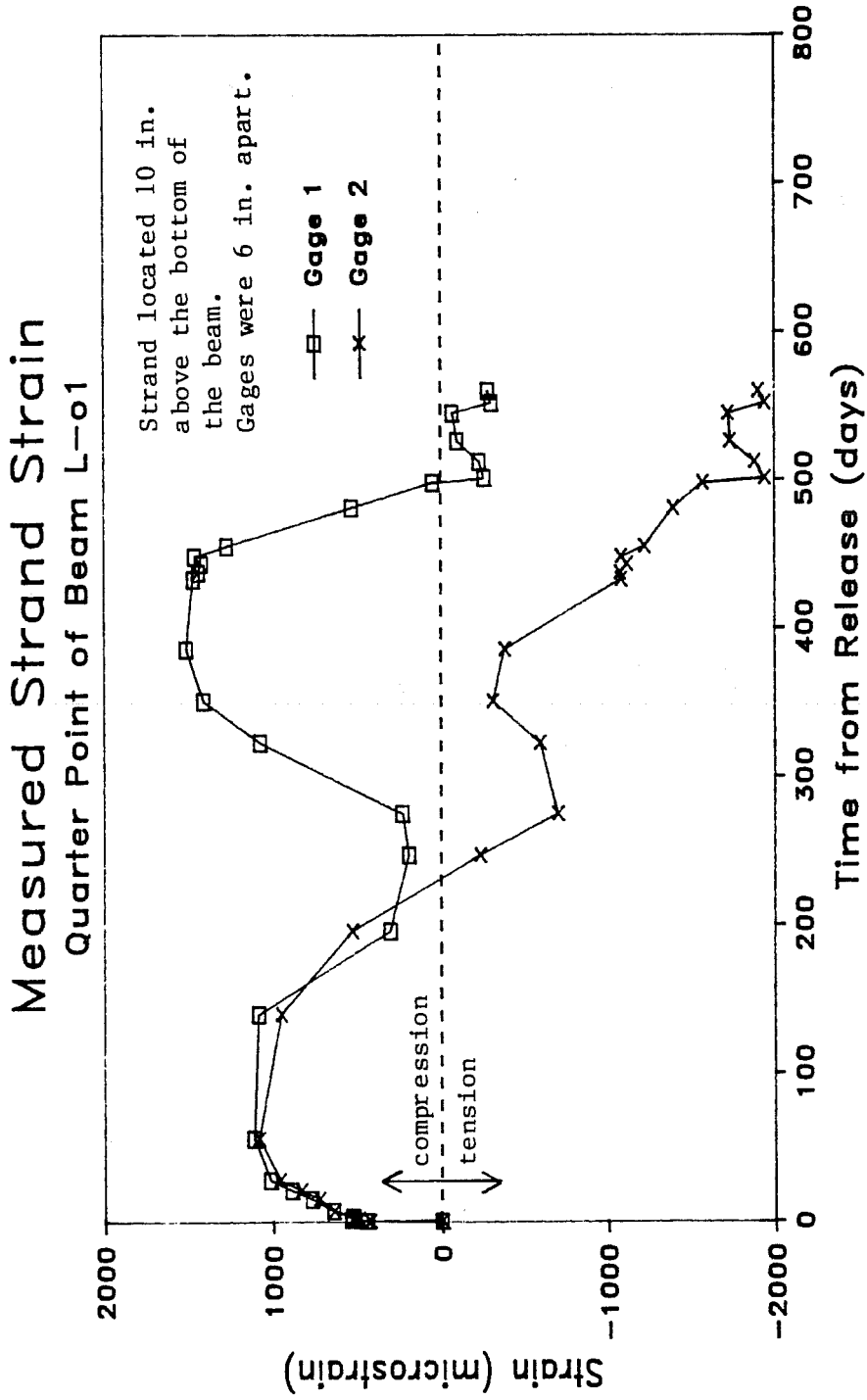
The strain readings in Fig. 4.13 appear to be reasonable and are in good agreement with each other for the first 100 days. The measured strain at this stage was approximately 1100 microstrain. This corresponds to a strand stress loss of approximately 16%. This loss calculation excludes the loss due to relaxation which would be an additional 1 to 3% for low-relaxation strand.

After about 100 days, the strain readings of each gage began to deviate from one another and became very erratic. Eventually the gages began to indicate tensile strains. This was impossible since only strand compressive strain changes caused by elastic shortening, creep, and shrinkage should have occurred during this time period as confirmed by the deflection observations.

All of the strain gages eventually gave very erratic readings. Most gages were no longer providing reasonable readings when they were only one month old. After 150 days, all gages were indicating strains that could not have existed. The electrical resistance integrity could not be maintained in the system used, and so the bulk of the strand strain measurements were useless.

4.2.4 Concrete Temperature Variations. Temperature distributions in bridges are effected by air temperature, wind, humidity, intensity of solar radiation, and type of material [35]. In order to gain an understanding of how the temperature in the bridge varied, internal temperatures of four composite beams were measured. The beam and slab temperatures were also observed in an effort to correlate them with the magnitude of thermal movements which will be discussed in Sec. 4.4. When measuring the internal beam temperatures, particular attention was given to observing the difference between the ambient and concrete temperatures, as well as the types and magnitudes of thermal gradients. Typical temperature readings are presented in this section to support the conclusions and generalizations drawn from the temperature data.

Changes in air temperature are caused by two basic cycles [36]: the yearly cycle and the daily cycle. The yearly cycle is created by changes in position and distance of the earth relative to the sun. The



Note. The measured strain is the strain that occurred after the tendon was initially tensioned.

Fig. 4.13 Typical measured strand strain

effect of the yearly cycle is to change the average temperature of the bridge. The average bridge temperature during the summer was higher than the average temperature during the winter. This is shown in Figs. 4.14 and 4.15 in which the average beam temperature was 85° F at 9 a.m. on July 12, 1984 and 29° F at 11 a.m. on January 22, 1985. The daily cycle provides temperature variations and gradients throughout the different parts of the structure. This is shown in all of the figures included in this section.

In general, the internal concrete temperature was warmer than the ambient temperature in the morning and cooler than it in the afternoon. Figure 4.14 shows the temperature readings in the morning of a sunny summer day. The average temperature of the beam was 4° F warmer than the ambient temperature. The average beam temperature shown in Fig. 4.16 (temperatures recorded during the afternoon of a hot summer day) was 13° F cooler than the ambient temperature.

While in storage, the observed thermal gradients were generally linear. Nearly linear gradients are shown in Figs. 4.14 to 4.17. In the morning, the top flange of the beam was usually cooler than the bottom flange as shown in Fig. 4.14. Throughout the morning, the temperature of the top flange would rise, and by the afternoon the top flange would normally be warmer than the bottom flange as shown in Fig. 4.16. On a sunny day, one can generally expect thermal gradients of 5 to 15° F to develop in a beam without a slab as shown in Fig. 4.16. On overcast days, the measured internal temperatures of a beam tend to be much more uniform as shown in Figs. 4.15 and 4.17. Thermal gradients of only a few degrees can be expected to develop on an overcast day.

After the cast-in-place slab was added to the right main lane bridge, detailed temperature data were collected during three days. Temperature readings were taken several times throughout the day on February 22, 1986, February 18, 1986, and March 11, 1986.

February 22, 1986 was chosen to represent a typical winter day in Austin. The ambient temperature varied from a low of 38° F to a high of 64° F throughout the day. The temperature variations at the midspan, southern quarter point, and south end of beam L-11 are presented in Figs. 4.18, 4.19, and 4.20, respectively. The maximum temperature gradient was measured at the quarter point station. At 4:10 p.m., the difference between the temperature in the center of the deck and in the top flange was 6° F.

February 18, 1986 was chosen because it was an unseasonably warm day. Through the course of the day, the ambient temperature changed 39° F from a low of 52° F to a high of 91° F. This variation was expected to produce a greater than normal thermal gradient. The observed temperature variations in beam L-11 are shown in Figs. 4.21 to 4.23. The greatest gradient occurred at both the midspan and quarter

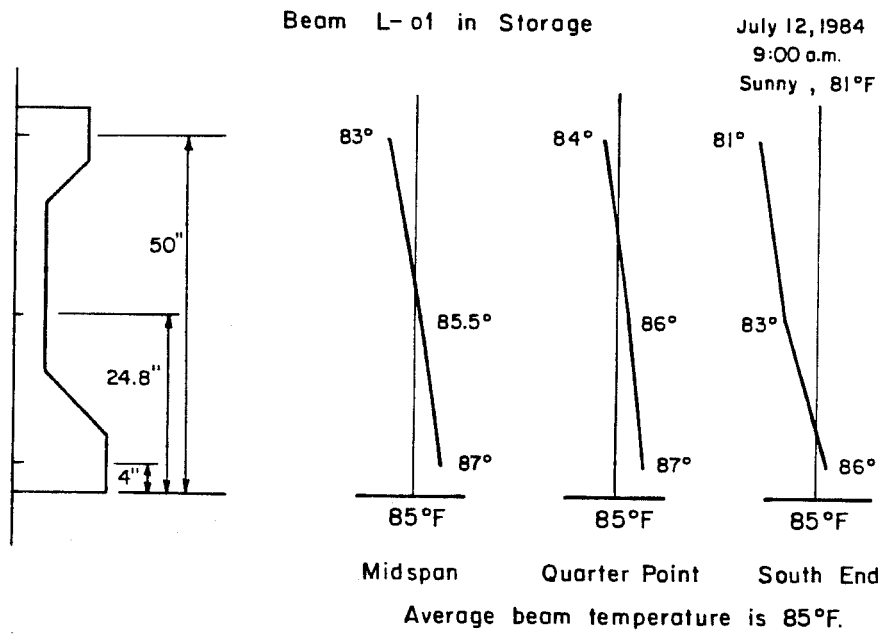


Fig. 4.14 Temperature distribution in a beam during the morning of a sunny summer day

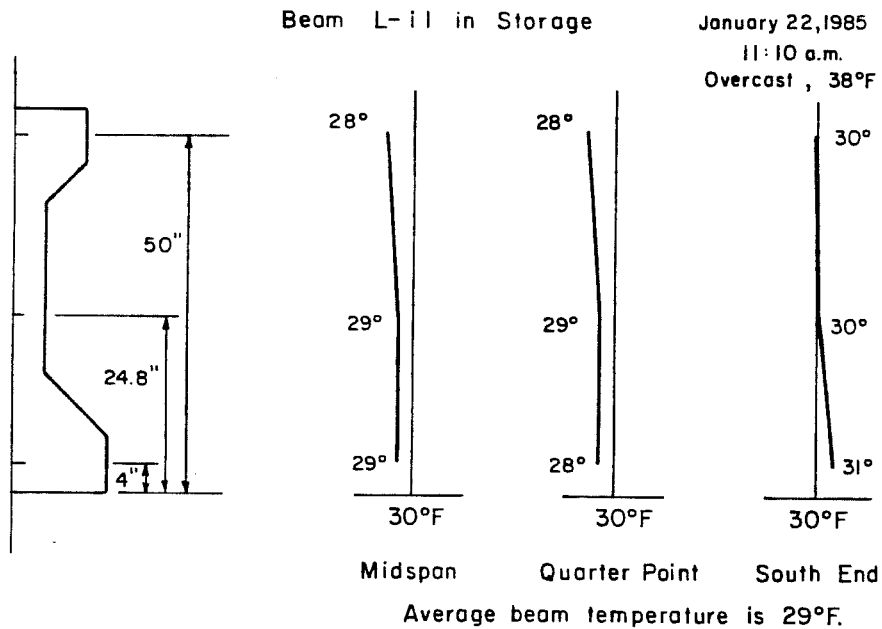


Fig. 4.15 Temperature distribution in a beam on a cold, overcast winter day

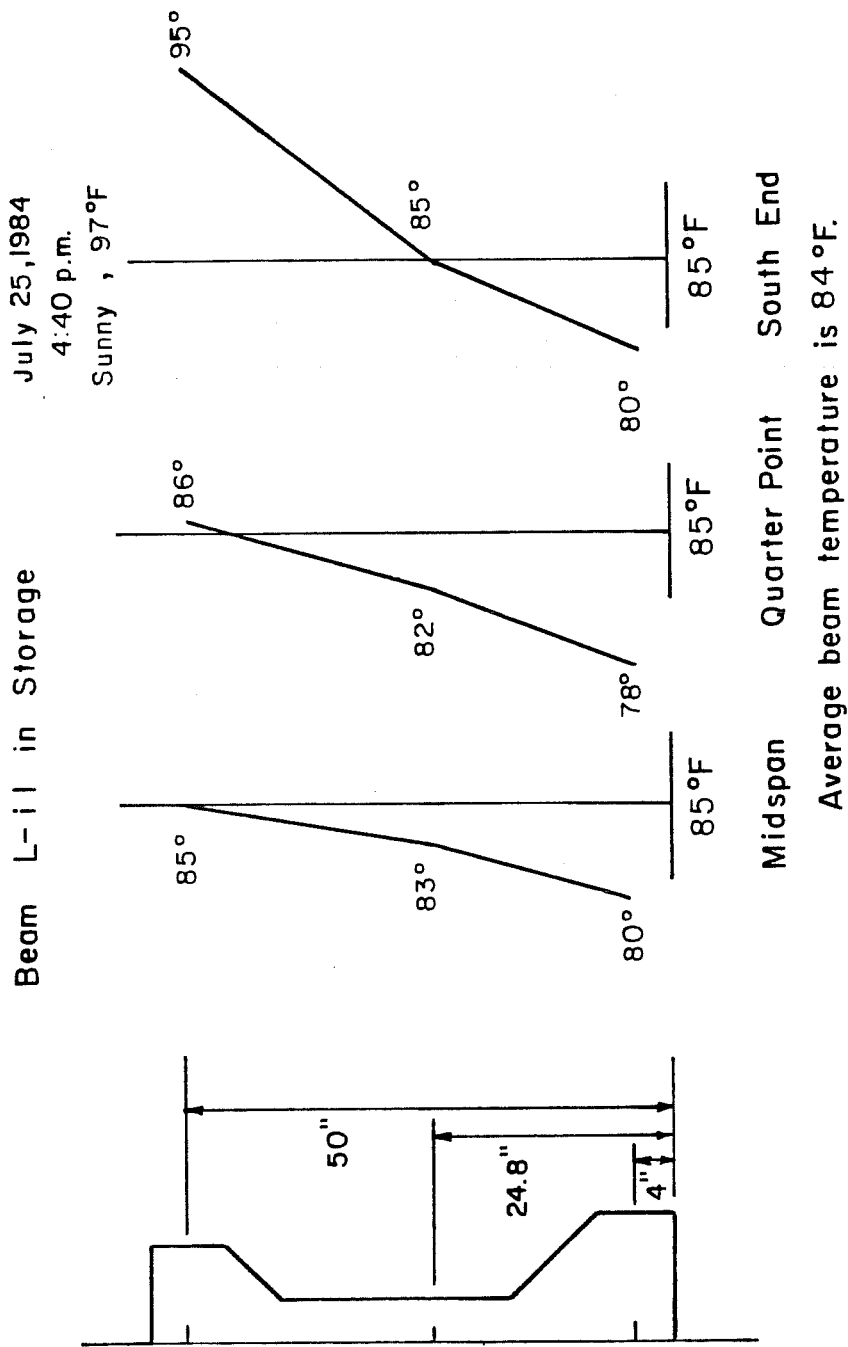


Fig. 4.16 Temperature distribution in a beam on a hot summer day

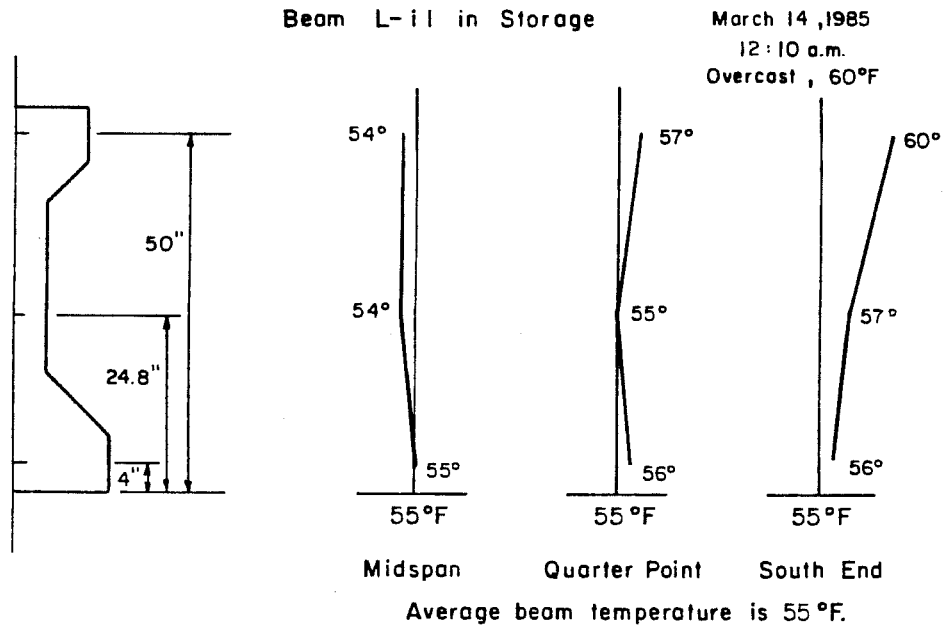


Fig. 4.17 Temperature distribution on an overcast spring day while in storage

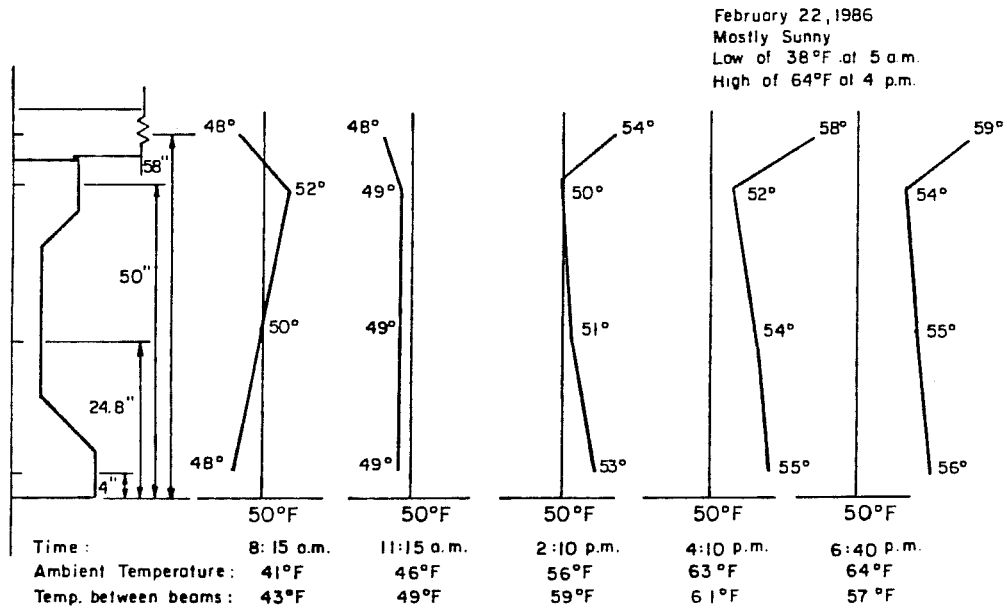


Fig. 4.18 Midspan temperature distributions in composite beam L-11 on a sunny winter day

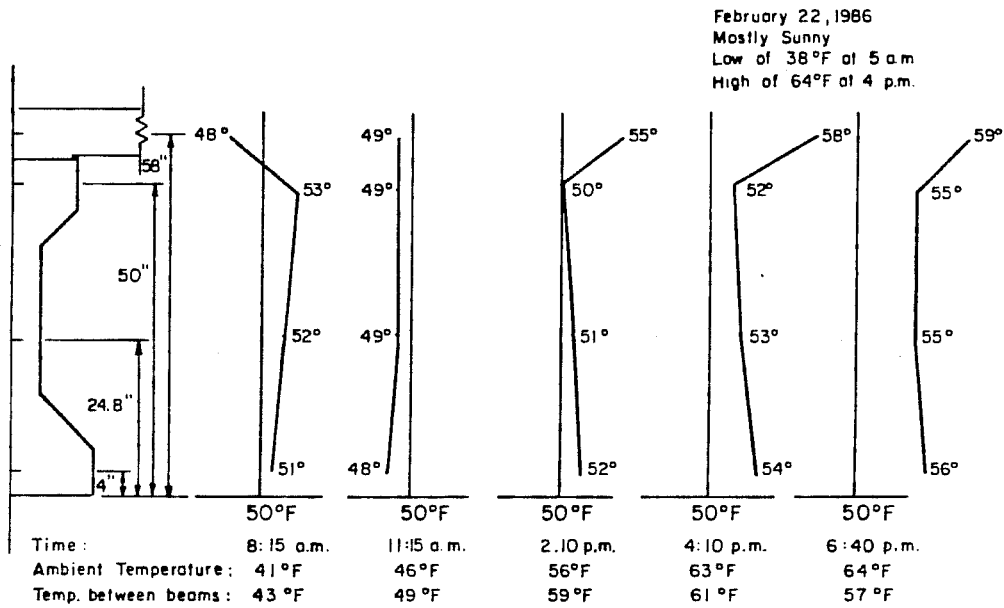


Fig. 4.19 Quarter point temperature distribution in composite beam L-11 on a sunny winter day

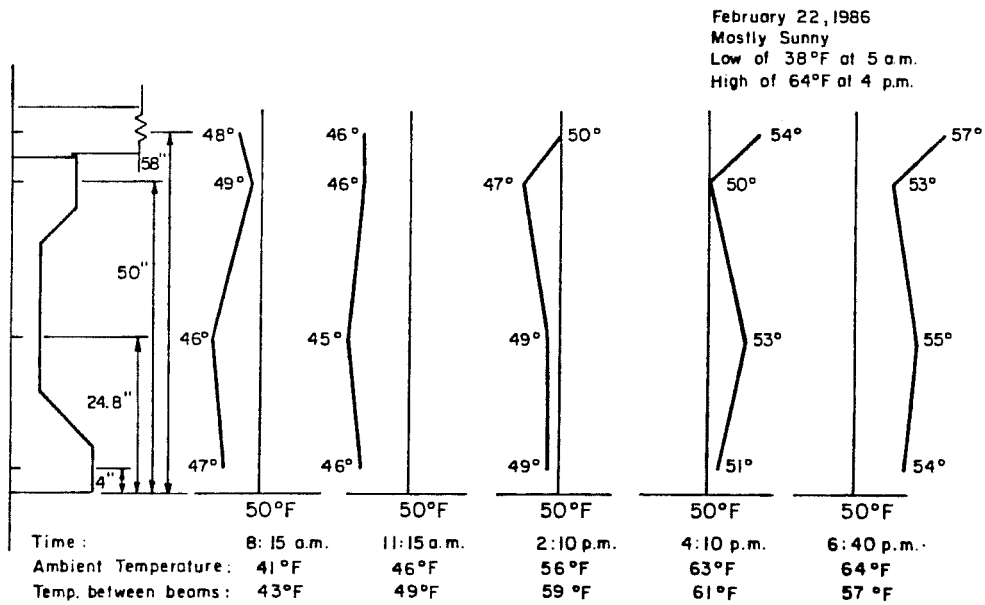


Fig. 4.20 South end temperature distribution in composite beam L-11 on a sunny winter day

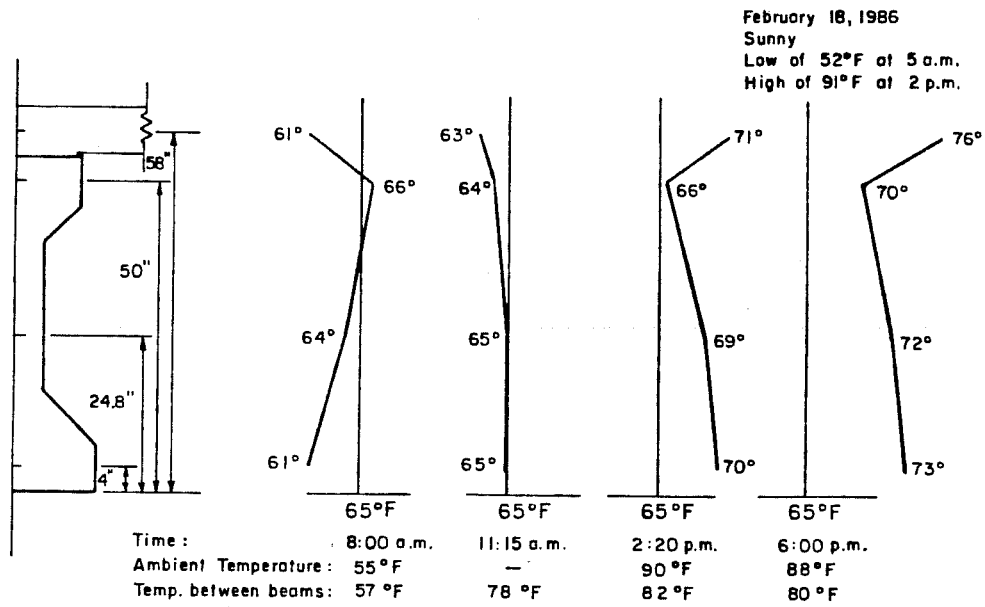


Fig. 4.21 Midspan temperature distributions in composite beam L-11 on an unusually hot winter day

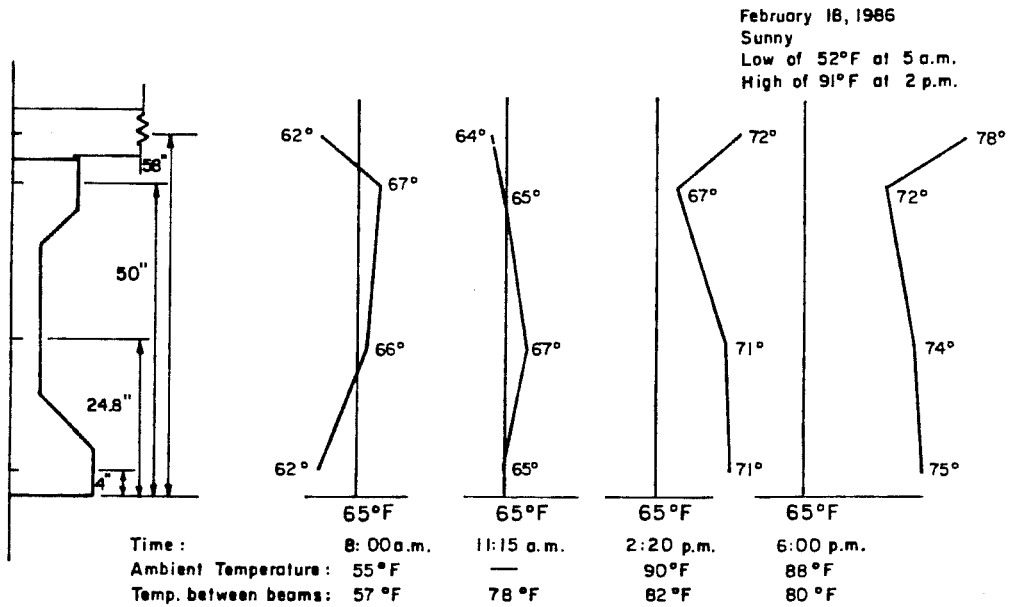


Fig. 4.22 Quarter point temperature distributions in composite beam L-11 on an unusually hot winter day

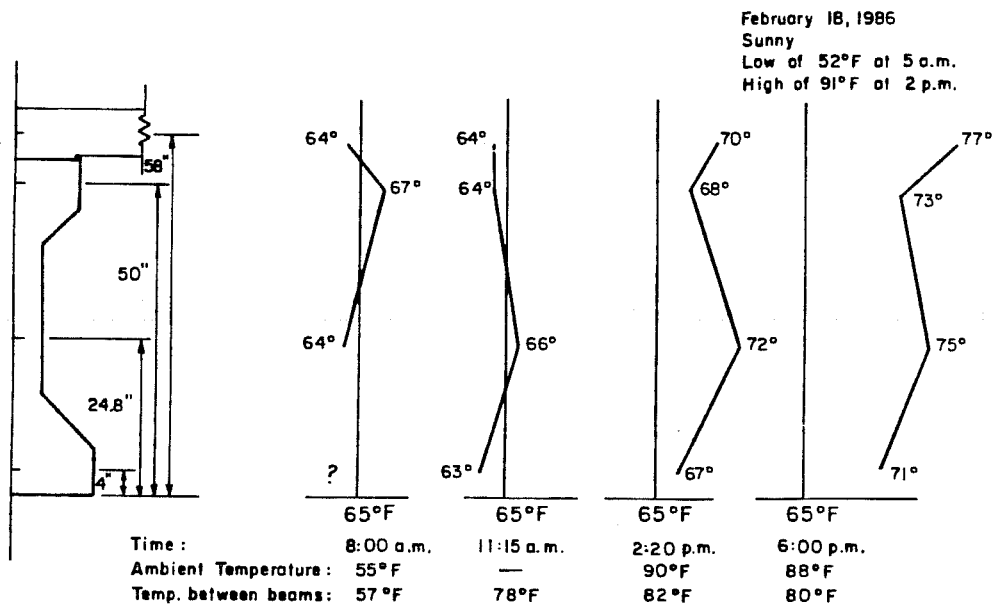


Fig. 4.23 South end temperature distributions in composite beam L-11 on an unusually hot winter day

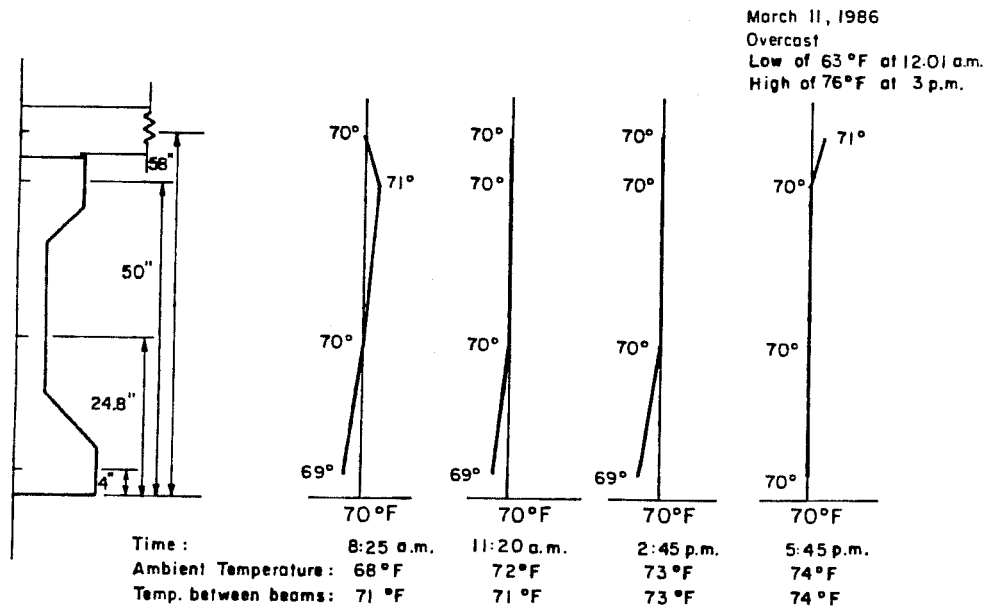


Fig. 4.24 Midspan temperature distributions in composite beam L-11 on an overcast spring day

point stations. At 6:00 p.m., a difference of 6° F was measured between the center of the deck and the top flange. This gradient was no greater than the gradient measured on February 22, 1986.

Temperature measurements were taken on March 11, 1986 because it was overcast. The ambient temperature varied from a low of 63° F to a high of 76° F. The observed temperature variations in beam L-11 during this day are shown in Figs. 4.24 to 4.26. The maximum, measured temperature gradient was only 3° F.

Out of the three days on which temperatures were closely monitored, the largest measured temperature variations occurred February 18, 1986. During this day, the temperature at the center of the deck changed 15° F. This was approximately equal to 40% of the change in ambient temperature. On February 22, 1986 the deck experienced an 11° F change which was also approximately 40% of the change in ambient temperature. The temperature gradients on these two days were of similar shape and magnitude.

Because March 11, 1986 was an overcast day, the beam did not experience as large temperature changes as occurred on the other two days. The temperature variations were less and the gradients more uniform because the slab absorbed less solar radiation.

4.3 Companion Tests

4.3.1 Concrete Compressive Strength. The variation with time of cylinder compressive strengths corresponding to beams L-11 and L-12 are shown in Fig. 4.27. An expanded view of the strengths of cylinders broken during the first 100 days after casting is shown in Fig. 4.28.

The concrete gained most of its strength at an early age, because Type III cement was used. As shown in Figs. 4.27 and 4.28, the average strength at 28 days was 8620 psi. This is 86% of the average strength at 527 days. The strength gain of concrete for the other six beams exhibited similar behavior. The cylinder strengths versus time for these beams are shown in Figs. 4.29 to 4.31.

Since the concrete mix and aggregate source were similar for all the beams, one would expect the variation of concrete strengths at a given age to be small. Figure 4.32 is a histogram of cylinder strengths at 14 days. The mean strength was 9670 psi with a standard deviation of only 183 psi. The cylinders included in the histogram were made and tested by the Texas SDHPT. They correspond to the beams cast on 7/9/84, 10/2/84, and 11/12/84. The cylinders were stored in saturated lime water at 73.4 plus or minus 3° F. Since the cylinders were stored at the same temperature for the same length of time, the

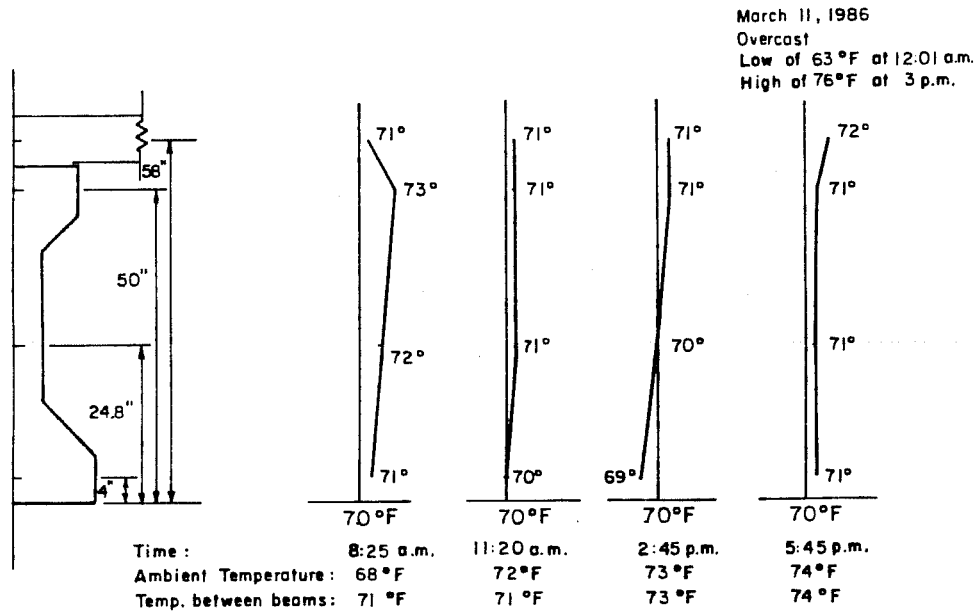


Fig. 4.25 Quarter point temperature distributions in composite beam L-11 on an overcast spring day

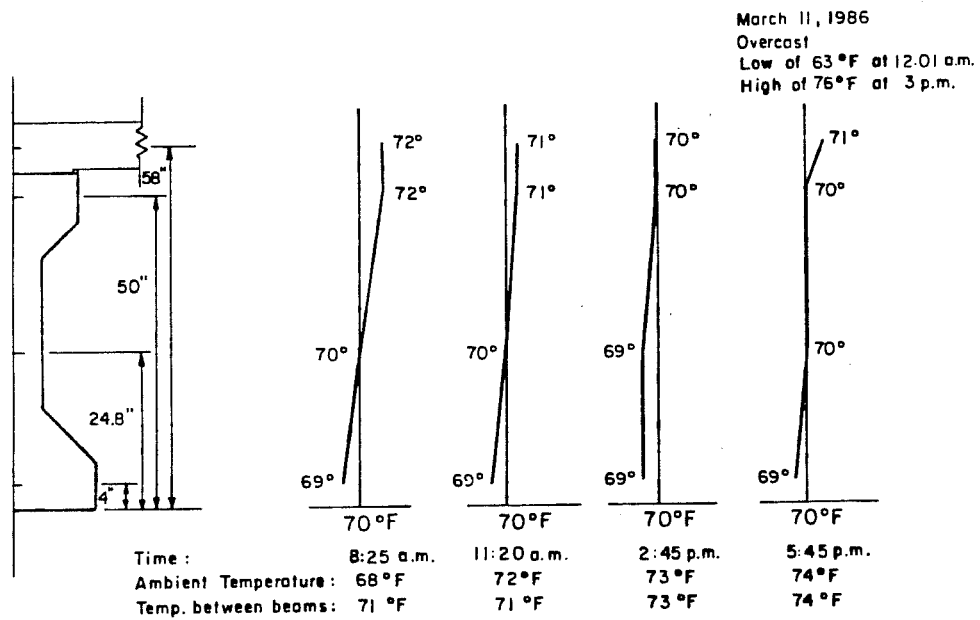


Fig. 4.26 South end temperature distributions in composite beam L-11 on an overcast spring day

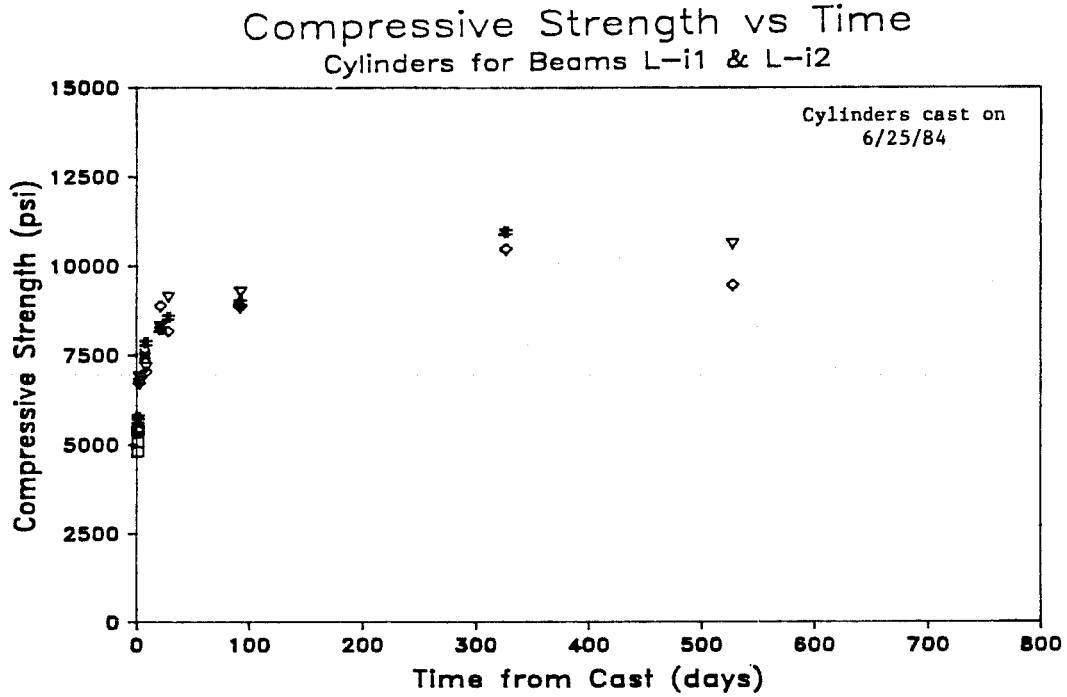


Fig. 4.27 Cylinder compressive strengths corresponding to beams L-i1 and L-i2

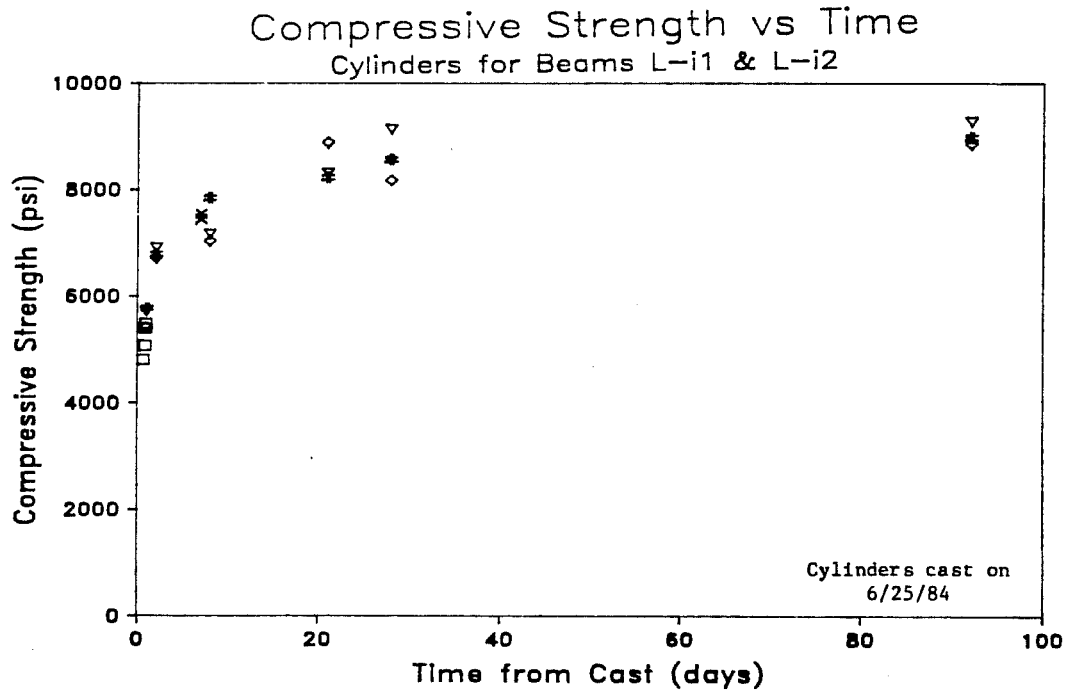


Fig. 4.28 Cylinder compressive strengths corresponding to beams L-i1 and L-i2 that were broken the first 100 days after casting

Compressive Strength vs Time Cylinders for Beams L-o1 & L-o2

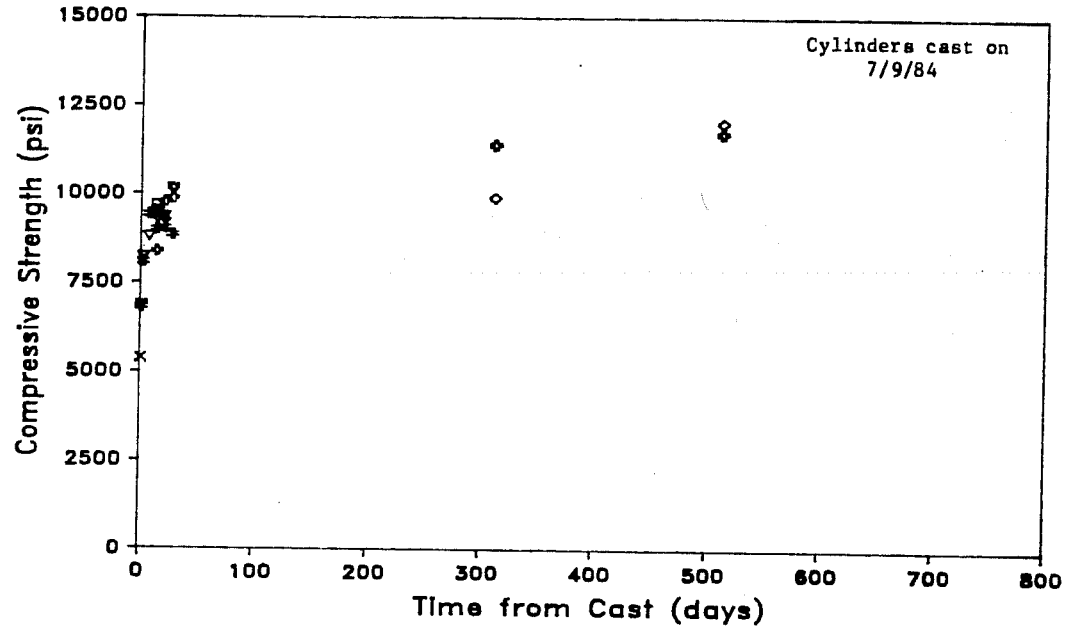


Fig. 4.29 Cylinder compressive strengths corresponding to beams L-o1 and L-o2

Compressive Strength vs Time Cylinders for Beams H-o1 & H-o2

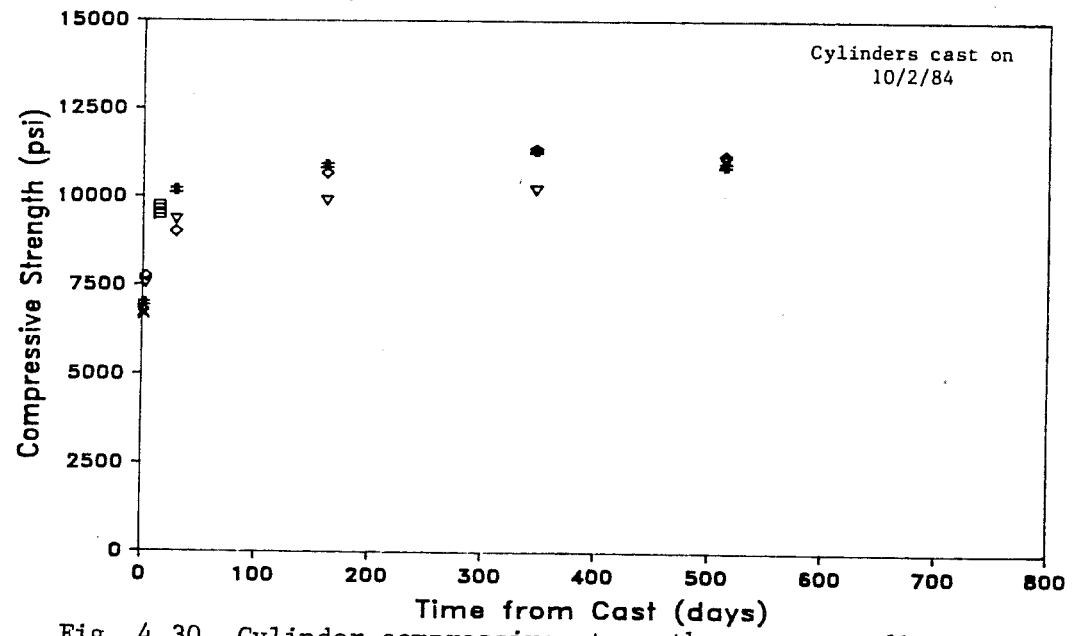


Fig. 4.30 Cylinder compressive strengths corresponding to beams H-o1 and H-o2

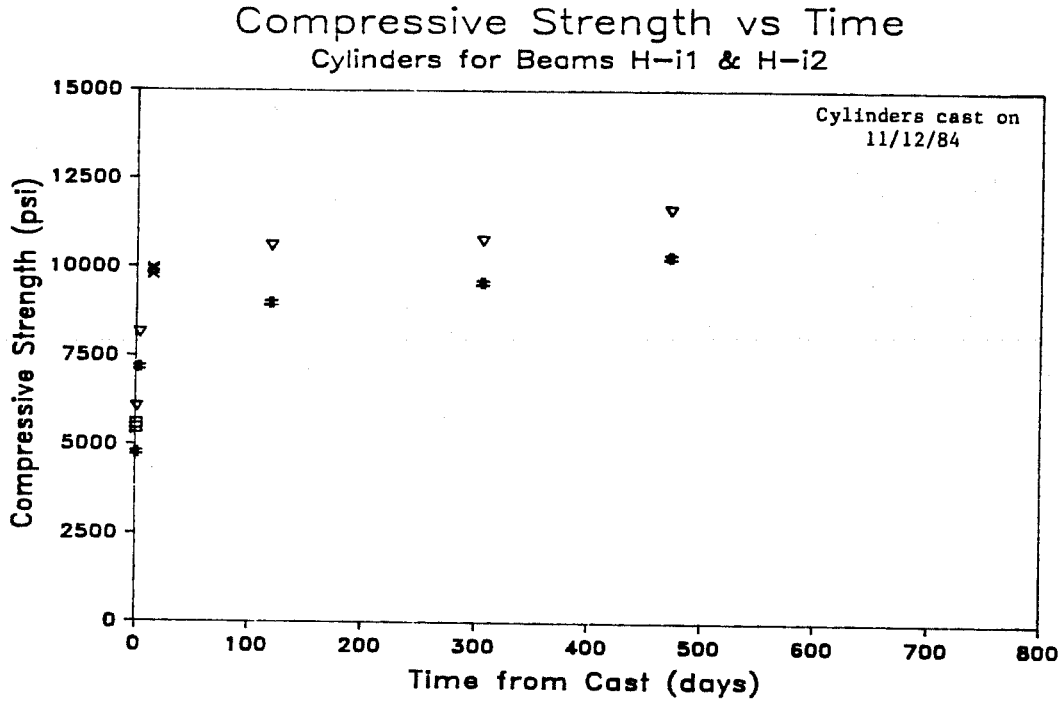


Fig. 4.31 Cylinder compressive strengths corresponding to beams H-01 and H-i2

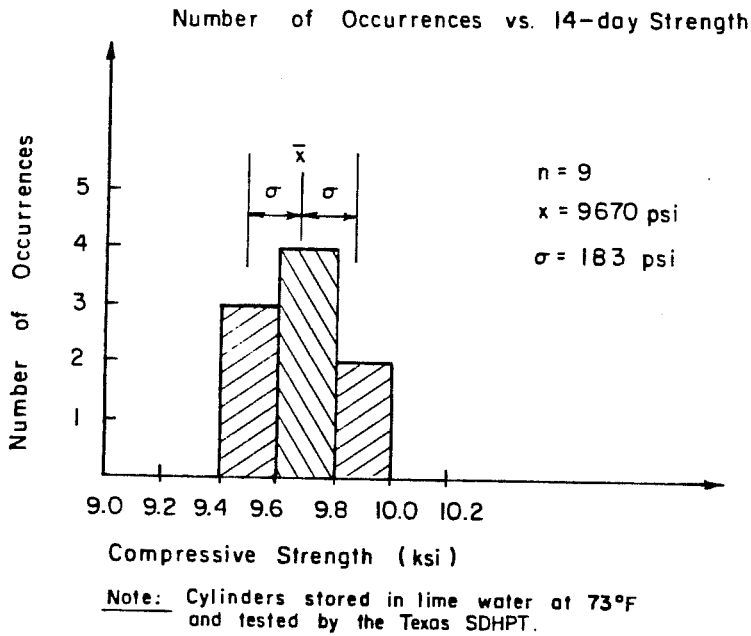


Fig. 4.32 Variation of 14-day strength of beam cylinders

maturity (integrated temperature-days of curing) of these cylinders was the same.

If the maturity of the tested cylinders is not equal, the scatter of strengths at a given age is increased. Figure 4.33 is a histogram of 28-day concrete strength of cylinders cured in an uncontrolled environment. The mean strength was 9340 psi with a standard deviation of 714 psi. These cylinders were cast on 6/25/84, 7/9/84, and 10/2/84. They were stored in an uncontrolled environment similar to the environment to which the beams were exposed. The standard deviation for these cylinders was substantially greater than the standard deviation for the controlled curing cylinders shown in Fig. 4.32. The standard deviation is significantly greater because the maturities of the cylinders were not equal.

The environment to which concrete is exposed should be carefully considered in determining the concrete strength and dependent parameters such as deformations in actual beams. Based on the data in Figs. 4.32 and 4.33, one might assume that the average strength at 14 days based on the controlled curing material tests is greater than the actual beam strength at 28 days. This is clearly because the cylinders broken at 14 days were in a much more favorable curing environment as compared to the beams and the 28-day cylinders. Cylinders stored in saturated lime water such as the 14-day cylinders indicate material potential but most likely overestimate the actual concrete strength in the beam and should not be relied on for deformation predictions.

4.3.2 Elastic Modulus of Concrete. The measured elastic modulus versus the compressive strength of cylinders made with concrete used to cast the instrumented beams is shown in Fig. 4.34. The elastic modulus versus strength curve representing the AASHTO formula [22] is also included in Fig. 4.34. This curve was calculated assuming the unit weight of concrete was 145 pcf.

Based on the data shown in Fig. 4.34, the AASHTO formula appears to overestimate the elastic modulus of cylinders with strengths above 9000 psi. As shown in Fig. 4.35, Pauw [37] developed the formula adopted by AASHTO and ACI 318 [38] using cylinders with strengths of 6000 psi and less. The scatter of the data used to develop this formula was also large (at least plus or minus 20%). Based on the data shown in Fig. 4.34 and the criteria for which this formula was developed, care should be taken when using the AASHTO formula to predict the elastic modulus of concrete with strengths greater than 9000 psi.

ACI Committee 363 [39] has recommended a formula for calculating the elastic modulus of concretes with strengths greater than 6000 psi. This formula generally underestimates the measured elastic modulus for the cylinders shown in Fig. 4.34 and replotted in Fig. 4.36.

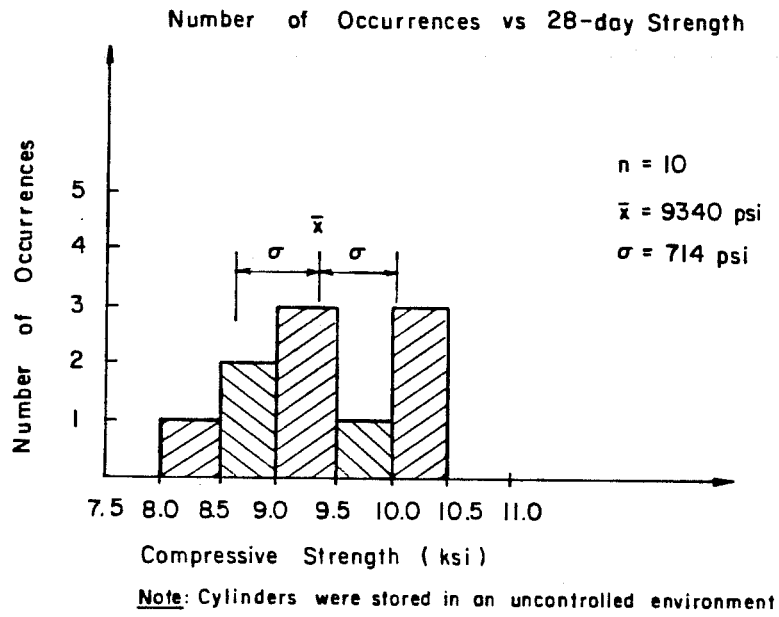


Fig. 4.33 Variation of 28-day strength of beam cylinders

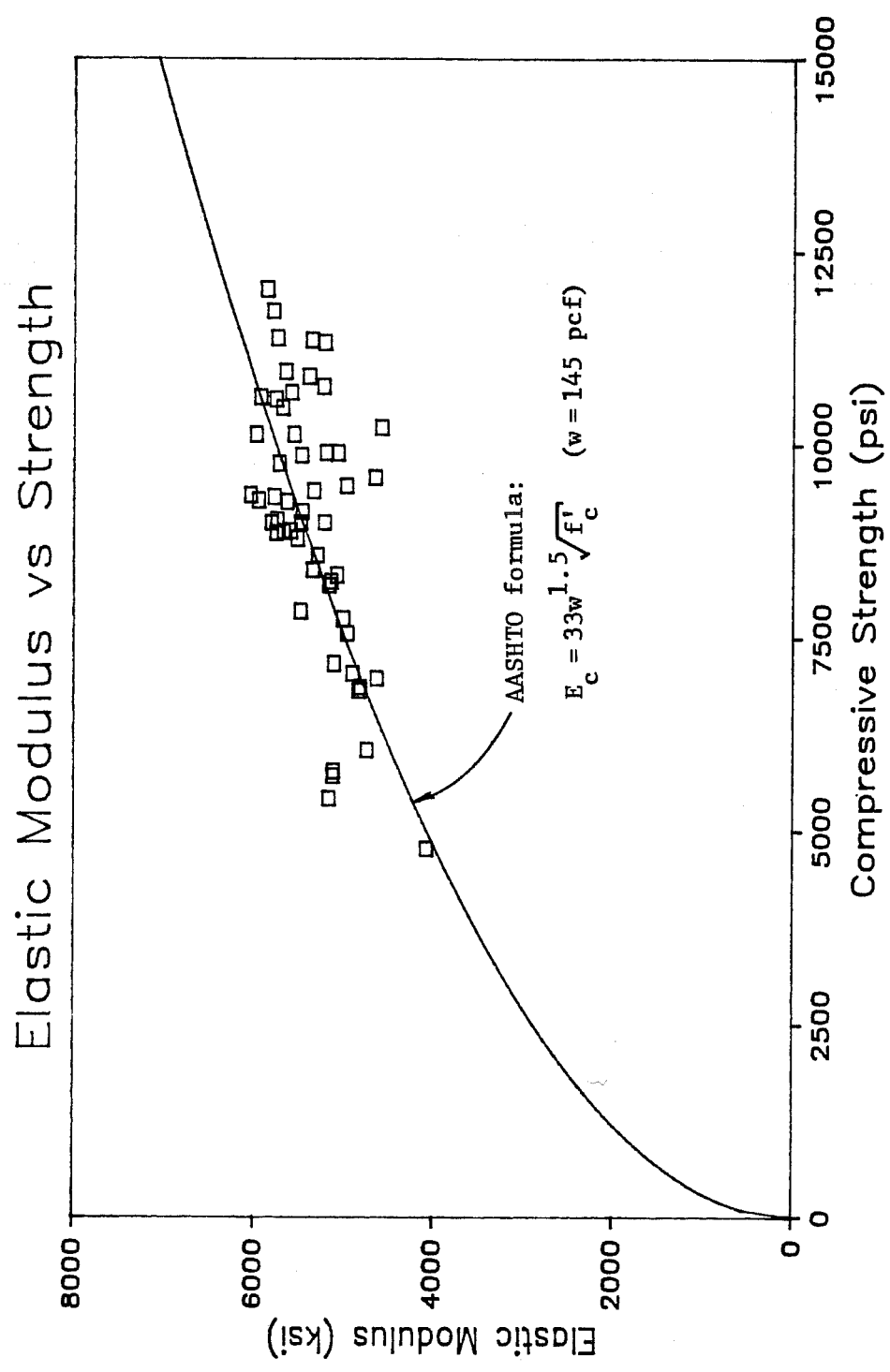


Fig. 4.34 Elastic modulus vs the compressive strength for the beam concrete

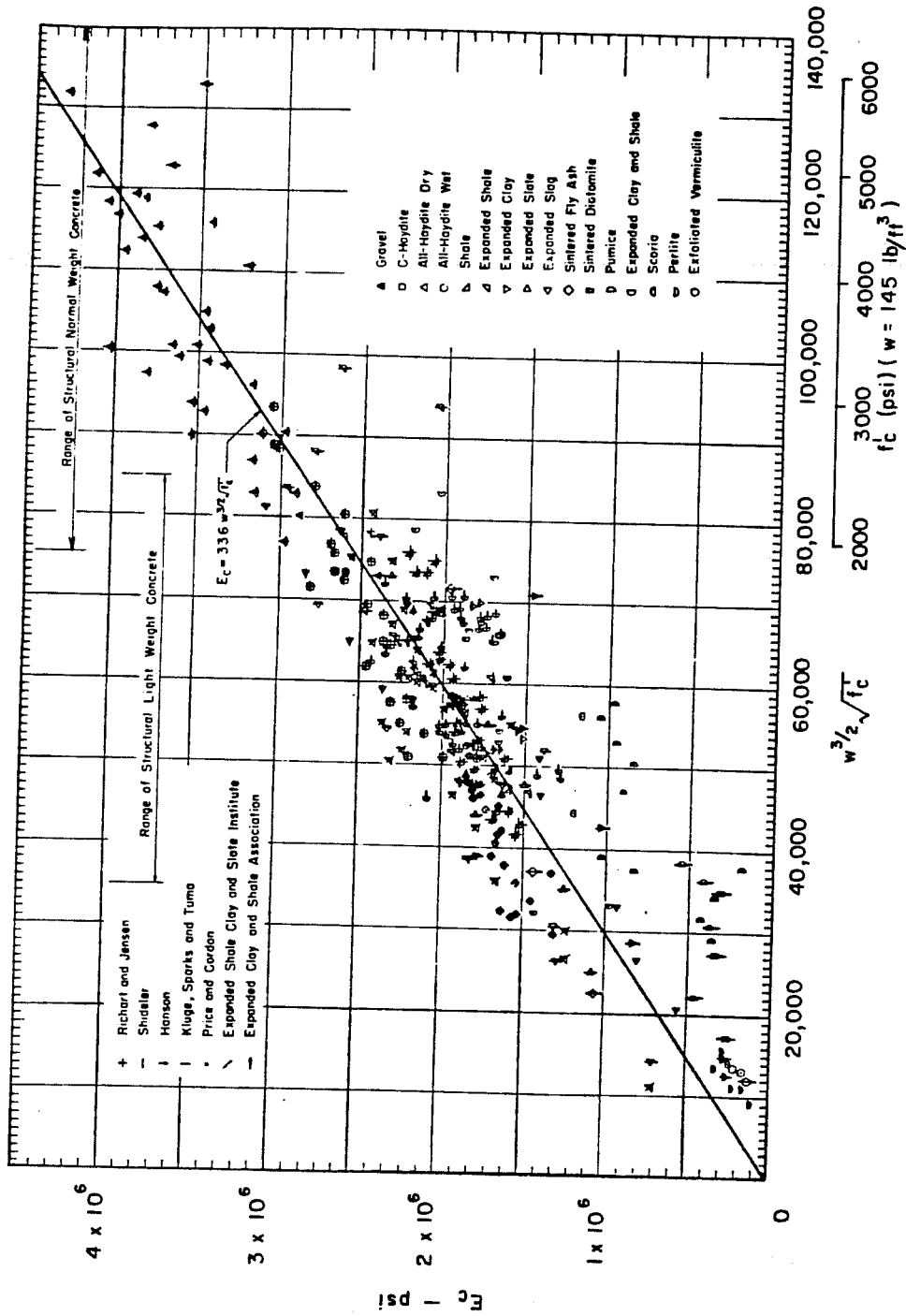


Fig. 4.35 Data Pauw used to develop the formula that AASHTO recommends to be used for calculating concrete elastic modulus (from Reference 37)

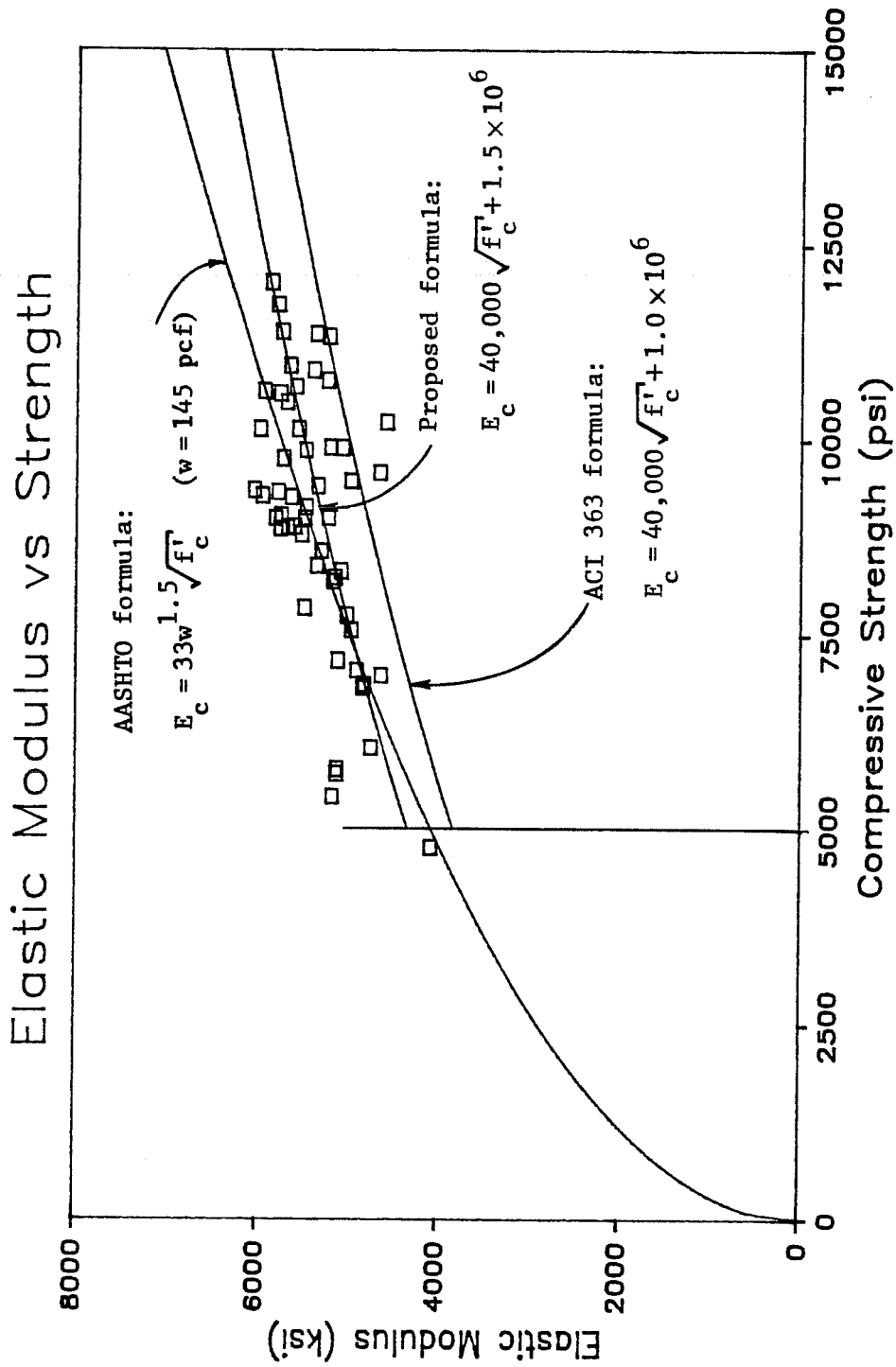


Fig. 4.36 Elastic modulus predicted using AASHTO, ACI 363, and a proposed formula vs measured values

This formula was developed by Carrasquillo [40] using cylinders with strengths between 3000 and 12,000 psi. Most of these cylinders were made using gravel aggregate, although several were made with crushed limestone aggregate. In general, Carrasquillo found that for the same compressive strength, cylinders made with crushed limestone aggregate had a higher elastic modulus than cylinders made with gravel aggregate. Because this formula was developed using both concretes with crushed limestone aggregate and concretes with gravel aggregate, it tends to underestimate the elastic modulus of concretes made with crushed limestone aggregate as in this study as shown in Fig. 4.36.

A more realistic estimate for the elastic modulus (psi) of concrete made with crushed limestone aggregate can be obtained using

$$E_c = 40,000 \sqrt{f'_c} + 1.5 \times 10^{-6} \quad (4.1)$$

This formula was developed by modifying the ACI 363 formula to fit the data presented in Fig. 4.34. As shown in Fig. 4.36, this formula works well for the data obtained for this project.

4.3.3 Concrete Creep and Shrinkage. The results of a creep test performed using cylinders made from the concrete used to cast beams L-i1 and L-i2 are shown in Fig. 4.37. The creep coefficient which appears on the vertical axis in the figure is defined as $\epsilon_t/\epsilon_o - 1.0$, where ϵ_t is the total strain (elastic and time dependent) minus the shrinkage and thermal strains, and ϵ_o is the initial elastic strain. The creep coefficient in Fig. 4.37 increased rapidly for approximately 100 days, and after 100 days it increased more gradually. The maximum creep coefficient was approximately 2.5.

The combined shrinkage and thermal strain was measured using cylinders stored next to the creep test. The average strain of the unloaded cylinders versus time is shown in Fig. 4.38. Large variations in this strain were created by changes in temperature and relative humidity. A temperature change of 50° F could cause the strain to change by as much as 300 microstrain. Throughout the year, temperature variations of this magnitude do occur. Such changes could account for the variation that appears in Fig. 4.38.

In an attempt to separate the thermal strain from the shrinkage strain, the average strain of the unloaded cylinders was adjusted using the variation of ambient temperature. This assumes the ambient and cylinder temperatures were equal. The coefficient of thermal expansion for concrete was assumed to be equal to 5.5 microstrain/° F. Strains were corrected assuming a base temperature of 93° F which was the ambient temperature when the cylinders were initially loaded.

Creep Coefficient vs Time Cylinders for Beams L-i1 & L-i2

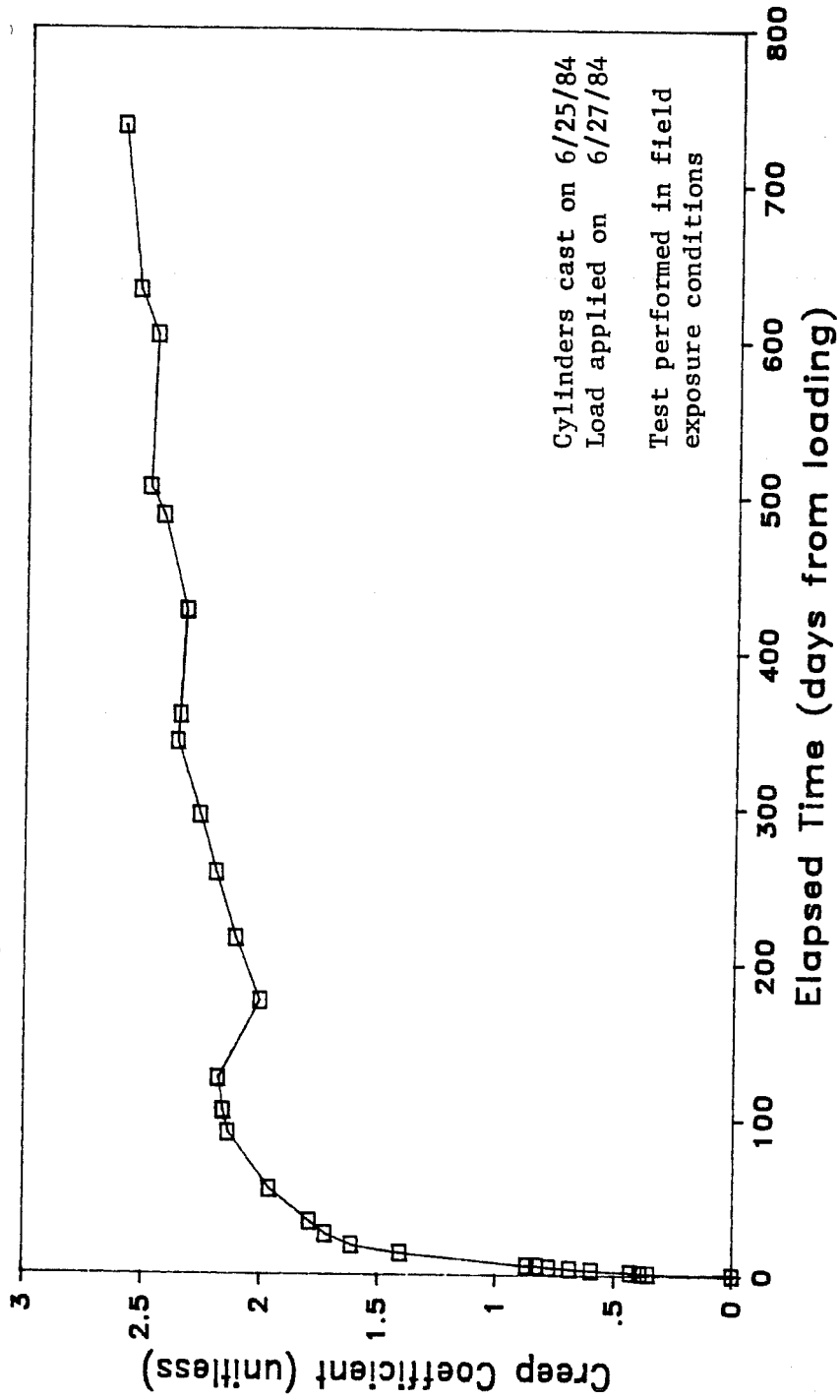


Fig. 4.37 Creep coefficient for cylinders corresponding to beams L-i1 and L-i2

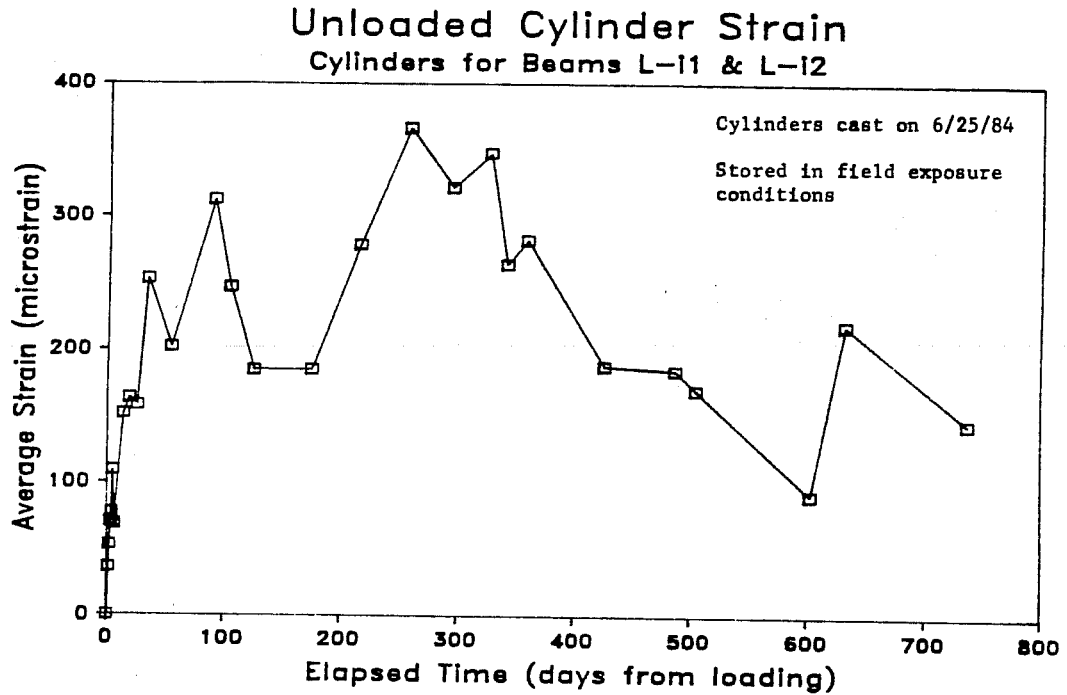


Fig. 4.38 Shrinkage and thermal strain of unloaded cylinders corresponding to beams L-11 and L-12

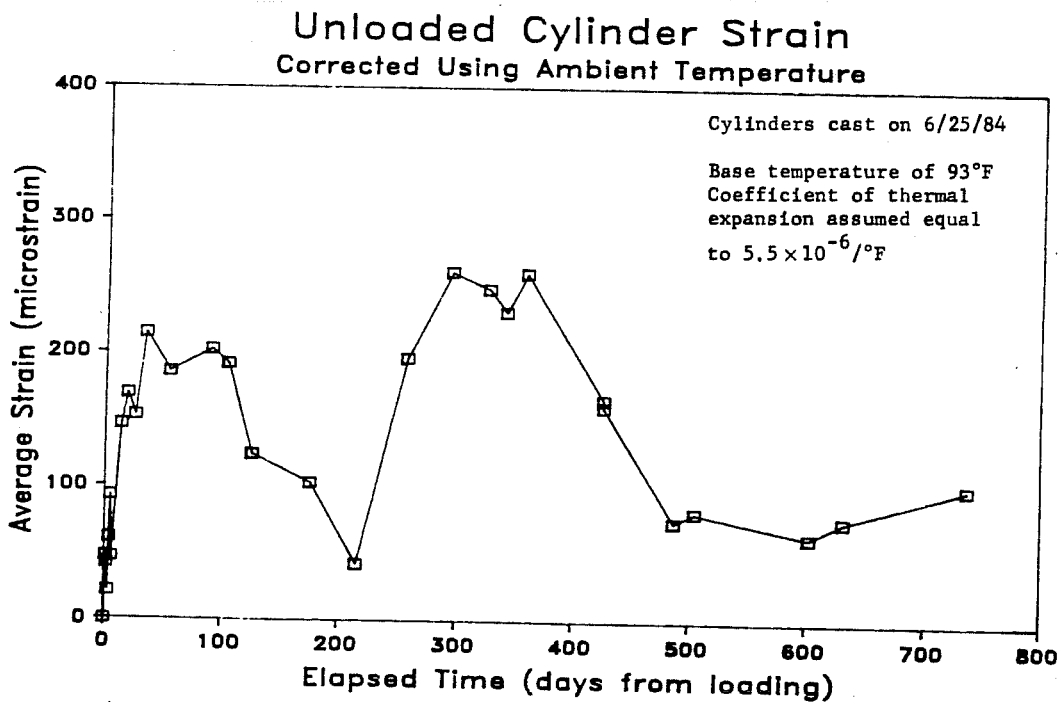


Fig. 4.39 Strain of unloaded cylinders corrected for thermal effects using changes of ambient temperatures

Creep Coefficient vs Time Cylinders for Beams H-01 & H-02

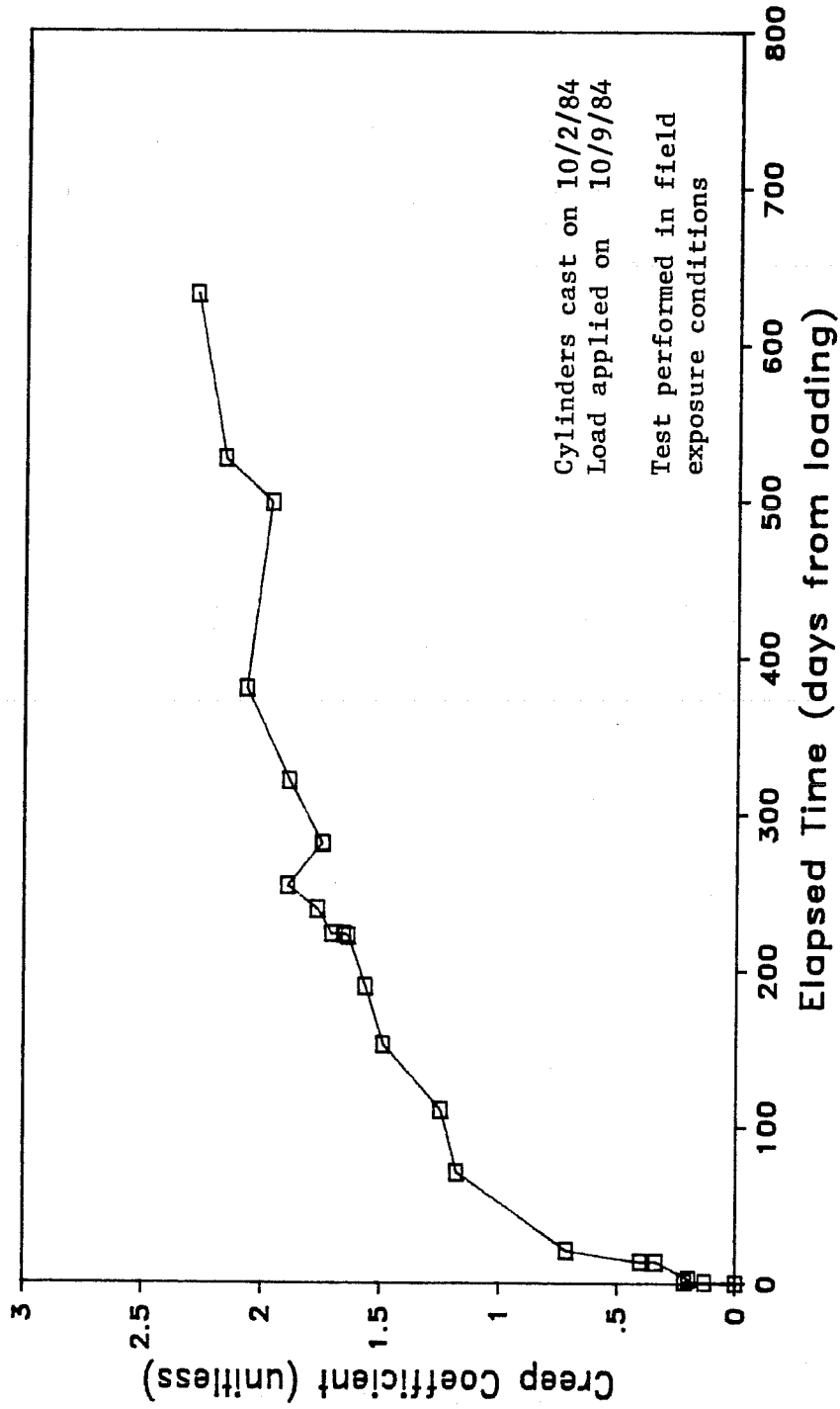


Fig. 4.40 Creep coefficient for cylinders corresponding to beams H-01 and H-02

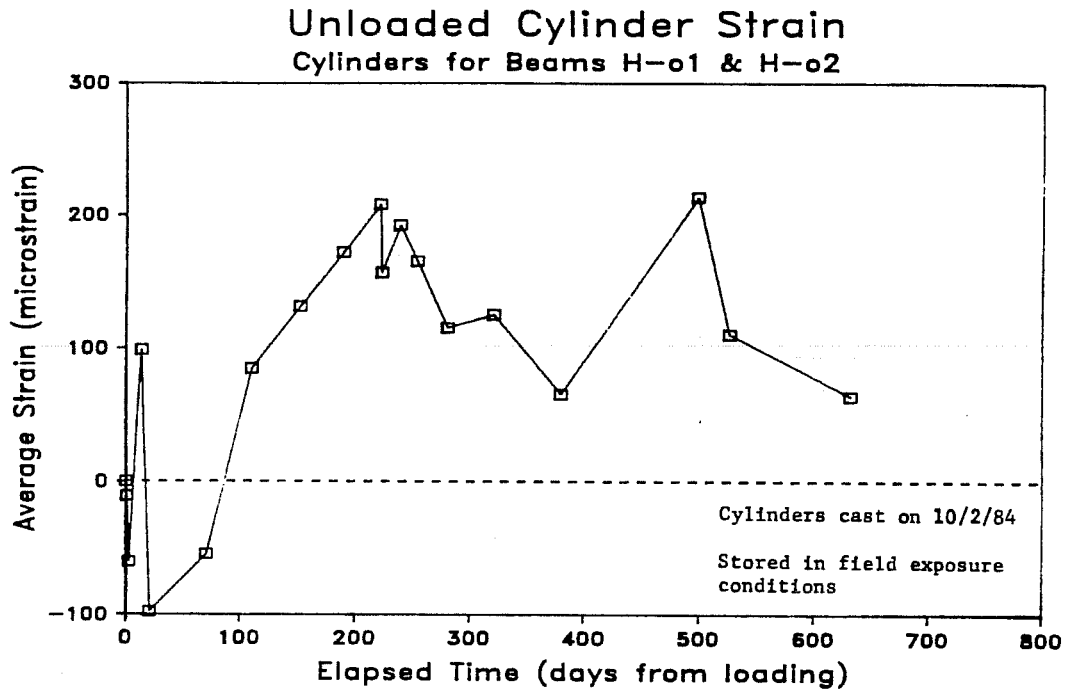


Fig. 4.41 Shrinkage and thermal strain of unloaded cylinders corresponding to beams H-01 and H-02

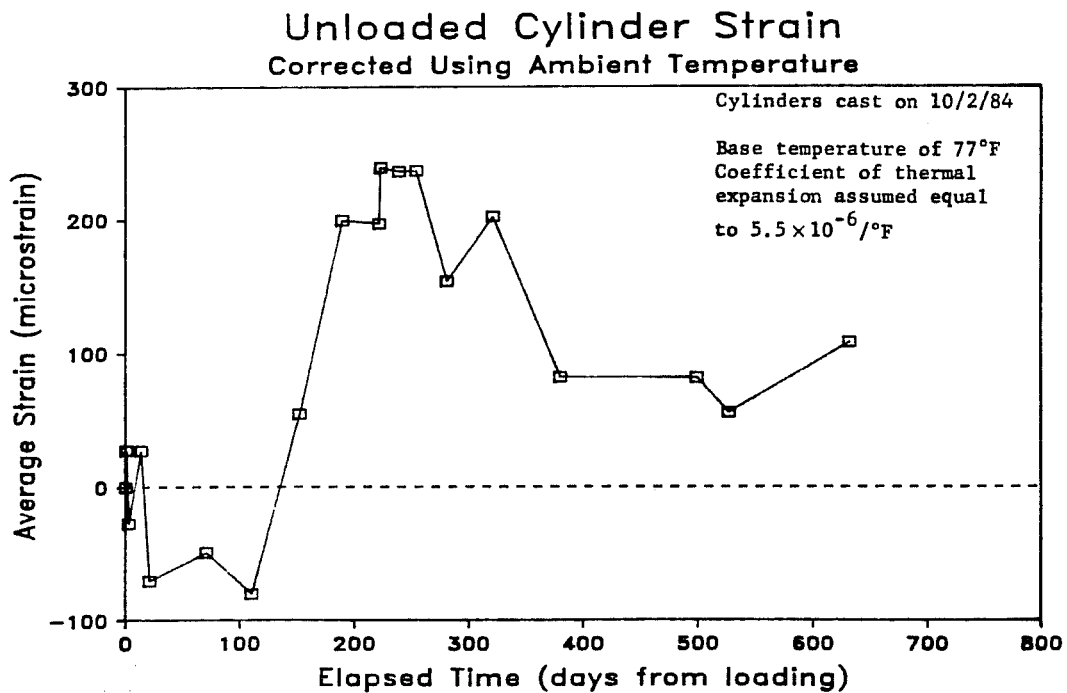


Fig. 4.42 Strain of unloaded cylinders corrected for thermal effects using changes of ambient temperatures

BEAM L-11

February 18, 1986
 Sunny
 Low of 52°F at 5 a.m.
 Base readings taken at 8:00 a.m.: 55°F High of 91°F at 2 p.m.

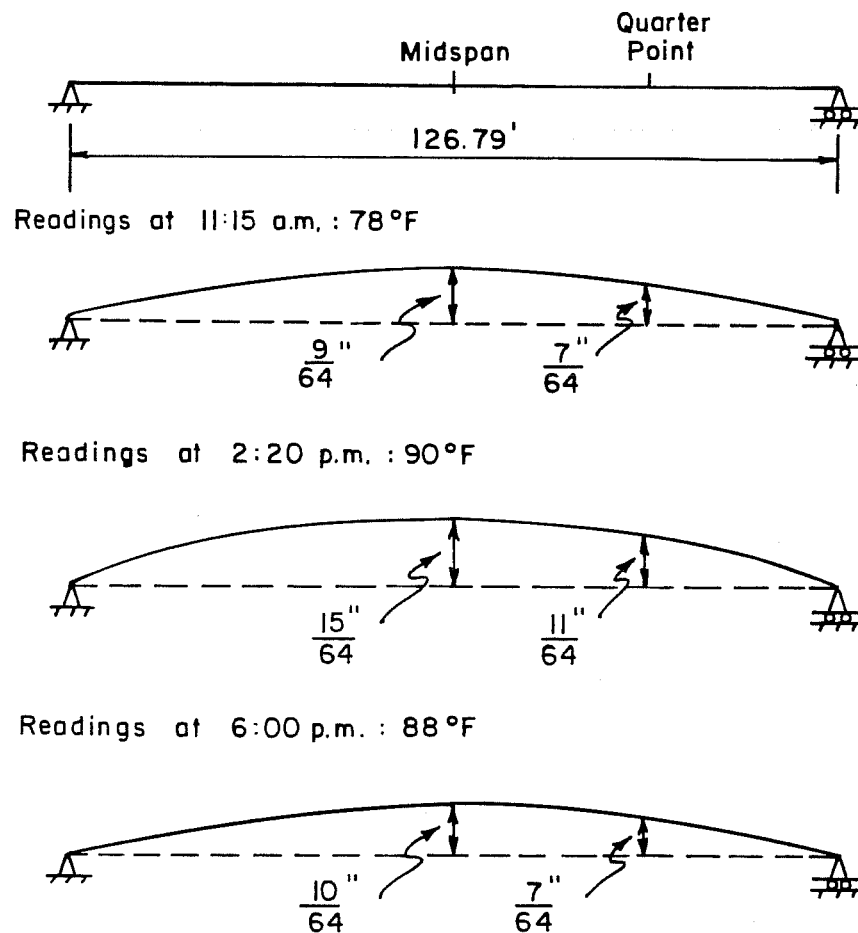
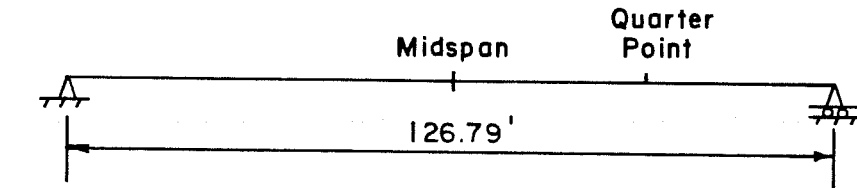
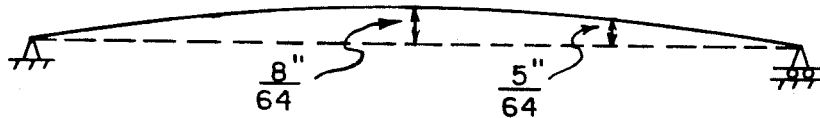


Fig. 4.43 Temperature induced camber in a composite beam on an unseasonably warm winter day

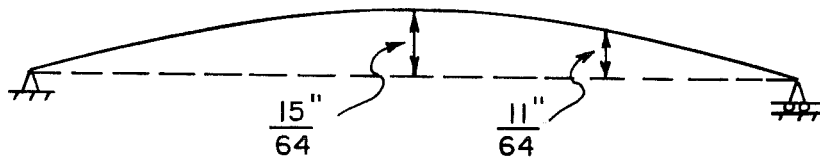
BEAM L-11
 February 22, 1986
 Sunny
 Low of 38°F at 5 a.m.
 Base readings taken at 8:00 a.m.: 41°F High of 64°F at 4 p.m.



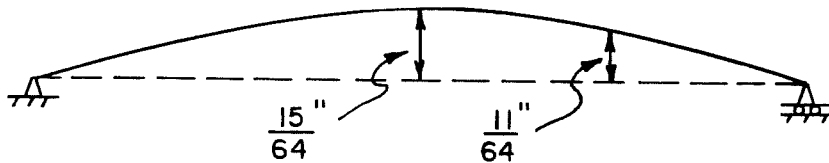
Readings at 11:15 a.m. : 46°F



Readings at 2:10 p.m. : 56°F



Readings at 4:10 p.m. : 63°F



Readings at 6:40 p.m. : 64°F

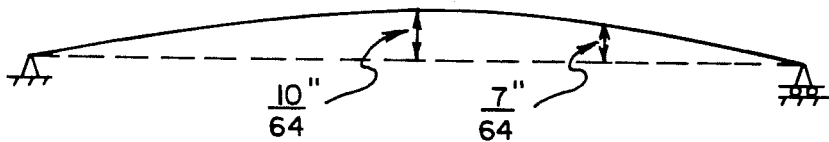


Fig. 4.44 Temperature induced camber in a composite beam on a sunny winter day

BEAM L-ii

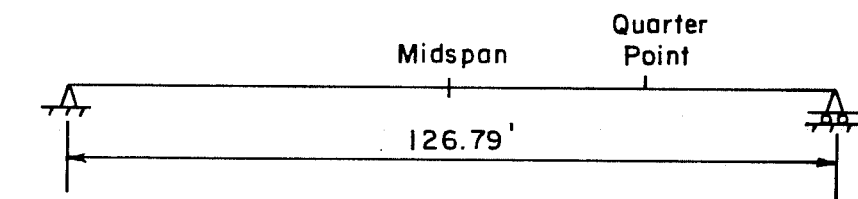
March 11, 1986

Overcast

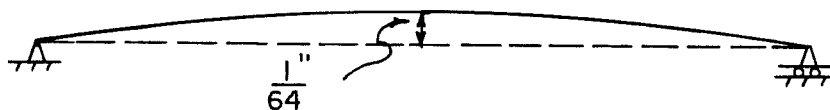
Low of 63°F at 12:01 a.m.

High of 76°F at 3 p.m.

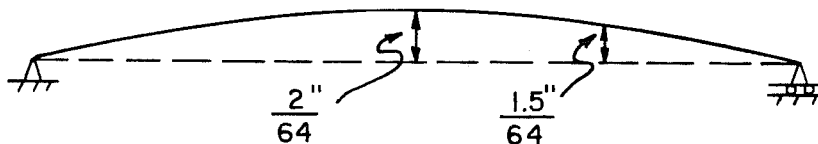
Base readings taken at 8:25 a.m. : 68°F



Readings at 11:20 a.m. : 72°F



Readings at 2:45 p.m. : 73°F



Readings at 5:45 p.m. : 74°F

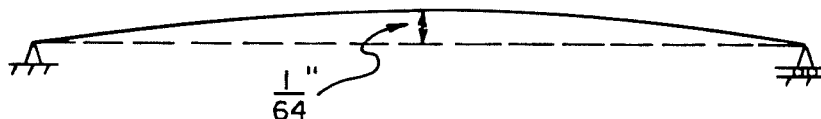


Fig. 4.45 Temperature induced camber in a composite beam on an overcast day

2/64 of an inch. The thermal camber during this day was less, because the temperature gradients were more uniform than the gradients on a sunny day.

4.5 Comparison of Observed Behavior

4.5.1 Creep Curves. The creep curves presented in Sec. 4.3.3 are compared in Fig. 4.46. The curve for cylinders corresponding to beams L-i1 and L-i2 has a higher creep coefficient and a steeper initial slope than the curve for cylinders corresponding to beams H-o1 and H-o2. The differences in the curves are caused by differences in the age at loading, the concrete compressive strength at loading, and the environment. In this section, the test performed using cylinders corresponding to beams L-i1 and L-i2 will be called Test 1, and the test performed using cylinders corresponding to beams H-o1 and H-o2 will be called Test 2.

The age at loading affects the magnitude of the creep coefficient at any given time. The cylinders used for Test 1 were loaded two days after they were cast, and the cylinders for Test 2 were loaded seven days after they were cast. If PCI creep factors for various ages of prestress [6] are applied to the results of Test 2, an equivalent creep coefficient, had the cylinders been loaded two days after being cast, can be estimated. The factor would be 1.18. When the maximum creep coefficient, 2.1, is multiplied by this factor, an equivalent maximum creep coefficient of 2.5 is obtained. This is equal to the maximum value obtained from Test 1.

Relative humidity and temperature affect the rate at which creep occurs [1]. Lower relative humidity and higher temperatures will cause a higher creep strain rate. The average relative humidity and temperature during the first 100 days of Test 1 were 59% and 81° F. This average relative humidity was significantly lower and the temperature higher than the equivalent values of 76% and 59° F for Test 2. The difference in slope of the curves shown in Fig. 4.46 during the first 100 days of each test reflects the effect that the environment had on the rate of creep. After 100 days, approximately 85% of the maximum creep strain had occurred in Test 1 compared to only 60% for Test 2.

After approximately 100 days, the slope of the curve for Test 1 is less than the slope of the curve for Test 2. At this time, Test 1 entered winter, a period of higher relative humidity and lower temperature. This resulted in a large reduction in the rate of creep strain. Test 2 was beginning to enter a period of lower relative humidity and higher temperature. Therefore, the strain rate did not reduce very much. Some reduction in the strain rate should be expected due to the nature of creep strain that occurs in environmentally controlled conditions.

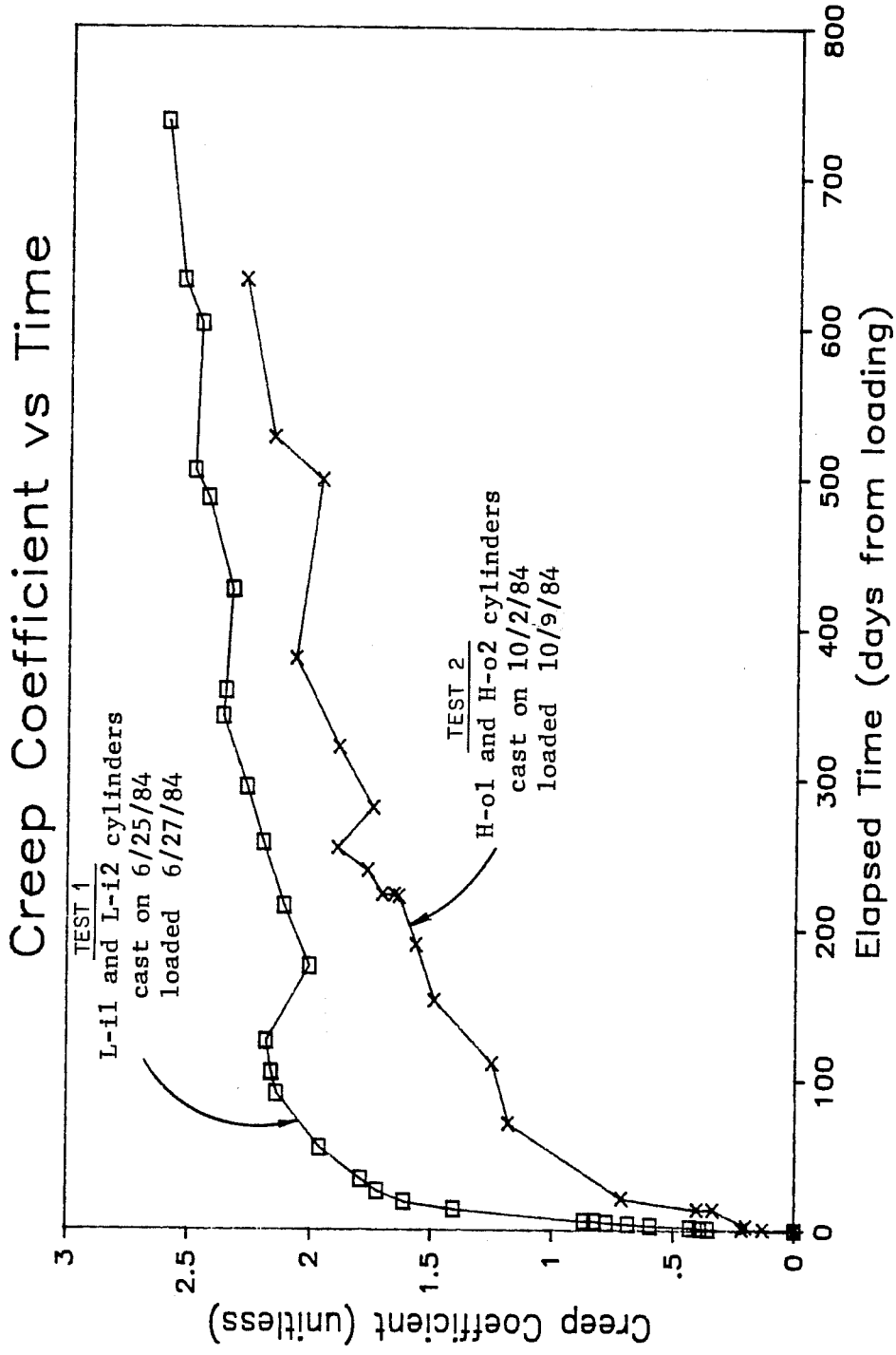


Fig. 4.46 Comparison of creep curves

As the tests continued through the seasons, fluctuations in the strain rates were caused by changes in the environment. However, after approximately one year only small increases in the maximum creep coefficient were observed.

4.5.2 L-Series Camber and Deflection Response. The camber and deflection responses of the L-series beams are shown together in Fig. 4.47. Differences in the shapes of the camber curves were discussed in Sec. 4.2.1. Differences in the magnitude of the responses are discussed in this section.

The initial midspan cambers, while still in the prestressing bed, were 1.89 and 1.71 in. for beams L-o1 and L-o2, respectively. Initial readings of beams L-i1 and L-i2 were not taken while in the prestressing bed. However, their initial support conditions in storage were very similar, span lengths of 118.4 and 118.2 ft, and so the initial readings in storage can be compared to each other. The initial midspan cambers were 2.81 and 2.66 in. for beams L-i1 and L-i2, respectively. For both sets of beams, the initial camber of the beam cast in casting position 1 of the prestressing bed had a higher initial camber. It is not understood why the beams in casting position 1 had the greater cambers. It may be related to the order in which the strands are depressed at the hold down points, or it may have just been a coincidence.

While in storage, the camber of all the beams grew similar amounts. Some of the difference in camber that occurred while in storage can be attributed to the difference in the support conditions. When first placed in the bridge, the midspan cambers were 3.91, 3.78, 4.05, and 3.76 in. for beams L-i1, L-i2, L-o1, and L-o2, respectively. As should be expected, beams L-i1 and L-o1 which had the greater initial cambers also had the greater cambers when placed in the bridge. The average camber for all L-series beams at this stage was 3.88 in. with a standard deviation of 0.13 in. and a range of 0.29 in. Considering the age of the beams at this stage, the difference in these readings are small.

The deflections caused by the weight of the deck panels and cast-in-place slab were 1.94 and 1.81 in. for beams L-i1 and L-i2. These deflections were determined using the difference between the last measurements before deck panels were added and the first measurements after the slab was cast. They include any time dependent deflection that occurred between the measurements. They may also include some error if there was a difference in the magnitudes of the thermal cambers when the measurements were taken. The deflection of beam L-i1 was most likely greater than that of beam L-i2 due to the time dependent effect caused by the additional half layer of deck panels that were stored on beam L-i1. However, there is only a 7% difference between these

Time Dependent Beam Camber L-series Beams

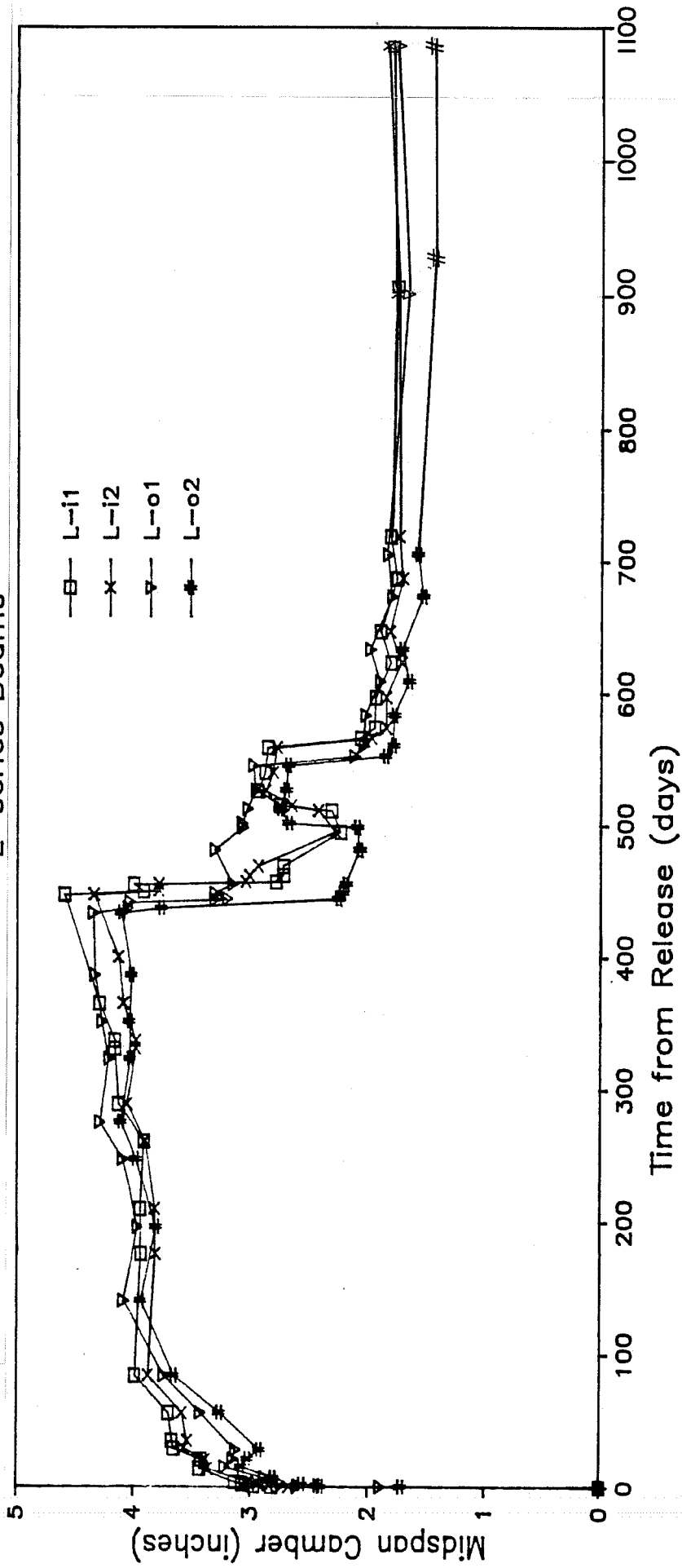


Fig. 4.47 Camber and deflection responses of the L-series beams

deflection values, and so the difference in time dependent effect must have been small.

Beams L-o1 and L-o2 each deflected downward 1.91 in. due to the weight of the deck panels and slab. The time dependent effect of temporarily storing the second layer of deck panels on top of beam L-o2 must have been very small. Because these beams were over 400 days old when the panels were placed on them, one should expect the time dependent effects to be small.

After the slab was cast, the behavior of the beams were similar. The average camber of the L-series beams was 2.0 in. just after the slab was cast. With time, each of these beams lost a small amount of camber. The average camber was 1.74 in. 153 days after the slab was cast.

4.5.3 H-Series Camber and Deflection Response. The time dependent camber and deflection responses of the H-series beams are shown in Fig. 4.48. There was a noticeable difference in the magnitude of the camber between the two pairs of beams. However, the responses of the beams cast on the same day were similar.

The initial midspan cambers, while in the prestressing bed, were 1.45, 1.33, 1.59, and 1.68 in. for beams H-o1, H-o2, H-i1, and H-i2, respectively. The average initial camber of beams H-o1 and H-o2, 1.39 in., was a quarter of an inch less than the average initial camber of 1.64 in. for beams H-i1 and H-i2. This difference in initial camber was most likely caused by a difference in the concrete stiffness at release. The average strength of cylinders tested just before release of the prestressing force was 6694 psi for beams H-o1 and H-o2 compared to only 5505 psi for beams H-i1 and H-i2. Because these beams were stiffer, their initial cambers were less. This illustrates the high sensitivity of prestressed members to release conditions.

While in storage, the camber of beams H-i1 and H-i2 grew significantly more than the camber of beams H-o1 and H-o2. When first placed in the bridge, the average camber of 3.01 in. for beams H-i1 and H-i2 was 0.53 in. greater than the average camber of 2.48 in. for beams H-o1 and H-o2. Less time dependent response occurred in beams H-o1 and H-o2 because the initial elastic camber was less. As mentioned in Sec. 4.3.3, creep is a function of the elastic strain multiplied by the creep coefficient. Because the elastic strain was less, the creep strain and time dependent camber were also less.

The deflections caused by the addition of the deck panels and the cast-in-place slab were 2.14, 1.93, 1.90, and 1.87 in. for beams H-o1, H-o2, H-i1, and H-i2, respectively. Beam H-o1 deflected the most, because the greatest volume of concrete was placed on top of it. Beam

Time Dependent Beam Camber H-series Beams

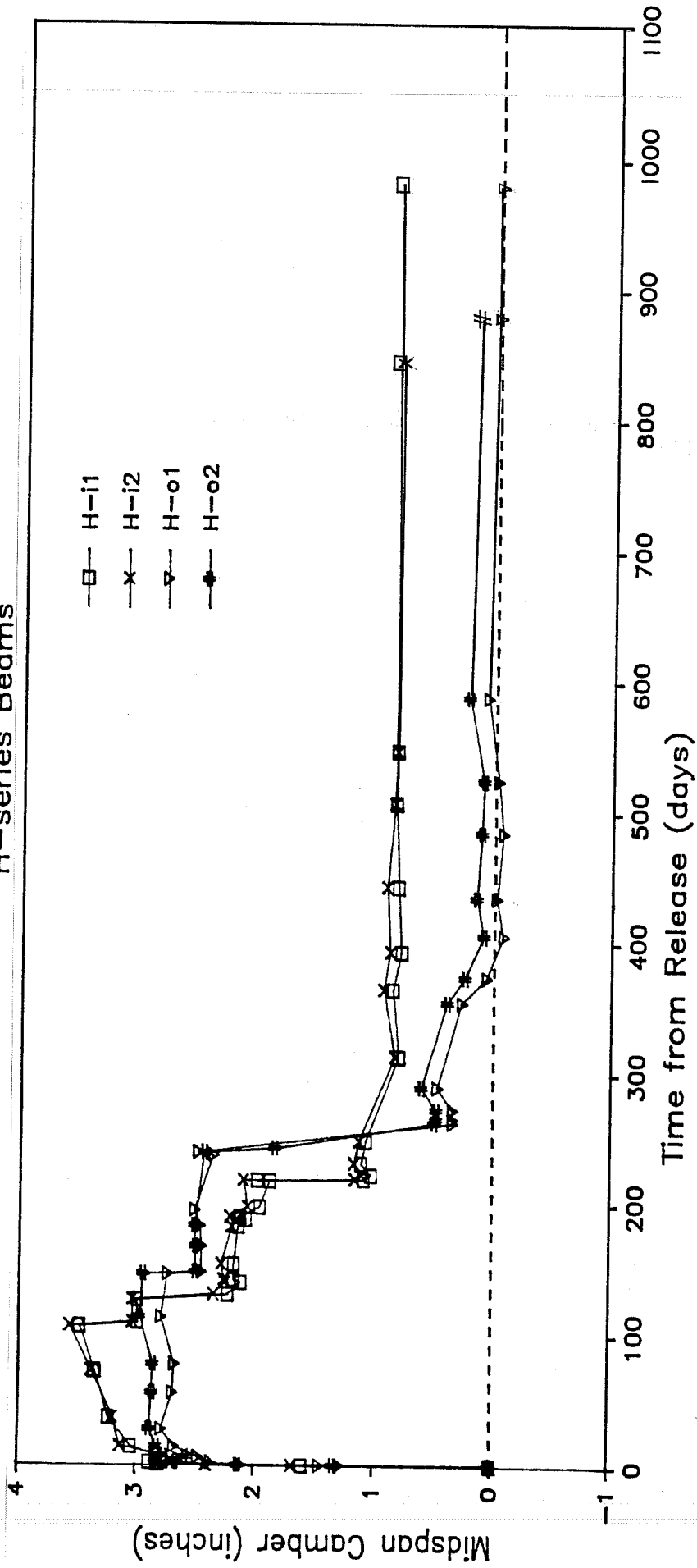


Fig. 4.48 Camber and deflection responses of the H-series beams

H-o1 had to support the weight of the slab overhang which extended 3 ft from the center of the beam to the edge of the slab. Therefore, beam H-o1 had to support a portion of the bridge deck which was 5.3 ft wide compared to only 4.6 ft for the other beams. The deflection of beam H-o2 was greater than those of beams H-i1 and H-i2, because the deck thickness was approximately $\frac{3}{4}$ of an inch thicker (see Table 3.4). The difference in the deflections of beams H-i1 and H-i2 was only 0.03 in. This difference is only about twice the $\frac{1}{64}$ in. accuracy of the measuring system. After the slab was cast, beams H-o1, H-o2, H-i1, and H-i2 had 0.35, 0.50, 1.09, and 1.16 in. of camber, respectively.

After the slab was cast all of the beams continued to deflect downward with time. The average camber of beams H-o1 and H-o2 was 0.15 in. 328 days after the slab was cast compared to 0.84 in. for beams H-i1 and H-i2. All of these beams lost approximately 0.28 in. of camber, even though beams H-o1 and H-o2 supported a greater portion of the weight of the traffic rail on the east side of the bridge.

4.5.4 L-Series vs H-Series Camber and Deflection Response. The time dependent camber and deflection responses of beams L-o1 and H-i2 are shown in Fig. 4.49. The responses of these beams were typical for their respective series. They are shown together in Fig. 4.49 so that comparisons of the responses for the two series can be seen.

Compared to the H-series beams, the L-series beams had a greater initial camber at release, they reached a greater maximum camber while in storage, and had a greater final camber after the slab was cast. These differences are shown in Fig. 4.49. These differences were caused primarily by differences in the magnitudes of the effective prestressing force, the initial stiffness, the length of time in storage, and the creep strains.

The average initial camber of beams L-o1 and L-o2 was approximately 0.3 in. greater than the average initial camber of the H-series beams. Differences in the effective prestress forces combined with differences in the strand eccentricity can account for approximately two-thirds of this difference. The other one-third can be accounted for by differences in the initial stiffness.

The initial upward camber is caused by the prestressing moment which at any point along the beam equals the effective prestress force multiplied by the strand eccentricity. Using the iteration method recommended by PCI [6], effective prestress forces immediately after release equal to 1378 and 1311 kips were calculated for beams L-o1 and H-i2, respectively. These forces were used to represent their respective series in using moment area equations to calculate initial prestress force cambers of 5.85 and 5.64 in. for the L- and H-series beams. These cambers are only the component of initial camber due to

Time Dependent Beam Camber

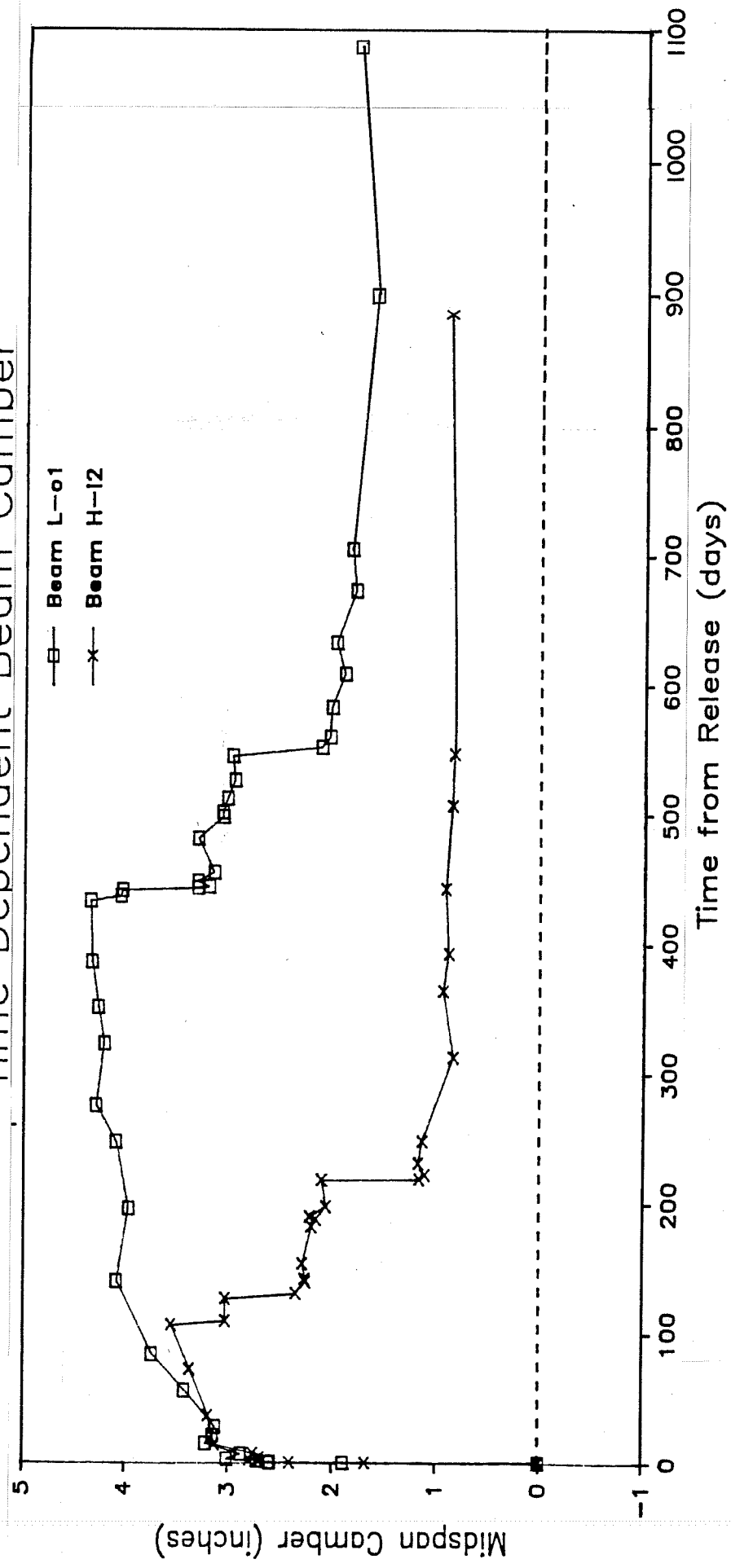


Fig. 4.49 Camber and deflection responses of typical L- and H-series beams

the prestressing force; they do not include the component of deflection caused by the weight of the beam. However, the beam weight deflection components calculated by moment area equations are equal, and so the difference of 0.21 in. in the prestress force camber components equals the difference that would be observed in the total initial camber. An average elastic modulus of 4500 ksi was used for the calculations, and so the initial stiffness did not enter into the comparison.

The average initial stiffness of the H-series beams was greater than that of the L-series beams. The average strength of cylinders for the H-series beams broken just before release was 6100 psi compared to an average cylinder strength of 5427 psi for beams L-01 and L-02. Elastic moduli equal to 4500 and 4245 ksi for the H- and L-series were calculated using the AASHTO formula for elastic modulus with these strengths and 145 pcf for the unit weight of concrete. Initial cambers equal to 1.56 and 1.88 in. for the H- and L-series beams were calculated using moment area equations with these moduli and the prestressing forces used above. Approximately 0.21 in. of the 0.32 in. difference in these initial cambers was caused by the difference in the prestressing force and strand eccentricity. The other 0.11 in. is caused by the difference in the initial elastic moduli (stiffness).

When first placed in the bridge, the average midspan camber of the L-series beams was more than 1.0 in. greater than the average camber of the H-series beams. This difference was caused primarily by the difference in the amount of creep strain that had occurred.

The creep strain equals the elastic strain multiplied by the creep coefficient. Therefore, it is a function of the concrete stresses applied by the prestressing force and beam weight along with the shape and magnitude of the creep coefficient curve. Since the effective prestressing forces acting on the L-series beams were greater than those acting on the H-series beams, greater creep strains and time dependent cambers were expected to occur in the L-series beams even if everything else had been equal.

Because the L-series beams remained in storage for a much longer period of time, a greater amount of creep had occurred. The average age of a L-series beam when first placed in the bridge was 443 days compared to only 129 days for the H-series beams. Using the creep curves in Fig. 4.46 to represent each series of beams, the creep coefficients when the beams were placed in the bridges were approximately 2.3 and 1.3 for the L- and H-series beams, respectively. As mentioned in Sec. 4.5.1, the creep coefficient for Test 2 must be multiplied by the age of loading correction factor 1.18 in order to compare it to the coefficient for Test 1. Therefore, the creep coefficient for the H-series beams should be 1.5. Because approximately 50%

more creep has occurred in the L-series beams at this stage, a greater amount of time dependent camber should be expected.

The average deflections caused by the weight of the deck panels and cast-in-place slab were very similar for both series of beams. The average deflection of the L-series beams was 1.89 in., and the average deflection of beams H-i1, H-i2, and H-o2 was 1.90 in. The difference in these deflections is less than the accuracy of the measuring system. The deflection of beam H-o1 was not included since it had to support a greater volume of concrete.

After the slabs were cast, all of the beams gradually lost some additional camber. At the time this report was written, the camber was decreasing only a very small amount if decreasing at all.

CHAPTER 5

ANALYTICAL TECHNIQUES AND RESULTS

5.1 General

In recent years, several analytical techniques for predicting the behavior of prestressed concrete members have been developed. These techniques vary in complexity from simple procedures which can easily be performed by hand, to complex computer programs which account for variables that would otherwise be difficult to include. However, the main objective of using each of these techniques is to estimate the magnitude of the prestress force loss, or the time dependent camber and deflection of a prestressed concrete member.

In each of the following sections, an analytical technique is presented, and the results obtained using the procedure are shown. At the end of each deflection predicting section, results for beams L-01 and H-12 predicted using that technique are compared to the measured responses. These beams were chosen as typical beams from the L- and H-series. The comparison gives the reader an idea of the accuracy of the technique. The results for the other beams compare favorably.

When comparing the results for an analytical technique to the measured response, all of the measured values were used in developing the shape of the curves. However, only point markers for measured camber immediately before and after an elastic response are shown. to minimize confusion when comparing the response to analytical results.

Subsequent to the completion of the study, the comprehensive work of Huang [49] on prediction of prestress losses was pointed out to the authors. This work had been examined in detail in connection with earlier phases of the project as reported in Ref. 21 and compared with the program PBEAM in Ref. 25. It was not felt necessary to reexamine it in detail in comparison with these girders. Huang's work was examined for applicability and sample calculations made to see if the present series could be interpreted and used for verification of Huang's procedure. Since the strain gages had yielded inconclusive loss measurements and since Huang's procedure predicts losses only, it was not possible to make a direct check. The procedure supported by Huang is too complex to check results without a major computer investigation and thus further checks were not feasible.

5.2 SDHPT's PSTRS10- Prestress Loss, Maximum Camber, and Slab Dead Load Deflection

PSTRS10 is a prestressed concrete beam design program used by the Texas SDHPT. This program was developed by Ingram and Butler [41] in 1970 and is periodically updated by the SDHPT. The program is used to design simply-supported I-shaped beams with normal relaxation stress-relieved strand.

When designing a beam, the program also predicts the percent prestress loss, the maximum camber, and the dead load deflection at the midspan and quarter points caused by the weight of the slab. As originally documented [41], the prestress loss and maximum camber were predicted by the hyperbolic function method developed by Sinno and Furr [26]. Periodic updatings have been made to the program. No input of time schedule is made in the program input.

PSTRS10 was used to design the L-series beams (the beams for the first span of the right main lane bridge). The results included predictions of a 26.59% prestress loss, a 3.25-in. maximum camber, and deflections of 1.73 and 1.24 in. at the midspan and quarter points caused by the weight of the slab.

The predicted loss of 26.59% is greater than what one would expect to occur in the actual beams. The loss should be less because low-relaxation strand was actually used rather than the normal relaxation stress-relieved strand assumed in the calculations. If low-relaxation strand had been assumed in the loss calculation, the predicted loss would be close to 20%. This is based on the results of the AASHTO and PCI Design Handbook procedures which will be presented in Sections 5.3 and 5.4.1.

The maximum camber prediction of 3.25 in. is significantly less than the average camber of 3.89 in. for the L-series beams measured just before the deck panels were placed on the beams. This can be accounted for in part by the greater prestressing force which remains acting in the beam, because low-relaxation strand was actually used.

The predicted midspan deflection of 1.73 in. caused by the weight of the slab (this calculation includes the deck panels as part of the slab) is greater than the average measured deflection of 1.58 in.

The difference between the predicted and measured deflections is best explained by the differences between the design and actual concrete strength and the change in deck thickness. The average measured concrete strength of the L-series beams was approximately 11,000 psi when the slab was cast. This is much greater than the assumed minimum design strength of only 6660 psi. To account for the difference

between actual and design strengths, the field engineer normally assumes the actual deflection will only be a portion of the deflection predicted by PSTRS10. This estimate may vary from 50% to 100% depending on the district involved with most districts using percentages in the 50% to 75% range. In the early 1960's field experience and actual measurements led to use of an estimate of 80%. Using this figure, the field engineer would have expected the beams to deflect 1.38 in. The measured deflections were greater than this value primarily because the actual deck thickness was greater than the design thickness. The average measured deck thickness was 7.88 in. compared to the design thickness of 7.25 in. used to predict the deflection.

PSTRS10 required alteration for use in designing beams made with low-relaxation prestressing strand. It did not predict the beam camber or deflection at the end of its service life. PSTRS10 was updated to PSTRS14 which uses the 1985 AASHTO Interim equation for estimating relaxation loss of low-relaxation strands. PSTRS14 gives the option of using either low- or normal-relaxation strands. Improvement in design predictions should be accompanied by development of comprehensive and rational field policies for predicting actual deflections to be expected considering updated material properties and construction schedules as the project progresses. Program CAMBER (described later in this report) allows such updating to be done on a microcomputer.

5.3 AASHTO - Prestress Losses

The American Association of State Highway and Transportation Officials has adopted a technique for calculating prestress loss [22,48] which can easily be performed without the aid of a computer. The total prestress loss includes components caused by elastic shortening, creep, shrinkage, and relaxation. The equations for the different components of loss were developed assuming the use of normal weight concrete and seven wire, normal relaxation stress-relieved prestressing strand. Recommendations for low-relaxation strand losses were added in the 1985 Interim Specifications [48]. A brief description of the procedure and prestress force losses calculated using the AASHTO Specifications are presented in this section.

The elastic shortening component of loss is a function of the concrete stress at the level of the prestressing steel center of gravity, and the modular ratio of prestressing steel to concrete during the transfer of prestressing force. The force in the strand immediately after transfer is assumed equal to 0.9 times the initial force for stress relieved strand and $0.92 (0.69 f'_s / 0.75 f'_s)$ for low relaxation strand. The initial elastic modulus of concrete is calculated using AASHTO's formula and the concrete strength at release.

The equation for the component of loss due to creep is a function of the concrete stress at the centroidal axis of the prestressing steel. It includes the concrete stress immediately after prestress force transfer and the additional stress caused by permanent dead load such as the composite slab. For an initial modular ratio of 6, this procedure applies an ultimate creep coefficient of 2.0 to the initial concrete strain just after release at the prestressing steel center of gravity. A smaller creep coefficient is applied to the strain caused by permanent dead load, because the beam is loaded at a later age. The loss caused by the permanent dead load should also be less, because the modular ratio becomes smaller as the concrete gets stronger.

The equation for the shrinkage component of loss is a function of only relative humidity. It does not account for different volume-to-surface ratios of members. The average annual relative humidity in Austin is approximately 65%. The resulting shrinkage strain is estimated to be 260 microstrain.

Until the 1985 AASHTO Interim Specification was published in 1986, the relaxation component of loss was specified assuming that normal relaxation stress-relieved strand, initially stressed to 0.70 times its guaranteed ultimate strength, would be used. The relaxation loss which would occur if the strain corresponding to the initial stress were maintained is reduced by fractions of the other components of loss. This reduction is made because the initial strand strain is reduced by the other components of loss.

In the 1985 AASHTO Interim Specification an equation for estimating the relaxation loss for low-relaxation strand is provided. However, that expression was not available when this investigation was actively underway. In order to calculate the relaxation loss for the beams under investigation, the generally similar relaxation loss equation which is part of the PCI Design Handbook [23] procedure for calculating loss was used.

Prestress losses were calculated for beams using: (1) design properties; (2) measured properties; (3) transformed sections; and, (4) the proposed elastic modulus formula for high strength concrete. Prestress loss was also calculated using stress-relieved strand along with the design properties for the L-series beams. Figures 5.1 and 5.2 show the losses predicted for the L-series and H-series beams, respectively. Except as noted in the figures, the losses were calculated using the minimum concrete release strength, the design slab thickness, low-relaxation strand, gross cross section properties, and the AASHTO formula for elastic modulus of concrete. The slab thickness is used to calculate the moment caused by the slab weight. Moments created by the beam and slab weight were calculated assuming the weight

AASHTO Prestress Losses L-series Beams

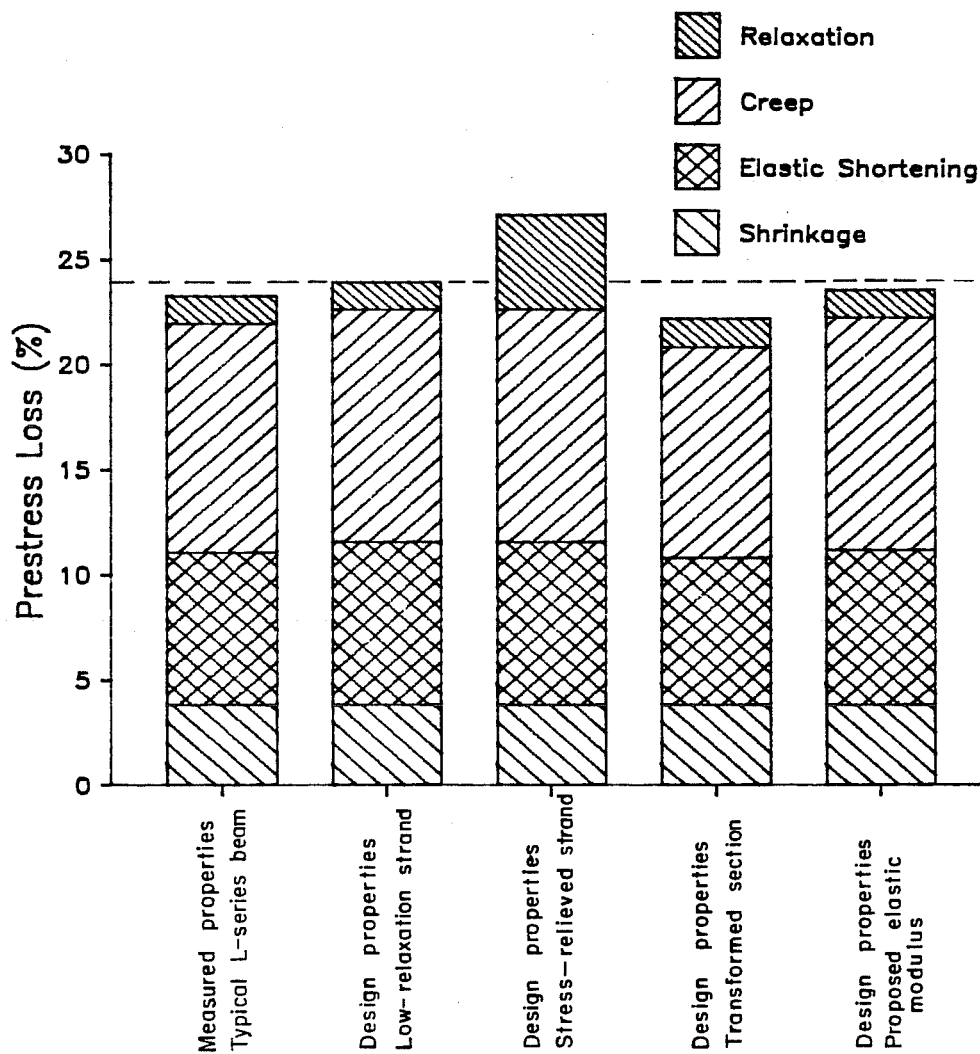


Fig. 5.1 Comparison of prestress losses for the L-series beams calculated using AASHTO specifications

AASHTO Prestress Losses H-series Beams

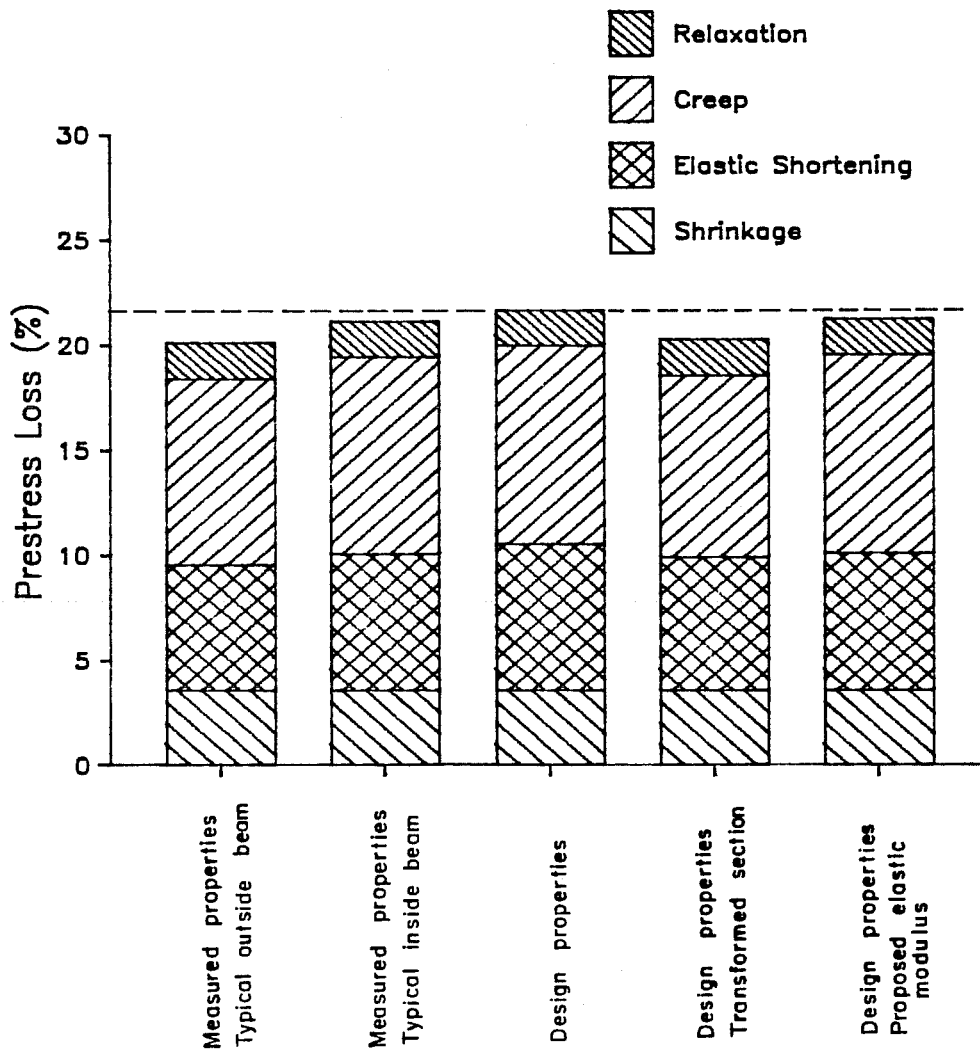


Fig. 5.2 Comparison of prestress losses for the H-series beams calculated using the AASHTO specifications

of reinforced concrete is equal to 150 pcf. The values for the design parameters are listed in Table 5.1.

The measured properties used to calculate the loss for the instrumented beams were the concrete strength at release and the slab thickness. Losses were calculated for beams L-o1 and L-o2, H-i1 and H-i2, and H-o2. The concrete strengths and moments created by the slab weight for these beams are listed in Table 5.2.

The cross section properties used to calculate the prestress losses using the transformed sections are listed in Table 5.3. The properties at 28 days were determined using 28-day concrete strengths of 7500 and 7200 psi for the L- and H-series beams, respectively. These values were used rather than the minimum 28-day design strengths, because the design strengths were unrealistically low. In general, the release strength is approximately 70% of the 28-day strength [42]. The 28-day strengths were determined using this percentage and the minimum release strengths.

The elastic modulus formula for high strength concrete which was presented in Sec. 4.3, along with the other design parameters, was used to calculate the prestress loss. The initial elastic moduli used were 4400 and 4340 ksi for the L- and H-series beams, respectively. The 28-day elastic moduli used were 4960 and 4890 ksi.

As shown in Fig. 5.1, the total losses calculated for the L-series beams are all between 22 and 27.1%. The loss calculated using the gross section design properties assuming low-relaxation strand was 24% (42.2 ksi). This included losses of 3.8% (7.2 ksi), 7.7% (14.6 ksi), 11.1% (20.9 ksi), and 1.3% (2.5 ksi) due to shrinkage, elastic shortening, creep, and relaxation, respectively. Based on these results, creep and elastic shortening have the greatest effect on the total loss. These values are used as a base to which the other calculated loss values are compared.

The use of measured concrete strength and slab thickness reduced the calculated loss only a small amount as shown in Fig. 5.1. The elastic shortening and creep components of loss were each reduced but the amount of reduction is insignificant.

The use of the proposed formula for elastic modulus of high strength concrete also had only a minor effect on the loss prediction. The effect was small because at the transfer concrete strength, 5270 psi, the value for the initial elastic modulus of the concrete was only increased from 4180 to 4400 ksi. This caused a small reduction in the elastic shortening loss, but at the same time it also increased the creep loss. The net result was a reduction of less than 0.4% prestress loss.

TABLE 5.1 Design Values Used to Calculate Prestress Loss

Parameter	L-Series	H-Series
Release Strength (psi)	5270	5025
Initial Elastic Modulus (ksi)	4180	4080
Initial Force (kips)	1504	1425
Eccentricity of Prestressing Steel (in.)	19.29	19.79
Gross Moment of Inertia (in. ⁴)	260,403	260,403
Moment Caused by Beam Weight (in.K)	19,790	19,790
Moment Caused by Slab weight (in.K)	10,280	10,280

TABLE 5.2 Parameters Used to Calculate Prestress Losses for Instrumented Beams

Beams	Concrete Release Strength (psi)	Moment Caused by Slab Wt (in.K)
L-01 and L-02	6010	10,970
H-i1 and H-i2	5765	10,625
H-02	6820	11,660

TABLE 5.3 Transformed Cross Section Properties
Used to Calculate Prestress Loss

Property	L-Series Design Beam	H-Series Design Beam
Area (in. ²)	870	867
Moment of Inertia at Release (in. ⁴)	304,420	304,370
Eccentricity at Release (in.)	19.43	20.03
Moment of Inertia at 28 days (in. ⁴)	296,000	296,000
Eccentricity at 28 days (in.)	19.41	19.99

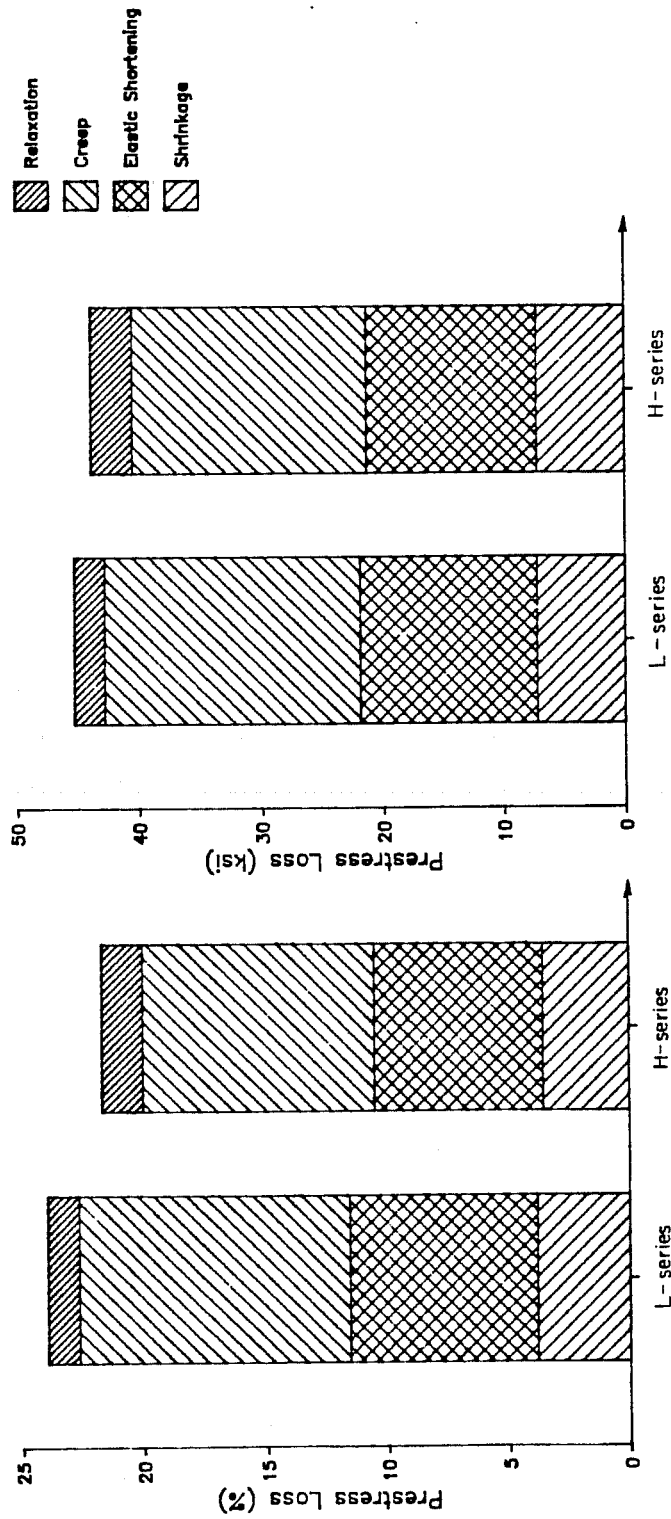
The prestress loss calculated assuming the use of normal relaxation stress-relieved strand was 27.1% (51 ksi). The percentage prestress loss due to relaxation was 4.5% (8.5 ksi) for stress-relieved strand compared to 1.3% (2.5 ksi) for low-relaxation strand.

Using transformed rather than gross cross sectional properties resulted in a lower total prestress loss (22.2%). This was calculated using a prestress force immediately after release equal to 0.90 times the initial force. The transformed moment of inertia was approximately 15% greater than the gross moment of inertia. The greater moment of inertia caused a reduction in the concrete stress at the prestressing steel center of gravity. The reduced stress resulted in smaller elastic shortening (7.0%) and creep (10.0%) losses. Had an exact solution been used to calculate the force immediately after release, a force greater than 0.90 times the initial force would have been obtained. This would increase the loss due to creep, and so the total loss would be closer to that calculated using gross section properties.

Similar calculated losses for the H-series beams are shown in Fig. 5.2. The total prestress loss calculated using the gross section design properties assuming low-relaxation strand was 21.7% (43.9 ksi). This loss included components of 3.6% (7.2 ksi), 7.0% (14.1 ksi), 9.5% (19.2 ksi), and 1.7% (3.4 ksi) due to shrinkage, elastic shortening, creep, and relaxation, respectively. The calculated losses for the other cases shown in Fig. 5.2 varied as did those of the L-series.

Figure 5.3 is a comparison of prestress losses for the L- and H-series beams calculated using gross section design properties. The total loss for the L-series beam is 24.0% (45.2 ksi) compared to 21.7% (43.9 ksi) for the H-series beam. The L-series beam has larger elastic shortening and creep losses which are caused by the higher initial concrete stress at the level of prestressing strand. The greater relaxation loss for the H-series beam occurs because the strand was initially tensioned to a higher stress level.

Although there is little difference in the total stress lost between the L- and H-series design beams as shown in Fig. 5.3b, the difference in percentage loss is significant. The percentage loss for the H-series beam is less than that of the L-series beam, because the strands were initially tensioned to a higher stress level. Therefore, the H-series beams will retain a greater percentage of the initial prestress force throughout the service life of the bridges.



a. Comparison using percent loss b. Comparison using stress loss (ksi)

Fig. 5.3 Comparison of prestress losses for the L- and H-series design beams calculated using the AASHTO specifications

5.4 PCI Design Handbook--Prestress Loss, Elastic Cambers and Deflections, and Longtime Camber or Deflection

5.4.1 Prestress Loss. The procedure for calculating prestress loss provided in the PCI Design Handbook [23] was taken from "Estimating Prestress Losses" [43]. This procedure considers the initial stress level, stress caused by the permanent dead load, type of strand, environmental conditions, and member shape in its equations for calculating components of loss. The concepts used to calculate loss are similar to those used by AASHTO. These concepts were discussed in Sec. 5.3. Variations from these concepts are discussed below.

In calculating the component of loss due to shrinkage, both the average relative humidity and member shape are considered. The member shape is considered by using the volume-to-surface ratio of the member. For an AASHTO type IV beam stored in 65% relative humidity, the shrinkage strain applied to the beam concrete is approximately 210 microstrain.

In calculating the loss due to creep, a creep coefficient of 2.0 is applied. The same creep coefficient is applied to the initial stress and the stress caused by permanent dead load. The equation does not account for the difference in the age of the concrete when these stresses are first applied.

As mentioned in Sec. 5.3, the equation for calculating the loss due to relaxation accounts for different types of prestressing steel. This includes both stress-relieved and low-relaxation strand. The equation also works for any initial stress level in the prestressing steel.

The calculated losses for the L-series beams are shown in Fig. 5.4. These losses were calculated using the same values that were used with the AASHTO procedure. The values of applicable parameters appear in Tables 5.1 to 5.3. The total loss for the case in which only gross section design properties along with low-relaxation strand were used was 20.6% (39.0 ksi). This consists of a 3.0% (5.7 ksi) shrinkage loss, a 7.7% (14.6 ksi) elastic shortening loss, an 8.4% (16.0 ksi) creep loss, and a 1.4% (2.7 ksi) relaxation loss. These loss values are used as a base to which the other calculated losses are compared.

The use of measured (greater) concrete strength increases the modulus and of measured (greater) slab thickness increases the dead load moment. Both tend to reduce the total loss. As shown in Fig. 5.4, the use of stress-relieved strand rather than low-relaxation strand caused the greatest change in calculated loss. The total loss was increased from 20.6 to 26.9%. The relaxation loss increased from 1.4 to 7.7%.

PCI Prestress Losses L-series Beams

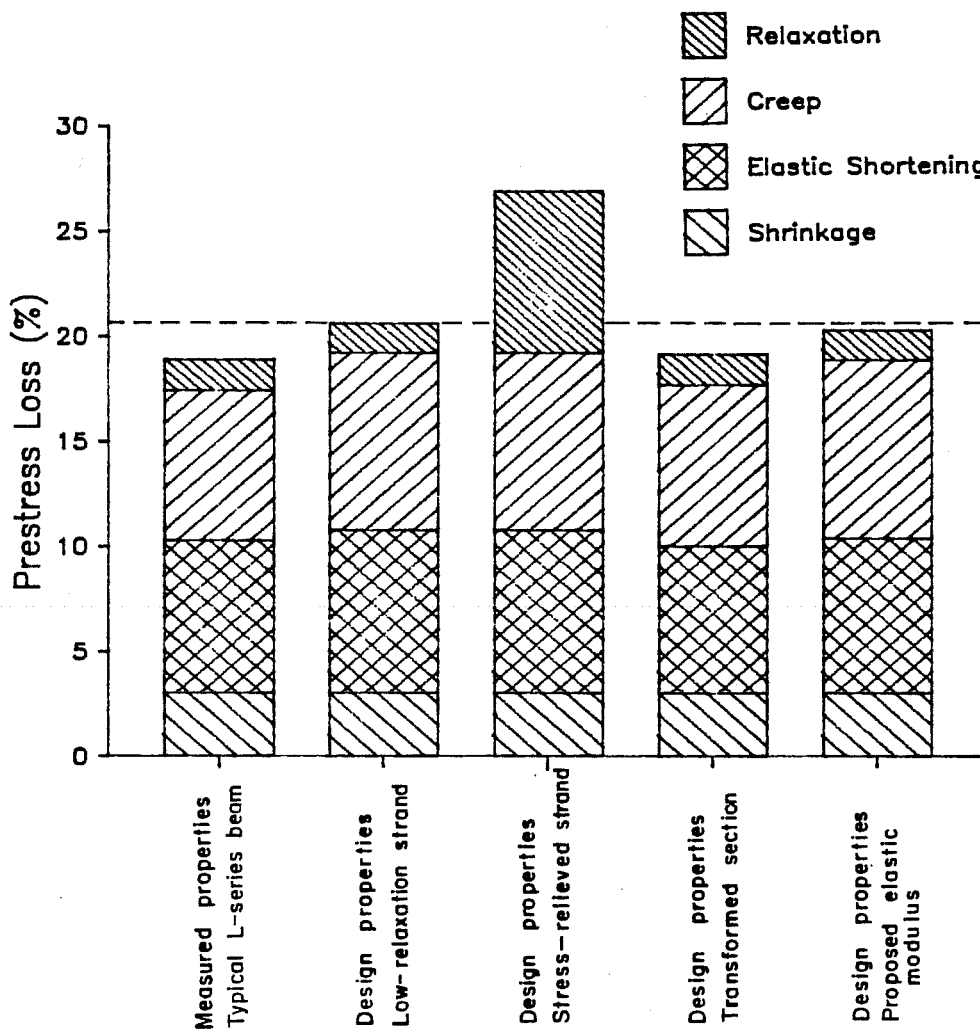


Fig. 5.4 Comparison of prestress losses for the L-series beams calculated using the PCI Design Handbook (1985)

The use of the transformed section or the proposed formula for high strength concrete had little affect on the total loss. In both cases the loss was reduced a small amount, because the stiffness of the beam was increased.

Similar calculated losses for the H-series beams are shown in Fig. 5.5. The total calculated loss using gross section design properties was 18.8% (16.4 ksi). This included a 2.8% (5.7 ksi) shrinkage loss, a 7.0% (14.1 ksi) elastic shortening loss, a 7.2% (14.6 ksi) creep loss, and a 1.8% (3.6 ksi) relaxation loss. The calculated losses for variations from the design properties were affected in the same manner in which the comparable cases for the L-series beams were affected.

The losses for the L- and H-series beams calculated using gross section design properties and low-relaxation strand are compared in Fig. 5.6. Although the H-series beam lost only 1.0 ksi less stress than the L-series beam, the difference in percentage prestress lost was 1.8% less. The greater difference in percent loss is a result of the higher initial prestressing strand stress for the H-series design beam. The smaller elastic shortening and creep losses for the H-series beam is a result of the lower total initial prestress force in the strands (1425 kips compared to 1504 kips). The calculated relaxation loss for the H-series beam is greater than that of the L-series beam, because the strand was initially tensioned to a greater stress.

5.4.2 Elastic Camber and Deflection. The PCI Design Handbook equations for initial camber and elastic deflections were derived using conventional moment-area equations. The equation for midspan initial camber caused by the prestressing force of a beam with a two point depressed strand pattern is shown in Fig. 5.7. The beams under investigation have this type of strand pattern. P_0 is the force in the prestressing strand immediately after transfer. This is normally taken to be 0.9 times the initial force in the strand. The equation for midspan deflection caused by a uniformly distributed load, such as the weight of the beam, also appears in this figure.

Elastic camber and deflections were calculated using both design and measured properties. Gross section properties and a 126.79-ft beam length were used for all calculations. The AASHTO formula elastic moduli used for the calculations are provided in Table 5.4. The elastic moduli for the nominal or design beams were calculated using the specified minimum compressive strength at release, and a 28-day strength which is 43% greater than the release strength (i.e. the release strength is 70% of the 28-day strength). Measured concrete strengths were used to calculate the moduli for each actual set of beams. Drapage points located 7 ft-5 in. on each side of the beam center line were used to calculate the initial response of the nominal or design beams.

PCI Prestress Losses H-series Beams

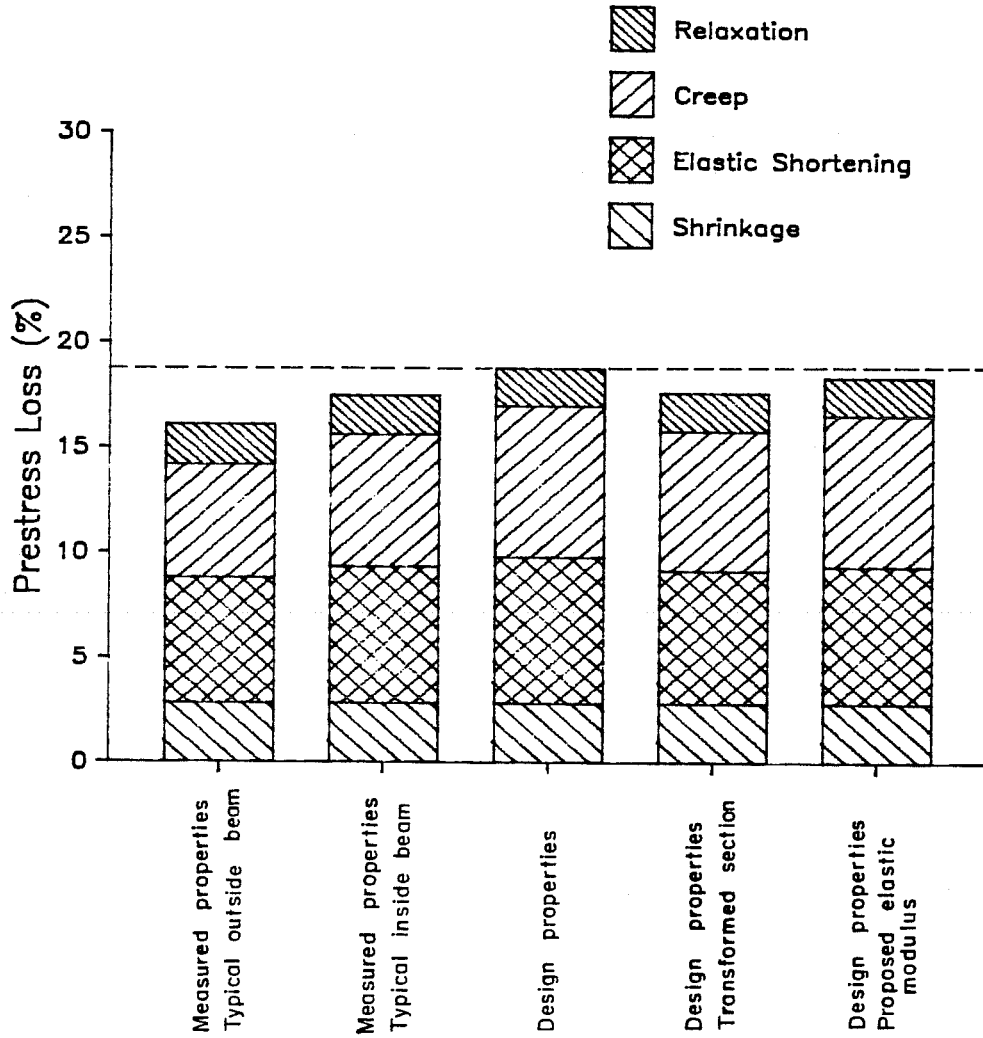
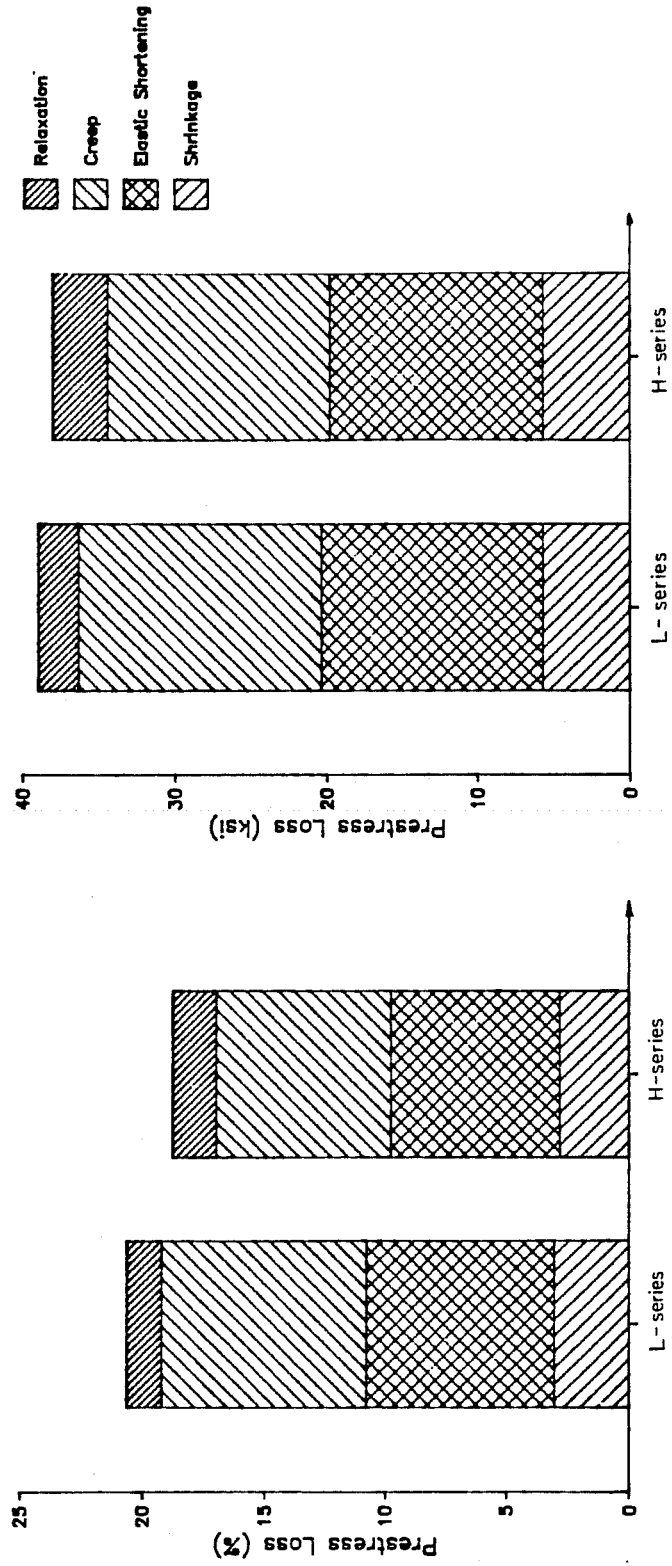
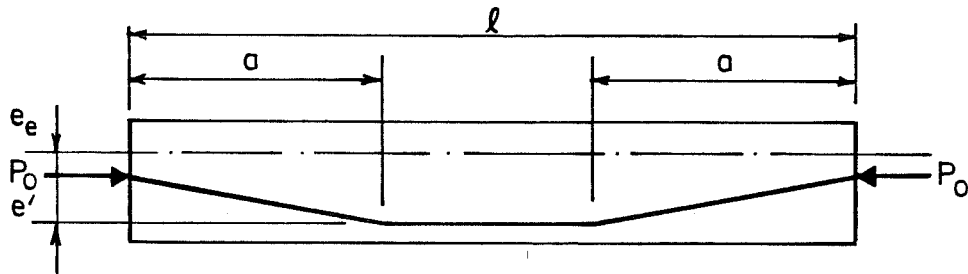


Fig. 5.5 Comparison of prestress losses for the H-series beams calculated using the PCI Design Handbook (1985)



a. Comparison using percent loss b. Comparison using stress loss (ksi)

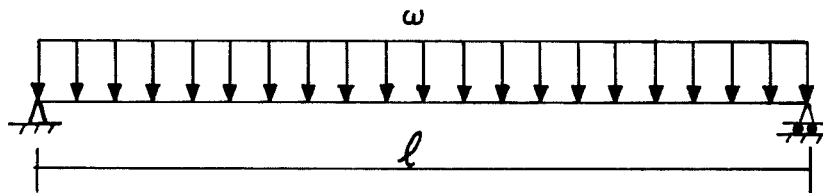
Fig. 5.6 Comparison of prestress losses for the L- and H-series design beams calculated using the PCI Design Handbook (1985)



Two point depressed

$$\Delta \uparrow = \frac{P_0 e_e l^2}{8EI} + \frac{P_0 e'}{EI} \left(\frac{l^2}{8} - \frac{a^2}{6} \right)$$

a. Midspan camber caused by prestressing force



$$\Delta \downarrow = \frac{5 w l^4}{384EI}$$

b. Midspan deflection caused by beam weight

Fig. 5.7 Initial response at midspan of a beam with a two-point depressed strand pattern

TABLE 5.4 Concrete Elastic Moduli (ksi) Used to Calculate Elastic Response

Event	B e a m					
	L-design	L-i1 L-i2	L-o1 L-o2	H-design	H-o1 H-o2	H-i1 H-i2
Release	4180	4250	4470	4080	4760	4370
Erection	5000	5770	6170	4880	5900	5700
Panels Added	5000	5770	6170	4880	5970	5710
Panels Removed	5000	5770	6260	4880		
Slab Cast	5000	5770	6280	4880	5970	5760
Rail Cast	5000			4880	6310	
ACP Overlay Added	5000	5780	6280	4880	6310	6040

Nominal design dimensions were used to calculate the weight of the deck panels and the cast-in-place slab for the nominal or design beams. Measured drapeline point locations and slab thickness were used to calculate the response of the instrumented beams.

The calculated elastic responses for the design and instrumented beams are shown in Table 5.5. The response is given for both components of the initial camber, the addition of deck panels, the removal of deck panels that were stacked on the beams, the addition of the cast-in-place slab, the addition of the asphaltic concrete pavement overlay, and casting of the east rail for the right main lane bridge.

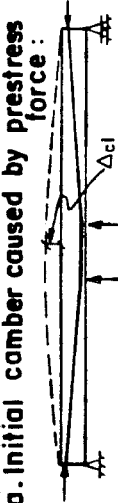
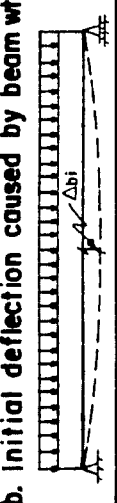
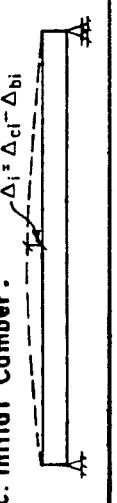
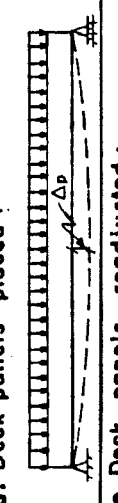
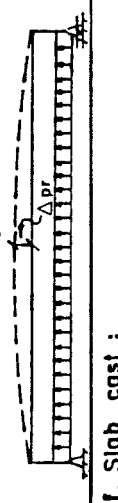
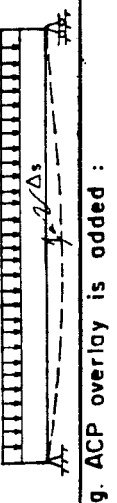
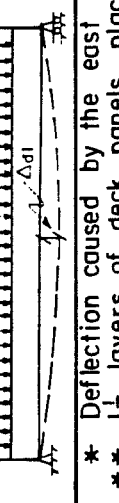
The calculated initial camber varied from a minimum of 1.37 in. for beams H-o1 and H-o2 to a maximum of 1.80 in. for the L-series design beam. The net initial cambers were small compared to the sum of the absolute values of the components. For example, the sum of the absolute value of the components was 10.58 in. for the L-series design beam and 9.09 in. for beams H-o1 and H-o2.

The deflection caused by placing panels on the beams varied from 0.35 in. for H-o1 to 1.36 in. for L-o2. The deflection for beam H-o1 is low because only half a layer of deck panels was placed on it. The deflection for beam L-o2 was high because two layers of deck panels were placed on it. The average calculated deflection caused by one layer of panels was 0.71 in. for the instrumented beams compared to 0.85 in. for the design beams. This difference is caused by the difference in strengths of concrete, and thus elastic moduli, at the time the panels were placed on the beams. The average measured strength for the instrumented beams was 10,500 psi which is 43% greater than the average strength of 7350 psi for the nominal design beams.

The calculated deflection caused by the weight of the cast-in-place slab varied from a minimum of 0.96 in. for beams L-o1 and L-o2 to a maximum of 1.61 in. for beam H-o1. The deflection for beam H-o1 is significantly greater than the deflection for the other beams, because the deck above this beam included an overhang and only a half layer of panels rather than a full layer.

The average deflection caused by the cast-in-place slab was 1.03 in. for the instrumented beams excluding beam H-o1. This is only 5% lower than the average deflection of 1.08 in. for the design beams. This percentage difference is misleading. Because the average concrete strength of 10,660 psi was 45% greater than the average strength for the design beams, one would expect a difference of approximately 20% for the calculated deflections. However, the average slab thickness measured from the top of the panels to the top of the slab was 3.8 in. compared to the design thickness of 3.25 in. The greater average slab thickness increases the calculated deflection by approximately 15%. Therefore,

TABLE 5.5 Elastic Response Calculated using the PCI Design Handbook Moment Area Equations

Event	Beam						H-i1	
	L-Design L-i1	L-i2	L-o1	L-o2	H-Design H-o1	H-o2	H-i2	H-i2
a. Initial camber caused by prestress force : 	6.19	6.08	5.78	5.78	6.09	5.23	5.23	5.67
b. Initial deflection caused by beam wt. 	4.39	4.32	4.11	4.11	4.50	3.86	3.86	4.20
c. Initial Camber : $\Delta_i = \Delta_{cl} - \Delta_{bi}$ 	1.80	1.76	1.67	1.67	1.59	1.37	1.37	1.47
d. Deck panels placed : 	0.84	**	1.10	0.73	0.68	0.86	**	0.73
e. Deck panels readjusted : 		0.37		0.67				
f. Slab cast : 	1.07	1.10	0.96	0.96	1.10	1.61	1.11	0.99
g. ACP overlay is added : 	0.21	0.19	0.18	0.18	0.21	0.27*	0.14*	0.18

* Deflection caused by the east rail in the LML bridge.
 ** 1 1/2 layers of deck panels placed on L-i1, 2 layers on L-o2, and 1/2 on H-o1

the average calculated deflection for the instrumented beams should be approximately 5% less than the deflection for the design beams.

The calculated deflections for beams H-o1 and H-o2 caused by the weight of the traffic rail were 0.27 and 0.14 in., respectively. These deflections were calculated assuming 50% of the weight of the rail was carried by beam H-o1 and 25% by beam H-o2. These load distributions were determined using Alani's research [44] as a guideline.

The average calculated deflection caused by the weight of the asphaltic concrete pavement was 0.18 in. for the instrumented beams. This was calculated using a composite beam moment of inertia equal to 542,000 in.⁴ The deflection for the instrumented beams is once again less than that of the design beams because the concrete strength is greater.

The measured and calculated initial camber and deflections caused by the weight of panels and the cast-in-place slab for beams L-o1 and H-i2 are compared in Table 5.6. Differences between the measured and calculated values are caused by differences in assumed and actual values for properties such as elastic moduli, moment of inertia, and strand eccentricity, as well as the value for the force left in the strand immediately after prestress force transfer. Thermal movements also introduce error into the measured responses.

The measured initial camber is approximately 0.2 in. greater than the calculated initial camber for both beams. The probable reason that the measured camber was greater than the calculated camber is the force in the strand immediately after transfer was probably greater than 0.9 times the initial force which was used to calculate the initial camber. If the force in the strand immediately after transfer is determined by the iterative method used for design example 2 in "Recommendations for Estimating Prestress Losses" [6], forces equal to 0.916 and 0.920 times the initial force would be obtained for beams L-o1 and H-i2, respectively. These values were determined using gross section properties and the relaxation loss equation provided in that paper. If the initial camber is calculated using these coefficients to determine the force in the strand, the calculated cambers would be increased by 0.1 in. The rest of the error is caused by differences between assumed and actual material and cross section properties.

Differences between the measured and calculated deflections caused by the weight of the panels are small enough that they could be caused by error introduced by thermal movements.

The measured deflection caused by the weight of the slab is smaller than the calculated deflection for both beams. However the actual differences are very small and could be easily due to minor

variations in slab thickness, ignoring reinforcement in computing gross moment of inertia, or thermal gradients from the heat of hydration of the fresh concrete placed on the upper surface of the beam. In addition, the placement of the slab produces tension in the strands, effectively reducing the losses (See Figs. 5.20 and 5.21). A 1% reduction in the losses would result in a calculated camber increment of 0.06-0.07 in. which would result in better agreement.

5.4.3 Longtime Camber and Deflection. The PCI Design Handbook includes multipliers for determining the longtime cambers and deflections in precast, prestressed members. The longtime response is estimated by multiplying elastic responses by appropriate multipliers. These multipliers which are given in Table 5.7 were developed by Martin [42]. The following assumptions were made in developing these multipliers:

1. The basic time dependent factor is 2.0
2. Initial loss of prestress is 8.0%
3. Time dependent loss of prestress is 15.0%
4. Percent of total camber and deflection change at erection is 50%
5. The ratio of noncomposite to composite moment of inertia is 0.65

The designer assumes the times of construction events or, if known, actual times of events can be used. However, the same multipliers are applied no matter what the times of events are. Therefore, the sequence of events has little effect on the responses predicted with these multipliers. However, this was not the case in the field as was shown in Sec. 4.5.4 and will be shown analytically in Sec. 6.4.8. Longtime response of the beams of this study using both design properties and conditions (design beams) and measured properties and conditions (instrumented beams) were predicted by multiplying the elastic cambers and deflections that were presented in Sec. 5.4.2 by these multipliers.

The predicted behavior for the L- and H-series design beams are shown in Figs. 5.8 and 5.9. The responses shown in these figures are what the designer would expect before construction begins. Erection was assumed to occur 45 days after release. Forty-five days was chosen, because Martin developed the multipliers assuming most beams are between 30 and 60 days old during erection. The asphaltic concrete pavement overlay was assumed to be added when the beams were 100 days old. The behavior for the L- and H-series design beams are similar. A greater

TABLE 5.7 Multipliers Suggested by PCI to Be Used as a Guide in Estimating Longtime Cambers and Deflections For Typical Members [23]

	Without Composite Topping	With Composite Topping
At Erection:		
Deflection (downward) component - apply to the elastic deflection due to the member weight at release of prestress	1.85	1.85
Camber (upward) component - apply to the elastic camber due to prestress at the time of release of prestress	1.80	1.80
Final:		
Deflection (downward) component - apply to the elastic deflection due to the member weight at release of prestress	2.70	2.40
Camber (upward) component - apply to the elastic camber due to prestress at the time of release of prestress	2.45	2.20
Deflection (downward) - apply to elastic deflection due to superimposed dead load only	3.00	3.00
Deflection (downward) - apply to elastic deflection caused by the composite topping	-	2.30

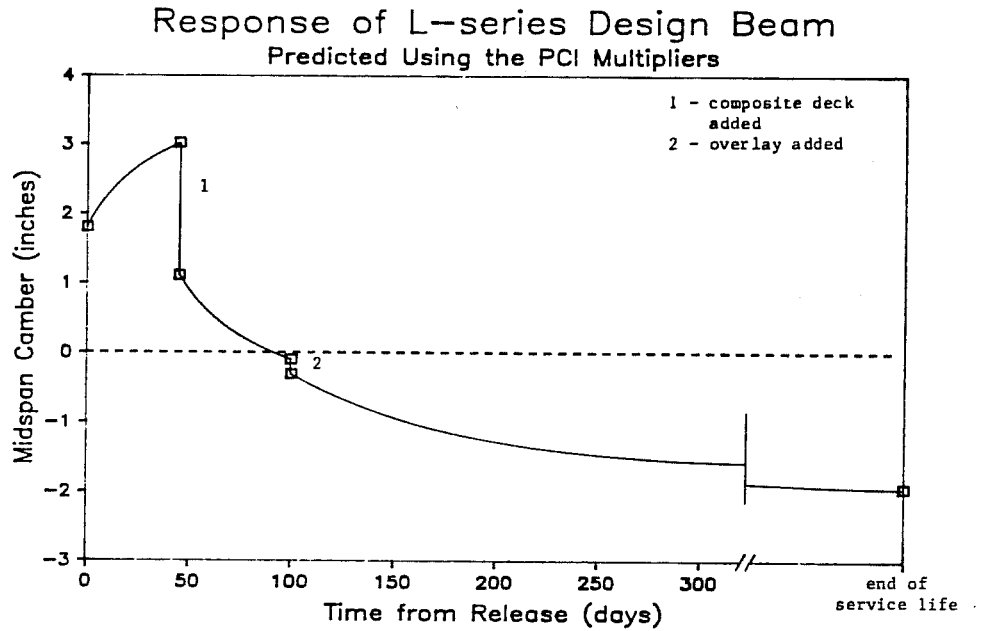


Fig. 5.8 Longtime response for the L-series design beam predicted using PCI multipliers and designer assumed timing of events

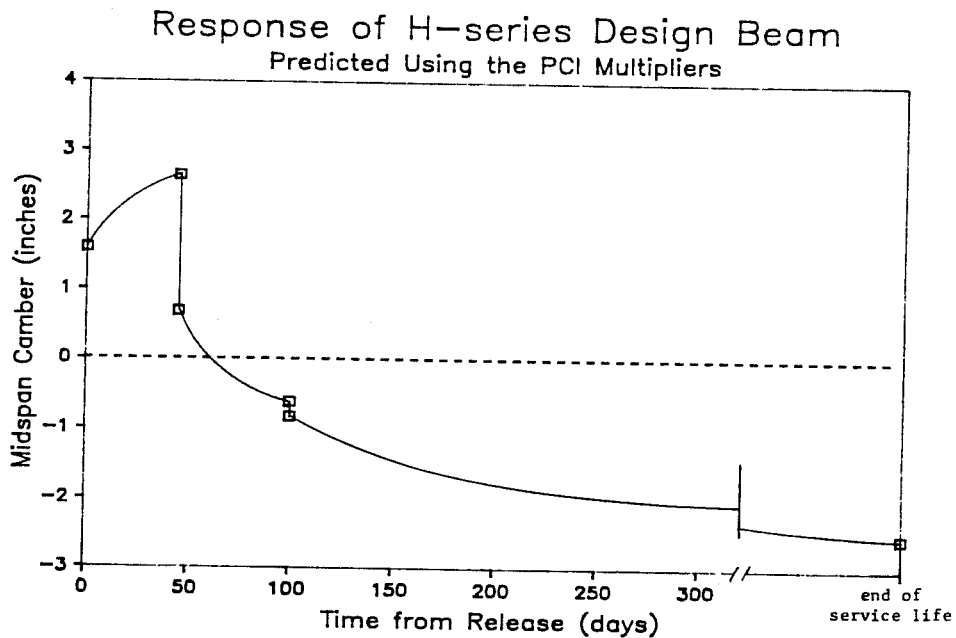


Fig. 5.9 Longtime response for the H-series design beam predicted using PCI multipliers and designer assumed timing of events

final deflection is predicted for the H-series beam, because the initial camber was less and the elastic deflections were greater than those of the L-series beam.

The longtime response for the instrumented beams were determined using actual ages for the occurrences of construction events. Elastic camber caused by the reduced span length while the beam is in storage was not included, because Martin did not consider it when developing the multipliers. The multiplier for elastic deflection caused by the composite topping was applied to deflections caused by the deck panels and the cast-in-place slab. Time dependent behavior was assumed to not occur between the time the panels were placed on the beams and the time the slab was cast. It was assumed that two-thirds of the time dependent response had occurred before the overlay was added.

The predicted responses for the instrumented beams are shown in Figs. 5.10 to 5.13. The predicted behavior for these beams are all similar. The maximum predicted camber at erection, 2.95 in. for beams L-i1 and L-i2 (see Fig. 5.10), was slightly less than 3.02 in. which was predicted for the L-series design beam. The minimum predicted camber at erection, 2.27 in. for beams H-o1 and H-o2 (see Fig. 5.12), was 0.37 in. less than the camber predicted for the H-series design beam. The maximum and minimum camber at erection is lower than those for the design beams because the initial elastic responses (initial stiffness) were smaller. In each case, the beams are predicted to be sagging before the end of the service life of the bridge. The amount of sag varies from a maximum of 3.0 in. for beam H-o1 to a minimum of 1.4 in. for beams L-o1 and L-o2 (see Fig. 5.11). These maximum and minimum final deflections are slightly greater and less than the final deflections of 2.54 and 1.94 in. calculated for the H- and L-series design beams.

The responses for beams L-o1 and H-i2 predicted using the PCI multipliers and the actual timing of events are compared to measured responses in Figs. 5.14 and 5.15. In both cases, the predicted camber at erection was less than the measured camber. This difference was caused in part by the difference in the assumed and actual age of the beams during erection. Because the beams were erected at an age much greater than the age which Martin assumed, 30 to 60 days, the percent of total camber and deflection change at erection should be greater than 50%.

The predicted final deflections were much greater than one would expect from observing the actual change that has occurred since the slab was cast. The multipliers were developed assuming the time-factor of 2.0 should be applied to all elastic deflections. The time-factor is equivalent to an ultimate creep coefficient. However, when concrete is loaded at an older age, less creep occurs. Therefore, the

Longtime Response of Beams L-i1 & L-i2
 Predicted Using the PCI Multipliers

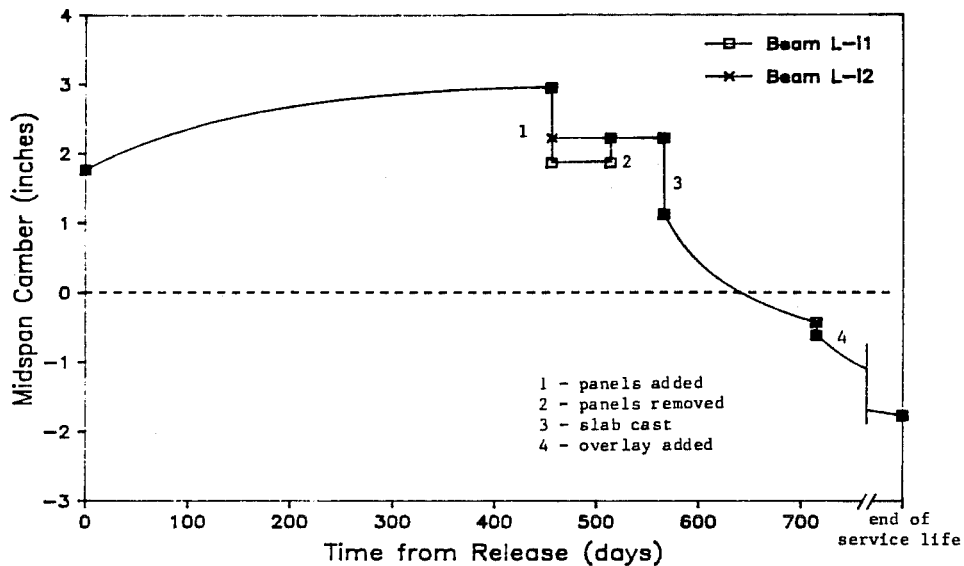


Fig. 5.10 Longtime response for beams L-i1 and L-i2 predicted using PCI multipliers and actual timing of events

Longtime Response of Beams L-o1 & L-o2
 Predicted Using the PCI Multipliers

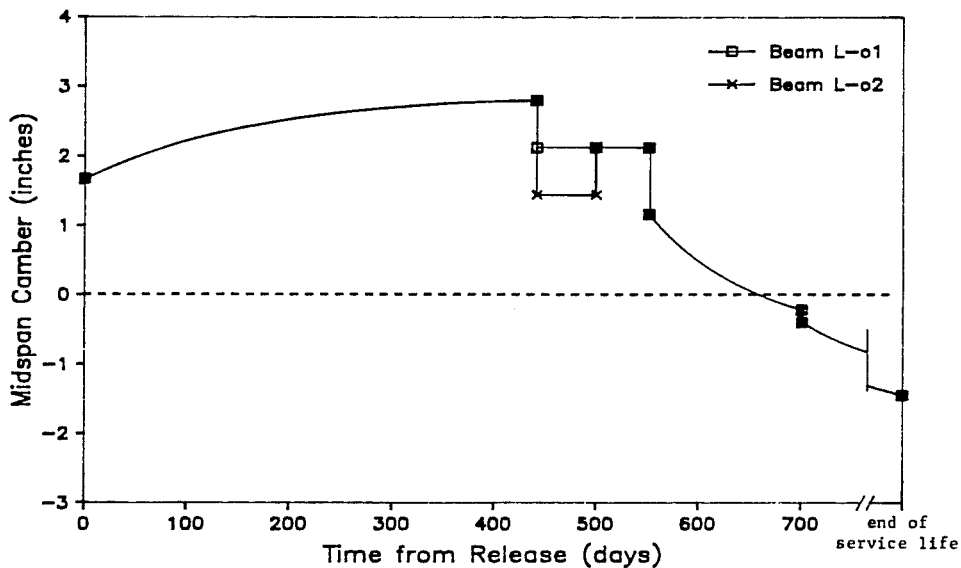


Fig. 5.11 Longtime response for beams L-o1 and L-o2 predicted using PCI multipliers and actual timing of events

Longtime Response of Beams H-o1 & H-o2
 Predicted Using the PCI Multipliers

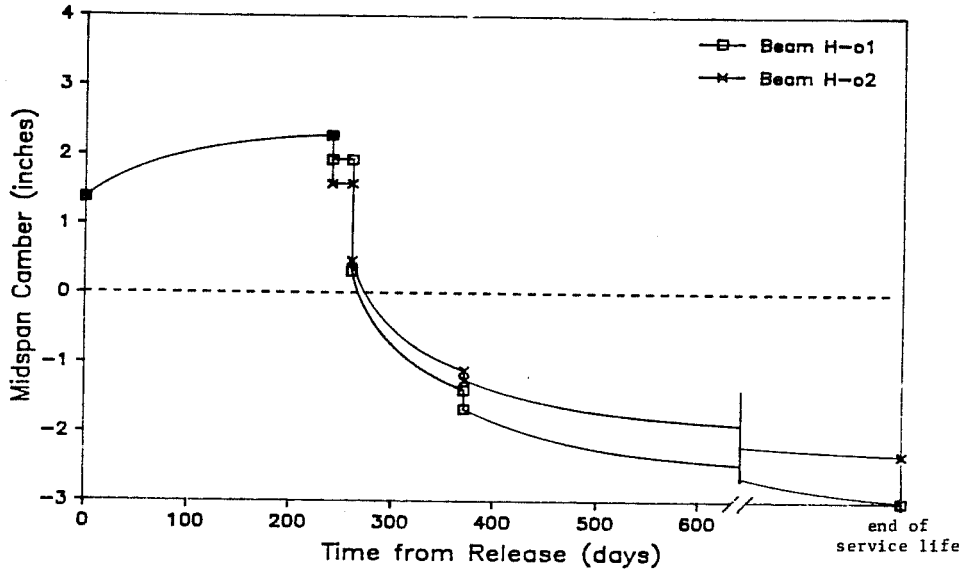


Fig. 5.12 Longtime response for beams H-o1 and H-o2 predicted using PCI multipliers and actual timing of events

Longtime Response of Beams H-i1 & H-i2
 Predicted Using the PCI Multipliers

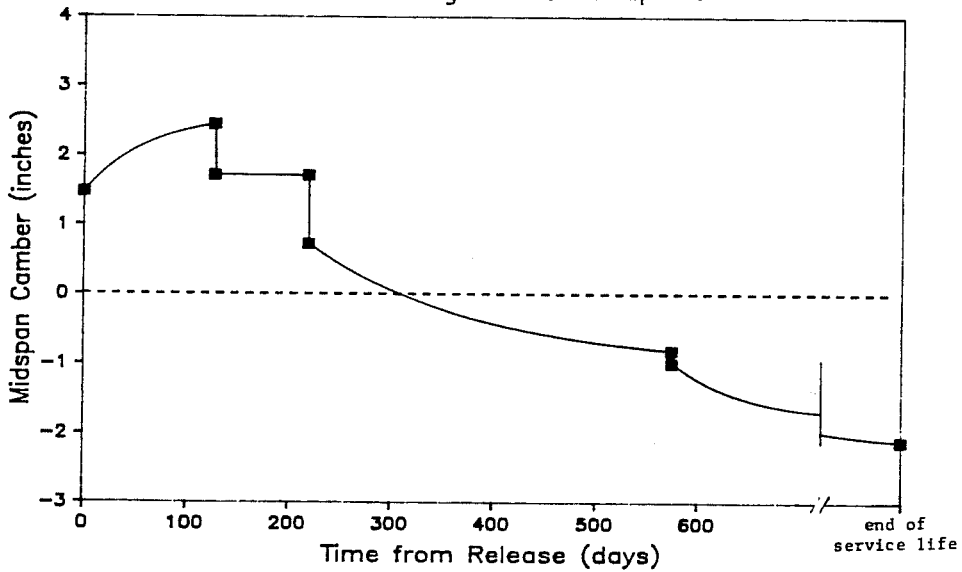


Fig. 5.13 Longtime response for beams H-i1 and H-i2 predicted using PCI multipliers and actual timing of events

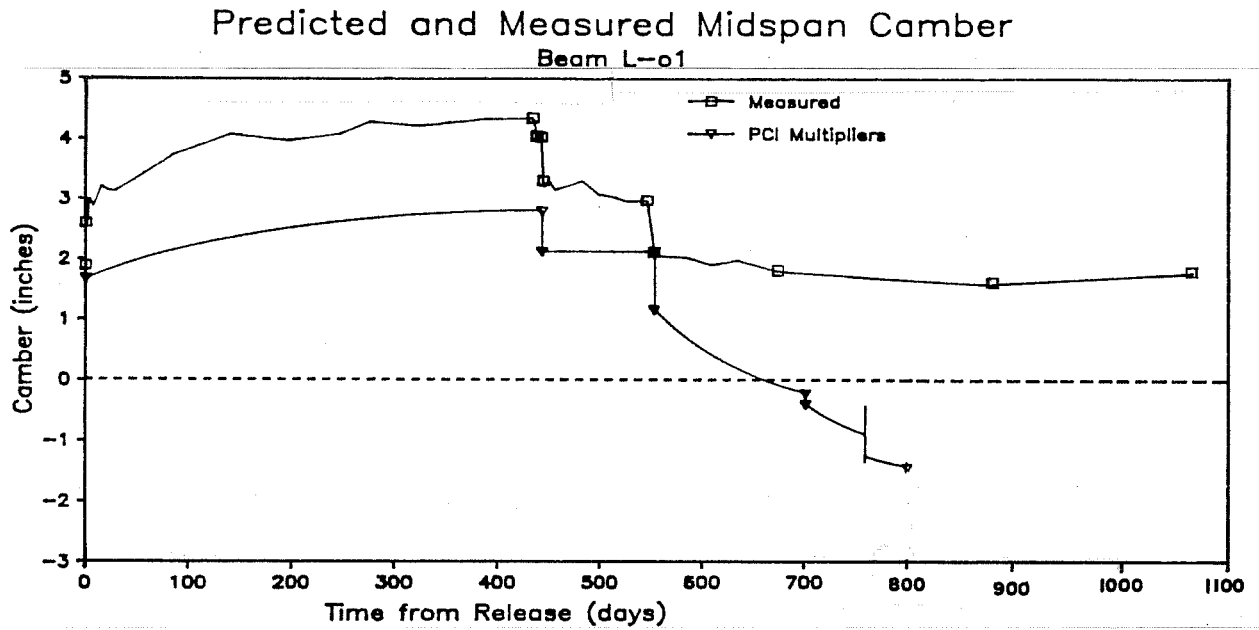


Fig. 5.14 Comparison of time dependent camber predicted using PCI multipliers and the measured response for beam L-o1

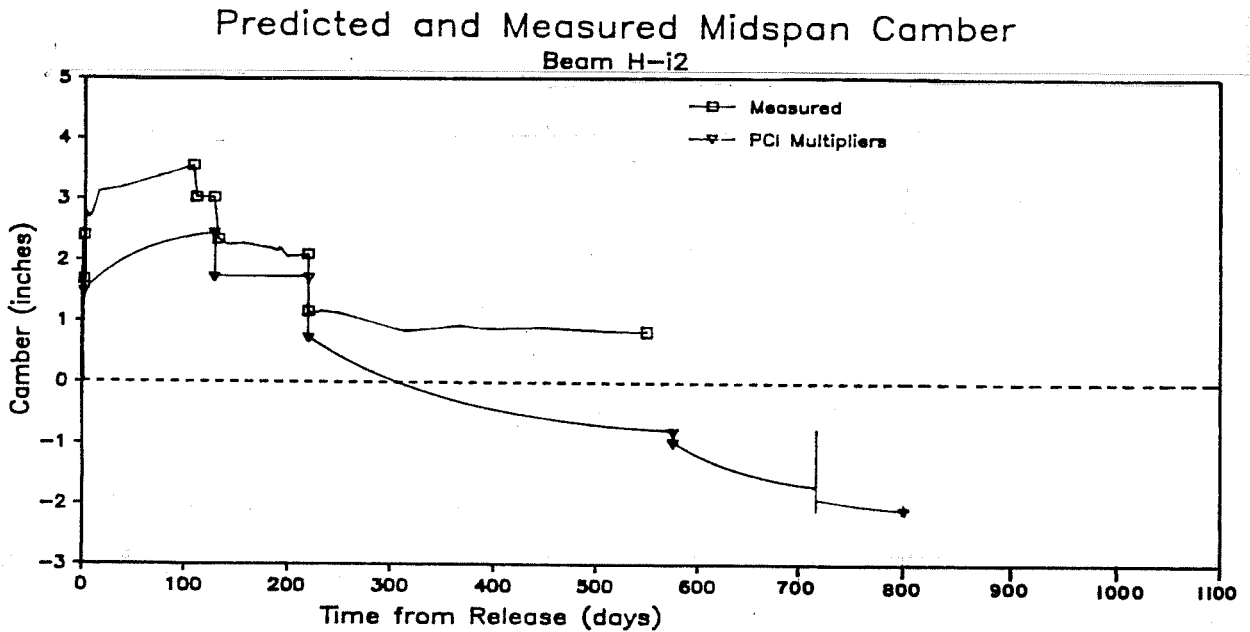


Fig. 5.15 Comparison of time dependent camber predicted using PCI multipliers and the measured response for beam H-i2

multiplier for the deflection caused by the composite topping should have been based on a time-factor which is less than 2.0. Because it was not, the time dependent deflection caused by the composite topping and the deflection at the end of the service life is overpredicted.

The predicted final deflection is also overestimated, because the assumed value for the ratio of noncomposite to composite moment of inertia was too high. A value of 0.65 was used in developing the multipliers, because Martin was considering members used in buildings. The actual value for the beams used in this investigation is closer to 0.5. In developing the multipliers, the time-factor applied to the deflection caused by the composite topping is reduced by the ratio of noncomposite to composite moment of inertia. Because the assumed ratio is greater than the actual ratio, the time dependent deflection is overestimated.

5.5 Suttikan's PBEAM- Prestress Loss, Elastic Cambers and Deflections, and Time Dependent Response

5.5.1 PBEAM. PBEAM is a computer program, developed by Suttikan [25], which is capable of analyzing noncomposite or composite prestressed concrete members of any cross-sectional shape. The program can be used to analyze both instantaneous and time dependent response. When calculating the time dependent response, variations with time of concrete strength, creep, shrinkage, and prestressing steel relaxation are considered.

The instantaneous response is analyzed by an iterative procedure in which the member is modeled using a discrete element method. The beam length is divided into several segments connected at joints. The cross section is broken down into several rectangles. The instantaneous response is calculated whenever a load is placed on the member, or a new portion of the cross section, such as the deck panels and cast-in-place slab, are added to the member.

The time dependent response is calculated at times specified as part of the input. The time dependent response is also calculated just before each instantaneous response.

When using PBEAM, one has the option to use either experimental values or internally provided equations for the material properties. When using experimental values as input, the program will linearly interpolate between values. If internally provided equations are used, coefficients for the equations must be included as input. Therefore, the coefficients for a best fit curve of experimental data may also be used.

The beam cross section is modeled using rectangles. The type of material, width, depth, and the distance to the center of gravity of the rectangle from a fixed vertical reference must be defined for each rectangle. Each rectangle may be divided into several subrectangles in order to increase the accuracy of the solution.

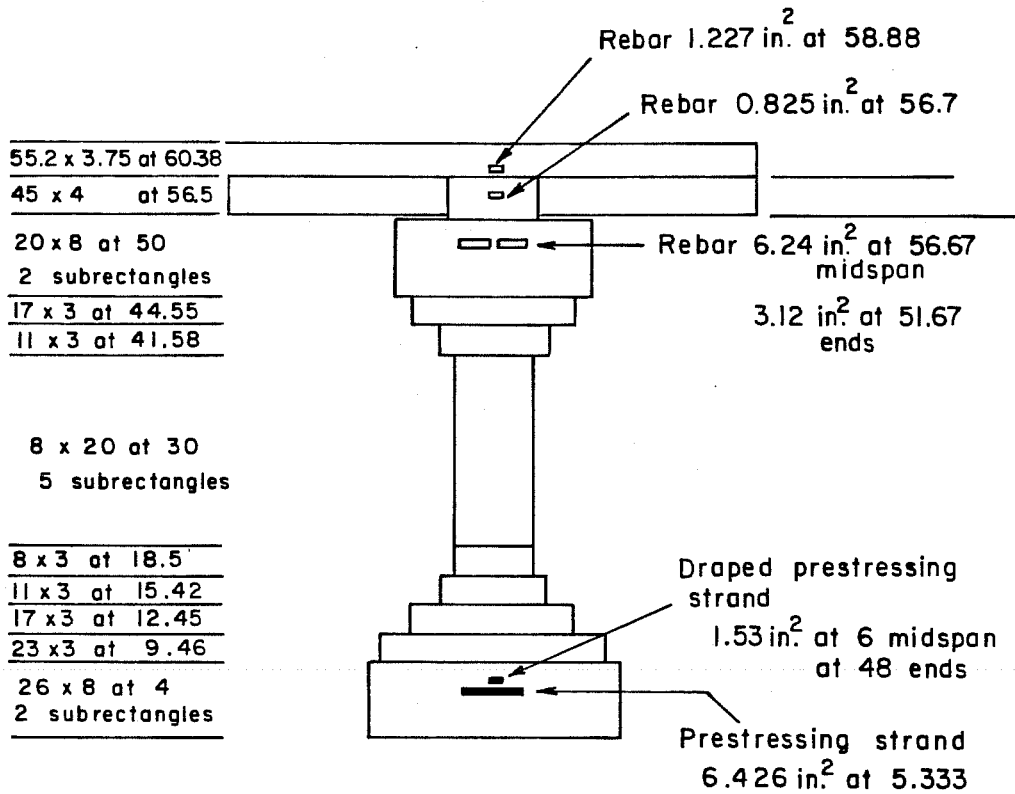
Three times must be defined for each rectangle: the time when cast, the time when added to the member, and the time when it can carry load. The time when cast is used as a reference for estimating aging and creep effects. When a rectangle is added to the member, its gravity load is applied to the member. Each rectangle has zero strain before the time when it can carry load. Shrinkage also starts when the rectangle can carry load. Shored construction can be modeled by making the time when a slab rectangle is added to the member greater than the time when it can carry load.

The results of PBEAM include camber or deflection, strains, and stresses at each time step. Camber or deflection and rotations are calculated for each joint. Strains and stresses are calculated for each subrectangle of the cross section in each beam segment. When running PBEAM, the output of camber or deflection, strains, or stresses may be suppressed.

PBEAM was used to analyze the time dependent response for each instrumented beam. Experimental values for material properties were used whenever possible. The beam cross section was modeled as shown in Fig. 5.16 except for beam H-01 which had only half a panel and a wider slab. The thickness of the top rectangle used to model the slab also varied depending on what the average measured slab thickness above the beam was.

Internally provided stress-strain curves were used for the beam, deck panel, and slab concretes. The form of the curve is shown in Fig. 5.17. Experimental values for the strength of beam concrete at different ages, f'_c , were used. The ACI Committee 209 recommended age strength gain curve [1] was used for the deck panel and cast-in-place slab concrete. Twenty-eight day concrete strengths of 7000, 6500, and 5500 psi were used for the deck panels, right main lane slab, and left main lane slab, respectively. The modulus of elasticity, E_c , was determined using the proposed formula presented in Sec. 4.3.2.

A perfectly elasto-plastic stress-strain curve with a modulus of elasticity of 29,000 ksi, and a yield stress of 60 ksi was used for the reinforcing steel. The stress-strain curve for the prestressing steel was assumed to be perfectly elastic with a modulus of elasticity of 28,000 ksi.



Note :

All dimensions are in inches unless otherwise noted.
 The distance to the center of gravity of each rectangle is measured from the bottom of the beam.

Fig. 5.16 Model cross section of beam used to run PBEAM

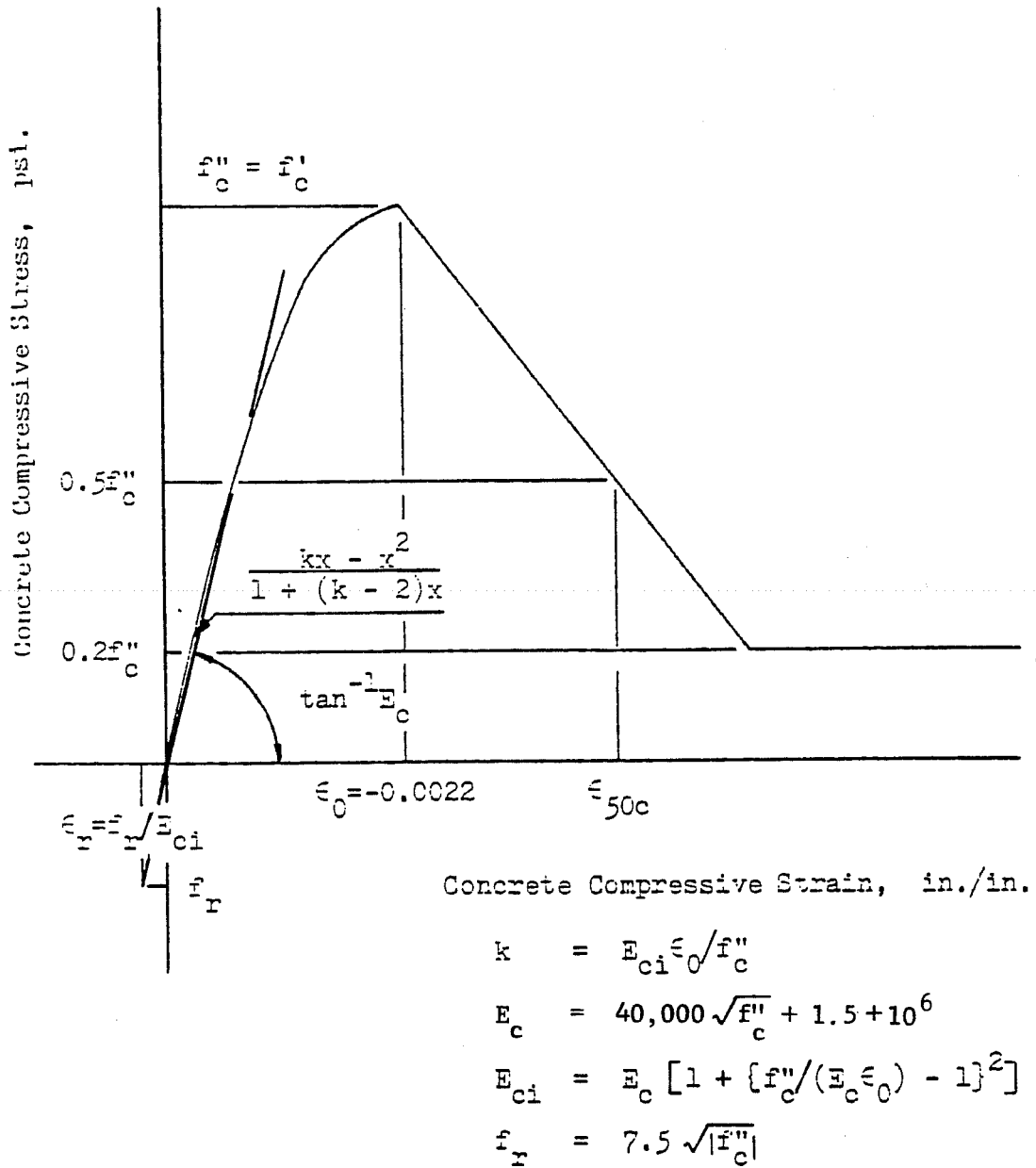


Fig. 5.17 Concrete stress-strain curve used for PBEAM [25]

Experimental values were used for the creep of the beam concrete. An experimental curve is input using an ultimate creep coefficient, and a curve which defines the fraction of ultimate creep that has occurred with time. Results from the experimental creep curves presented in Sec. 4.3.3 were used to determine the ultimate creep coefficients and the shapes of the creep curves. The curves shown in Figs. 5.18 and 5.19 were used for the L- and H-series beams, respectively. The ultimate creep coefficients shown in these figures are for a load applied to the beam concrete when it is seven days old. Because the creep tests were performed on 6-in. diameter cylinders, the ultimate creep coefficient was reduced to account for the effect of the greater volume-to-surface ratio for the beams. The ACI Committee 209 recommendation for correction of age at loading was applied to the creep coefficients for loads applied to the beam after they were seven days old. Between zero and seven days old, the correction factor was linearly interpolated between values of 1.25 and 1.0 [6].

An internally provided creep curve was used for the deck panel and cast-in-place slab concretes. The creep curve and correction for age at loading were those recommended by ACI Committee 209. An ultimate creep coefficient of 1.92 was used. This is the recommended value of 2.35 corrected for an average relative humidity of 65% and a deck thickness of 7 in.

Ultimate shrinkage strains of 170 and 140 microstrains were used for the L- and H-series beam concretes. These values were obtained using the ultimate shrinkage strains estimated from the tests presented in Sec. 4.3.3 with a 0.68 volume-to-surface ratio correction factor [1] applied to them. The ACI Committee 209 shrinkage curve was used to define the fraction of ultimate shrinkage that has occurred versus time.

The ultimate shrinkage strains used for the deck panels were 40 and 70 microstrains for the L- and H-series beams, respectively. These values were determined using the values recommended by ACI Committee 209 with proper correction factors applied to the ultimate shrinkage. These values are small, because the panels were an average of 520 and 240 days old for the right and left main lane bridges when they became part of the cross section. PBEAM does not start to calculate shrinkage strain until after a subrectangle is able to carry load. Because panels can not carry load as part of the cross section until after the slab has been cast, only the fraction of shrinkage that had not occurred at the time the slab was cast was used as the ultimate shrinkage strain.

The ultimate shrinkage strain used for the slab concrete was 560 microstrain. This is the value recommended by ACI Committee 209 after corrections for an average relative humidity of 65% and a deck thickness of 7 in. are applied.

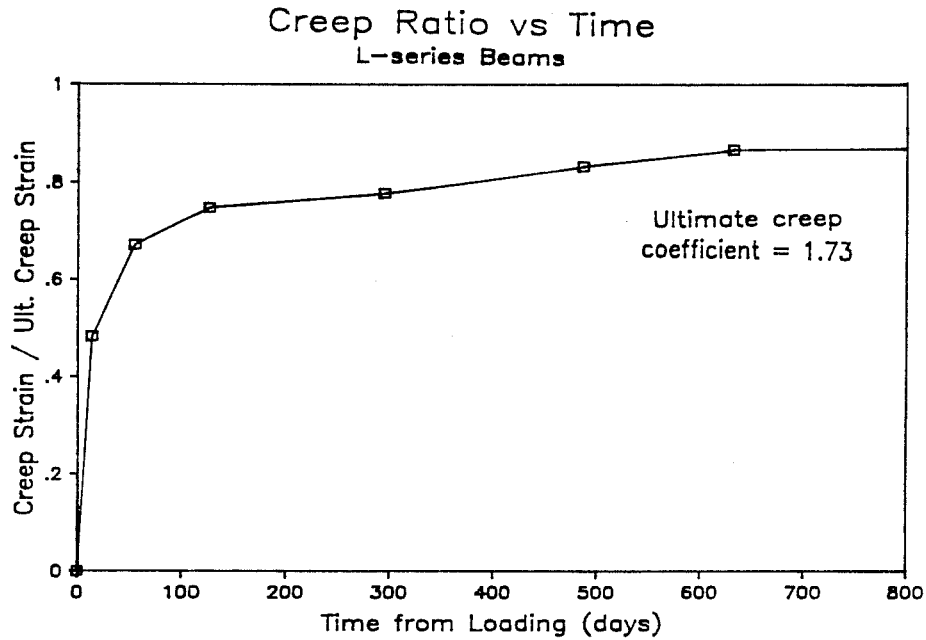


Fig. 5.18 Creep curve for the L-series beams used as input for PBEAM

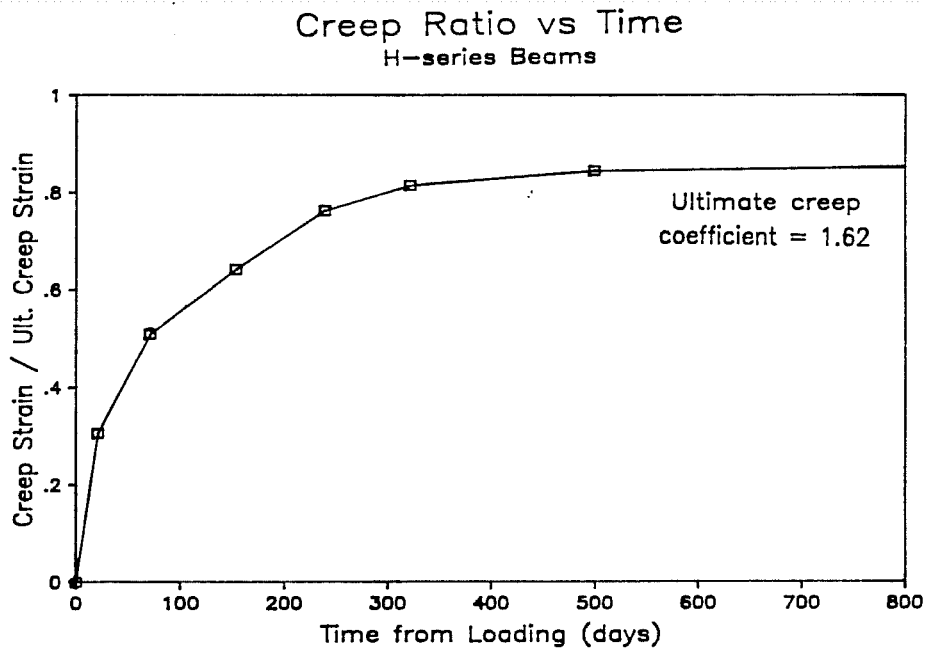


Fig. 5.19 Creep curve for the H-series beams used as input for PBEAM

Experimental values were used to model the relaxation of the prestressing strand. Results of relaxation tests performed by the strand manufacturers were used to define the shape and magnitude of the relaxation curve. These tests were performed at a stress level of 0.7 times the strands guaranteed ultimate strength. An ultimate relaxation of 2.0% was estimated from the results of both manufactures.

The effect of stress level on relaxation was accounted for by using the equation for relaxation that appears in "Recommendations for Estimating Prestress Losses" [6]. This equation was used to calculate the amount of relaxation that occurs at several different stress levels. These values were then divided by the calculated relaxation that occurs at a stress level of 0.7 times the guaranteed ultimate strength. These ratios were then applied to the relaxation curves measured by the manufacturers to obtain the relaxation for different stress levels. The relaxation of the prestressing strand was input into PBEAM using two curves: the fraction of ultimate relaxation that has occurred versus time, and the ratio of ultimate relaxation stress divided by the initial stress for different stress levels.

The PBEAM data files for beams L-01 and H-i2 are provided by Kelly in Appendix Tables A.2 and A.3 of Ref. 46. Those files can serve as examples to be used with the user's guide, which does not explain how to input experimental data very well. The length and complexity of those input data files and the lengthy running time (approximately 160 seconds on the University of Texas at Austin Cyber system for a single beam life) indicate PBEAM is not a practical program for everyday use in a design office.

5.5.2 Prestress Loss. The prestress loss predicted using PBEAM was determined by taking the difference between the initial stress and the stress that remains in the rectangles used to model the strand. The percent prestress losses at midspan for beams L-01 and H-i2 are shown in Figs. 5.20 and 5.21.

The predicted loss immediately after release equaled 7.96% for beam L-01 and 7.36% for beam H-i2. These initial losses included the loss due to relaxation from the time strand was initially tensioned until release and the loss due to elastic shortening. The losses due to just elastic shortening were 7.16% and 6.3% for beams L-01 and H-i2, respectively.

The maximum predicted prestress loss for beam L-01 occurred just before the beam was removed from storage, while the maximum loss for beam H-i2 occurred just before the slab was cast. The maximum calculated losses were 21.6% for beam L-01 and 16.5% for beam H-i2. The maximum loss for beam L-01 was greater than that of beam H-i2, because the moment caused by the prestress force along the length of the beam

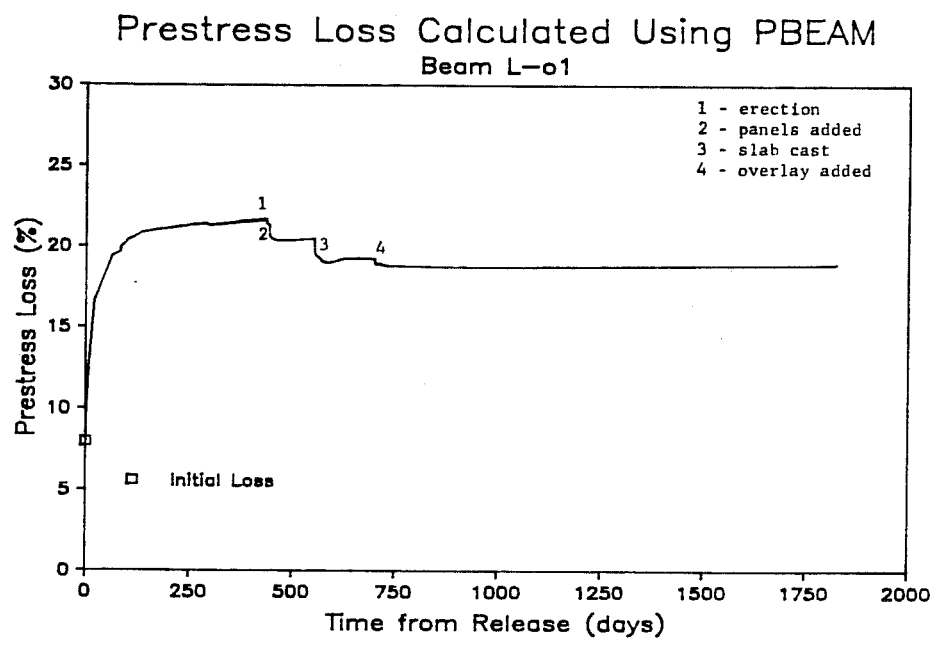


Fig. 5.20 Time dependent prestress loss for beam L-o1 predicted using PBEAM

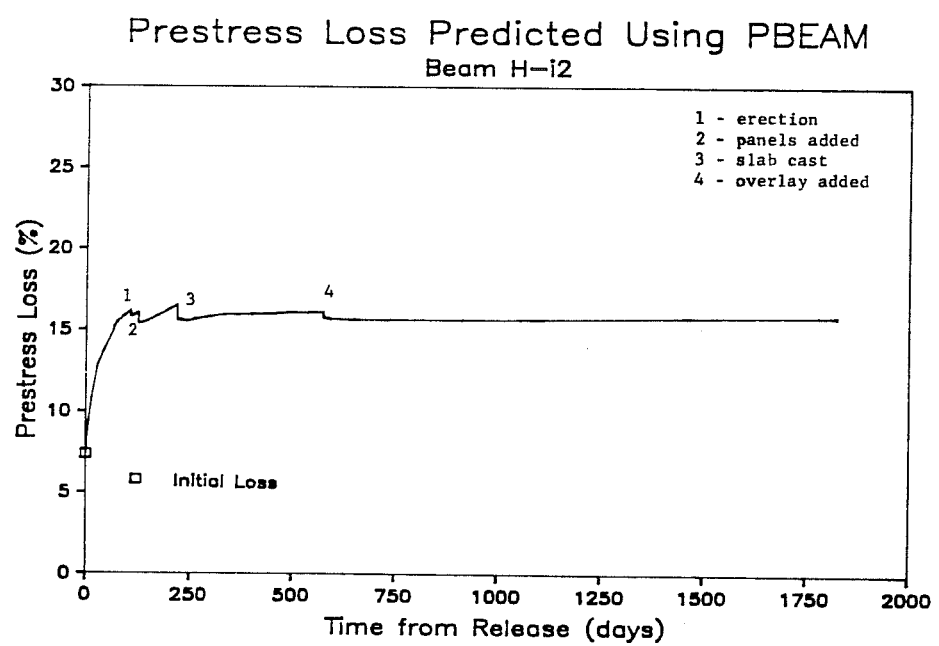


Fig. 5.21 Time dependent prestress loss for beam H-i2 predicted using PBEAM

and the creep coefficient of beam L-01 were greater. A greater loss also occurred in beam L-01, because it remained in storage for a longer time.

The predicted prestress losses were reduced when the beams were placed in the bridge, panels were placed on the beams, the slab was cast, and the overlay was placed on the bridge deck. During these events, a moment opposite in sense to the moment caused by the prestressing force was applied to the beam. This causes the strand below the beam center of gravity to stretch, and therefore, some of the prestress force which was lost was then regained.

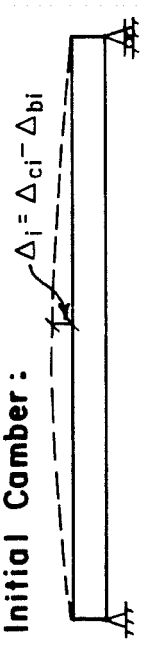
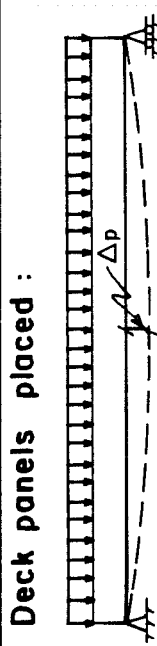
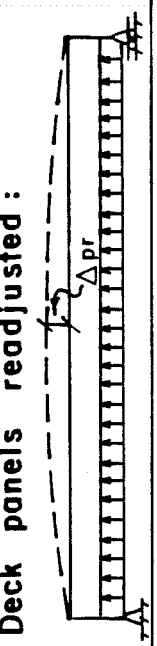
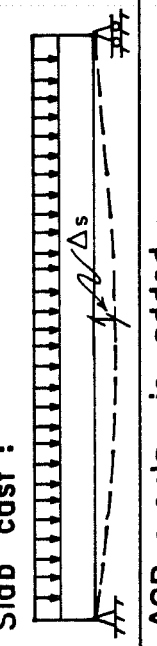
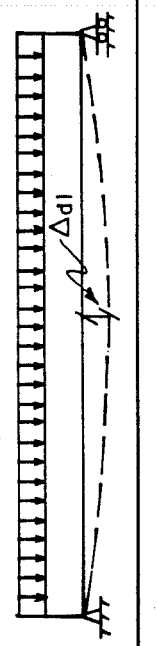
The prestress losses predicted for five years after the beams were cast are 18.9% for beam L-01 and 15.9% for beam H-i2. The prestress losses were predicted to increase only a few tenths of a percent between the time the overlays were placed on the deck and five years after the beams were cast.

5.5.3 Elastic Camber and Deflection. The elastic cambers and deflections calculated using PBEAM are listed in Table 5.8. The calculated initial cambers varied from a minimum of 1.59 in. for beams H-01 and H-02 to a maximum of 1.99 in. for beams L-i1 and L-i2. The average initial cambers were 1.96 and 1.64 in. for the L- and H-series beams, respectively. The initial cambers for the H-series beams were less, because the concrete strengths at release were greater and the moment caused by the prestressing force was less than those for the L-series beams.

The average calculated deflections caused by the deck panels and the cast-in-place slabs agreed well with the measured values. The average calculated deflection caused by one layer of deck panels was 0.64 in. compared to a measured value of 0.73 in. The average calculated deflection caused by the cast-in-place slabs (excluding beams H-01 and H-02) was 0.89 in. compared to the average measured value of 0.85 in.

A comparison of measured and calculated elastic cambers and deflections for beams L-01 and H-i2 are shown in Table 5.9. In both cases, the calculated initial camber is in excellent agreement with the measured values. The calculated deflections caused by the weight of the deck panels and cast-in-place slab are also in good agreement with the measured values. The maximum error was only 0.11 in. (15%) for the deflection of beam L-01 caused by the weight of panels. This error is less than half the magnitude of thermal movements that occur on a sunny day. Therefore, the error may be caused entirely by the error in the measured values due to thermal movement. The good agreement between these measured and calculated values also indicate that the proposed formula for elastic modulus of high strength concrete presented in Sec. 4.3.2 is accurate.

TABLE 5.8 Elastic Cambers and Deflections Predicted Using PBEAM

Event	Beam				H-i1	
	L-i1	L-i2	L-o1	L-o2	H-o1	H-i2
a. Initial Camber : 	1.99	1.99	1.92	1.59	1.59	1.69
b. Deck panels placed : 	1.04	0.65	0.62	1.24	0.32	0.63
c. Deck panels readjusted : 	0.34			0.61		
d. Slab cast : 	1.01	0.94	0.85	0.85	1.45	0.85
e. ACP overlay is added : 	0.25	0.24	0.20	0.23	0.26*	0.23

* Deflection caused by the east rail in the LML bridge.

5.5.4 Time Dependent Camber and Deflection. PBEAM was used to analyze the time dependent response for each instrumented beam. In general, the shape of the responses were similar to the actual responses discussed in Sec. 4.2.1.

The predicted response for beam L-i1 is shown in Fig. 5.22. The camber grew to a maximum of 6.05 in. just before it was removed from storage. The camber was decreased by elastic deflections when the beam was placed in the bridge, deck panels were placed on it, the slab was cast, and the overlay was placed on the deck. The camber increased when the extra half layer of deck panels were removed.

Immediately after the slab was cast, PBEAM predicted that the beam should continue to deflect downward for a few weeks, and then it should camber upward for a few weeks. The time dependent downward motion was primarily caused by shrinkage of the slab concrete. As the slab concrete shrinks, differential strains were developed between the slab and beam concrete. In order to minimize the differential strain, the beam deflected downward. Because the panel and beam concrete prevented the slab from freely shrinking, tensile stresses were developed in the slab concrete. After a few weeks, these stresses became great enough to cause the slab concrete to crack. When the slab concrete cracked, differential strains between the beam and slab concretes were relieved. The beam then begins to return to the calculated camber which was in the beam immediately after the slab was cast. The beam never fully returns to that camber, because time effects caused by creep and relaxation have occurred.

The time dependent responses for the other instrumented beams are shown in Figs. 5.23 to 5.29. Except for beam H-o1, the shape of the predicted response curves for these beams were similar to the actual beams. The time dependent deflection of beam H-o1 caused by the slab continues to grow beyond a few weeks. This occurred because the volume of slab concrete was greater for this beam. The tensile stress in the slab never reached a stress great enough to cause cracking. Therefore, the beam continued to deflect as the slab concrete shrank.

Comparisons of the measured and predicted time dependent camber and deflection responses for beams L-o1 and H-i2 are shown in Figs. 5.30 and 5.31. As shown in these figures, the maximum cambers predicted using PBEAM were greater than the maximum measured values. The predicted time dependent response that occurred between the time the beams were placed in storage to the time the beams were placed in the bridge was much greater than what was measured. The predicted growth in camber for beam L-o1 was 3.24 in. compared to the measured growth of 1.75 in. The difference was most likely caused by less creep and more relaxation actually occurring compared to what was assumed when using PBEAM. The difference in creep was the greater factor and could be

Camber Predicted Using PBEAM
Beam L-i1

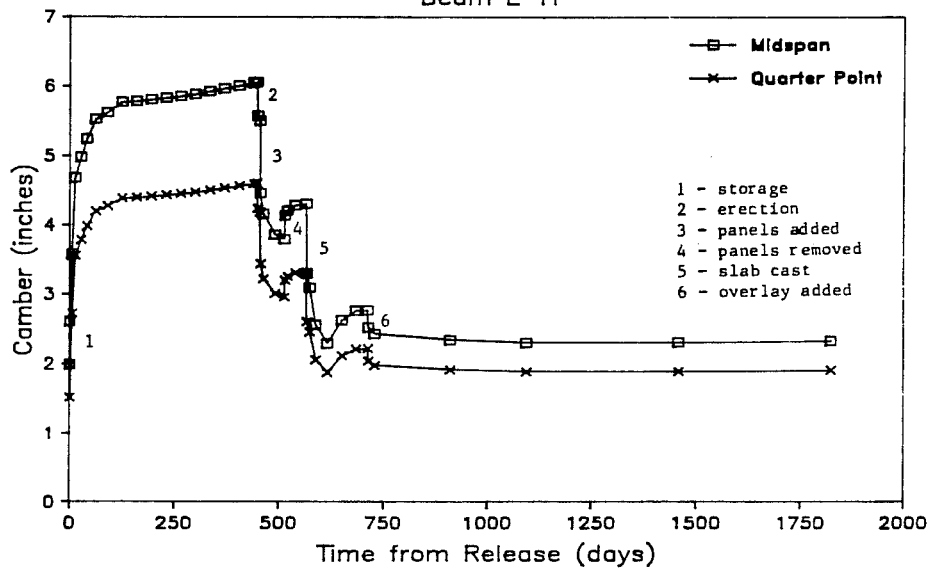


Fig. 5.22 Time dependent camber for beam L-i1 predicted using PBEAM

Camber Predicted Using PBEAM
Beam L-i2

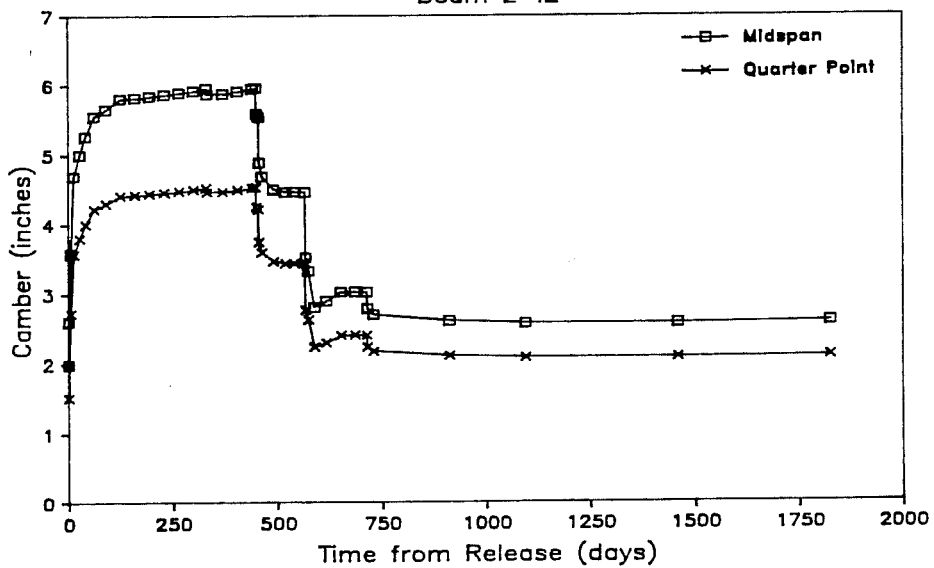


Fig. 5.23 Time dependent camber for beam L-i2 predicted using PBEAM

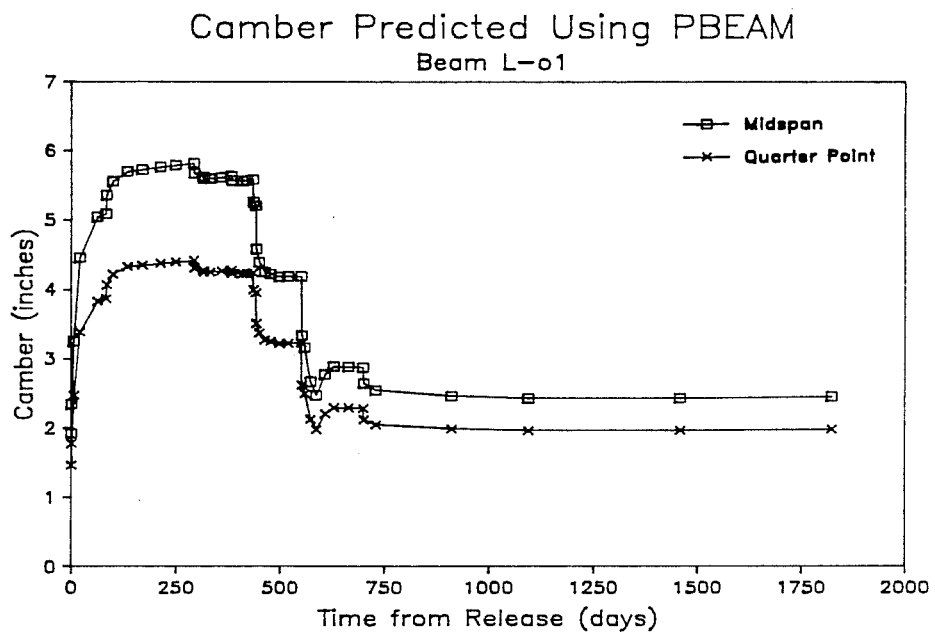


Fig. 5.24 Time dependent camber for beam L-01 predicted using PBEAM

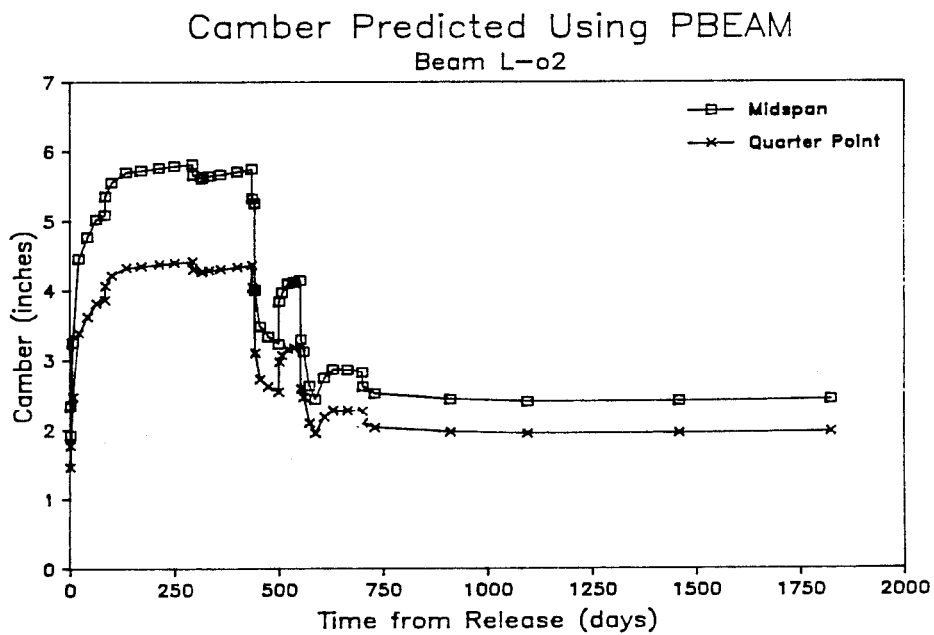


Fig. 5.25 Time dependent camber for beam L-02 predicted using PBEAM

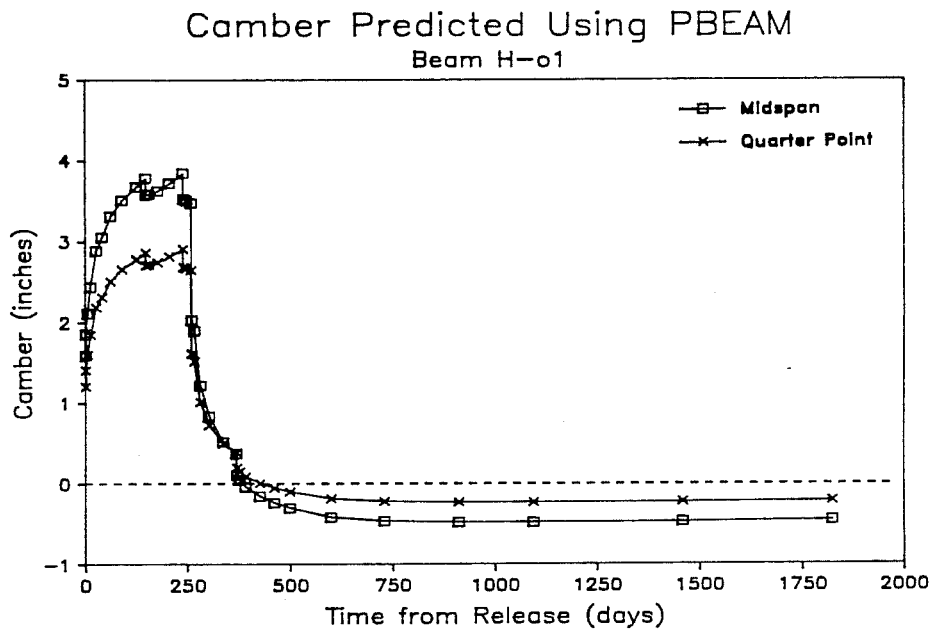


Fig. 5.26 Time dependent camber for beam H-o1 predicted using PBEAM

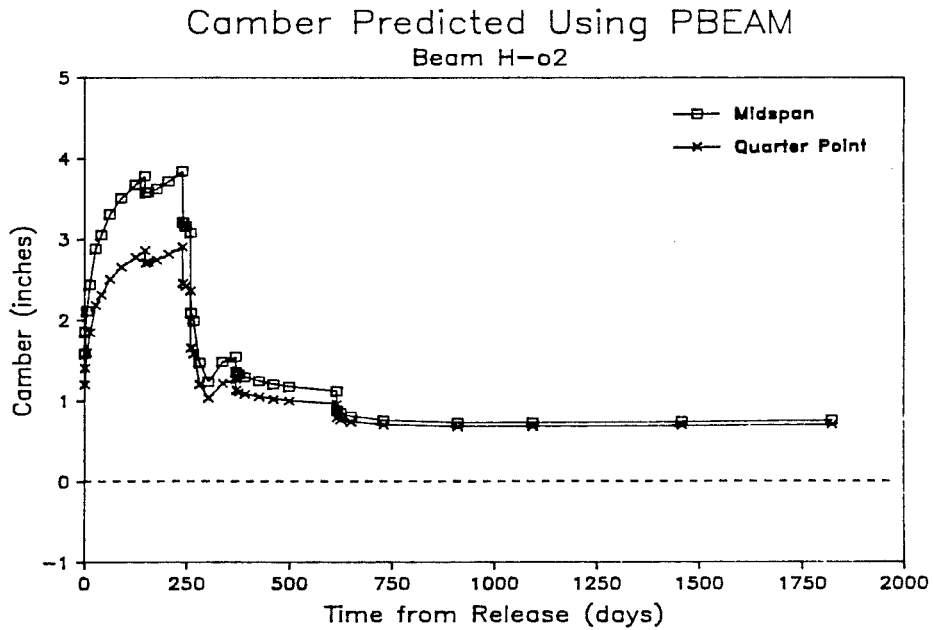


Fig. 5.27 Time dependent camber for beam H-o2 predicted using PBEAM

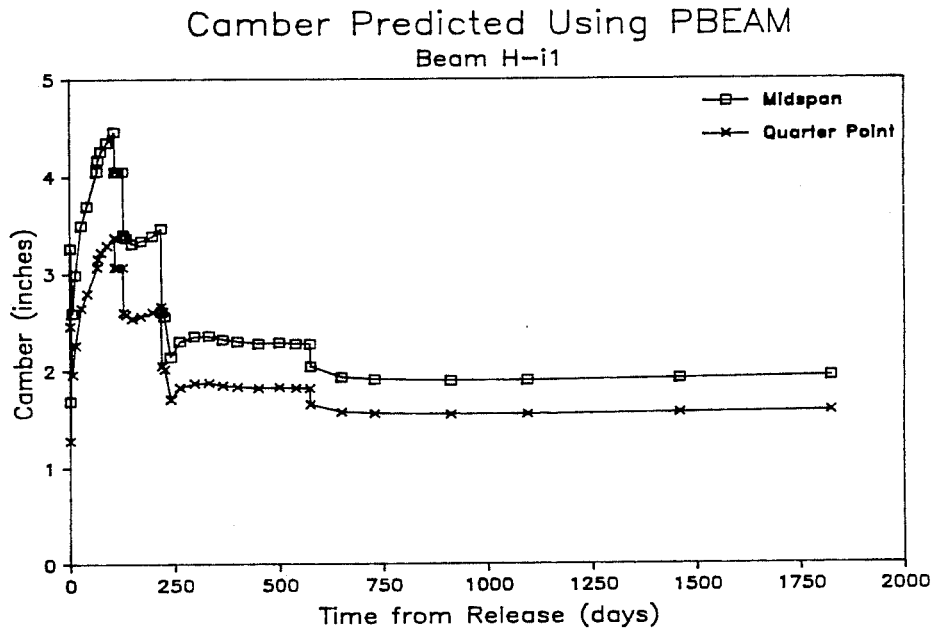


Fig. 5.28 Time dependent camber for beam H-i1 predicted using PBEAM

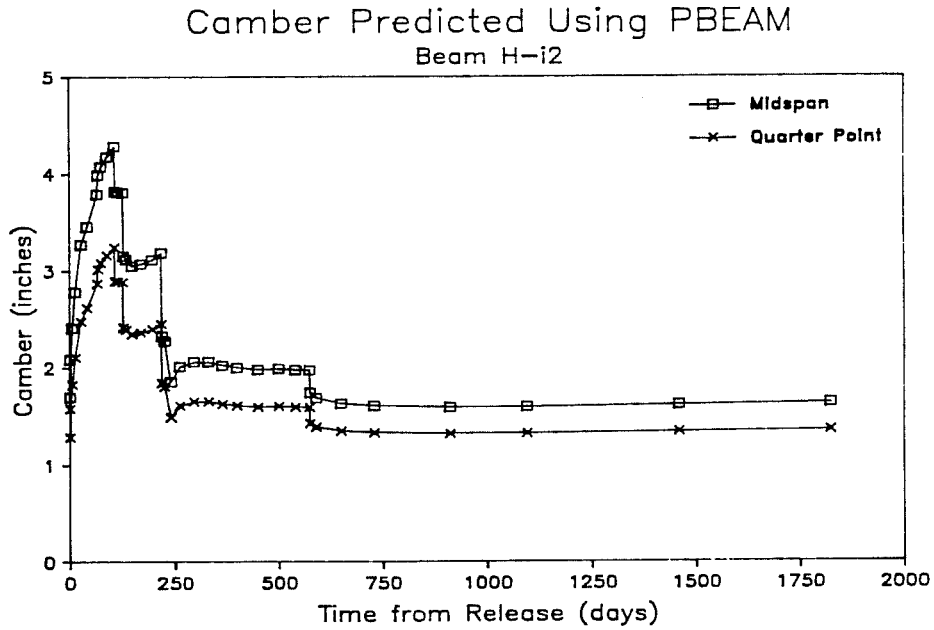


Fig. 5.29 Time dependent camber for beam H-i2 predicted using PBEAM

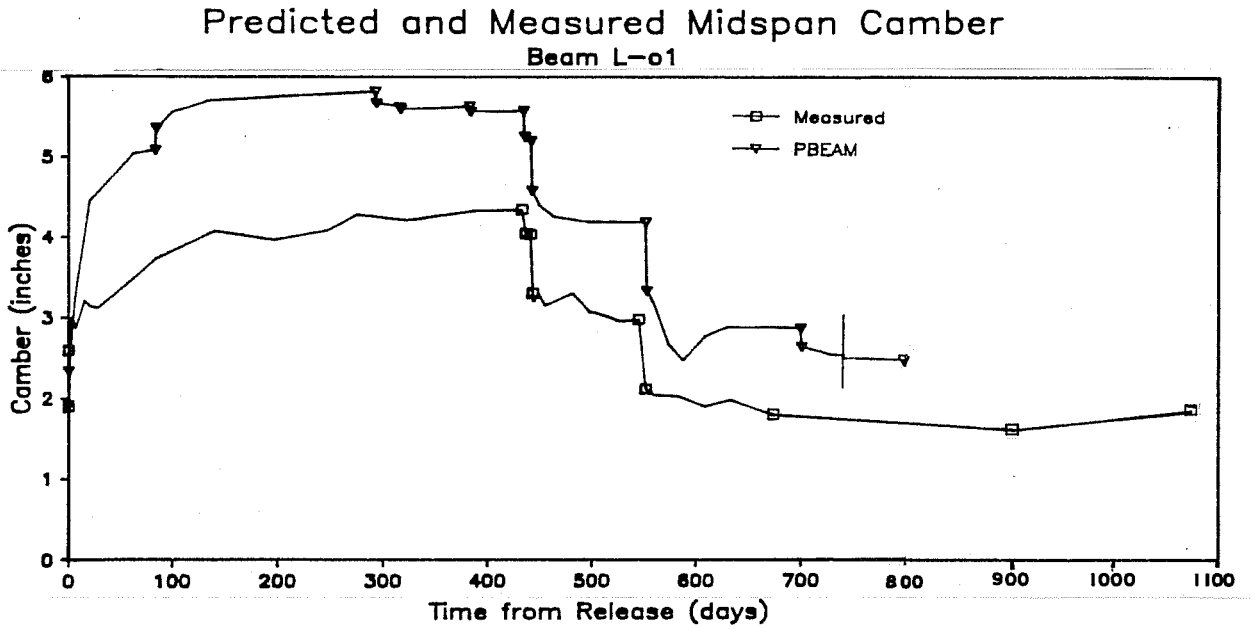


Fig. 5.30 Comparison of time dependent camber predicted using PBEAM and measured camber for beam L-01

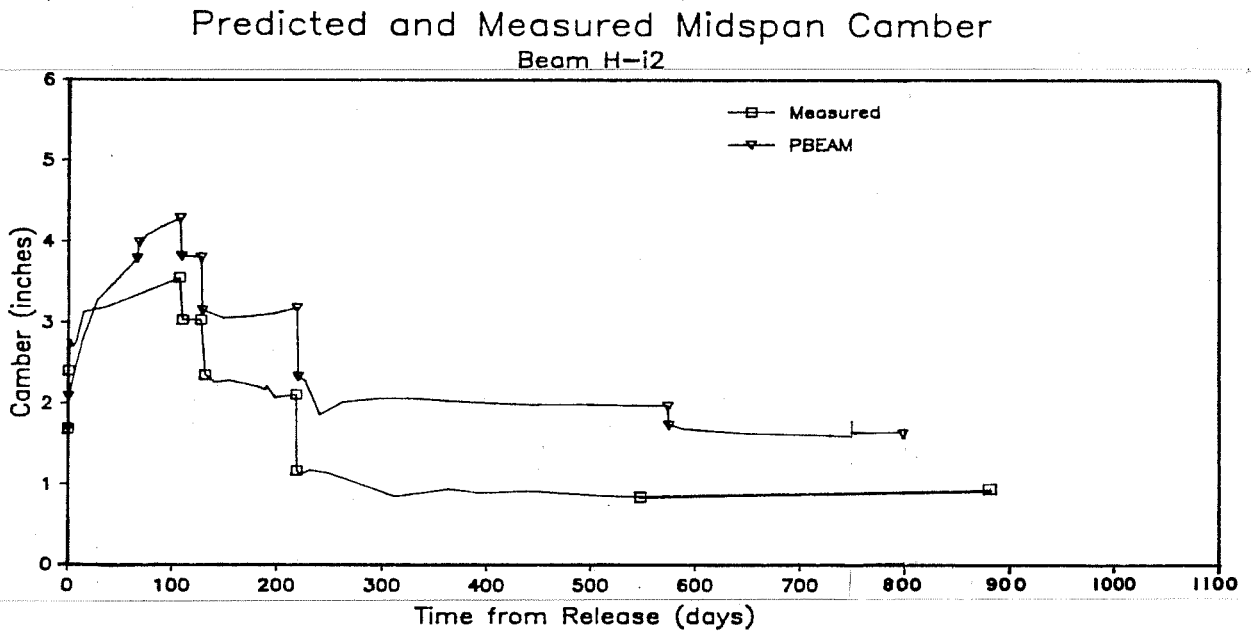


Fig. 5.31 Comparison of time dependent camber predicted using PBEAM and measured camber for beam H-i2

caused by error in the companion creep test results, or error in the volume-to-surface ratio correction factor that was used. Buckler and Scribner [8], and Koretsky and Pritchard [45] measured greater relaxation losses than reported by manufacturers. Differences of 1 to 2% relaxation loss were measured.

The predicted and measured responses that occurred during the first month after the slab was cast were also different. As shown in Figs. 5.30 and 5.31, PBEAM predicted that the beams should have deflected downward at first after the slab was cast and then camber up, while the measured response shows only a small decrease in camber. This difference may be caused by the actual slab cracking very soon after the slab was cast. Such cracks could have been caused by thermal differentials between the slab and the beam. The difference may also be caused by the difference in actual and assumed shrinkage of the slab. The ultimate shrinkage used for the slab was 560 microstrain. When compared to the shrinkage strain measured for the beam concrete, one might feel the assumed value for the slab shrinkage may have been too high. If a smaller shrinkage strain had been assumed, the beam would not have deflected as much, since the differential shrinkage strain would not have been as great.

Although PBEAM did not accurately predict the measured response, it is a very good program. The response was not accurately predicted because the time dependent material properties were not accurately modeled.

5.6 Proposed Multipliers- Time Dependent Camber and Deflection

Time dependent cambers and deflections are primarily a function of prestress loss and creep. If appropriate values are used for prestress loss and creep, multipliers can be developed which can be used to accurately predict time dependent cambers and deflections. In this section a method for determining such multipliers is presented. The ideas and principles used to develop these multipliers are similar to those used for an analytical technique presented by Branson and Kripanarayanan [28] and for the multipliers developed by Martin [42].

Time dependent beam camber or deflection at any time is equal to the elastic response plus the time dependent response. Equation 5.1 describes the response of an individual component of camber or deflection such as the deflection caused by the weight of the beam.

$$\Delta_i = \Delta_{ei} + \Delta_{tdi} \quad (5.1)$$

Such a component of deflection consists of both an elastic, Δ_{ei} , and a time dependent, Δ_{tdi} , response. The total beam camber or deflection equals the sum of the individuals components.

The total beam camber or deflection at any time can be predicted by multiplying each elastic camber and deflection component by an appropriate coefficient and summing the results as in Eq. 5.2.

$$\Delta_t = \sum M_i \Delta_{ei} \quad (5.2)$$

These coefficients, M_i , which are referred to as multipliers in this report, account for the elastic response and time dependent effects of prestress loss and creep. Each multiplier equals one plus a time dependent factor as in Eq. 5.3.

$$M_i = 1.0 + F_i \quad (5.3)$$

The time dependent factors, F_i , account for the time dependent response only. The time dependent response (not including the initial elastic response) caused by an individual camber or deflection component equals the elastic component multiplied by an appropriate time dependent factor. Each multiplier equals one plus a time dependent factor, because the total response at any time equals the initial elastic response ($1.0 * \Delta_{ei}$) plus the time dependent response ($F_i * \Delta_{ei}$).

When developing such multipliers, one must consider the magnitude and shape of the concrete creep and prestress force loss curves. The multipliers used for this project were developed using the ACI Committee 209 recommended creep expression of Eq. 5.4,

$$C_t = C_{ult} * t^{0.6} / (10 + t^{0.6}) \quad (5.4)$$

where C_t is the creep coefficient at time t after the load is applied, and C_{ult} is the ultimate creep coefficient. Because creep is the major component of time dependent prestress loss, $t^{0.6} / (10 + t^{0.6})$ was also used as the shape of the curve for time dependent prestress loss. The ACI Committee 209 recommended creep correction factors for concrete age at loading, volume to surface ratio, and relative humidity were also used.

Time dependent deflections caused by permanent dead loads, such as the weight of the beam, are a function of creep. If only the weight

of the beam were to remain acting on a noncomposite beam until the concrete stopped creeping, the final deflection would equal

$$\Delta_{bf} = (1.0 + C_{ult})\Delta_{eb} \quad (5.5)$$

The final life-time factor, F_{bf} , for time dependent deflection is equal to the ultimate creep coefficient. The final life-time multiplier to be applied to the initial deflection caused by the weight of the beam equals

$$M_{pf} = 1.0 + C_{ult} \quad (5.6)$$

The time dependent camber caused by the prestressing force is a function of the prestress force loss and creep coefficient at any time. With time, the elastic camber decreases due to the loss of prestress force, while the time dependent camber grows due to creep. If only the prestress force were to act on a beam, the multiplier to determine the final camber could be estimated as

$$M_{pf} = 1.0 + (1.0 - PL)C_{ult} \quad (5.7)$$

where PL is the time dependent prestress loss (percent loss divided by 100). The factor for final time dependent camber is

$$F_{pf} = (1.0 - PL)C_{ult} \quad (5.8)$$

Note that F_{pf} is always less than the lifetime factor applied to the beam weight deflection ($F_{bf} = C_{ult}$). If a step-wise analysis with small time steps, Δt , was being performed it would be desirable to reflect the gradual reduction of prestress and the resultant decrease in creep induced camber growth by a "weighted average loss" term βPL in Eq. 5.8. β would be determined from the shape of the prestress loss vs. time curve.

The two time dependent factors, F_{bf} and F_{pf} , described above are the basic factors from which multipliers at different times and for different loads are determined. In this study, multipliers were formed to calculate the responses caused by the weight of the beam, the prestressing force, the reduced span length when beams are placed in

storage, the increased span length when beams are placed in the bridge, the weight of deck panels, the weight of the cast-in-place slab, and a permanent dead load applied to the composite beam. The time dependent response was calculated when the beams were placed in the bridge, the panels were placed on the beams, the slab was cast, the permanent dead load was placed on the beam, and at the end of the service life of the bridge.

The multipliers for deflections caused by the weight of the beam, the increased span length when placed in the bridge, the weight of deck panels, the weight of the slab, and the camber that occurs due to the decreased span length when a beam is placed in storage are all determined as follows. The first step is to determine the final time dependent response factor equal to the ultimate creep coefficient. The ultimate creep coefficient must be corrected for the age of the beam concrete when the load is initially applied, the average relative humidity, and the beam volume-to-surface ratio. In order to determine the factor for time dependent response that has occurred at any time before the composite slab is added, the final time dependent response factor is multiplied by the fraction of creep that has occurred. The fraction of creep or time dependent response is calculated using

$$FR_t = t^{0.6}/(10 + t^{0.6}) \quad (5.9)$$

where t is the time since the load was first applied. The multiplier is determined by multiplying this response factor by F_{bf} and adding one.

Once the composite slab has been added to the beam, the moment of inertia is increased. This reduces the time dependent response that would have occurred. The time dependent response that has not yet occurred is reduced by the ratio of noncomposite to composite moment of inertia. For example, the factor for time dependent response caused by the beam weight at sometime after the composite slab has been cast is

$$F_{bct} = F_{bf}[FR_c + (FR_{ct} - FR_c)I_o/I_c] \quad (5.10)$$

where FR_c and FR_{ct} are the fractions of time dependent response that have occurred just before and at sometime after the composite slab is cast. They are calculated using Eq. 5.9. I_o/I_c is the ratio of noncomposite to composite beam moment of inertia.

The factor for time dependent response caused by the prestressing force is calculated in a similar manner to the other factors, however, the factor must include a reduction which represents the prestress force loss. This reduction equals one minus the fraction

of the prestress force that has been lost. Therefore, the factor for the time dependent camber caused by the prestressing force at any time before the composite slab has been cast is

$$F_{pt} = F_{bf}FR_t(1.0 - PL_t) \quad (5.11)$$

where PL_t is the time dependent prestress loss expressed as a decimal (percent loss divided by 100). The factor for the time dependent camber at sometime after the composite slab has been cast is

$$F_{pct} = F_{pc} + (F_{pt} - F_{pc})I_o/I_c \quad (5.12)$$

where F_{pc} is the response factor at the time the slab is cast calculated using Eq. 5.11. F_{pt} is also calculated using Eq. 5.11 even though t is greater than the time when the slab is cast.

Multipliers were determined and used to calculate the time dependent response for each instrumented beam. Two sets of multipliers were developed for each beam. The first set was determined using the ultimate creep coefficients obtained from the creep tests, along with the time dependent prestress loss which was determined by the AASHTO procedure. These creep coefficients were corrected for the volume-to-surface ratio of the beam. The second set was determined using the ACI Committee 209 recommended creep coefficient of 2.35, and a time dependent prestress loss of 15%. The creep coefficient was corrected for a volume-to-surface ratio of 4.75 and an average relative humidity of 65%.

The time dependent response was calculated using the elastic responses calculated with the moment area equations which are in the PCI Design Handbook. These cambers and deflections are listed in Table 5.5. The elastic cambers and deflections used to represent when the beams were placed in and then taken out of storage are listed in Table 5.10. These values were calculated using moment area equations for deflection and the average support conditions while the beams were in storage. Measured values were used for the elastic camber and then deflection for when beams H-01 and H-02 were placed in and then taken out of storage. Measured values were used, because the actual spans of the temporary supports were never measured.

Figure 5.32 shows the time dependent responses for beam L-11 determined using the two sets of multipliers. Point markers are used to show the calculated values for the responses. Smooth lines were used to connect the points. The general shape of the lines are correct, but they do not represent the exact values that could be determined using

TABLE 5.10 Calculated Elastic Camber and Deflection
That Occurs When a Beam Is Placed Into
and Taken Out of Storage

Beam	Camber when Placed in Storage (in.)	Deflection when Removed from Storage (in.)
L-i1 and L-i2	0.68	0.50
L-o1 and L-o2	0.65	0.47
H-o1	0.66	0.28
H-o2	0.80	0.44
H-i1 and H-i2	0.57	0.44

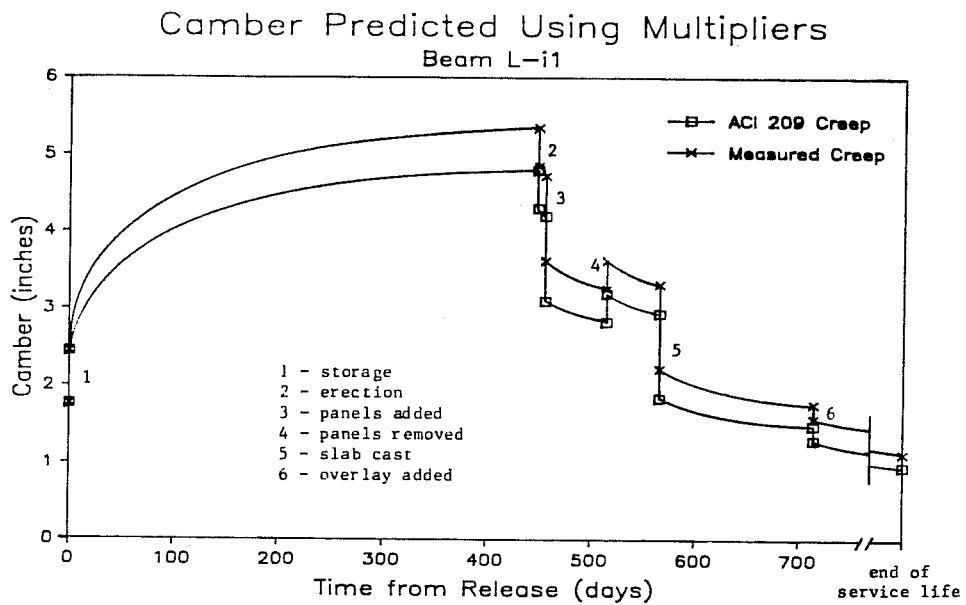


Fig. 5.32 Time dependent camber for beam L-i1 predicted using the proposed multipliers

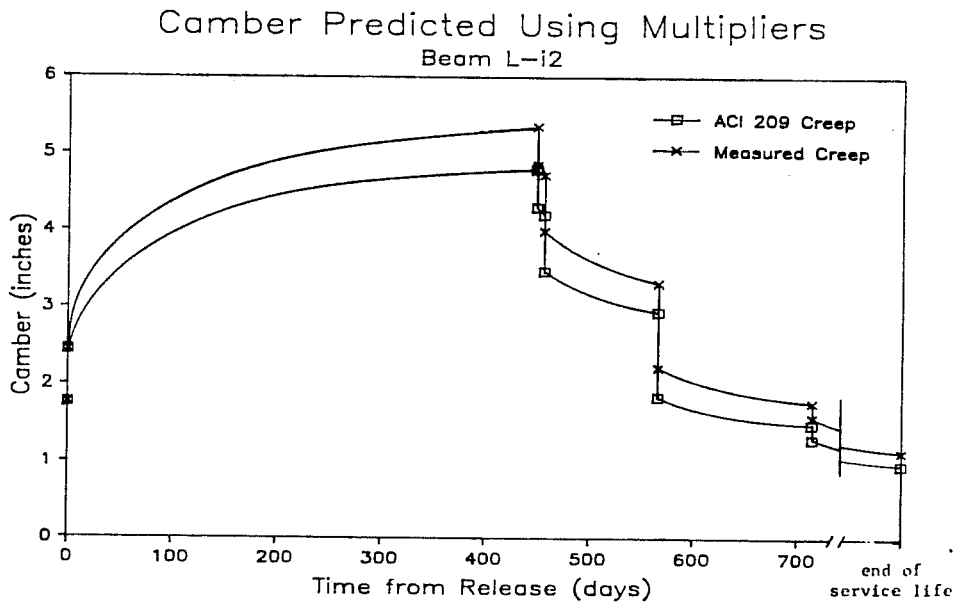


Fig. 5.33 Time dependent camber for beam L-i2 predicted using the proposed multipliers

this method. Time dependent response due to the extra half layer of panels stored on beam L-i1 was assumed to not occur. The general shape of the responses are similar to the actual response. The calculated responses for the other instrumented beams are shown in Figs. 5.33 to 5.38.

The responses calculated using the multipliers are compared to the measured responses of beams L-o1 and H-i2 in Figs. 5.39 and 5.40, respectively. As shown in these figures, the response calculated using the recommended creep coefficient more closely represents the actual response. This creep coefficient is smaller than the measured creep coefficients. This supports the idea presented in Sec. 5.5.4 that the measured creep coefficient is too large or else the volume-to-surface ratio reduction factor is not great enough.

5.7 General

The results of several analytical techniques were presented in this chapter. Prestress losses were calculated using PSTRS10, AASHTO Specifications, the PCI Design Handbook, and PBEAM. The loss predictions were not compared to measured values because the strand strain measuring system did not work properly. Cambers and Deflections, both elastic and time dependent were calculated with PSTRS10, the PCI Design Handbook, PBEAM, and a proposed multiplier technique. The elastic cambers and deflections were accurately predicted using the PCI equations and PBEAM. In general, the time dependent response was underpredicted by PSTRS10 and the PCI longtime multipliers, and the response was overpredicted by PBEAM and the proposed multipliers when the measured creep coefficients were used. The time dependent response was accurately predicted using the proposed multipliers with the ACI 209 recommendations for creep.

In the next chapter, the results of the analytical techniques will be compared to one another and the measured response. Calculated losses will be compared to one another and the measured camber and deflection will be used as a datum for determining which technique is most accurate. The time dependent camber and deflection responses for all the procedures will be compared using plots similar to Figs. 5.39 and 5.40. The predicted responses will all be included on the same plot along with the measured response. These plots will be used to show which techniques are most accurate and how the predicted results compare to one another.

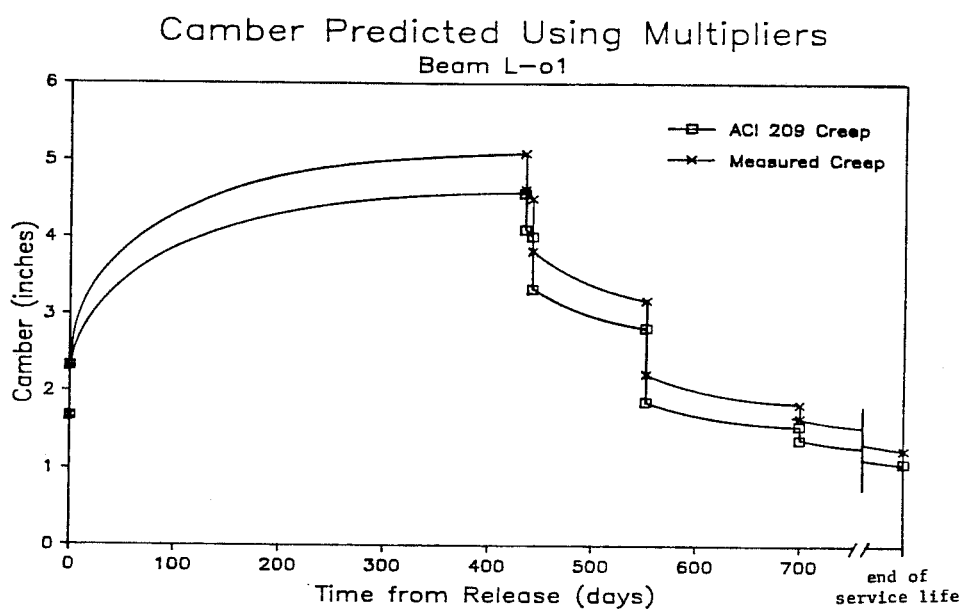


Fig. 5.34 Time dependent camber for beam L-o1 predicted using the proposed multipliers

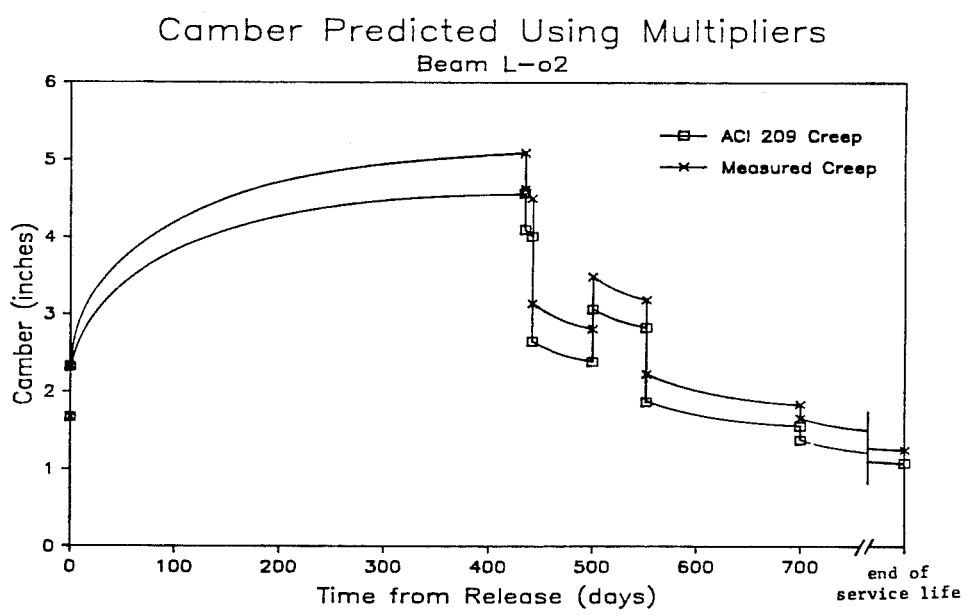


Fig. 5.35 Time dependent camber for beam L-o2 predicted using the proposed multipliers

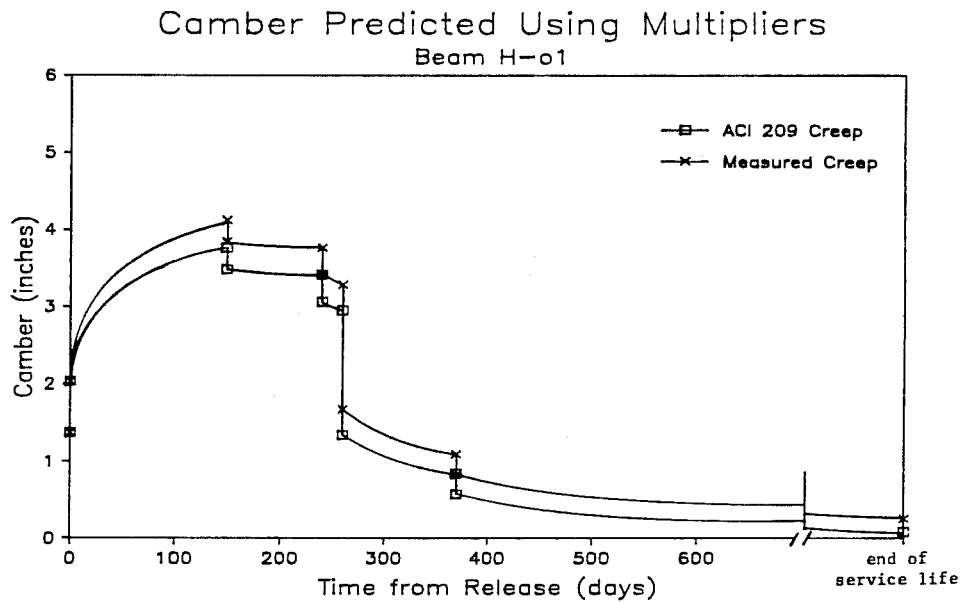


Fig. 5.36 Time dependent camber for beam H-o1 predicted using the proposed multipliers

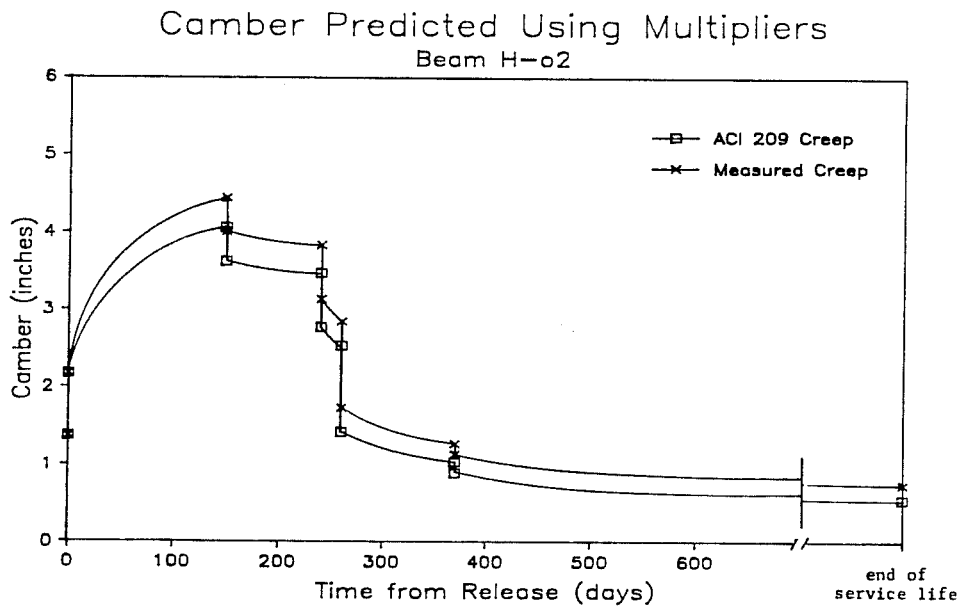


Fig. 5.37 Time dependent camber for beam H-o2 predicted using the proposed multipliers

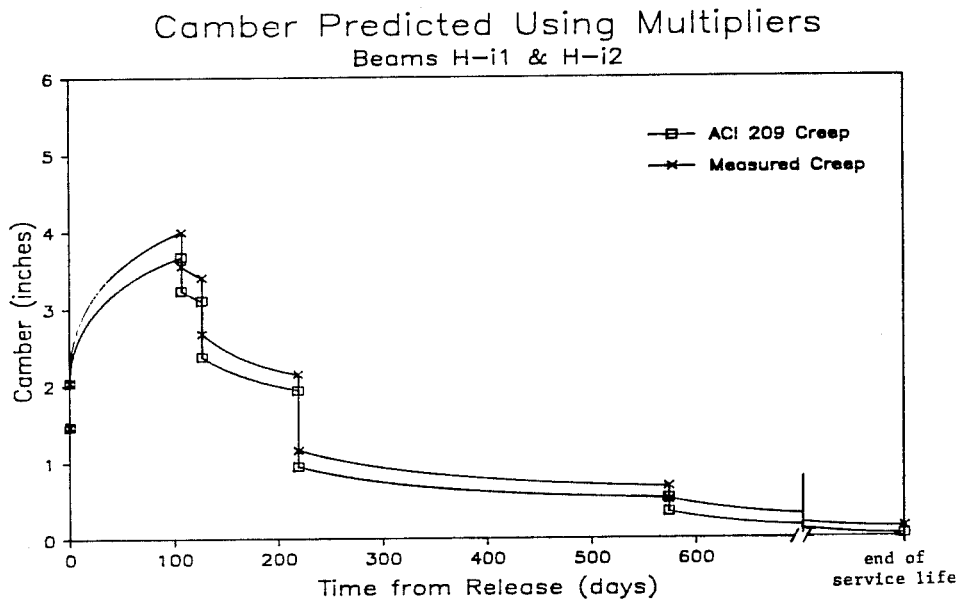


Fig. 5.38 Time dependent camber for beams H-i1 and H-i2 predicted using the proposed multipliers

Predicted and Measured Midspan Camber Beam L-o1

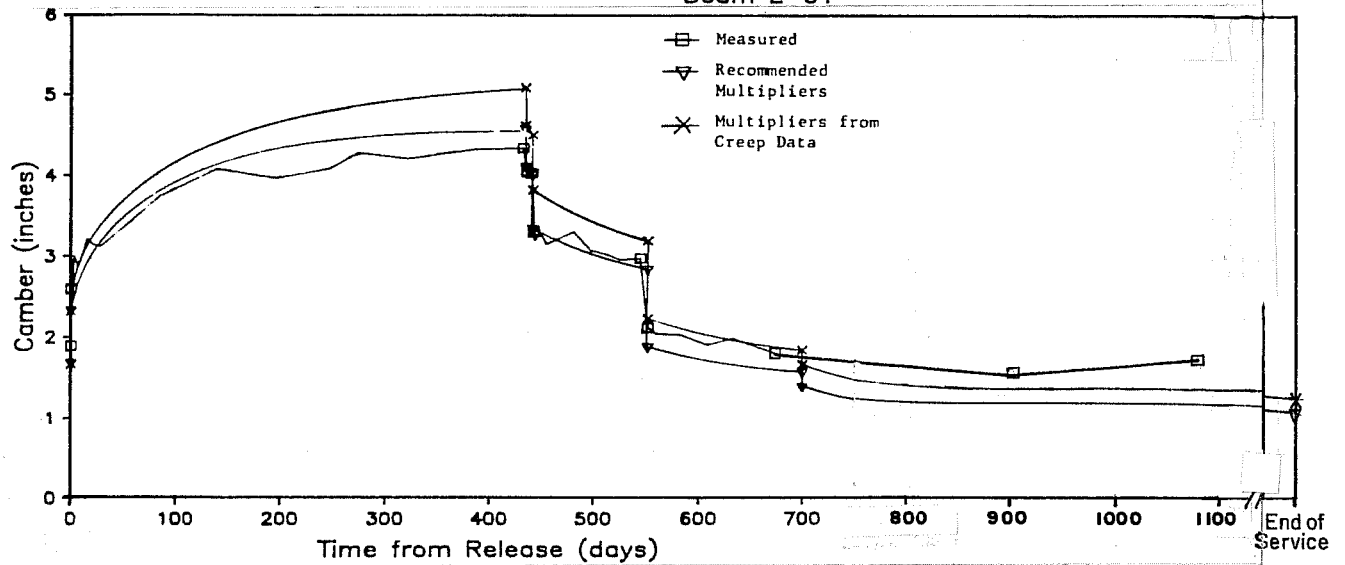


Fig. 5.39 Comparison of time dependent camber predicted using proposed multipliers and measured camber for beam L-o1

Predicted and Measured Midspan Camber Beam H-i2

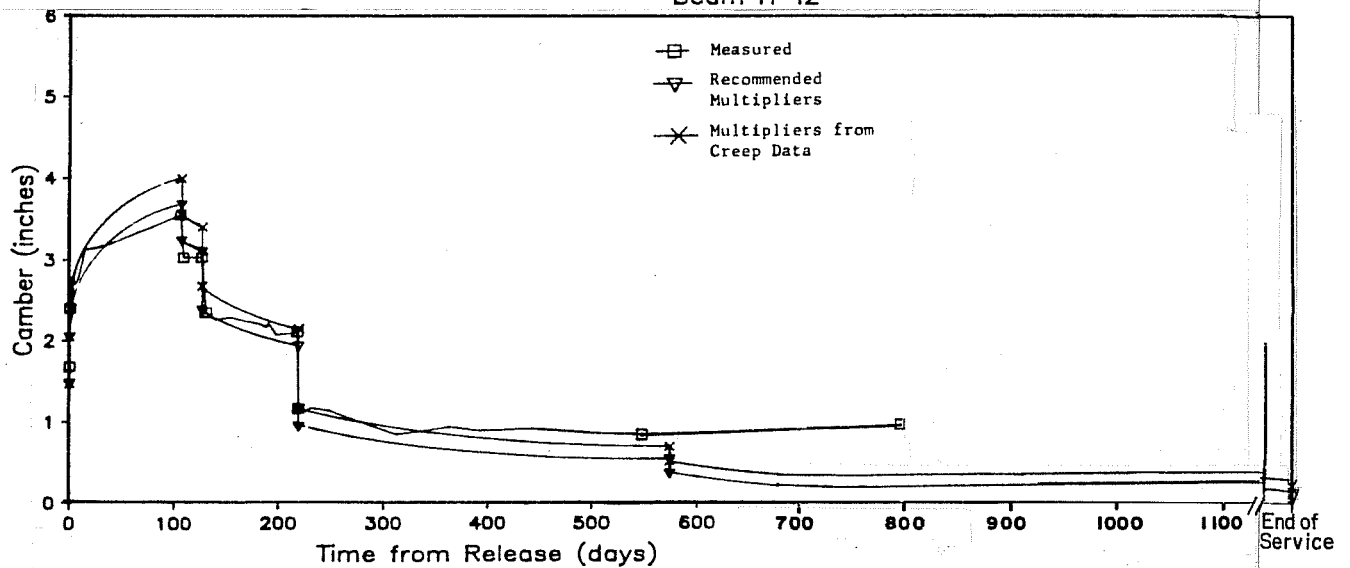


Fig. 5.40 Comparison of time dependent camber predicted using proposed multipliers and measured camber for beam H-i2

CHAPTER 6

ASSESSMENT OF ANALYTICAL TECHNIQUES

6.1 Prestress Loss

In this section, prestress losses calculated using PSTRS10, the AASHTO Specifications, the PCI Design Handbook, and PBEAM are compared. Based on the comparisons, recommendations are made to improve the accuracy of loss prediction.

The losses for the L-series beam with nominal material properties and $f_{sp} = 0.7f'_s = 0.7 f_{pu}$ calculated using PSTRS10, AASHTO Specifications, and the PCI Design Handbook are compared in Fig. 6.1. The total prestress loss calculated using each procedure was approximately 27% for the nominal properties beam with stress-relieved strand. However, the loss due to each component varies among the methods. For example, the 11.1% loss due to creep which was calculated with the AASHTO procedure is greater than the 8.4% loss calculated using the PCI procedure. This difference was partly offset by the 4.5% relaxation loss calculated with the AASHTO procedure compared to the 7.7% loss for the PCI procedure. Since none of the instrumented beams contained stress-relieved strand, none of the current data are applicable for verifying these losses.

The prestress losses calculated for the same nominal properties L-series beam but with low-relaxation strand substituted for the stress-relieved strand are also shown in Fig. 6.1. The version of program PSTRS10 used did not correctly express the relaxation loss for low-relaxation strand but has been subsequently modified to do so. The total loss calculated with the AASHTO procedure (24%) was greater than that calculated with the PCI procedure (20.6%). The difference was primarily caused by the greater creep loss (11.1 vs 8.4%). The AASHTO creep loss was greater, because it applies different creep coefficients to the compressive stress applied at release and the tensile stress applied when the slab was cast. A greater coefficient is applied to the initial stress at release, because the concrete is loaded at an earlier age. In the PCI procedure, the same creep coefficient was applied to each of these stresses. This difference was masked in the earlier comparison with stress-relieved strand by the offsetting difference in assumed relaxation losses.

The prestress losses for beams L-01 and H-i2 (both with low relaxation strand) calculated using the AASHTO procedure, the PCI procedure, and PBEAM are shown in Fig. 6.2. Elastic shortening losses of 7.2 and 6.5% were calculated for beams L-01 and H-i2, respectively.

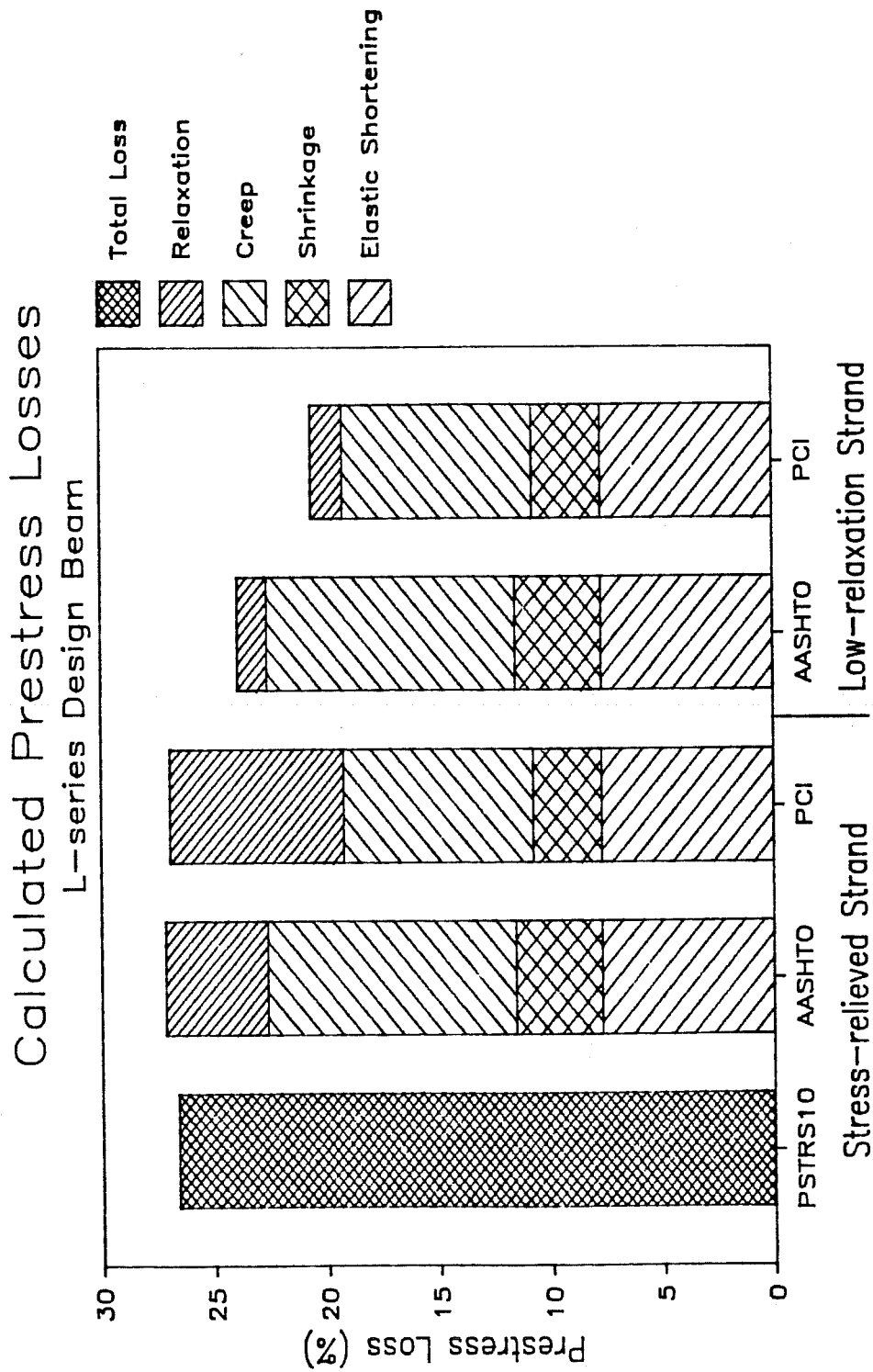


Fig. 6.1 Comparison of calculated prestress losses for the L-series design beams

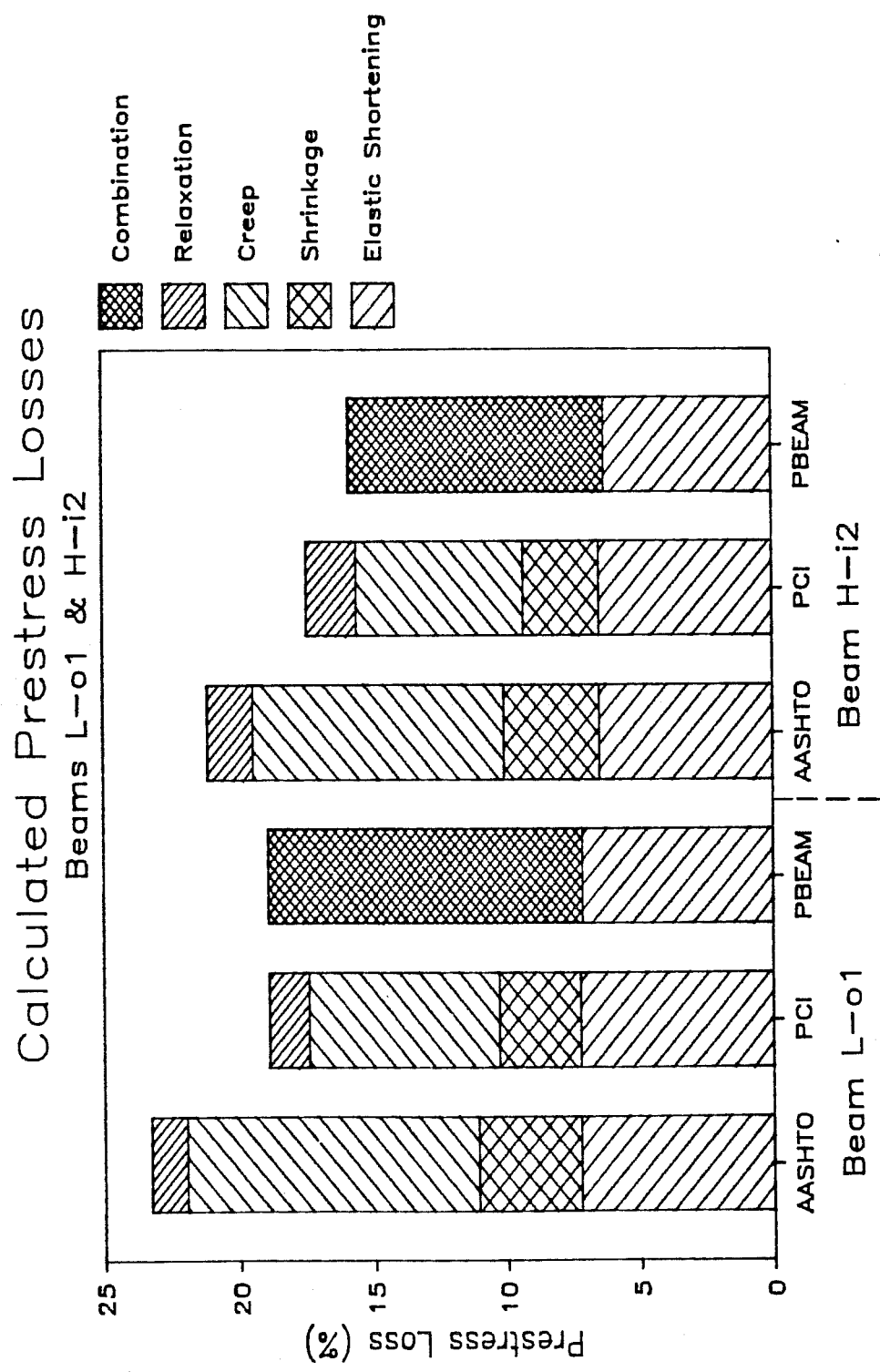


Fig. 6.2 Comparison of calculated prestress losses for beams L-01 and H-i2

These losses were approximately equal for all the procedures. Because the initial cambers calculated using PBEAM were very close to the measured values, the initial losses calculated using all of these procedures were probably also accurate.

For both of these beams, PBEAM predicts the least amount of time dependent loss. The prestress loss predicted by PBEAM is probably an underestimate. If it were underestimated, the time dependent beam camber would have been overestimated. In Sec. 5.5.3, the time dependent camber predicted by PBEAM was indeed shown to be overestimated, primarily due to the high value for the creep coefficient, as well as the low estimate for the loss due to relaxation. A difference of 2% in the calculation of the percentage loss can cause a difference of 0.13 in. in the elastic camber, and a difference of as much as 0.4 in. in the total camber. Based on the comparison of the PBEAM predictions for the time dependent beam camber with the measured values, the prestress losses may have been underestimated by as much as 2 to 4% loss in the PBEAM solution. This means the PCI losses would also be underestimates.

The AASHTO prestress loss predictions for these beams were the greatest. The prestress loss calculated by the AASHTO procedure was most likely overestimated by a 1 to 2% loss. The greatest component of loss was caused by creep. The equation used to calculate the creep loss (ksi) was

$$CR_c = 12f_{cir} - 7f_{cds} \quad (6.1)$$

where f_{cir} is the initial concrete stress at the centroid of the prestressing strand, and f_{cds} is the tensile stress caused by the permanent dead load. Using the ACI Committee 209 recommendations for creep, the actual concrete strengths, and the actual construction time schedule for beam L-01, a similar equation with different coefficients can be obtained:

$$CR_c = 9.2f_{cir} - 2.4f_{cds} \quad (6.2)$$

A creep loss of 9.6% is predicted with this equation compared to 11.1% predicted using Eq. 6.1. This difference is only apparent when actual material properties and construction schedules are known. Such accuracy is not generally possible in the design stage.

Overall, it is the authors' opinion that the AASHTO procedure for calculating the total prestress loss provided the most accurate results for the instrumented beams. This procedure most accurately

represented the influence of various loading stages in the equation for creep loss when this project was active in 1984-6, AASHTO did not include an equation for estimating the relaxation loss for low-relaxation strand. AASHTO did adopt such an equation in the 1985 Interim published in 1986. Equation 6.3A which is part of the PCI procedure was adopted for use in this project. The relaxation loss (ksi) for grade 270, low-relaxation strand initially tensioned to 0.75 times the guaranteed ultimate tensile stress is

$$CR_S = 5000 - 0.04(SH + CR_C + ES) \quad (6.3A)$$

where SH, CR_C , and ES are the losses due to shrinkage, creep, and elastic shortening, respectively. The generally similar AASHTO Equation 9-10A adopted in the 1985 Interim is

$$CR_S = 50000 - 0.10 ES - 0.05 (SH + CR_C) \quad (6.3B)$$

The accuracy of the AASHTO loss prediction could be further improved by providing several equations for the loss due to creep. Important factors which should be considered are the volume-to-surface ratio of the beam, the age of the beam when the slab is cast, the average percent relative humidity, and the ultimate creep coefficient.

In Texas, the three most commonly used standard beams are the Texas Type C and 54 beams, and AASHTO Type IV beams. These beams have volume-to-surface ratios ranging from 3.33 to 4.75 in. For this range, the ACI Committee 209 recommendations for the creep volume-to-surface ratio correction factor varies from 0.725 to 0.79. This variation is not great enough to warrant separate equations. However, for these beams an average correction factor of 0.75 should be used in developing creep loss equations.

During the design phase, the designer can only guess what the construction schedule will be. Therefore, it would be difficult to include the actual age of the beam when the slab is cast in the loss equation. However, most beams are generally less than one year old when the slab is cast. Using one year as the age when the slab is cast will safely overpredict the loss due to creep for most beams.

The relative humidity has a large effect on the amount of creep that occurs. Based on the ACI Committee 209 recommendations, for the same concrete, the amount of creep that occurs in a city with 75% relative humidity, such as Houston, is only 77% of the creep that occurs in a city such as El Paso which has 40% average relative humidity. Using the same principles that were used to develop the deflection

multipliers presented in Sec. 5.6, equations to predict the prestress loss due to creep can be developed. For a typical creep coefficient, the loss due to creep in a city with high relative humidity can be estimated using

$$CR_c = 9f_{cir} - 2f_{cds} \quad (6.4)$$

and in a city with low humidity,

$$CR_c = 11f_{cir} - 3f_{cds} \quad (6.5)$$

These equations were developed using a volume-to-surface ratio of 4.0, a creep coefficient of 2.35, release at 1 day, and the slab cast one year after the beam.

Sometimes a designer knows ahead of time that a beam will be cast using concrete which is known to have a large amount of creep, such as lightweight concrete, or a very small amount of creep, such as the concrete from a particular prestress plant. For these cases, the designer may want to use a more accurate equation for estimating the prestress loss due to creep. The creep loss for beams made of concrete with a high creep coefficient could be estimated using

$$CR_c = 12f_{cir} - 3f_{cds} \quad (6.6)$$

The creep loss for beams made of concrete with a low creep coefficient could be estimated using

$$CR_c = 5f_{cir} - f_{cds} \quad (6.7)$$

Equations 6.6 and 6.7 were developed using creep coefficients of 2.5 and 1.0, respectively. These coefficients were corrected for a beam volume-to-surface ratio of 4.0. Release was assumed to occur one day after a beam is cast, and the slab was assumed to be cast one year later.

6.2 Elastic Camber and Deflection

The measured and calculated initial elastic camber upon release of the pretensioning force and the later deflections caused by the addition of deck panels and subsequently the cast-in-place slab are

compared in Tables 6.1 and 6.2. The responses were calculated using program PBEAM and also using the moment area equations which appear in the PCI Design Handbook. The PCI procedures are included in the microcomputer program CAMBER developed as part of this study and discussed in Appendix A and listed in Ref. 46. The calculated responses are compared with the measured values for beams L-01 and H-i2. The percentage error for the initial camber was determined by dividing the difference in the measured and calculated camber by the sum of the absolute values of the components predicted using the PCI equations. This procedure is a more realistic assessment of accuracy in procedures which represent the difference of large numbers.

PBEAM predicted the initial elastic camber somewhat more accurately. However, both procedures were quite close on a percentage basis.

Similar numerical accuracy was obtained using PBEAM and CAMBER to predict the deflections caused by the deck panels and slab. In view of the small magnitude of the deflections involved, the accuracy is acceptable. It is impossible to determine which procedure was more accurate, since there was some probable error in the measured deflections caused by thermal movements which is probably of the order of magnitude of the differences between calculated values by the two methods.

Although the elastic responses predicted using both PBEAM and the PCI equations (Program CAMBER) were good, the authors recommend the use of the PCI equations because they are much easier to use. This is particularly true if the microcomputer program CAMBER is used. The accuracy of the initial camber predicted by this method could be improved by using 0.92 times the initial force for the force immediately after release. Currently PCI suggests 0.9, but 0.92 seems better for low-relaxation strand. As mentioned in Sec. 5.4.2, this will increase the initial camber for these girders by a tenth of an inch.

6.3 Time Dependent Camber and Deflection

In this section, time dependent camber and deflections calculated by the different techniques discussed in Chapter 5 are compared to one another and the measured response. Comparisons are made using the typical responses for beams L-01 and H-i2.

The time dependent responses calculated by the various methods for beam L-01 are compared in Fig. 6.3. The response calculated using the proposed multipliers which are included in microcomputer program CAMBER was the most accurate. The time dependent response predicted using the multipliers only slightly overestimates the camber during

TABLE 6.1 Comparison of Calculated and Measured Elastic Responses (in.) for Beam L-01

Response	Measured	(Program CAMBER)		PBEAM	
		PCI Calculated	Error (%)	Calculated	Error (%)
Initial Camber	1.89	1.67	2.2	1.92	0.3
Deck Panels	0.73	0.68	-6.8	0.62	-15.1
Cast-in-Place Slab	0.86	0.96	+11.6	0.85	-1.2

TABLE 6.2 Comparison of Calculated and Measured Elastic Responses (in.) for Beam H-i2

Response	Measured	(Program CAMBER)		PBEAM	
		PCI Calculated	Error (%)	Calculated	Error (%)
Initial Camber	1.68	1.47	2.1	1.69	0.1
Deck Panels	0.69	0.73	+5.8	0.65	-5.8
Cast-in-Place Slab	0.94	0.99	+5.3	0.85	-9.6

Predicted and Measured Midspan Camber

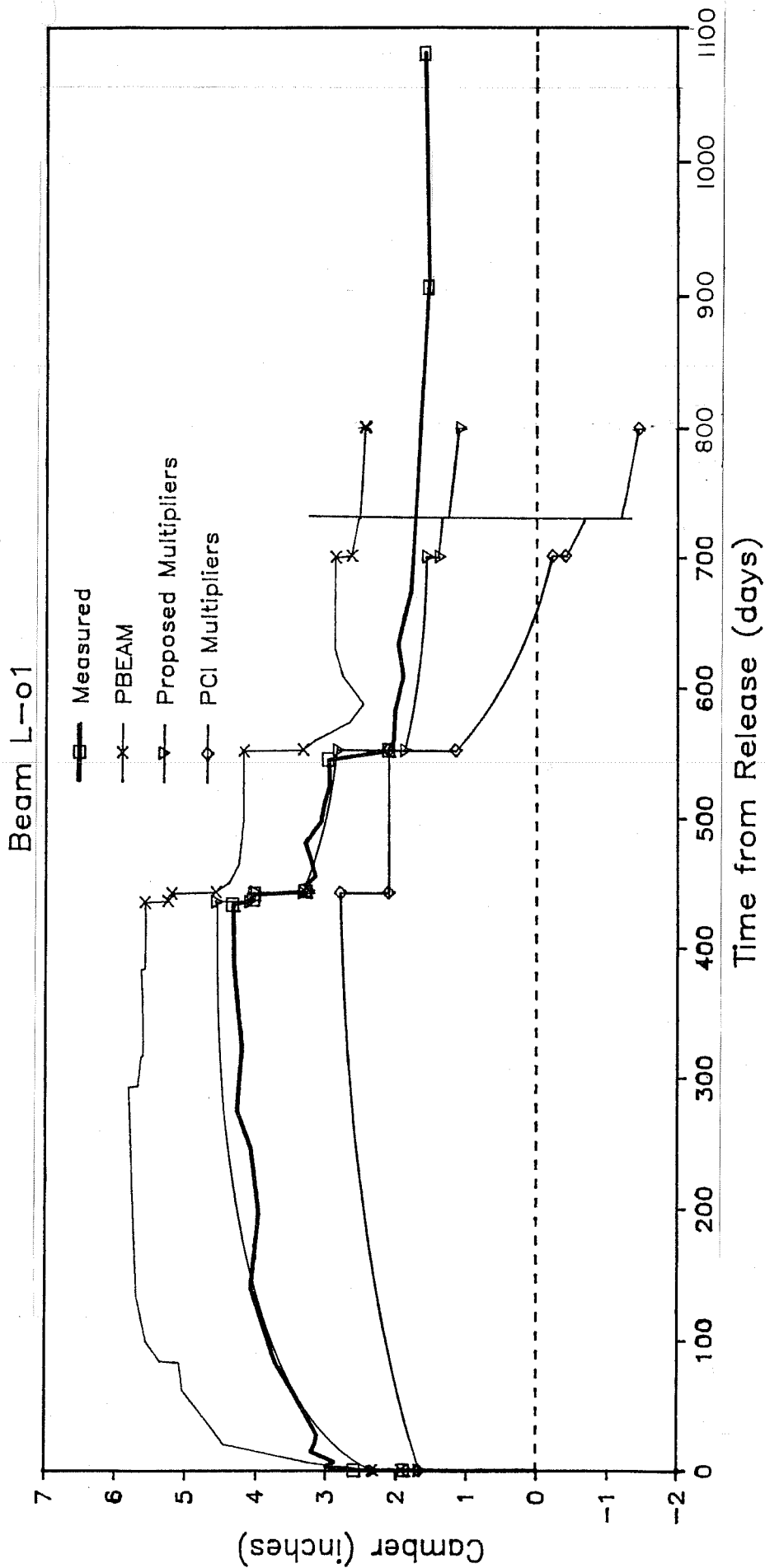


Fig. 6.3 Comparison of calculated time dependent camber for beam L-o1

erection and slightly underestimates it once the slab has been cast. The response predicted using PBEAM overestimated the time dependent camber at all times. PBEAM overestimates the camber primarily because the measured creep data on the companion cylinders were too high or the volume-to-surface ratio connection factor was too low. The response calculated using the PCI multipliers seriously underestimated the time dependent camber. Similar results were obtained for beam H-12, as shown in Fig. 6.4.

The proposed multipliers appear to work very well. Not only did they yield the best results, but they were also easy to use. These multipliers could be useful to the designer and the field engineer. The designer can obtain an estimate as to how much the beams will camber or deflect with time based on estimated construction schedules. The field engineer will be able to make more accurate estimates by calculating the response using the known actual age of the beam during important construction events, and the concrete strengths measured by the SDHPT at the prestressing plant. If the field engineer has access to a microcomputer such as the IBM AT with a math coprocessor chip (or equivalent), the calculated response can be easily updated using the program CAMBER described in Appendix A and listed in Ref. 46.

6.4 Sensitivity of Camber Predictions to Material Properties and Construction Schedule

6.4.1 General. There are many variables which affect the time dependent camber, and it would be difficult to systematically investigate all of them. In this section, the sensitivity of the calculated camber is investigated for typical ranges of several of the more important variables and construction schedules. The predictions are then compared for typical and unfavorable combinations of variables. The variations in the properties and the combinations that will be used do not necessarily represent the worst possible cases. However, the comparisons do provide an idea of how sensitive the camber is to certain variables, and how much variation should be expected in the field.

The sensitivity analysis was performed using the computer program CAMBER which is documented in Appendix A and which calculates the longtime camber using the proposed multipliers. Except where otherwise noted, the analysis was performed using the following general design and properties. The beam was a 127 ft span AASHTO Type IV beam similar in design to the H-series beams and assumed made with low-relaxation strand. The ratio of the prestress force just after release to the initial force was assumed equal to 0.92. The time dependent loss (excludes initial elastic shortening and relaxation which occurs before release) was assumed to be 15%. While in storage, the beams were

Predicted and Measured Midspan Camber Beam H-i2

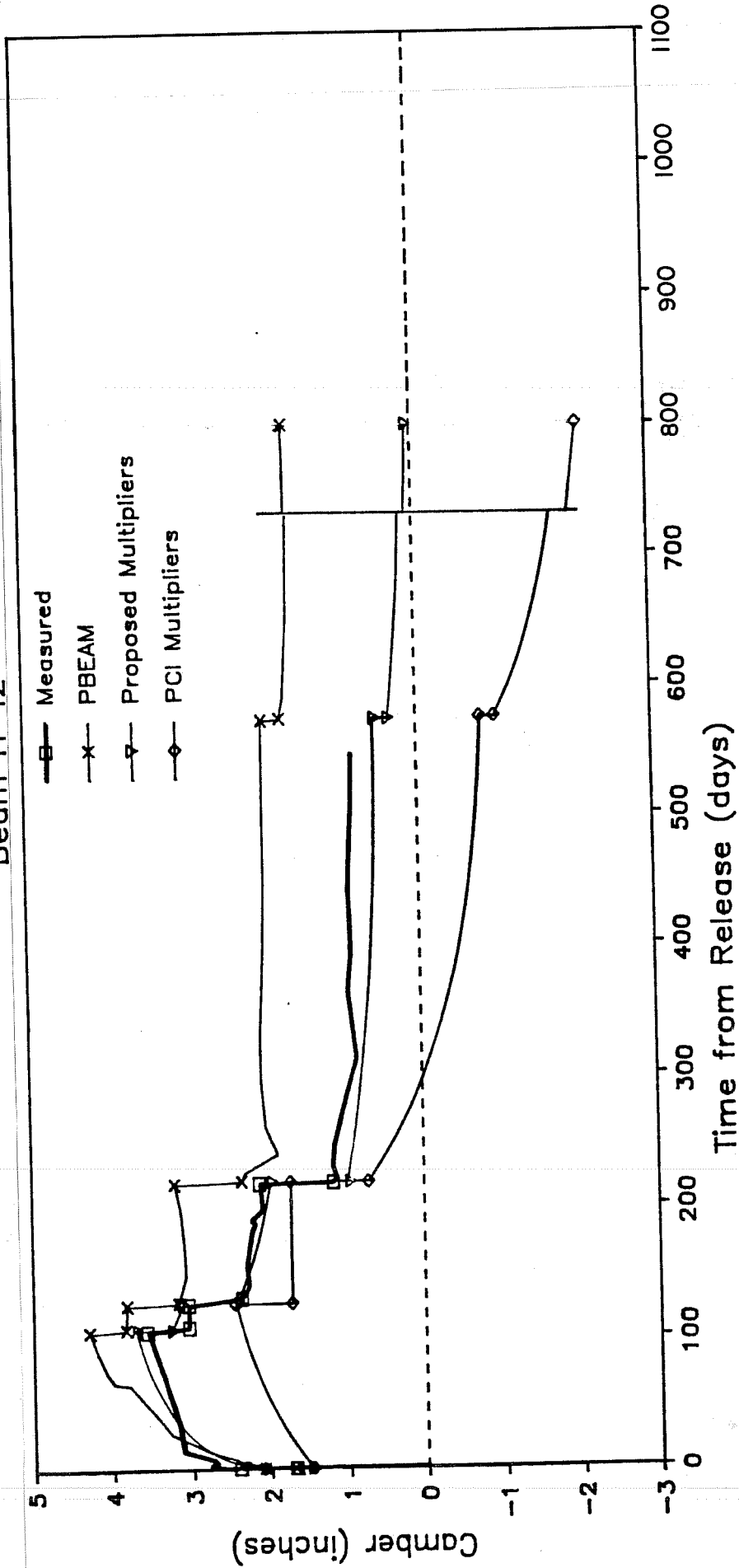


Fig. 6.4 Comparison of calculated time dependent camber for beam H-i2

assumed to be supported on blocks 4 ft from each end with a resultant span length 8 ft shorter than when in the bridge.

6.4.2 Concrete Strength. Long span Type IV beams have been designed by the Texas SDHPT to have concrete strengths from 5000 to over 10,000 psi. In recent years, these beams have been usually designed with specified concrete strengths from 5000 to 8000 psi with most in the 7000 to 7500 psi range. In the near future, it is anticipated that these beams will be designed to have concrete strengths of 9000 psi or higher. Strengths of this magnitude will generally be specified in the southern part of Texas where the cement and aggregate is of higher quality than in other parts of the State.

Three levels of concrete strengths were used to perform the sensitivity analysis. The lowest level included strengths of 4500, 6000, and 6500 psi at release, 28 days and one year, respectively. Corresponding strengths for the typical strength level were 5000, 7880, and 8500 psi. This 28-day strength is slightly greater than the most commonly specified range of 7000 to 7500 psi, because the actual strength is generally 5 to 10% greater than the specified strength. The strengths for the highest level were 6000, 10,050, and 12,000 psi at 20 hours, 28 days and one year, respectively. These later values were suggested by Jesse Lawrance who was superintendent of the Heldenfels Brothers, Inc. prestressing plant when the instrumented beams of this study were cast.

The analysis was performed assuming a construction sequence similar to that of the instrumented beams, but with a revised time schedule. The age of the beam during release was set equal to 0.8 days. The beam was then assumed to be erected at 112 days, have deck panels placed on it at 119 days, have the slab cast at 140 days, and have the overlay added at 196 days.

The ACI Committee 209 recommendation of 2.35 was used for the ultimate creep coefficient. These values seemed reasonable for the girders in this study. Smadi, Slate and Nilson [47] have reported that 60 day creep coefficients seem significantly less for very high strength concretes than for lower strength concretes. However, data is not available for longer periods to indicate what may be expected over a design lifetime. Appropriate corrections were made for the volume-to-surface ratio of a Type IV beam and an average relative humidity of 65%.

The results of the analysis are shown in Fig. 6.5. The highest strength concrete had the least amount of camber at erection, the smallest time dependent response, and the greatest final camber. Because higher strength concrete has a higher elastic modulus, the elastic responses were smaller. Less time dependent response occurs, because it is a function of the creep coefficient multiplied by the

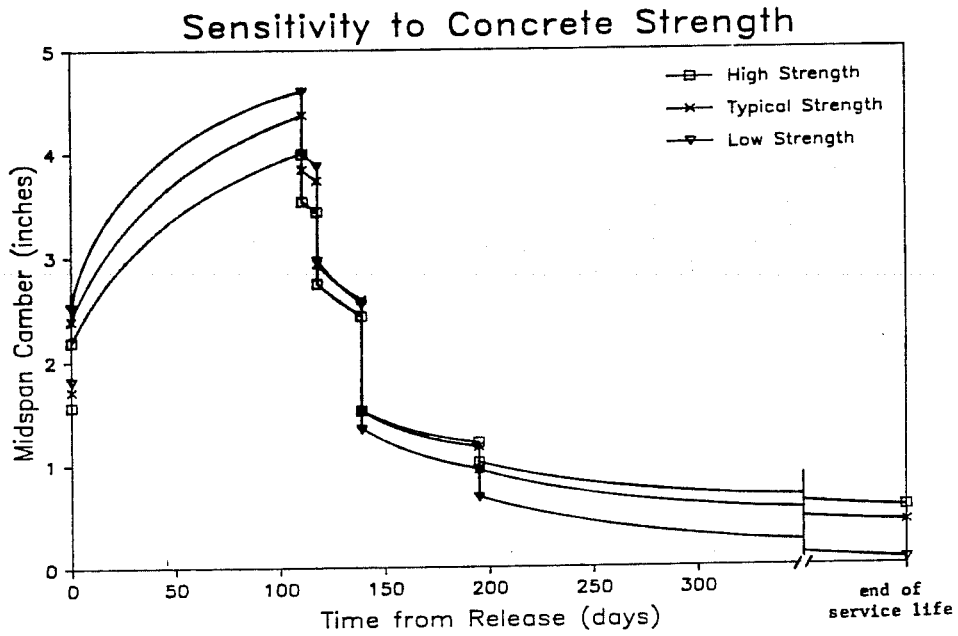


Fig. 6.5 Sensitivity of time dependent camber to concrete strength

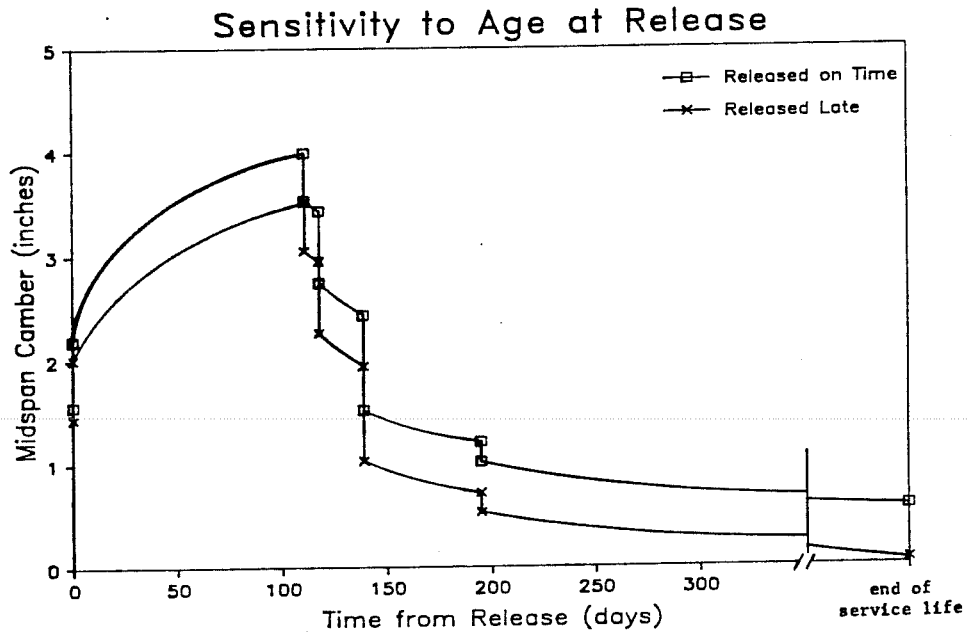


Fig. 6.6 Sensitivity of time dependent camber to beam age at release

elastic strains which were smaller. The greatest camber during erection, the greatest time dependent response, and least final camber was predicted for the lowest strength concrete. These results were caused by the smaller elastic modulus.

6.4.3 Age at Release. The prestress force for most pretensioned beams in Texas plants is released within 24 hours after the beam is cast. However, it is not uncommon for the force to be released as late as four days after the beam has been cast. This can occur when a beam is cast on a Friday and then it rains on the following Monday.

The calculated response of two otherwise identical beams, one released at 0.8 days and the other at 4 days after casting, are compared in Fig. 6.6. The same construction time schedule, creep coefficient, and the higher strength concrete used for the analysis in Sec. 6.4.2 were used. The high strength concrete was used for this analysis, because the age strength gain characteristics of this concrete at an early age were most accurately known. The beam four days old at release had a smaller initial response, and less camber during erection and at the end of the service life. The difference in camber was 0.5 in. throughout most of the construction period and service life.

6.4.4 Creep. Creep is a function of several factors such as the type of aggregate used, environmental conditions, concrete compressive strength and the age of concrete when stresses are applied. The resulting creep that is observed in the field can vary a large amount. Three different ultimate creep coefficients were used for this analysis. The low value used, 1.0, was measured by Sinno and Furr [12]. The ACI recommended value of 2.35 was used for the typical case, and 2.5 was used as the high coefficient. These coefficients were adjusted using the ACI Committee 209 recommendations for creep correction factors. The coefficients were corrected for a volume-to-surface ratio of 4.75. The low and typical coefficients were corrected for a relative humidity of 65%, while a correction factor for relative humidity was not applied to the maximum coefficient. The analysis was performed using the same construction schedule as in Sec. 6.4.2.

The results of the analysis are shown in Fig. 6.7. As shown by this figure, creep has an important effect on the time dependent camber of a beam. A maximum difference in camber of almost 2 in. is predicted at 112 days when the beams are placed in the bridge. The maximum difference in camber predicted at the end of the service life is only 0.5 in.

6.4.5 Humidity. Relative humidity affects the amount of creep, and therefore, the time dependent behavior of a beam. Using the construction time schedule in Sec. 6.4.2 and the typical creep coefficient used in Sec. 6.4.4, an analysis was performed for beams

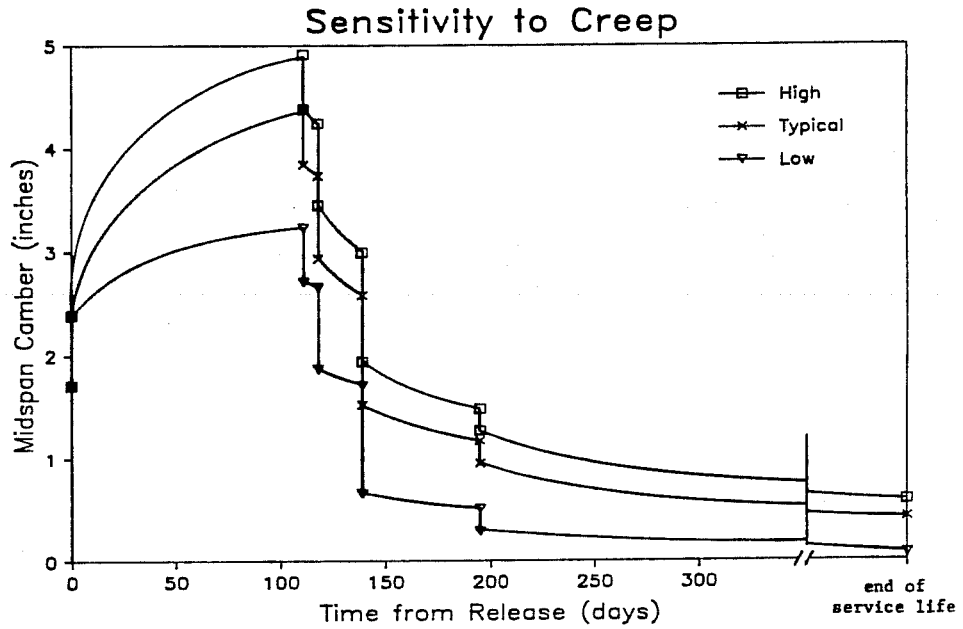


Fig. 6.7 Sensitivity of time dependent camber to the creep coefficient

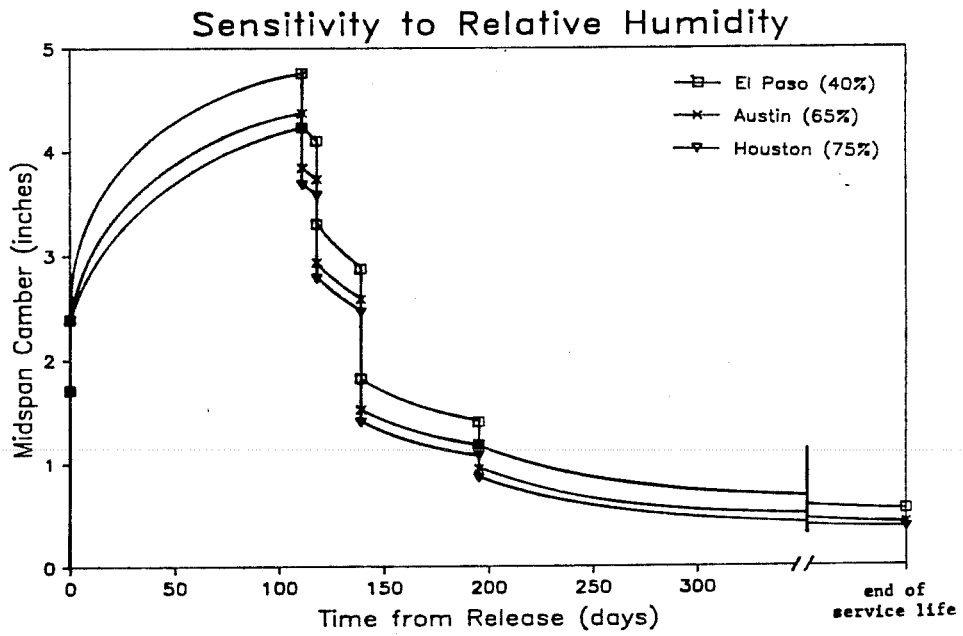


Fig. 6.8 Sensitivity of time dependent camber to the relative humidity

subjected to three average relative humidities. Relative humidities of 40, 65, and 75% were used to represent beams cast and erected near El Paso, Austin, and Houston, respectively. The analysis was performed using the ACI 209 recommendations for the creep correction factor for relative humidity.

The results of the analysis are shown in Fig. 6.8. The beam subjected to 40% relative humidity had the greatest time dependent response, while the beam subjected to 75% relative humidity had the least. A difference of more than half an inch of camber is predicted at the time the beams are shipped to the bridge site. However, there is very little difference in the camber at the end of the service life.

6.4.6 Low-Relaxation Strand Substituted for Stress-Relieved Strand. Because low-relaxation strand meets all the ASTM specification requirements for stress-relieved strand, a fabricator can substitute low-relaxation strand for stress-relieved strand at his discretion. Such substitutions are widely made. When such a substitution is made during fabrication, the beam design and initial strand stress level usually remain as specified for the beam as originally designed assuming it would be made with stress-relieved strand. In fact, this substitution was made for the L-series beams in this study with no notice to the design group.

The effect that such a substitution can have on the time dependent behavior was investigated. The responses for two otherwise identical 128 ft span beams, one made with stress-relieved strand and the other with low-relaxation strand substituted for the specified stress-relieved strand, were calculated. These beams were similar in design to an L-series beam. The typical values for concrete strength and the creep coefficient that were used in Sec. 6.4.2 were also used to calculate the responses for these beams. The response of the beam with stress-relieved strand was calculated using a value of 0.90 for the ratio of prestress force immediately after release to the initial prestress force and using a total time dependent loss of 20%. The response for the otherwise identical beam with low-relaxation strand was calculated using a value of 0.92 for the ratio of the force immediately after release to the initial force and using a total time dependent loss of 15% to reflect the improved relaxation characteristics.

Figure 6.9 shows that when low-relaxation strand is substituted for stress-relieved strand with no other changes, the camber at every time is increased. For the calculated responses, the camber at erection (112 days) was 0.5 in. greater for the beam made with low-relaxation strand. This difference increased to 0.71 in. at the end of the service life. In order to accurately predict the time dependent response, one must know which type of strand was or will be used.

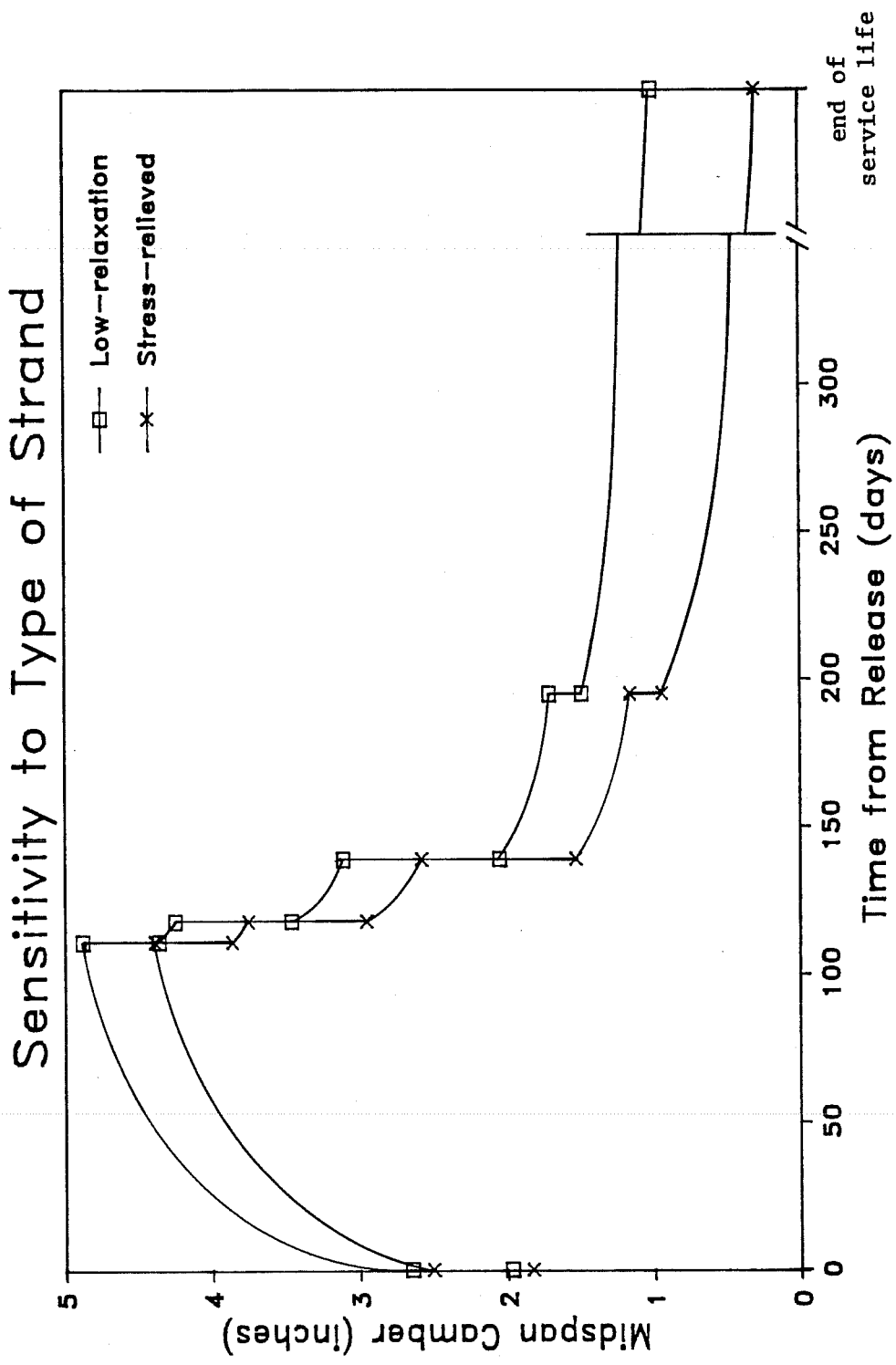


Fig. 6.9 Effect that substituting low-relaxation strand for stress-relieved strand without changing the design of the beam has on time dependent response

6.4.7 Replaced Beam. When constructing a bridge, a beam can be damaged and have to be replaced. When this occurs the new replacement beam may be much younger than the adjacent beams in the bridge, and so the camber may be significantly less. Using the typical strength concrete from Sec. 6.4.2 and the typical creep coefficient from Sec. 6.4.4, the responses for a typical beam and a replacement beam were calculated. The time dependent responses for these beams are shown in Fig. 6.10. The construction schedule used in Sec. 6.4.2 was used for the typical beam. It was assumed that the replacement beam was cast at 109 days after the original casting date. The schedule for the replacement beam was release at 0.8 days, erection at 7 days, deck panels added at 10 days, slab cast at 31 days, and the overlay added at 87 days. The erection is assumed to occur at 7 days since this is the earliest age at which the SDHPT allows beams to be taken from a prestress yard.

As shown in Fig. 6.10, the camber at erection for the adjacent (typical) beam is 1.0 in. greater than the camber of the replacement beam. Because the camber of beams adjacent to the replacement beam will be significantly greater than the camber of the replaced beam, the slab thickness above the replaced beam will have to be greater. The difference in camber at the end of the service life is shown to be almost 1 in. In reality, the response of the adjacent and replacement beams become highly indeterminate once the slab is cast. Ideally, one would like to have the beams respond the same amount once the slab is cast. The difference in camber at erection and the end of the service life could be reduced by supporting the replacement beam several feet (10 to 15 ft) from its ends while it is in storage, providing that the temporary negative overhang moments do not cause top fiber tensile stresses above permissible limits.

The response of the replacement beam was recalculated assuming it was supported 15 ft from each end while in storage. The calculated response is shown by the dashed line in Fig. 6.10. Using the reduced span length during storage was very effective in reducing the difference in camber between the replacement beam and the typical beam. The camber for the replacement beam with the reduced span length was only 0.26 in. less than the typical beam when placed in the bridge and at the end of their service lives. (No check was made of top fiber tensile stresses during the temporary support period. Such a check should be made to ensure that cracking does not occur.)

6.4.8 Construction Schedule. The effect that the construction schedule has on camber was investigated using a fast track and slow track construction schedule. According to Jesse Lawrance, formerly superintendent of Heldenfels Brothers, Inc., beams may be shipped to the construction site as early as 28 days and as late as two and a half years. Using these shipping dates, realistic construction schedules

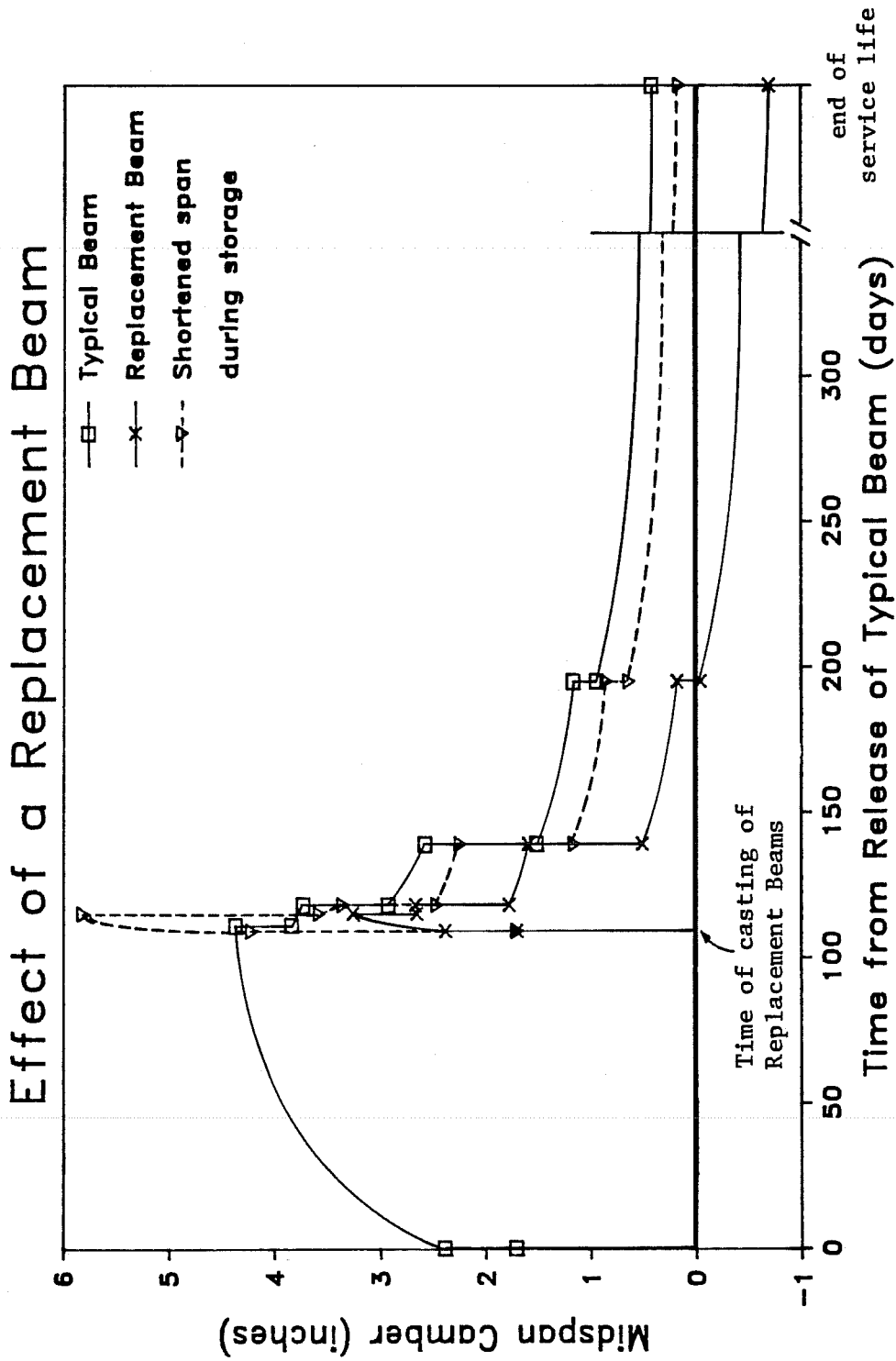


Fig. 6.10 Comparison of the cambers for a typical beam and a new beam which is used in place of a rejected beam

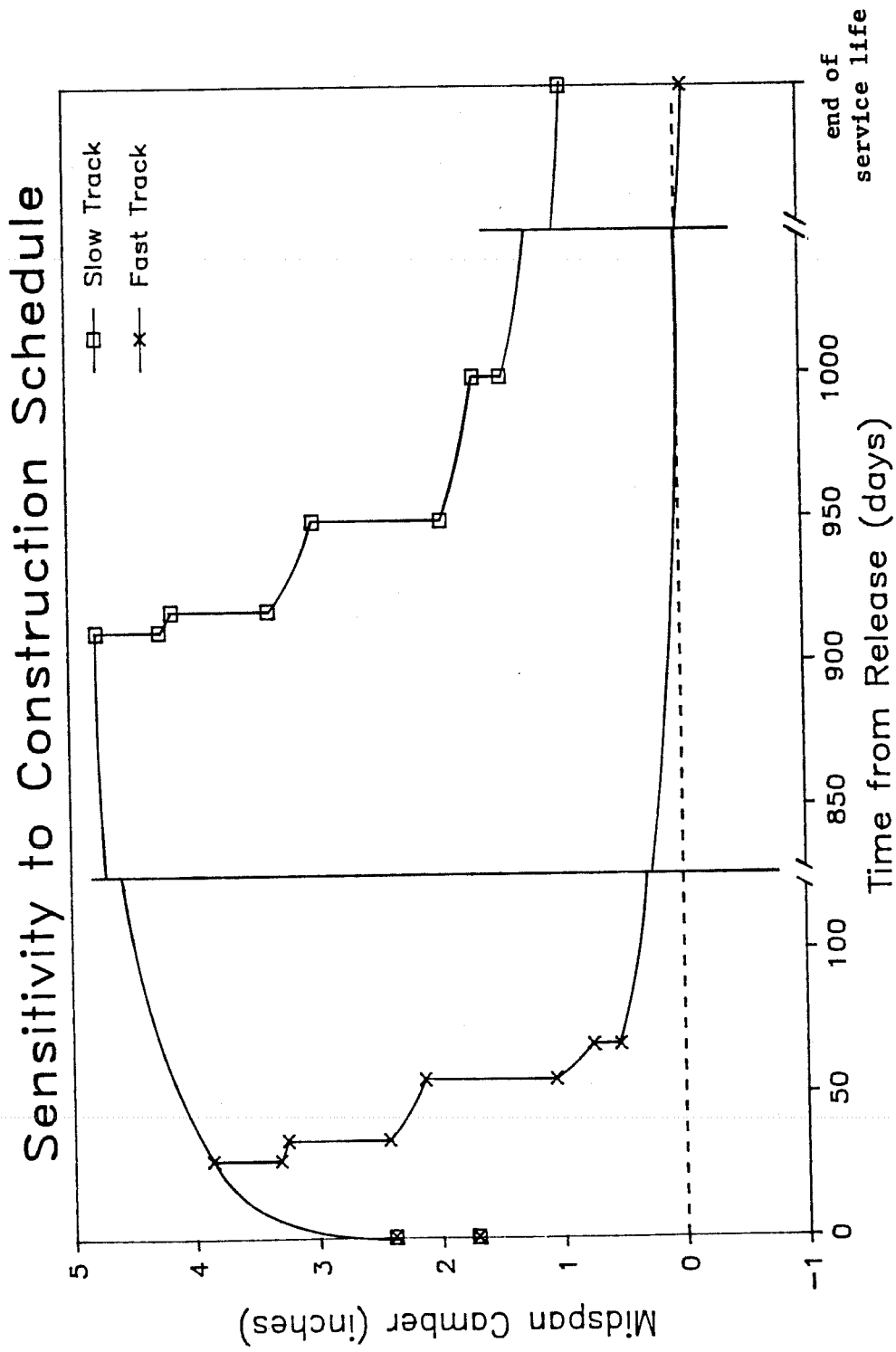
were made up. The fast track schedule used was erection at 28 days, deck panels added at 35 days, the slab cast at 56 days, and the overlay added at 98 days. The slow track schedule was erection at 912 days, deck panels placed at 917 days, the slab cast at 950 days, and the overlay added at 1000 days. A typical construction schedule was not used for this comparison, because David Hohmann of the SDHPT and Jesse Lawrance both felt that there was not a typical age or range when most beams are shipped to bridge sites.

The effect that the construction schedule can have on the time dependent camber is shown in Fig. 6.11. The beam camber during erection and at the end of the service life for the slow track construction was an inch greater than the camber for the fast track construction. Because the beam remained in storage for a much longer time, the initial camber grew to a greater value due to creep. The creep components for deflections caused by the deck panels and cast-in-place slab were small, because the beam was very old when they were added.

6.4.9 Combinations of Variables. As mentioned in Sec. 6.4.1, it would be difficult to include all of the variables that affect the time dependent response. However, it is the opinion of the authors that the most important factors are the strength of the concrete, magnitude of creep, and the construction schedule. The variations of concrete strength used in Sec. 6.4.2, creep in Sec. 6.4.4, and construction schedule in Sec. 6.4.7 were combined in all possible combinations to predict the time dependent response.

The predicted responses are shown together in Fig. 6.12. The responses fall into one of two main groups. These groups are distinguished by which construction schedule was used. In general, the beam camber during and after construction was greater for the slow track construction schedule. The response for beams constructed between the fast and slow track schedules would fall within or between the two groups. Thus, the non-shaded area between the two shaded areas is also a possible camber state.

When designing a bridge, an engineer should realize that before construction has begun it is impossible to accurately predict the camber at erection and the final camber. The engineer should recognize that the midspan camber at erection for a long span, Type IV beam ($l = 127$ ft) can vary in magnitude from values as low as 2.25 in. ($l/675$) up to at least 5.5 in. ($l/275$). He should also recognize that the final camber could be as low as -0.75 in. ($l/2030$) and as high as 2.0 in. ($l/760$). These values do not cover the full range of possible cambers at erection and final deflection, but they do give the engineer an idea of how much variation should be expected. It is generally not practical to anticipate or regulate construction schedules to provide more narrow ranges.



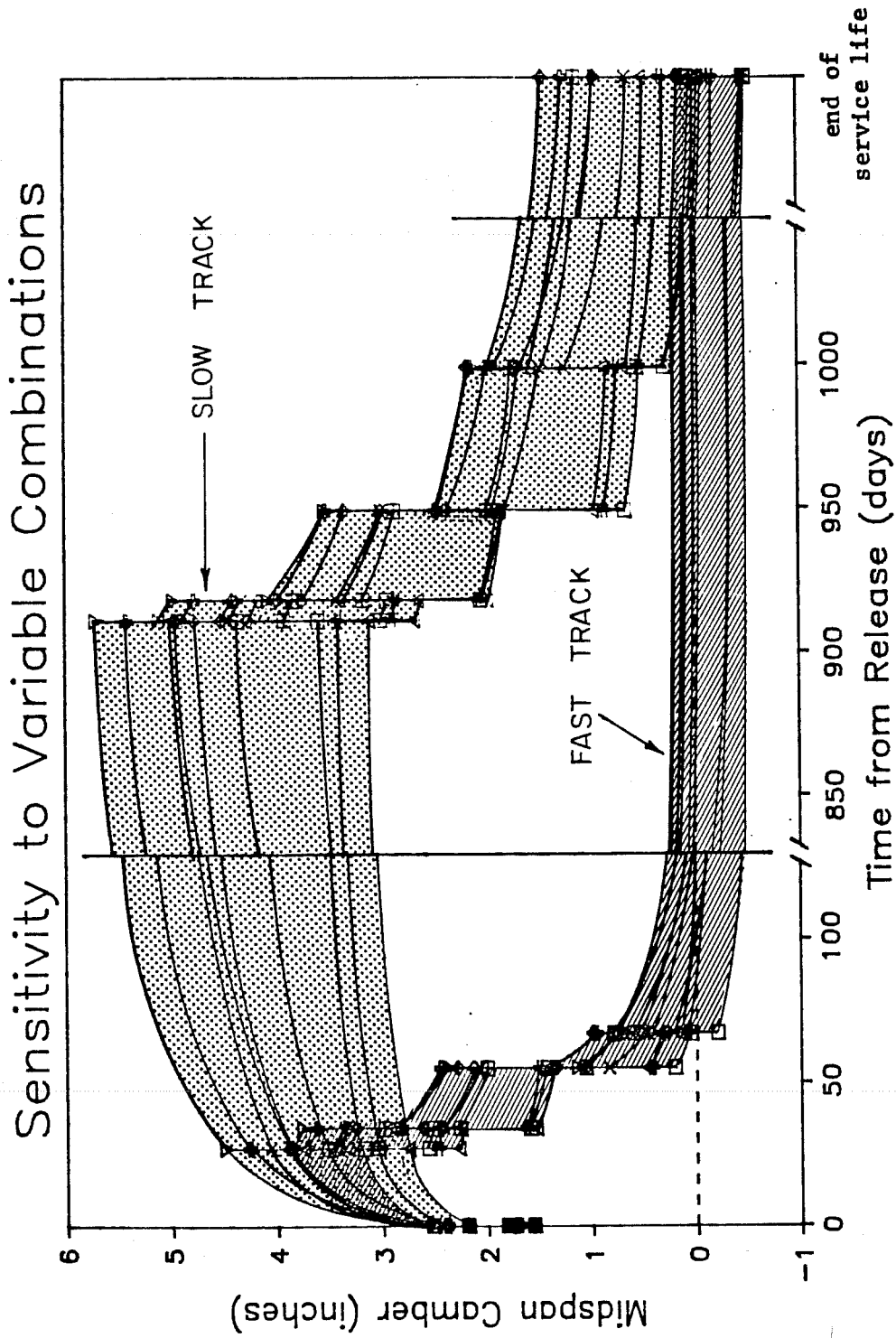


Fig. 6.12 Range of time dependent response predicted using combinations of variable concrete strengths, creep, and construction time schedule

However, with the use of the microcomputer program CAMBER the field engineer, fabricator, or erector can update the predicted response using the cylinder strengths that the SDHPT measures at the prestressing plant and the age of the beam during construction events. More accurate approximations for the creep coefficients can also be used if they are known or measured. As the calculated response is updated, the engineer can reduce the range of possible responses and narrow in on the correct response. By updating the prediction, the field engineer will be able to spot some potential problems. He can then take action such as varying storage support conditions or adjusting deck forms to prevent the problem from occurring or getting worse.

CHAPTER 7

SUMMARY, CONCLUSIONS, AND RECOMMENDATIONS

7.1 Summary

Eight prototype long span, pretensioned, prestressed concrete beams made with high strength concrete and low-relaxation prestressing strand were instrumented and monitored in the field. Time dependent camber, concrete surface strains, and prestressing strand strains were measured as well as the internal concrete temperatures of the beams. The concrete surface strain and prestressing strand strain measuring systems worked poorly, while the camber and internal temperature measuring instrumentation worked extremely well. Companion tests were performed to determine the time dependent material properties of the beam concrete.

Several analytical techniques were used to calculate the time dependent cambers and prestress losses of the instrumented beams. The beam cambers and deflections calculated by the different techniques were compared to one another and to the measured response to determine which technique was most accurate. A substantially modified version of a previously published deflection component multiplier technique was adapted for use on a microcomputer. This technique most accurately predicted the time dependent response of the beams. The calculated prestress losses were compared to one another to determine which technique most accurately predicted the loss using measured beam deflections as a datum. Recommendations were made to improve the accuracy of the AASHTO procedure for calculating prestress loss.

Finally, the proposed procedure for calculating time dependent camber was programmed for a microcomputer (CAMBER) and used to perform a sensitivity analysis. Realistic variations in material properties and construction schedules were explored to determine the effect on the upper and lower bounds of time dependent beam camber or deflection that could be expected in a given project.

7.2 Conclusions

The conclusions presented in this section are based largely on the measured responses, the results of the companion tests, and the results of the analytical techniques for the eight instrumented beams. When numerical values are present, they only apply to beams of similar length (128 ft) and dimensions as the instrumented beams.

1. When evaluating the measured or calculated camber or deflection of a pretensioned, prestressed concrete beam, one must view the net response as the small difference of several large components.
2. The actual support conditions of a beam through all phases of construction (including storage) must be considered when calculating beam response and comparing it to the actual response. Storage support conditions can dramatically affect camber. Specific support guidance should be given to fabricators.
3. The concrete strengths measured using cylinders stored in saturated lime water generally overestimate the actual concrete strength in a beam and should not be relied on for deformation predictions.
4. The AASHTO formula for predicting the elastic modulus of concrete should not be used for predicting deflections with high strength concrete (f'_c greater than 9000 psi). The formula proposed in Sec. 4.3.2 can be used for high strength concrete made with limestone aggregate.
5. Thermal gradients are nearly linear in a noncomposite beam, and highly nonlinear in a composite beam.
6. On a sunny day, thermal cambers of approximately 0.25 in. should be expected to occur in long span Type IV, pretensioned beams with an uncovered composite concrete slab.
7. The camber of a pretensioned beam is very sensitive to the age and strength of concrete at release. This was shown both in Sec. 4.5.3, when comparing the actual responses of the H-series beams to each other, and in Sec. 6.4.3 where the sensitivity study analytically examined the effect of age at release.
8. Elastic cambers and deflections can be accurately predicted using moment area equations, if known concrete strengths are used.
9. Initial elastic camber of a beam made with low-relaxation strand can be predicted more accurately if 0.92 is used for the ratio of prestressing force immediately after release to the initial force. As recommended in the 1985 Interim Revision to the AASHTO Specifications rather than the previously used value of 0.9 which is more appropriate for stress-relieved strand.

10. The actual time dependent beam camber can be accurately predicted using the proposed multipliers of Sec. 5.6 which were obtained using a substantially modified version of analytical techniques found in the literature.
11. The time dependent camber or deflection of a beam is extremely affected by the following variables: concrete age-strength gain characteristics; the concrete creep coefficient; the relative humidity; the age of concrete at release; and the construction schedule.
12. The difference in camber between a replacement beam (for a rejected beam) and the adjacent beams in the bridge can be substantially reduced by storing the replacement beam on a shortened span.
13. Field substitution of low-relaxation strand for stress-relieved strand without modifying the design increases the time dependent beam camber by a significant amount. Since low-relaxation strand meets all specification requirements for stress-relieved strand, such substitution is possible without designer approval.
14. Based on the results of the sensitivity investigation presented in Sec. 6.4.8, one could expect that the maximum camber of a long span (128 ft) Type IV beam can range from 2 to 6 in. The camber at the end of the service life can range from -0.75 to +2.0 in.

7.3 Recommendations

1. The piano wire measuring system for beam deflections described in Sec. 2.5.4 worked extremely well and its use is strongly recommended for future studies.
2. Further investigation is needed to develop a reliable system for measuring the long-term strain of strand in pretensioned, prestressed concrete beams.
3. In view of the importance of prestress losses in both camber calculations and in fatigue stress range determinations, an improved knowledge of prestress loss is required. The rapid introduction of new materials such as high strength concretes, low-relaxation strands, high range water reducing admixtures, fly ash, silica fumes, and strain gain accelerators means that early prestress loss

studies are becoming very outdated. A comprehensive study of current prestress losses is recommended.

4. The Texas SDHPT should use the program CAMBER to predict the time dependent camber of beams. The field engineer, fabricator, and contractor should update this prediction by using actual construction times and concrete strengths as they become known to ensure proper project control.

REFERENCES

1. ACI Committee 209, "Prediction of Creep, Shrinkage, and Temperature Effects in Concrete Structures," Designing for Creep and Shrinkage in Concrete Structures, SP-76, American Concrete Institute, Detroit, 1982.
2. Hansen, T.C. and Mattock, A. H., "Influence of Size and Shape of Member on the Shrinkage and Creep of Concrete," ACI Journal, Proceedings, V. 63, No. 2, Feb. 1966.
3. Ngab, A. S., Nilson, A. H., and Slate, F. O., "Shrinkage and Creep of High Strength Concrete," ACI Journal, Proceedings, V. 78, No. 4, July-Aug. 1981, pp. 255-261.
4. Carrasquillo, R. L., Slate, F.O., and Nilson, A. H., "Microcracking and Behavior of High Strength Concrete Subject to Short-Term Loading," ACI Journal, Proceedings, V. 78, No. 3, May-June 1981, pp. 179-186.
5. Magura, D. D., Sozen, M. A., and Siess, C. P., "A Study of Stress Relaxation in Prestressing Reinforcement," PCI Journal, V. 9, No. 2, April 1964, pp. 13-57.
6. PCI Committee on Prestress Losses, "Recommendations for Estimating Prestress Losses," PCI Journal, V. 20, No. 4, July-Aug. 1975, pp. 43-75.
7. Hernandez, H. D. and Gamble, W. L., "Time-Dependent Prestress Losses in Pretensioned Concrete Construction," Structural Research Series No. 417, Civil Engineering Studies, University of Illinois at Urbana-Champaign, Urbana, May 1975.
8. Buckler, J. D. and Scribner, C. F., "Relaxation Characteristics of Prestressing Strand," Structural Research Series No. 520, Civil Engineering Studies, University of Illinois at Urbana-Champaign, Urbana, Aug. 1985.
9. Rao, V. J. and Dilger, W. H., "Time-Dependent Deflections of Composite Prestressed Concrete Beams," Deflection of Concrete Structures, SP-43, American Concrete Institute, Detroit, 1974.

10. Corley, W. G., Sozen, M. A., and Siess, C. P., "Time-Dependent Deflections of Prestressed Concrete Beams," Bulletin No. 307, Highway Research Board, Washington, DC, 1961.
11. Zundeleovich, S., Lee, D. L. N., and Chia, A. N. L., "Camber and Deflection Behavior of Prestressed Concrete Beams," Technical Report CE71-R1, Civil Engineering Department, University of Hawaii, Honolulu, HI, Sept. 1971.
12. Furr, H. L. and Sinno, R., "Creep in Prestressed Lightweight Concrete," Research Report 69-2, Study 2-5-63-69, Texas Transportation Institute, Texas A&M University, College Station, TX, Oct. 1967.
13. Furr, H. L. Sinno, R., and Ingram, L. L., "Prestress Loss and Creep Camber in a Highway Bridge with Reinforced Concrete Slab on Pretensioned Prestressed Concrete Beams," Research Report 69-3 (Final), Study 2-5-63-69, Texas Transportation Institute, Texas A&M University, College Station, TX, Oct. 1968.
14. Branson, D. E., Meyers, B. L., and Kripanarayanan, K. M., "Loss of Prestress, Camber and Deflection of Noncomposite and Composite Structures Using Different Weight Concretes," Iowa Highway Commission Final Report, No. 70-6, Aug. 1970.
15. Sokal, Y. J. and Tyrer, P., "Time Dependent Deformation in Prestressed Concrete Girder: Measurement and Prediction," Research Report No. CE30, Department of Civil Engineering, University of Queensland, Queensland, Australia, Nov. 1981.
16. Gamble, W. L., "Field Investigation of a Continuous Composite Prestressed I-Beam Highway Bridge Located in Jefferson County, Illinois," Structural Research Series No. 360, Civil Engineering Studies, University of Illinois at Urbana-Champaign, Urbana, June 1970.
17. Houdeshell, D. M., Anderson, T. C., and Gamble, W. L., "Field Investigation of a Prestressed Concrete Highway Bridge Located in Douglas County, Illinois," Structural Research Series No. 375, Civil Engineering Studies, University of Illinois at Urbana-Champaign, Urbana, Feb. 1972.
18. Gamble, W. L., "Long-Term Behavior of a Prestressed I-Girder Highway Bridge in Champaign County, Illinois," Structural Research Series No. 470, Civil Engineering Studies, University of Illinois at Urbana-Champaign, Urbana, Dec. 1979.

19. Sinno, R., "The Time-Dependent Deflections of Prestressed Concrete Bridge Beams," unpublished Ph.D. dissertation, Texas A&M University, College Station, TX, 1968.
20. Comite Euro-International Du Beton-Federation Internationale De La Precontrainte, "Model Code for Concrete Structures," 1978.
21. Bradberry, T. E., "Time Dependent Deformation of Long Span Prestressed Concrete Beams Having Low Relaxation Strands," unpublished M.S. report for the Department of Civil Engineering, The University of Texas at Austin, May 1986.
22. American Association of State Highway and Transportation Officials, Standard Specification for Highway Bridges, Twelfth Edition, Washington, DC, 1977.
23. Prestressed Concrete Institute, PCI Design Handbook: Precast and Prestressed Concrete, Third Edition, Chicago, 1985.
24. Tadros, M. K., Ghali, A., and Dilger, W. H., "Time-Dependent Prestress Loss and Deflection in Prestressed Concrete Members," PCI Journal, V. 20, No. 3, May-June 1975, pp. 86-98.
25. Suttikan, C., "A Generalized Solution for Time-Dependent Response and Strength of Noncomposite and Composite Prestressed Concrete Beams," unpublished Ph.D. dissertation, The University of Texas at Austin, Aug. 1978.
26. Sinno, R. and Furr, H. L., "Hyperbolic Functions for Prestress Loss and Camber," Journal of the Structural Division, ASCE, V. 96, No. ST4, April 1970, pp. 803-821.
27. Sinno, R. and Furr, H. L., "Computer Program for Predicting Prestress Loss and Camber," PCI Journal, V. 17, No. 5, Sept.-Oct. 1972, pp. 27-38.
28. Branson, D. E. and Kripanarayanan, K. M., "Loss of Prestress, Camber and Deflection of Non-Composite and Composite Prestressed Concrete Structures," PCI Journal, Sept.-Oct. 1971, pp. 22-52.
29. Hernandez, H. D. and Gamble, W. L., "Time-Dependent Prestress Losses in Prestressed Concrete Construction," Structural Research Series No. 417, Civil Engineering Studies, University of Illinois at Urbana-Champaign, Urbana, May 1975.

30. Texas State Department of Highways and Public Transportation, Standard Specifications for Construction of Highways, Streets, and Bridges, 1982.
31. ASTM Committee C-9, Method C39-83b, "Standard Test Method for Compressive Strength of Cylindrical Concrete Specimens," 1983 Annual Book of ASTM Standards, V.C 04.02, American Society for Testing and Materials, 1983.
32. ASTM Committee C-9, Method C469-81, "Static Modulus of Elasticity and Poisson's Ratio of Concrete in Compression," 1983 Annual Book of ASTM Standards, V.C 04.02, American Society for Testing and Materials, 1983.
33. ASTM Committee C-9, Method C512-76, "Standard Test Method for Creep of Concrete in Compression," 1983 Annual Book of ASTM Standards, V. C 04.02, American Society for Testing and Materials, 1983.
34. Pauw, A. and Breen, J. E., "Field Testing and Analysis of Two Prestressed Concrete Girders," The University of Missouri Bulletin, V. 60, No. 52, Engineering Experiment Station Series, No. 46, University of Missouri, Department of Civil Engineering, Columbia, MO, Nov. 1959.
35. Zuk, W., "Thermal Behavior of Composite Bridges - Insulated and Uninsulated," Highway Research Record, No. 76, 1965, pp. 231-253.
36. Berwanger, C., "Thermal Stresses in Composite Bridges," Proceedings, ASCE Specialty Conference on Steel Structures, Engineering Extension Series, No. 15, University of Missouri-Columbia, Columbia, MO, June 1970, pp. 27-36.
37. Pauw, A., "Static Modulus of Elasticity of Concrete as Affected by Density," ACI Journal, Proceedings, V. 32, No. 6, Dec. 1960, pp. 679-687.
38. Building Code Requirements for Reinforced Concrete (ACI Standard 318-83), American Concrete Institute, Detroit, 1983.
39. ACI Committee 363, "State-of-the-Art Report on High-Strength Concrete," ACI Journal, Proceedings, V. 81, No. 4, July-Aug. 1984, pp. 364-411.

40. Carrasquillo, R. L., Nilson, A. H., and Slate, F. O., "Microcracking and Engineering Properties of High-Strength Concrete," Research Report No. 80-1, Department of Structural Engineering, Cornell University, Feb. 1980, 254 p.
41. Ingram, L. L. and Butler, H. D., "Prestressed Concrete Bridge Girder Design Program," Research Report 149-1 (Final), Texas Transportation Institute, Texas A&M University, College Station, TX, Nov. 1970.
42. Martin, L. D., "A Rational Method for Estimating Camber and Deflection of Precast Prestressed Members," PCI Journal, V. 22, No. 1, Jan.-Feb. 1977, pp. 100-108.
43. Zia, P., Preston, H. K., Scott, N. L., and Workman, E. B., "Estimating Prestress Losses," Concrete International, V. 1, No. 6, June 1979, pp. 32-38.
44. Alani, A. F., "Correlation of Physical Tests with Computer Simulation Models for Slab and Girder Bridge Systems," unpublished Ph.D. dissertation, The University of Texas at Austin, May 1971.
45. Koretsky, A. V. and Pritchard, R. W., "Assessment of Relaxation Loss Estimates for Strands," Journal of the Structural Division, ASCE, V. 108, N. ST12, Dec. 1982, pp. 2819-2836.
46. Kelly, D. J., "Time Dependent Deflections of Pretensioned Beams," unpublished M.S. thesis, The University of Texas at Austin, August 1986.
47. Smadi, M. M., Slate, F. O., and Nilson, A. H., "Shrinkage and Creep of High-, Medium-, and Low-Strength Concretes, Including Overloads," ACI Materials Journal, Title No. 84-M25, May-June 1987, pp. 224-234.
48. American Association of State Highway and Transportation Officials, Standard Specifications for Highway Bridges, 1985 Interim Revision, Washington, D.C., 1986.
49. Huang, T., "Study of Prestress Losses Conducted by Lehigh University," Journal of the Prestressed Concrete Institute, Vol. 27, No. 5, Sept./Oct. 1982, pp. 48-61.

A P P E N D I X A

USER'S GUIDE FOR COMPUTER PROGRAM CAMBER
TO CALCULATE PROPOSED MULTIPLIERS

- A.1 GENERAL
- A.2 DATA INPUT GUIDE
- A.3 COMPUTER OUTPUT
- A.4 USE
- A.5 EXAMPLE PROBLEMS

A.1 General

The computer program CAMBER discussed in this appendix was written by Dominic J. Kelly. It calculates long-time camber and deflection multipliers for a composite pretensioned prestressed concrete beam by the procedure discussed in Sec. 5.6. The user has the choice to output only these multipliers requiring the time dependent response to be calculated by hand, or the user can choose to use the program to calculate the deflections thus giving the response at important construction events and the end of the bridge's service life. If the time dependent response is to be calculated by the program, the user has further choice on the input. Either the externally computed elastic deflections can be included as input, or else some fundamental beam properties can be input and the program will compute elastic responses using moment area equations. This latter mode is the most likely input for conventional pretensioned girder layouts.

This program was written for beams in a rectangular span. The time dependent beam camber is calculated assuming each beam in the span acts individually. In reality the camber is affected by adjacent beams once the slab has been cast. It is reasonable to assume the beams act individually in a rectangular span, because the behavior of adjacent beams will be similar. This program can be used to estimate the response of beams in a skewed span. However, adjacent beams will have some effect on the time dependent camber once the slab is cast. In general, the response will be reduced.

This program was written in Fortran 77 computer language. A listing is given in Ref. 46. The program was compiled using PFORT and run on an IBM AT microcomputer which has a math coprocessor chip. The math coprocessor is essential with the FORTRAN compiler used.

A.2 Data Input Guide

The compiled version of this program must be run using a separate data file. Data is input using free format. This requires that the data must be entered on the correct lines and in the correct order, but the data does not have to be placed in predefined columns.

The first four lines of input are required no matter which of the basic computation options are used in the program. The data included in these lines are the information necessary to calculate the multipliers. The fifth input line is used to define whether only the multipliers will be output or whether the time dependent response will be calculated by the program. If the multipliers are to be the only output, no further lines of input are necessary. If the precalculated

elastic cambers and deflections are to be input, one more line defining the elastic responses is required. If the program is to be used to calculate the elastic responses which are limited to those of a simply supported beam, approximately 10 to 15 more data lines defining the beam properties, support conditions, and magnitude of a possible superimposed load are required.

The following is a list of data which must be included on each data line. As mentioned above the data does not have to appear in predefined columns, but they must be furnished in the order listed. Each datum must be separated by either a comma or one or more spaces. If an asterisk appears by the line number, remarks for the line are included just below the final datum.

*Line 1 Age of Beam at Time of Construction Events (days)

- tr - release of prestressing force
- te - placement in bridge (erection)
- tp - addition of a superimposed load to the noncomposite beam (ex. deck panels placed on the beam)
- ts - placement of the composite slab
- tsi - addition of a superimposed dead load to the composite beam (ex. the weight of an ACP overlay)

Remarks - Line 1

1. The age of the beam is always measured from the time it is cast and always in days. Decimal fractions of days are acceptable.
2. The age at which various events take place should be updated as actual construction schedules become known.

*Line 2. Creep Data and Moment of Inertia Ratio

- cult - ultimate creep coefficient
- vs - volume to surface ratio of beam (in.)
- rh - average relative humidity (%)
- inic - ratio of noncomposite to composite beam moment of inertia

Remark - Line 2

1. If measured data is used for the ultimate creep coefficient, vs should reflect the size of specimen and the environment in which the test was performed. For example, if standard 6-in. diameter cylinders were tested, the data would have to be corrected for the beam volume to surface properties. Thus, the volume to surface ratio input should equal that of the beam.

On the other hand, if the test specimens were similar in size and shape to the member, no further volume to surface ratio correction would be required so that the ratio should be set equal to 1.0.

2. If the test was performed in an environment similar to that in which the beam is stored, the relative humidity should be input as 40%. This corresponds to a correction factor of 1.0 (no correction). If tests were run at a relative humidity, x , and the beams stored at a relative humidity, y , the relative humidity should be input as $[40 + (y-x)]\%$. This will form the proper correction. Note that y or x should be set equal to 40% if it is less than 40%. If no tests were run, the data should be input as the probable average relative humidity at the site.

*Line 3 Time Dependent Prestress Loss

pl - time dependent prestress loss (%)

Remarks - Line 3

1. The time dependent prestress loss includes only the loss that occurs after the release of the prestress force. It does not include the loss due to elastic shortening or the relaxation loss that occurs before release. If no data is available 15% loss is recommended to be used for beams made with low-relaxation strand and 20% loss for beams made with stress-relieved strand.

Line 4 Steam or Moist Cured

steam - steam = 0 if moist cured, or steam = 1 if steam cured

Line 5 Output Control

defl - If only the multipliers are desired as output set defl = 0. If elastic responses will be input set defl = 1. If the elastic responses are to be calculated by this program set defl = 2.

*Line 6(A) Elastic Cambers and Deflections (in.)

drbw - deflection at release due to beam weight alone. Input downward as negative.
 crpf - camber at release due to prestress force alone. Input upward as positive.
 cstr - change in camber due to possible reduced span length when placed in storage. Input upward as positive.

- dstr - change in camber caused by the possible increase in span length when a beam is taken from storage and placed in the bridge. Input downward as negative.
- dpanel - deflection caused by a superimposed load added to the noncomposite beam (ex. deck panels). Input downward as negative.
- dslab - deflection caused by the weight of the cast-in-place slab. Input downward as negative.
- dover - deflection caused by a superimposed dead load placed on the composite beam (ex. the weight of an ACP overlay). Input downward as negative.

Remarks - Line 6(A)

1. This line is used if the time dependent response is to be calculated using input elastic responses (defl = 1 in line 5)

or *Line 6(B) Beam Dimensions

- ig - pretensioned beam moment of inertia (in.⁴)
- area - pretensioned beam cross sectional area (in.²)
- cg - center of gravity of the pretensioned section as measured from the bottom of the beam (in.)
- emid - prestressing steel eccentricity (positive when measured down from the center of gravity of the pretensioned section, in.)
- eend - prestressing steel eccentricity at the beam ends (positive when measured down from the center of gravity of the pretensioned section, in.)
- l - beam span length (ft)
- a - distance from end of beam to near drap point (ft). If only straight strands are used set a = 0.

Remarks - Line 6(B)

1. This line is only used in place of Line 6(A) if the time dependent response is to be calculated by the program from fundamental beam properties and loads.
2. All properties are for the noncomposite pretensioned beam only.

*Line 7 Prestress Force

- pi - initial prestress force (kips)
- rforce - ratio of prestress force at release to initial force

Remarks - Line 7

1. The ratio of prestressing forces is used to model the amount of relaxation loss before release and the loss due to elastic shortening during release. If no data is available, 0.9 is recommended for stress-relieved strand and 0.92 for low-relaxation strand.

*Line 8 Concrete Weight and Composite Deck Dimensions

unitw - unit weight of concrete (pcf)
 pwidth - deck panel width (in.)
 pthick - deck panel thickness (in.)
 sthick - thickness of cast-in-place slab above panel (in.)
 bspace - beam spacing center-to-center (ft)

Remarks - Line 8

1. If panels are not used for the composite deck set pwidth and pthick equal to zero, and set sthick equal to the total deck thickness.

*Line 9 Age-Strength Gain Curve

nage - number of points used to define the age-strength gain curve for the beam concrete

Remarks - Line 9

1. The maturity relation for the concrete is defined by inputting a series of discrete age-strength data points in Lines 10 to 9 + nage.
2. The number of points used to define the age-strength gain curve can be defined by no more than 9 points (nage \leq 9). The time for zero time and strength is already defined. A three point Lagrangian interpolation is used to determine the strength at times between those input. Two more points equal to the strength at the oldest given age are automatically defined at ages of 50 and 55 yr.
3. A minimum of at least three points should be input to define the age strength gain curve for concrete. These points could correspond to the strengths at release, 28 days, and 365 days. Strengths at the age when the deck panels are added or the slab is cast are even more desirable than the strengths at 28 or 365 days. The release and 28-day strengths are normally specified. If a strength at 365 days is not known, a strength 10% greater than the 28-day strength is recommended.

*Line 10 to 9 + nage Ages and Strengths

age(i) - age of concrete (days)
str(i) - concrete strength (psi)

Remarks - Lines 10 to 9 + nage

1. nage lines of input must be included. Each line must include an age in days and strength in psi for the concrete. The ages and strengths must be input in order of increasing age.

*Line 10 + nage Elastic Modulus

mod - If the AASHTO formula is to be used for the elastic modulus of concrete set mod = 0. If the proposed elastic modulus for high strength concrete is to be used, set mod = 1.

Remarks - Line 10 + nage

1. The AASHTO formula calculates the elastic modulus assuming normal weight concrete is used for the beam (unit weight = 145 pcf).
2. The proposed elastic modulus is recommended to be used for high strength concrete made with limestone aggregate. $E_c = 40,000 f'_c + 1.5 \times 10^6$

*Line 11 + nage Supports Locations in Storage

suploc - distance from the final support location (in bridge) to the temporary support location (ft)

Remarks - Line 11 + nage

1. The program assumes two simple supports will be used. The average measured distance from the ends of the beam to the temporary support locations minus the average distance from the ends to center of the bearing pads should be used if known. A value of 4 ft is recommended if it is not known. If significantly larger values are used to control cambers, the top fiber stresses at the support points should be checked to avoid cracking. The program does not make such checks.

*Line 12 + nage Superimposed Load

siload - magnitude of the superimposed load added to the composite beam (ex. the weight of an ACP overlay in lb/ft)

A.3 Computer Output

Two basic types of output options are available when using this program. These options are chosen and input on Line 5, Output Control. Their uses are discussed in this section.

The first option, $defl = 0$, is to print only the calculated multipliers. If this option is chosen, one would then have to calculate the time dependent behavior at the different stages of construction by hand. This option might be useful if the same multipliers are to be applied several times or if they are to be applied to continuous construction. It could also be used to gain an understanding of which cambers and deflections have the greatest time dependent effects. This is also the option that must be used if the total response of an individual camber or deflection component is desired.

The second basic option is to print out the time dependent camber or deflection at important construction events or service life times and at the end of the expected service life of the bridge. This option is chosen by using $defl = 1$ if precalculated elastic responses are to be input or by using $defl = 2$ if the program is to calculate elastic responses. This output option should be used to predict the time dependent behavior during the design phase based on estimated material properties and construction schedules. It can also be used to obtain the variation in camber or deflection that the designer might expect to occur. This would be done by running the program several times changing variables such as the concrete strength, creep, the prestress loss, and the time of construction events. This is also the option that the fabricator, erector, and field engineer should use to update the camber predictions as more specific information such as the actual concrete strength and the age of the beam during important construction events become available.

A.4 Use.

In order to assist the reader in preparation of data files, the actual data files used for three examples as well as the output from those files are included in Section A.5.

Datafiles can be speedily composed by using a text editor like WORDSTAR. The name of the datafile created is referred to as INFILE.

If an executable or compiled version of the program is available (CAMBER.EXE), it may be used directly with INFILE to run the problem and create an output file designated by the user but referred to as OUTFILE.

The command to do this if CAMBER.EXE and INFILE are resident on disk is:

```
C> CAMBER <INFILE >OUTFILE
```

(Note that a space is required after CAMBER and after INFILE)

This command executes the program. OUTFILE can then be sent to the screen by C> TYPE OUTFILE/P or sent to the printer by the appropriate command.

If a compiled version of the program is not available the FORTRAN source code CAMBER.FOR (Ref. 46) must be compiled using appropriate procedures with a compiler such as PFORT or PROFORT.

A.5 Example Problems

In this section, three data files and corresponding output files are presented. These files represent the different options available with the program.

Example 1. The data file in Table A.1 was used to obtain multipliers (See Table A.2) for typical concrete creep ($C_{ult} = 2.35$) and relative humidity (65%).

TABLE A.1 Data File for Example 1

```
.8,112,119,140,196  
2.35,4.75,65,0.5  
15  
0  
0
```

TABLE A.2 Output File for Example 1

Long-Time Deflection and Camber Multipliers

The age of the beam during significant events (days)

- | | | |
|----|--|------|
| 1. | Release of prestress force | 0.80 |
| 2. | Placed in the bridge (erection) | 112. |
| 3. | Super-imposed load is added to
the noncomposite beam (ex. the
weight of deck panels) | 119. |
| 4. | The composite slab is cast | 140. |
| 5. | Super-imposed load is added to
the composite beam (ex. the
weight of an asphalt overlay) | 196. |

The uncorrected ultimate creep coefficient is 2.35

The volume-to-surface ratio is 4.75 inches

The average percent relative humidity is 65.%

The ratio of noncomposite-to-composite moment of
inertia is 0.50

The total time dependent percent prestress loss
(not including the initial loss due to elastic
shortening) is 15.0 %

The beam is moist cured

TABLE A.2 (continued)

	Multipliers applied at the events listed above				
	2	3	4	5	End of design life
(1) Deflection (downward) component-apply to the elastic deflection due to the member weight at release of prestress	2.09	2.11	2.14	2.18	2.44
(2) Camber (upward) component-apply to the elastic camber due to prestress at the time of release of prestress	1.99	2.00	2.03	2.06	2.25
(3) Camber (upward)-apply to the elastic camber caused by the reduced span length when the beam is placed in storage	2.09	2.11	2.14	2.18	2.44
(4) Deflection (downward)-apply to the elastic deflection that occurs when the beam is first placed in the bridge		1.25	1.43	1.52	1.73
(5) Deflection (downward)-apply to the elastic deflection caused by a super-imposed dead load applied to the noncomposite beam (ex. the weight of deck panels)			1.39	1.48	1.70
(6) Deflection (downward)-apply to elastic deflection caused by the weight of the cast-in-place slab				1.26	1.50
(7) Deflection (downward)-apply to the super-imposed dead load added to the composite beam (ex. weight of an overlay)					1.95

Example 2. Cambers and deflections at the times of important construction events and at the end of the bridge's service life were obtained with the data file in Table A.3. Precalculated elastic cambers and deflections were read into the computer. This data file was used to calculate the response for beam H-i2, shown in Fig. 5.38.

TABLE A.3 Data File for Example 2

```
0.82,108,128,220,575
2.32,4.75,40,0.5
14.6
0
1
-4.2,5.67,0.57,-0.44,-0.73,-0.99,-0.18
```

TABLE A.4 Output File for Example 2

Long-Time Deflection and Camber Multipliers

The age of the beam during significant events (days)

1. Release of prestress force 0.82
2. Placed in the bridge (erection) 108.
3. Super-imposed load is added to 128.
the noncomposite beam (ex. the
weight of deck panels)
4. The composite slab is cast 220.
5. Super-imposed load is added to 575.
the composite beam (ex. the
weight of an asphalt overlay)

The uncorrected ultimate creep coefficient is 2.32

The volume-to-surface ratio is 4.75 inches

The average percent relative humidity is 40.%

The ratio of noncomposite-to-composite moment of
inertia is 0.50

The total time dependent percent prestress loss
(not including the initial loss due to elastic
shortening) is 14.6 %

The beam is moist cured

TABLE A.4 (continued)

The elastic cambers and deflections are :
 (Camber is positive, values are in inches)

- a. Deflection at release due to the weight of the beam -4.20
- b. Camber due to prestress force at release 5.67
- c. Camber due to the reduced span when placed in storage 0.57
- d. Deflection due to an increased span length when placed in the bridge -0.44
- e. Deflection due to a super-imposed load added to the noncomposite beam (ex. the weight of deck panels) -0.73
- f. Deflection due to the weight of the cast-in-place slab -0.99
- g. Deflection due to a super-imposed load added to the composite beam (ex. the weight of an ACP overlay) -0.18

Event listed above	Time from release (days)	Camber (inches)		Time to next event (days)	Camber just before the next event (inches)
		before	after		
1.	0.00	0.00	1.47	0.	1.47
Placed in storage	0.00	1.47	2.04	107.	3.99
2.	107.	3.99	3.55	20.	3.40
3.	127.	3.40	2.67	92.	2.14
4.	219.	2.14	1.15	355.	0.68
5.	574.	0.68	0.50		0.15
end of design life			0.15		

Example 3. Elastic and longtime cambers and deflections were calculated using the data file in Table A.5. Dimensions for the H-series beam studied in this project along with typical strength concrete and creep were used. The results shown in Table A.6 are the longtime cambers for a typical beam.

TABLE A.5 Data File for Example 3

```
.8,112,119,140,196
2.35,4.75,65,0.5
15
0
2
280403,788,24.75,19.79,10.66,126.79,56.5
1425,.92
150,45,4,3.5,4.6
7
.8,5000
14,7270
28,7880
100,8360
200,8460
365,8500
912,8540
0
4
103.5
```

TABLE A.6 Output File For Example 3

Long-Time Deflection and Camber Multipliers

The age of the beam during significant events (days)

1. Release of prestress force	0.80
2. Placed in the bridge (erection)	112.
3. Super-imposed load is added to the noncomposite beam (ex. the weight of deck panels)	119.
4. The composite slab is cast	140.
5. Super-imposed load is added to the composite beam (ex. the weight of an asphalt overlay)	196.

The uncorrected ultimate creep coefficient is 2.35

The volume-to-surface ratio is 4.75 inches

The average percent relative humidity is 65.%

The ratio of noncomposite-to-composite moment of
inertia is 0.50

The total time dependent percent prestress loss
(not including the initial loss due to elastic
shortening) is 15.0 %

The beam is moist cured

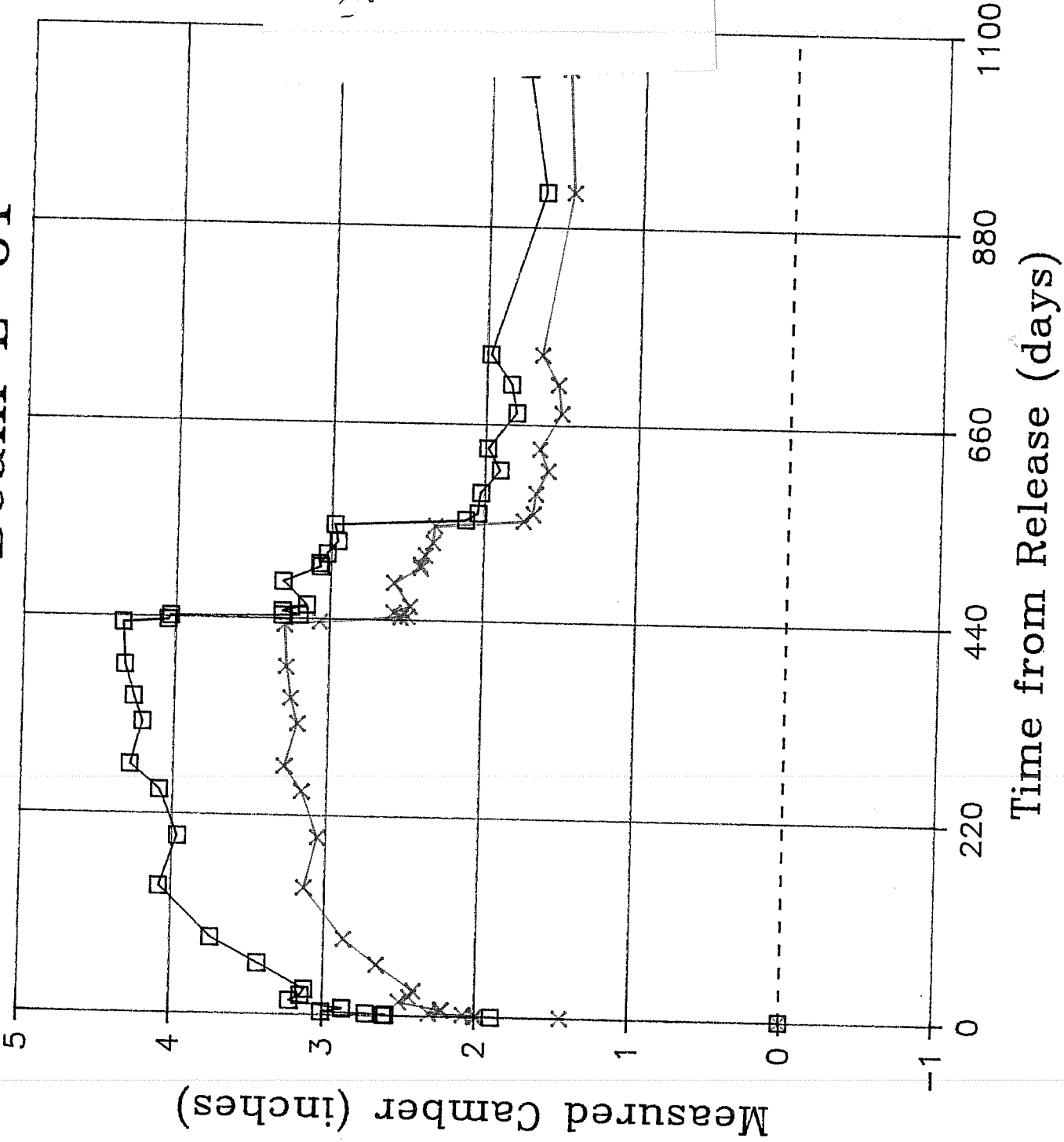
TABLE A.6 (continued)

The elastic cambers and deflections are :
 (Camber is positive, values are in inches)

- a. Deflection at release due to the weight of the beam -4.50
- b. Camber due to prestress force at release 6.21
- c. Camber due to the reduced span when placed in storage 0.68
- d. Deflection due to an increased span length when placed in the bridge -0.53
- e. Deflection due to a super-imposed load added to the noncomposite beam (ex. the weight of deck panels) -0.79
- f. Deflection due to the weight of the cast-in-place slab -1.05
- g. Deflection due to a super-imposed load added to the composite beam (ex. the weight of an ACP overlay) -0.22

Event listed above	Time from release (days)	Camber (inches)		Time to next event (days)	Camber just before the next event (inches)
		before	after		
1.	0.00	0.00	1.71	0.	1.71
Placed in storage	0.00	1.71	2.39	111.	4.37
2.	111.	4.37	3.84	7.	3.73
3.	118.	3.73	2.93	21.	2.58
4.	139.	2.58	1.52	56.	1.17
5.	195.	1.17	0.95		0.42
end of design life			0.42		

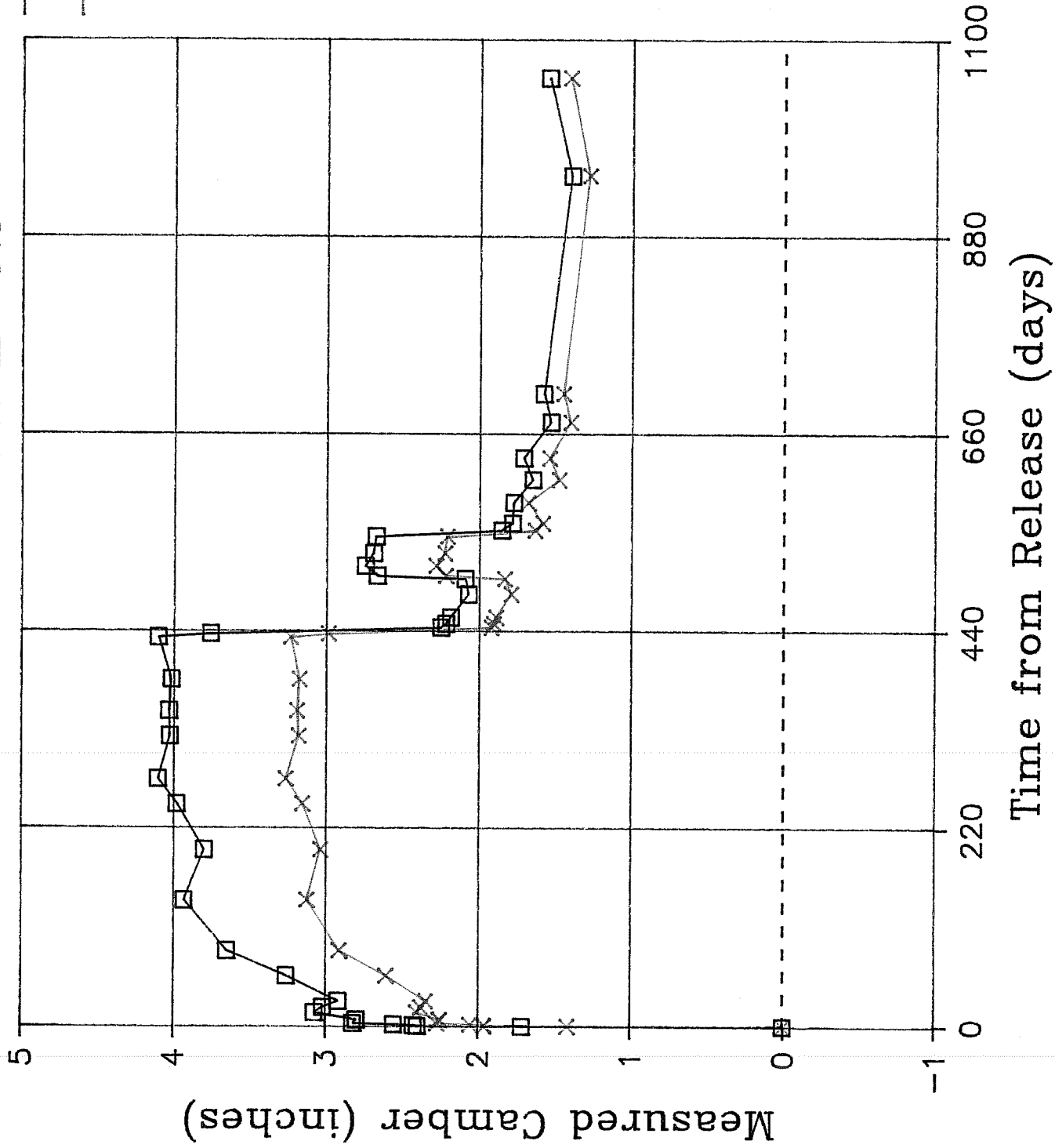
Beam L-01



Used these drawings for updating info. for figs. for report
June 5.
3/3/88
281-1

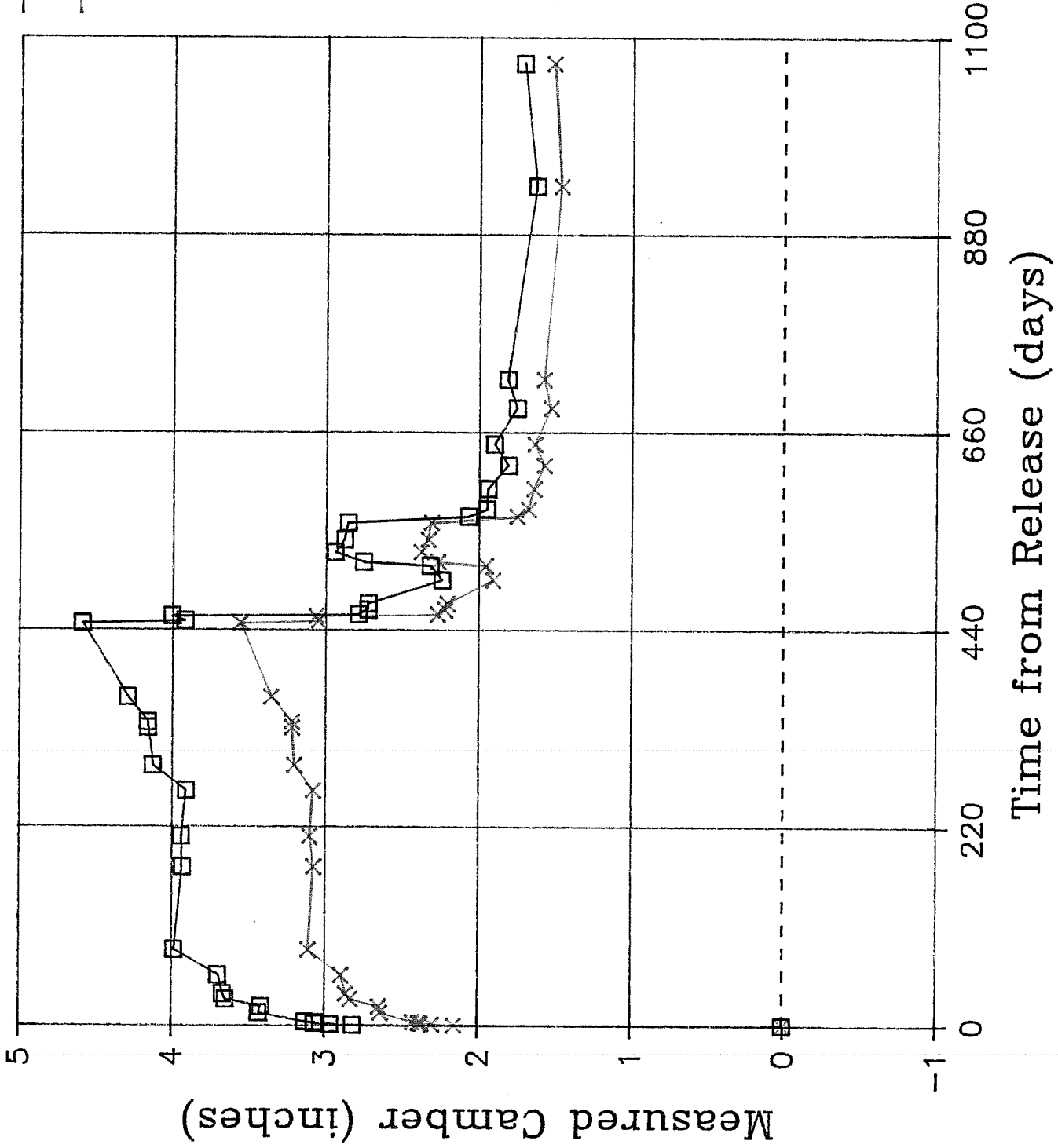
Beam L-02

—□— CENTER OF SPAN
—×— QUARTER POINT



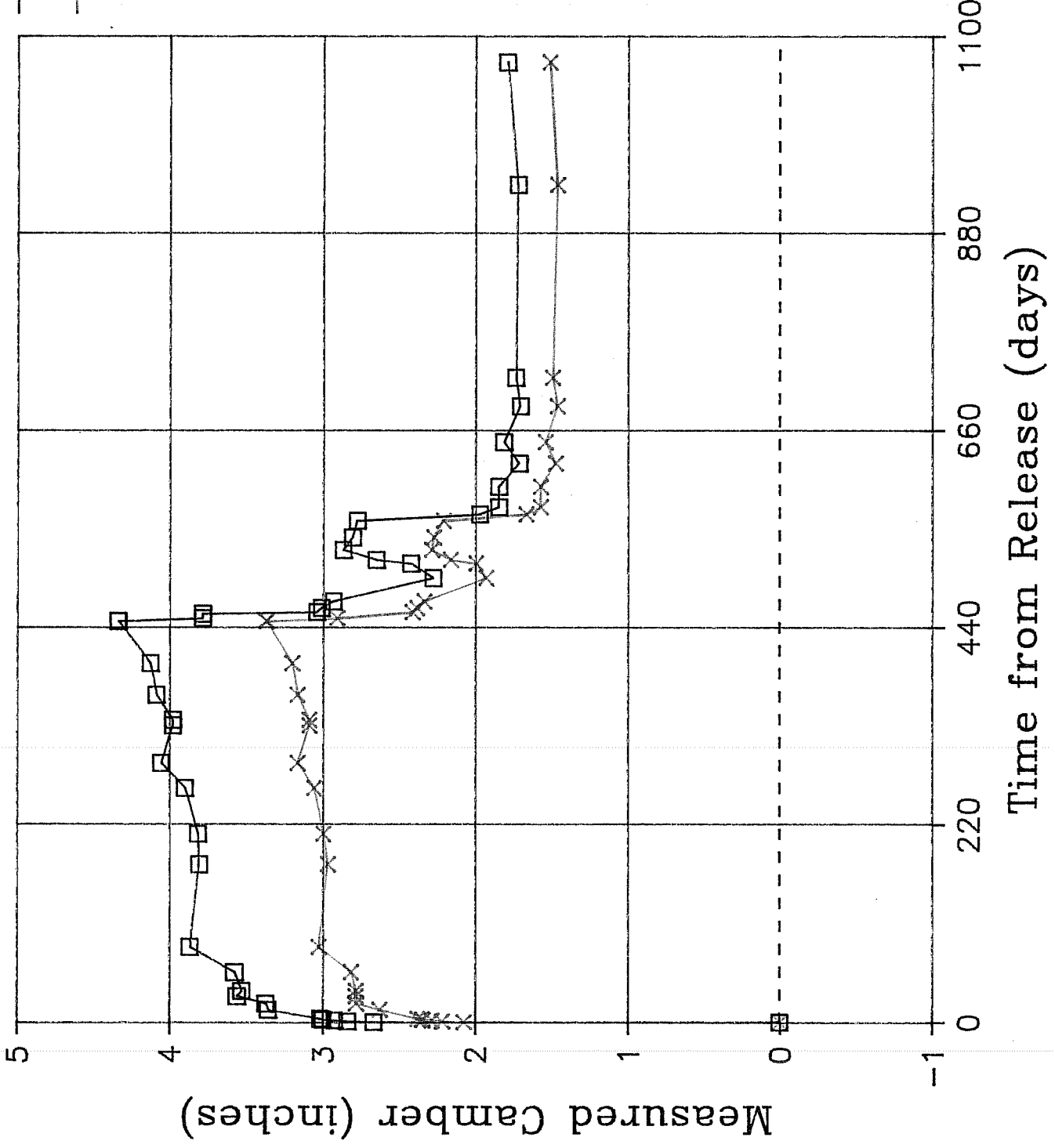
Beam L-i1

—□— CENTER OF SPAN
—×— QUARTER POINT



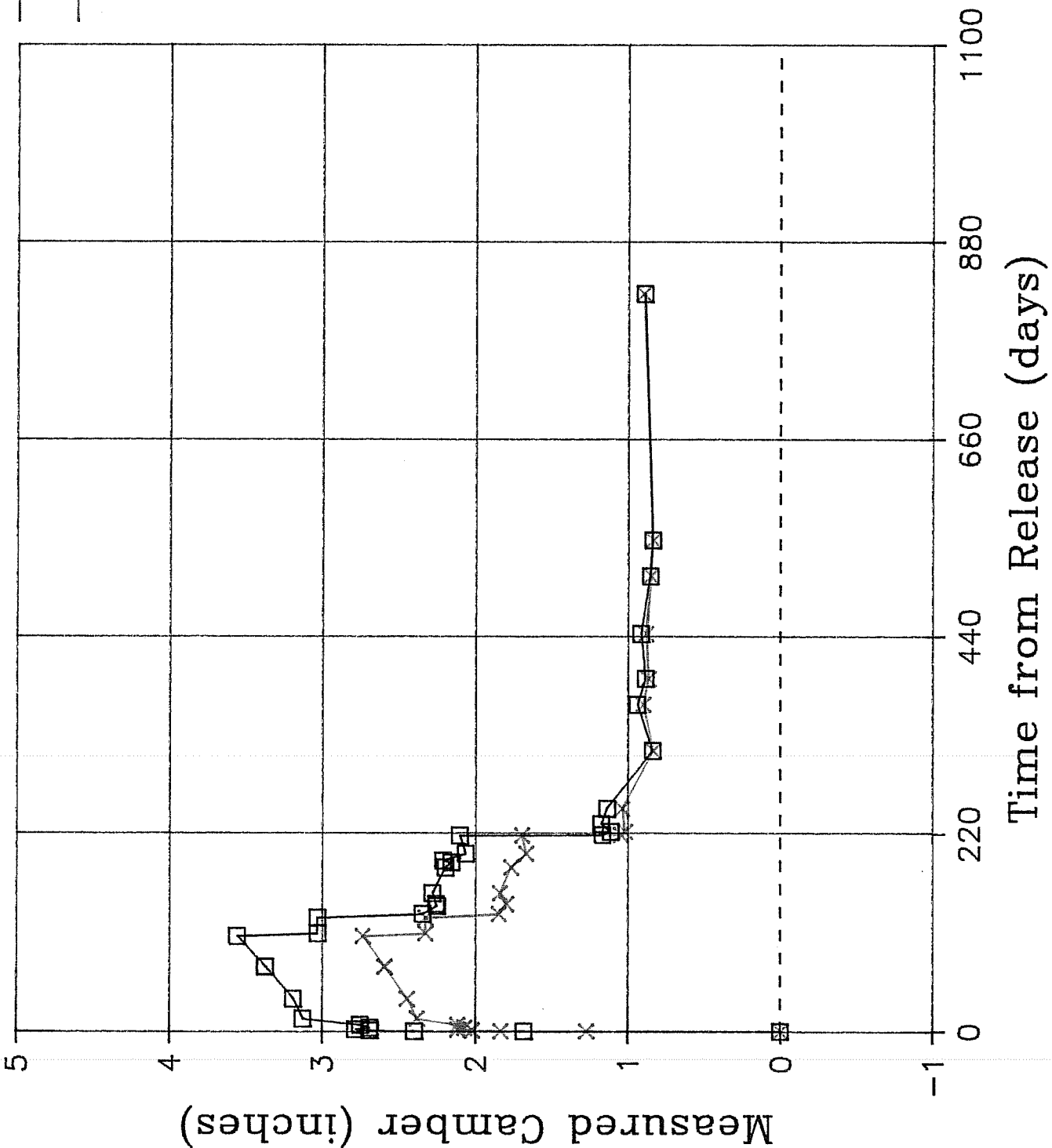
Beam L-i2

- CENTER OF SPAN
- ×— QUARTER POINT



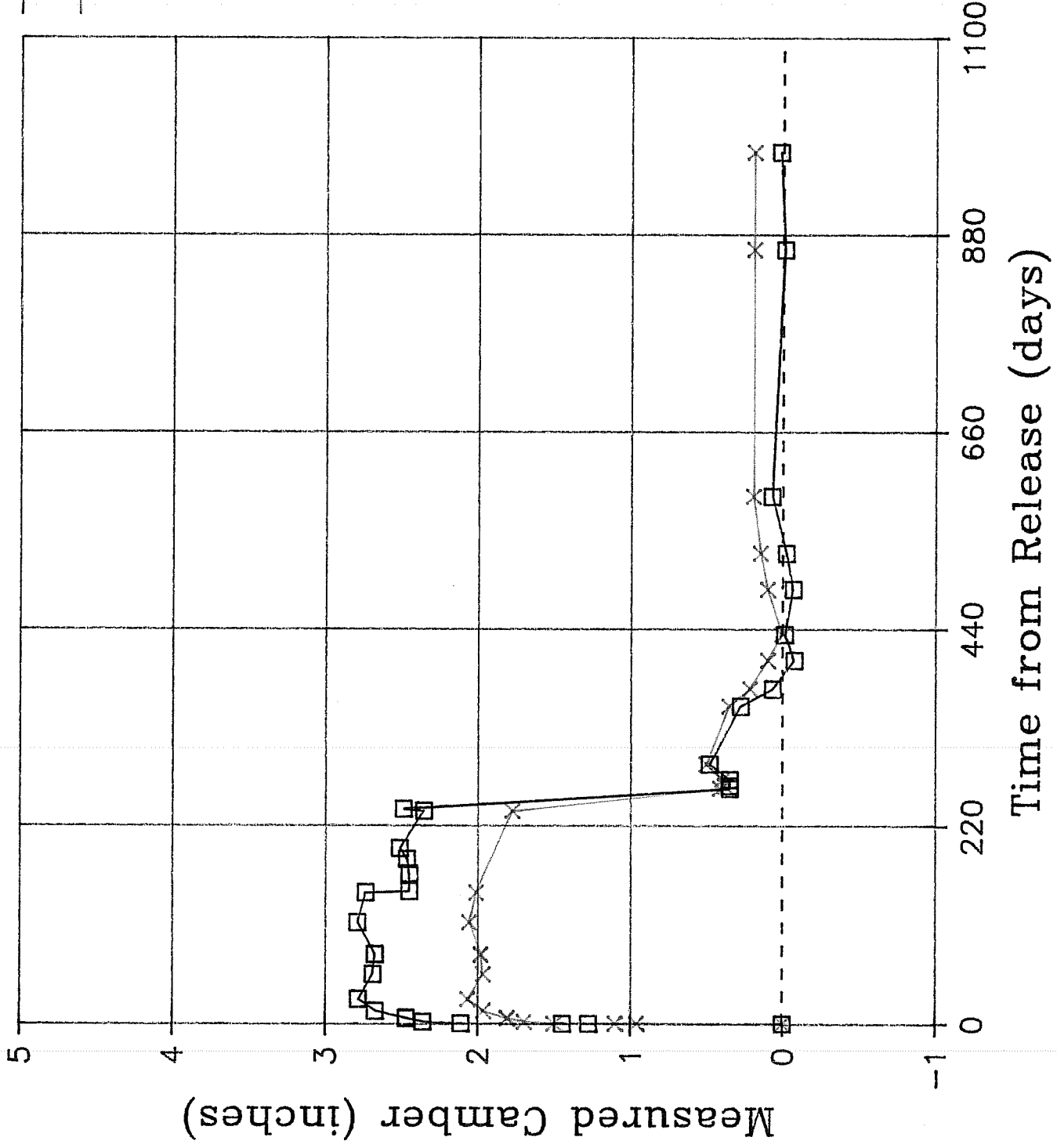
Beam H-i2

- CENTER OF SPAN
- *— QUARTER POINT



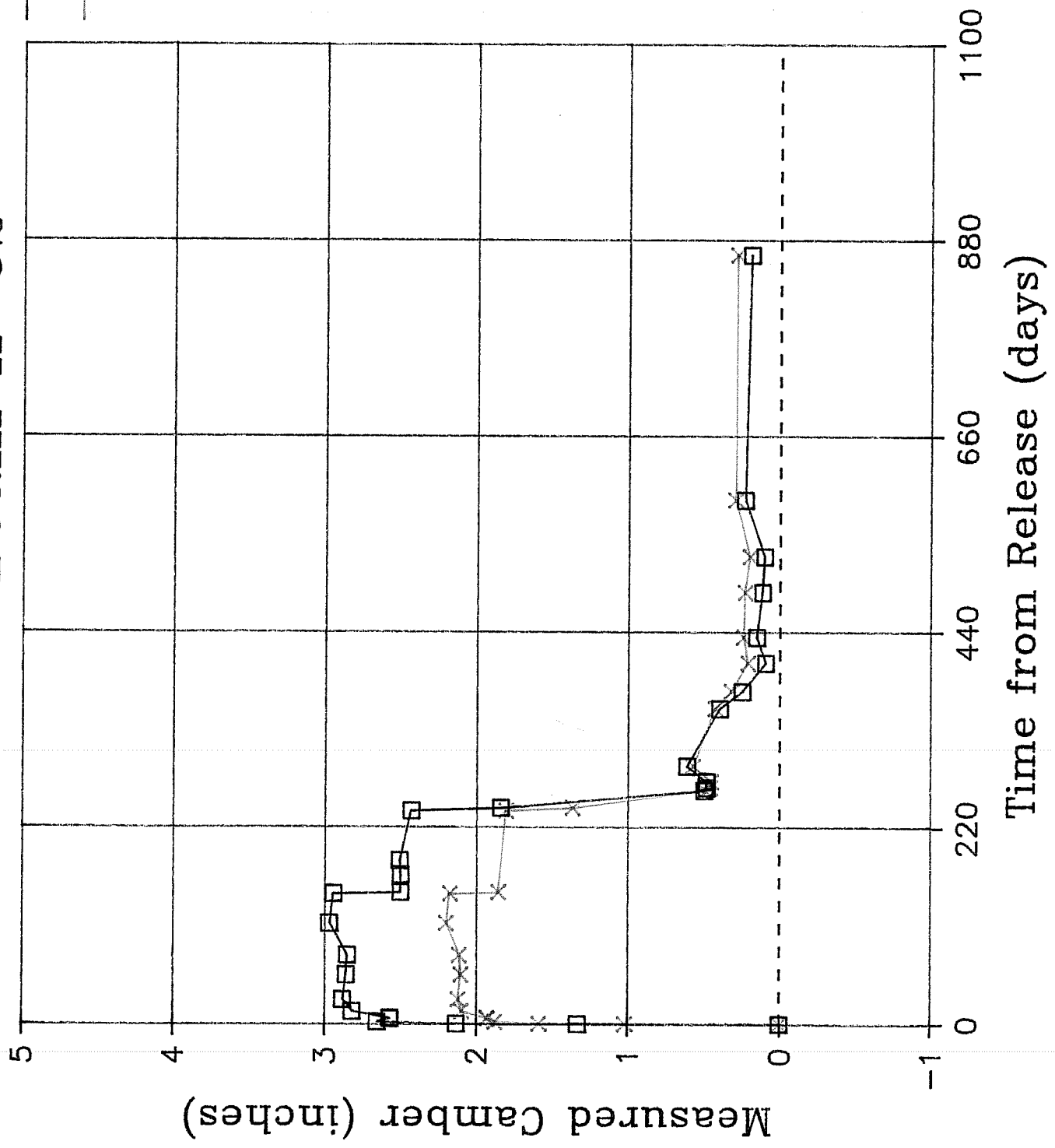
Beam H-01

—□— CENTER OF SPAN
—×— QUARTER POINT



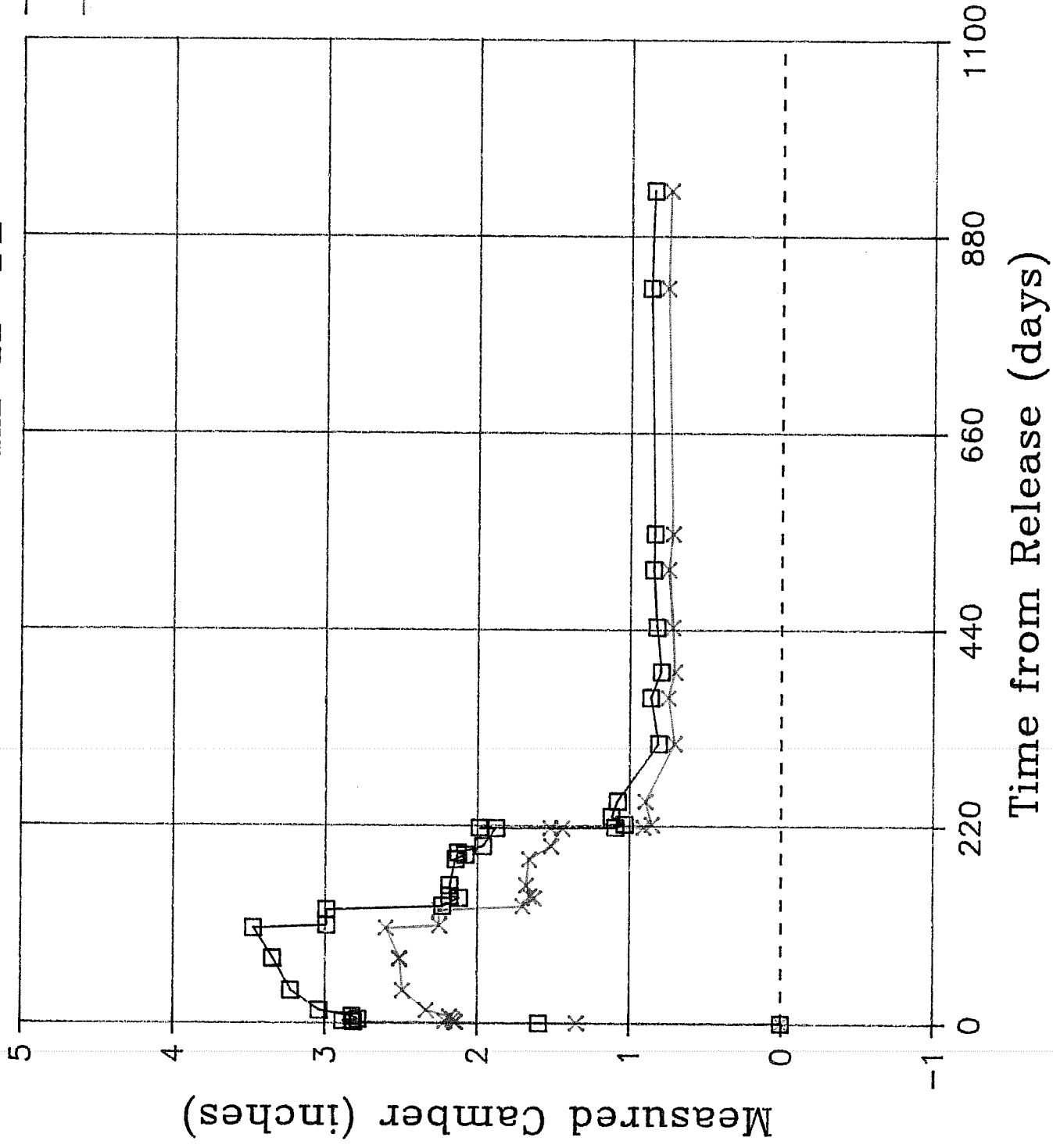
Beam H-02

—□— CENTER OF SPAN
—x— QUARTER POINT



Beam H-i1

—□— CENTER OF SPAN
—x— QUARTER POINT



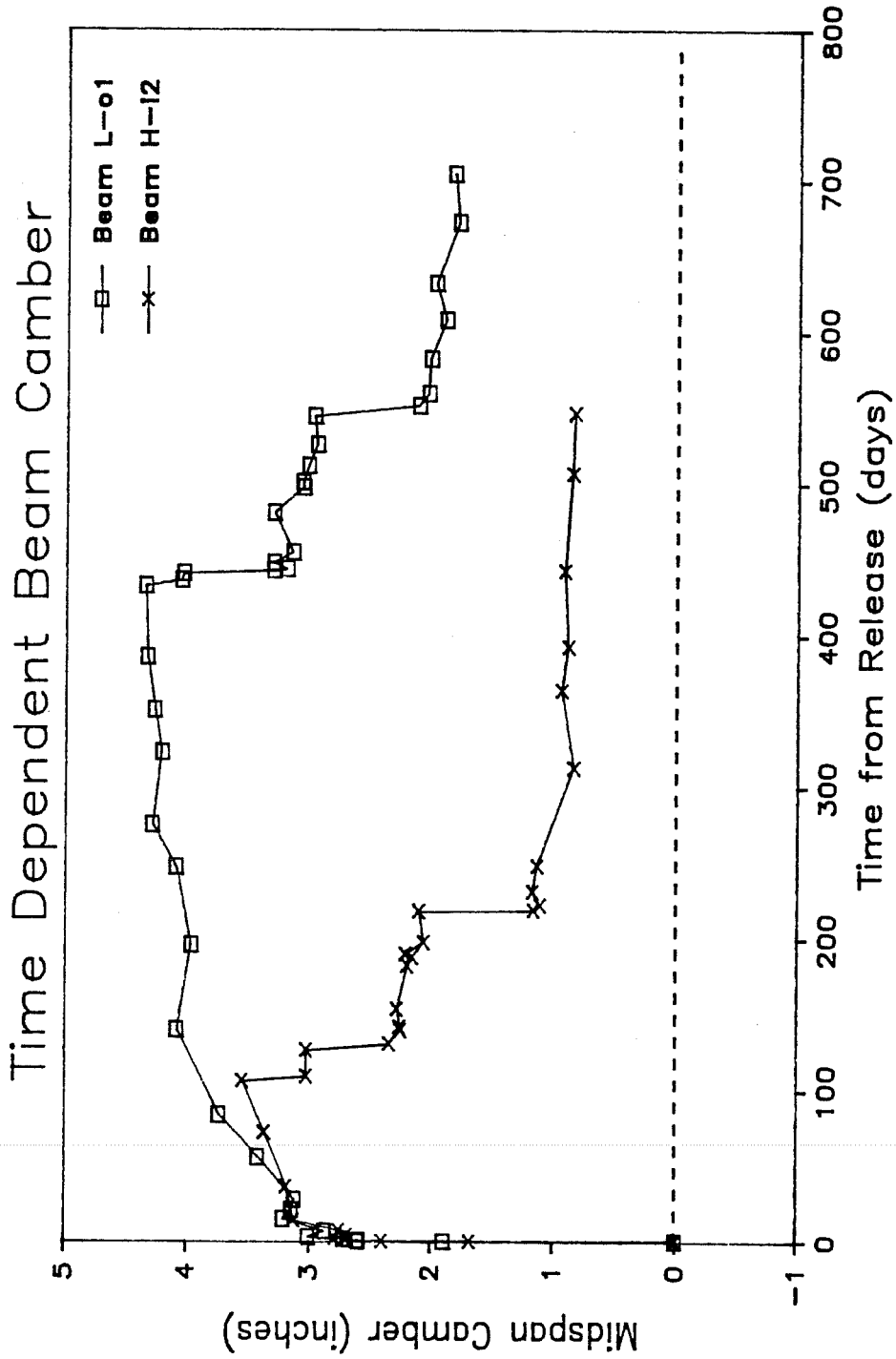


Fig. 4.49 Camber and deflection responses of typical L- and H-series beams

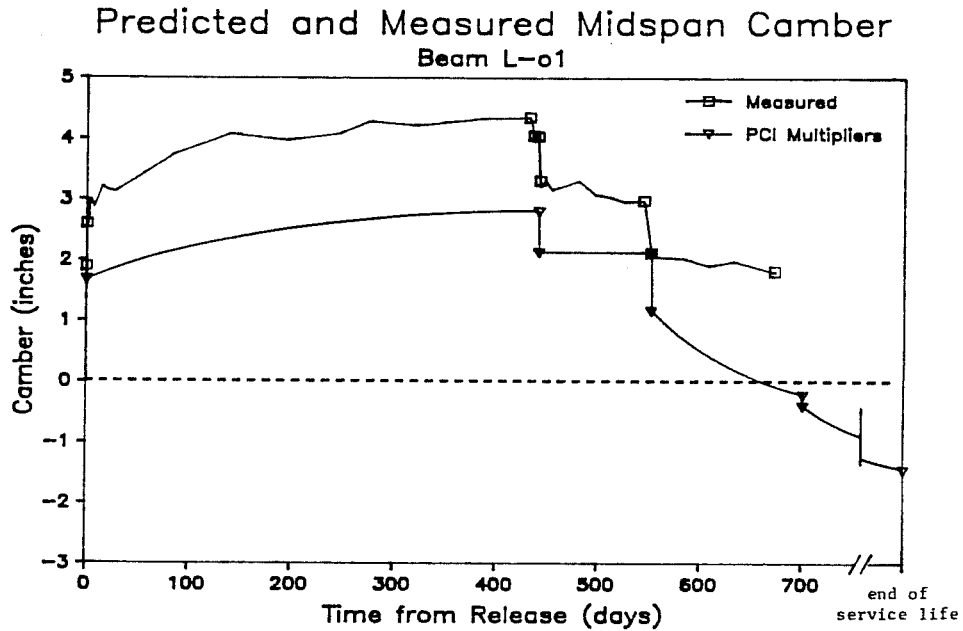


Fig. 5.14 Comparison of time dependent camber predicted using PCI multipliers and the measured response for beam L-01

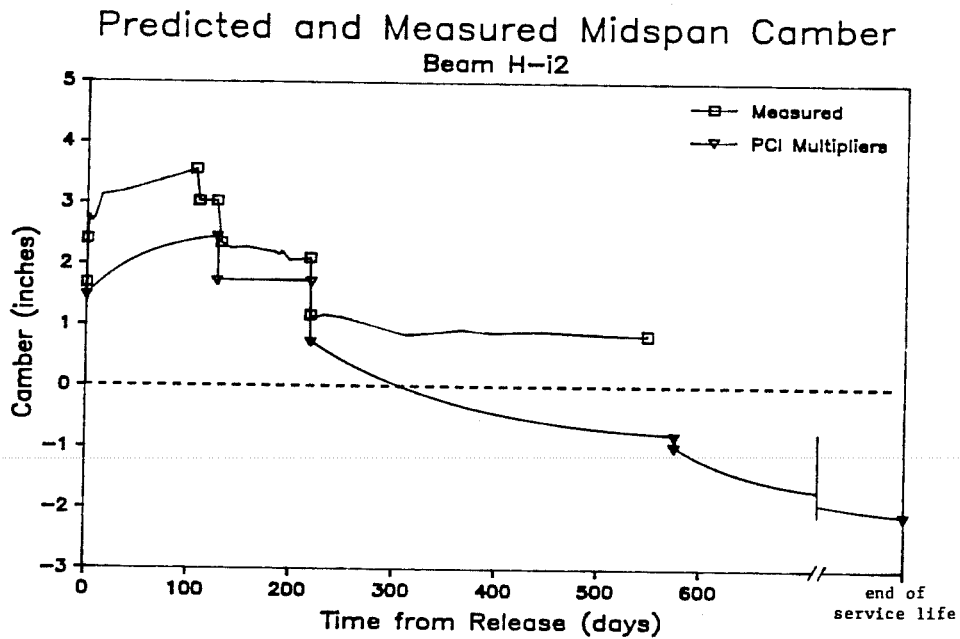


Fig. 5.15 Comparison of time dependent camber predicted using PCI multipliers and the measured response for beam H-i2

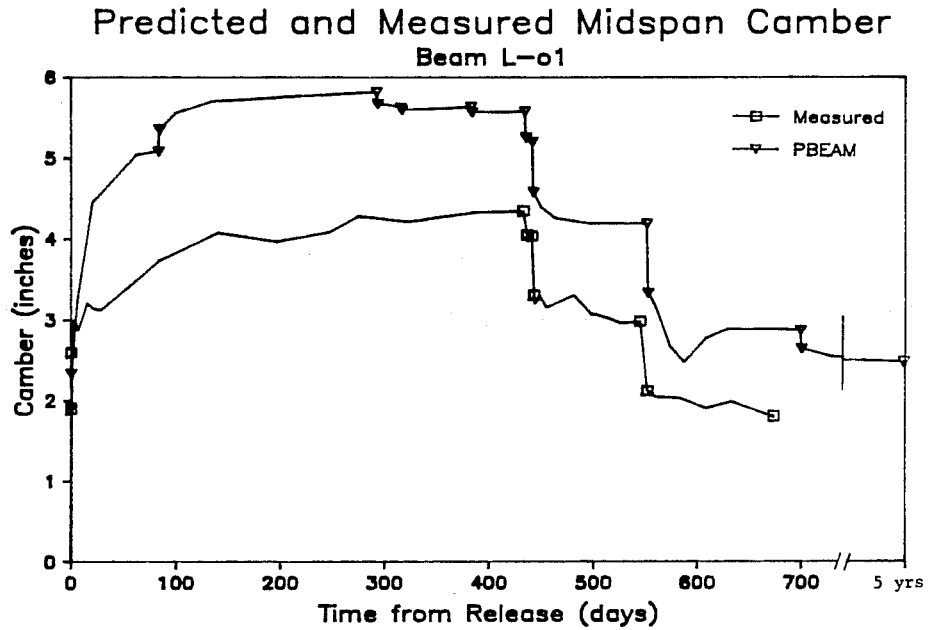


Fig. 5.30 Comparison of time dependent camber predicted using PBEAM and measured camber for beam L-01

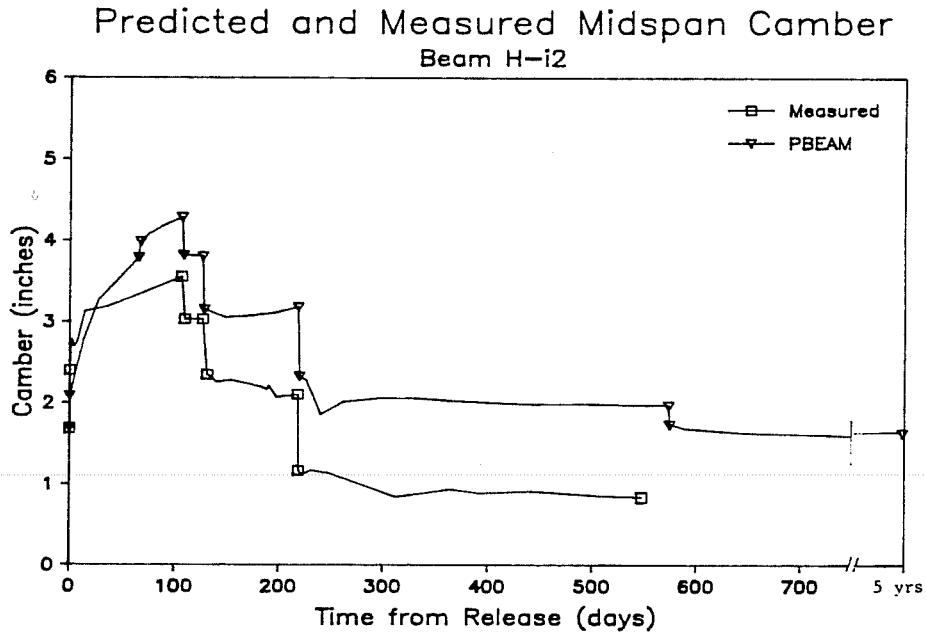


Fig. 5.31 Comparison of time dependent camber predicted using PBEAM and measured camber for beam H-i2

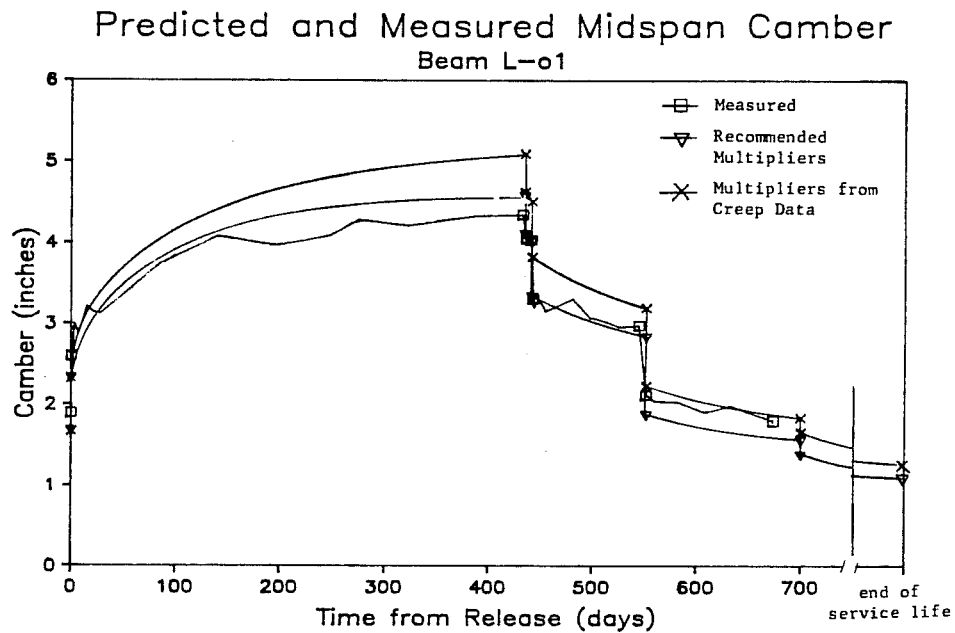


Fig. 5.39 Comparison of time dependent camber predicted using proposed multipliers and measured camber for beam L-o1

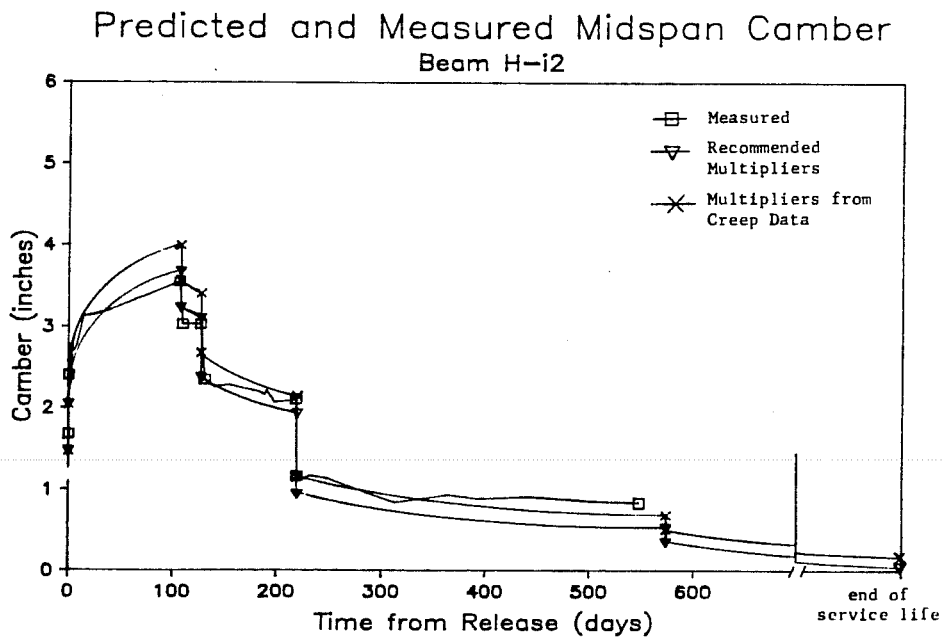


Fig. 5.40 Comparison of time dependent camber predicted using proposed multipliers and measured camber for beam H-i2

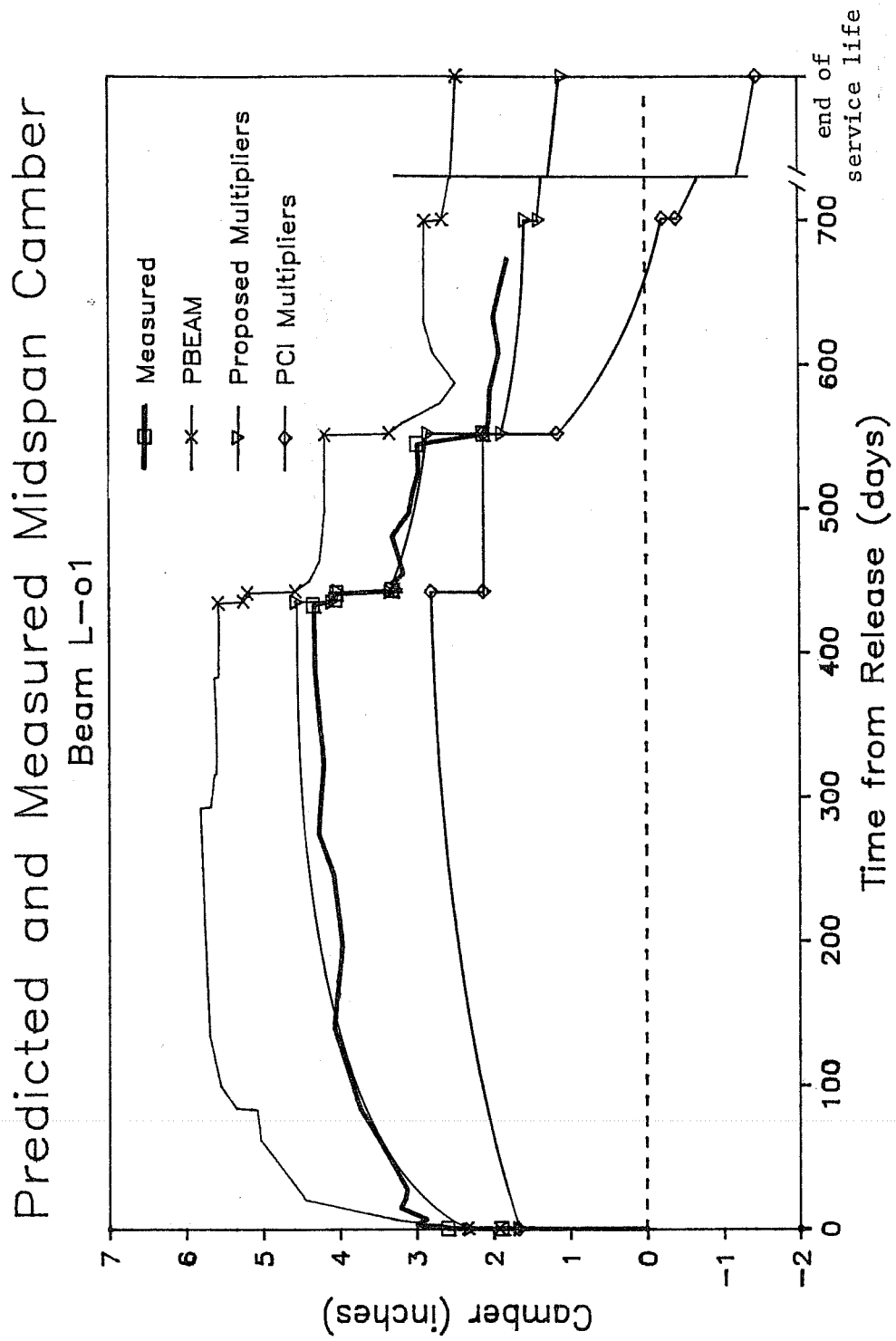


Fig. 6.3 Comparison of calculated time dependent camber for beam L-01

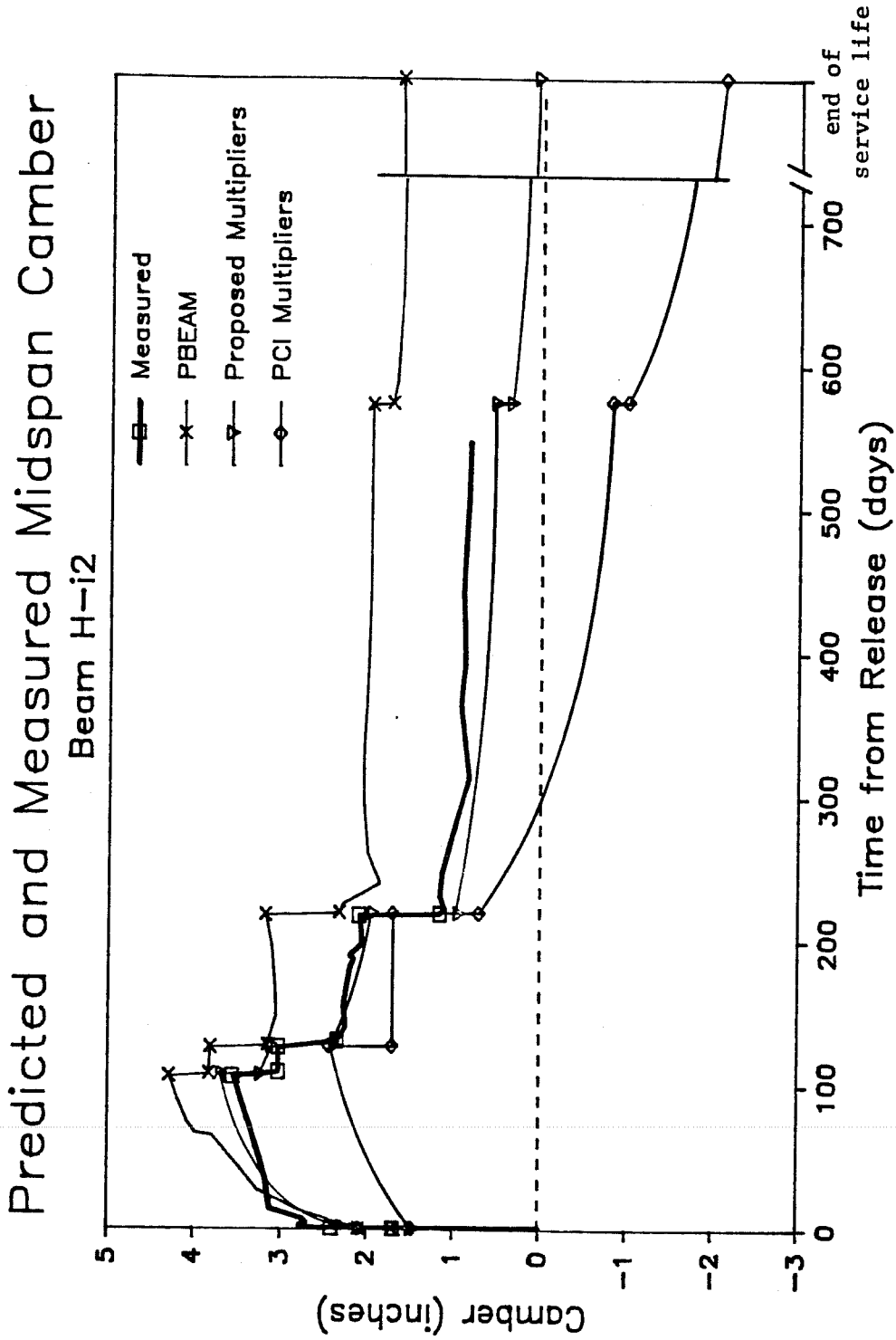


Fig. 6.4 Comparison of calculated time dependent camber for beam H-i2